# CATALYTIC REACTIONS OF ALKENES AND SUBSTITUTED CYCLOPROPANES ON ZEOLITES

By

CHRISTINE E. MARSDEN, B.Sc.

Thesis submitted for the Degree of

Doctor of Philosophy

University of Edinburgh

1978

*To my parents*

I declare that the work described in this thesis has not been submitted for any other degree and is the original work of the author except where acknowledgment is made by reference. The work has been carried out in the Chemistry Department of the University of Edinburgh between October 1974 and September 1977 under the supervision of Dr. H.F. Leach.

Post-graduate courses attended include: Computing (1 week Fortran programming course); High Speed Liquid Chromatography (5 lectures - Prof. J.H. Knox and Dr. J.H. Done); Biomimetic Organic Chemistry (5 lectures - Dr. R.M. Paton); Chemical Aspects of Oil Products Research (5 lectures - Staff of Shell Research Ltd.); Chemistry of the Upper Atmosphere (5 lectures - Dr. R.J. Donovan and Dr. M.F. Golde); Catalytic Group Seminars - 1974/75, 1975/76 and 1976/77.

## Acknowledgments

The author is indebted to her supervisor Dr. H.F. Leach for his interest and encouragement throughout the work and to Prof. C. Kemball for the provision of laboratory facilities. She also thanks the other members of the catalytic research group for the many useful discussions.

She is grateful for the assistance of the technical staff of the Chemistry Department in particular that of A. Anderson and J. Broom and in addition thanks Mrs. J. Gorrie for undertaking the typing.

Acknowledgment is also due to the University of Edinburgh for the award of a Vans Dunlop Scholarship for the duration of the research.

## ABSTRACT

A general review of molecular sieve zeolites precedes a more specialised account of the properties of the zeolites omega and erionite. It is these relatively unstudied zeolites which have been selected for a detailed catalytic characterisation utilising the isomerisation of the n-butenes and the methyl substituted cyclopropanes as test reactions. The resulting product distributions for each zeolite were indicative of carbonium ion type mechanisms. A study of the reaction of specifically labelled deuteropropene, $CD_2=CH-CH_3$, on the catalysts confirmed this mechanism and moreover, demonstrated that the intermediate carbonium ion was formed in an associative manner involving Brönsted acid sites.

A gravimetric study of the sorption of reactant and product molecules into the zeolites was also carried out. The wide pore zeolite omega exhibited rapid sorption and desorption of all three n-butenes and methylcyclopropane. Conversely, the rates of sorption of the n-butenes into erionite were a function of their dipole moments and structures, the order trans but-2-ene > but-1-ene > cis but-2-ene being observed. Furthermore, the sorption rates shown by erionite were dependent on the ionic composition of the erionite sample.

CONTENTS

# CHAPTER I

## Introduction to Catalysis

### 1.1. Historical

Processes, now described as catalytic, were used by the earliest civilisations with nature supplying the catalyst to unsuspecting man. Alcoholic fermentation, an enzyme reaction, appears quite commonly in ancient Chinese, Assyrian and Egyptian documents. Later, in the alchemical Middle Ages, some of the modern ideas of catalysis were incorporated in the ideas of the Philosopher's Stone[1].

The first scientific observation of a catalytic transformation appears to be due to van Marum[2] who, in 1796, reported the dehydrogenation of alcohol over silver, copper, lead and tin. Some years later, Kirchof[3] showed that hot aqueous mineral acids changed starch into dextrine and sugar, without themselves being altered by the reaction. Subsequently, Davy[4] observed that a slightly heated platinum spiral, introduced into a mixture of air and a combustible gas, became incandescent and caused the slow oxidation of the gas. This prompted the preparation of a spongy platinum catalyst which precipitated the reaction of hydrogen and oxygen at room temperature[5]. Similar observations over palladium and iridium were reported by Dulong and Thenard[6]. In 1831, Phillips[7] took out an English patent for making sulphuric acid by oxidation of sulphur dioxide on platinum. Phenomena of this kind, in which the presence of a material apparently having nothing to do with a reaction but which causes that reaction to take place, were coordinated by Berzelius[8] under the term catalysis.

In 1902, Ostwald[9] emphasised that a catalyst cannot change the equilibrium position in a reversible reaction. He introduced a quantitative meaning to catalysis by proposing that the rate of a

reaction was a measure of the catalyst activity. By correlating catalytic activity with a measurable quantity he laid the foundations upon which the modern ideas of catalysis are built.

## 1.2. Definition

Catalysis describes the action of a substance (the catalyst) which alters the rate at which a chemical reaction reaches equilibrium without appearing in the stoichiometric equation of the reaction. The equilibrium attained must be the same as that observed in the corresponding thermal reaction. Consequently the catalyst must affect both forward and reverse reactions equally. A catalyst can only alter the rate of a reaction which is thermodynamically favourable, it cannot initiate a reaction which involves an increase in free energy.

For a given reactant or group of reactants there may be several reaction paths leading to different products. By appropriate choice of catalyst any one of these paths may be 'selected'. For example, formic acid may undergo two alternative decompositions:

a) $HCOOH \rightleftharpoons H_2O + CO_2$

b) $HCOOH \rightleftharpoons H_2 + CO_2$.

The first of these reactions is catalysed by oxides such as alumina, the second by various metals.

In general, catalysed reactions may be classified as heterogeneous or homogeneous depending on the phase relationship between catalyst and reactants and products.

1) In heterogeneous catalysis the reaction takes place at an interface between two phases.

2) Homogeneous catalysis involves reaction in which the catalyst and reactants are in the same phase.

This thesis is concerned with heterogeneous catalysis and specifically deals with the reactions of gases on solid catalysts.

## 1.3. Heterogeneous Catalysis

In a heterogeneously-catalysed reaction at least one of the reactants must, for some finite time, be attached to the surface of the solid catalyst. A large amount of experimental evidence has been accumulated showing that adsorption of reactant molecules occurs at solid surfaces.

Berzelius[8], the first to define catalytic phenomena and to give them their name, did not really furnish any explanation for them and found only vague terms with which to characterise the 'catalytic force' which he regarded as the cause of reactions of this kind. A theory of "contact action" was proposed by Faraday[10], whereby physical forces of attraction between the catalyst and reactants led to increased reaction rates, due entirely to the increased concentrations of reactants in the condensed layer. However, a satisfactory explanation of the specificity of catalyst action was not given until Sabatier's[11] postulation of unstable surface compounds as reaction intermediates. In support of this concept, Langmuir[12] proposed that molecules, adsorbed on the surface, were held essentially by chemical bonds and that the nature of the adsorption depended on the catalyst surface sites.

## 1.4. Adsorption

Two types of adsorption are clearly distinguishable, physical adsorption and chemisorption.

### 1.4.1. Physical Adsorption

Physical adsorption can, in principle, occur between all gases and solids. The adsorbate molecules are held to the surface by weak forces similar to van der Waals forces between molecules.

These may be classified as forces associated with

a) permanent dipole moment in the adsorbed molecule

b) polarisation of the adsorbed molecule

c) dispersion effect

d) the short range repulsive effect.

Heats of adsorption are low ( 3 - 30kJ $mol^{-1}$) and similar to the latent heat of condensation of the adsorbate. Physical adsorption requires little activation energy and is thus rapid and reversible at low temperatures. Gases are not physically adsorbed at temperatures much greater than their critical temperature.

Since the forces involved are small and non-specific, physical adsorption is not considered to be of direct importance to the surface catalysed reactions of stable molecules. However, the non-selective nature of physical adsorption means that monolayer coverage is determined by the cross-sectional area of the adsorbate molecules and not by the number of specific surface sites. Hence measurement of physical adsorption at low temperatures provides a convenient method for the determination of surface areas. This is exemplified by the work of Brunauer, Emmett and Teller[13] whose methods are generally used for surface area determination.

### 1.4.2. Chemisorption

Chemisorption is the result of a chemical reaction involving redistribution of electrons between the adsorbate and the adsorbent. The bond formed may be either covalent or ionic in character. The forces involved in chemisorption are comparable with those leading to the formation of chemical compounds. Such adsorption may be regarded as the formation of a sort of surface compound, the heats evolved ranging from 40 to 400 kJ $mol^{-1}$.

Like other chemical reactions, chemisorption is usually an activated process and so it proceeds at a finite rate which increases rapidly with increasing temperature. Many chemisorptions are consequently irreversible especially at low temperatures, due to a slow desorption rate. Chemisorption is always confined to a single atomic or molecular layer and is invariably specific in nature, for example hydrogen is chemisorbed on nickel but not on copper.

Owing to the large energy changes which it brings about in a molecule, chemisorption of one or more of the reactants is considered to be a prerequisite of a catalytic reaction. The strength of adsorption is important, a too strongly chemisorbed reactant will be difficult to remove and may act as a poison, while a too weakly chemisorbed reactant may not remain on the surface long enough to react.

Infrared spectroscopy[14] and electron spin resonance[15] techniques have revealed that a gas may adsorb on a surface with the formation of a variety of species, often involving considerable rearrangement of the molecule.

## 1.5. The Mechanism of Heterogeneous Catalysis

A heterogeneously catalysed reaction may be considered as occurring in five elementary steps:

(1) Diffusion of reactant(s) to the surface from the gas phase.

(2) Chemisorption of one or more reactant species on the surface.

(3) Chemical reaction on the surface.

(4) Desorption of the products from the surface.

(5) Diffusion of the products away from the surface.

The overall reaction rate is determined by the slowest of these steps. In low pressure laboratory systems diffusion to and from the surface is usually rapid compared with the other steps. Nevertheless,

diffusion effects may be important in highly porous catalysts where an activated diffusion through the catalyst pores may occur. Low values for the activation energy are often indicative of such a diffusion controlled reaction.

The energy-reaction path diagram for a unimolecular reaction $X \rightarrow Y$ is represented in Fig. 1.1.

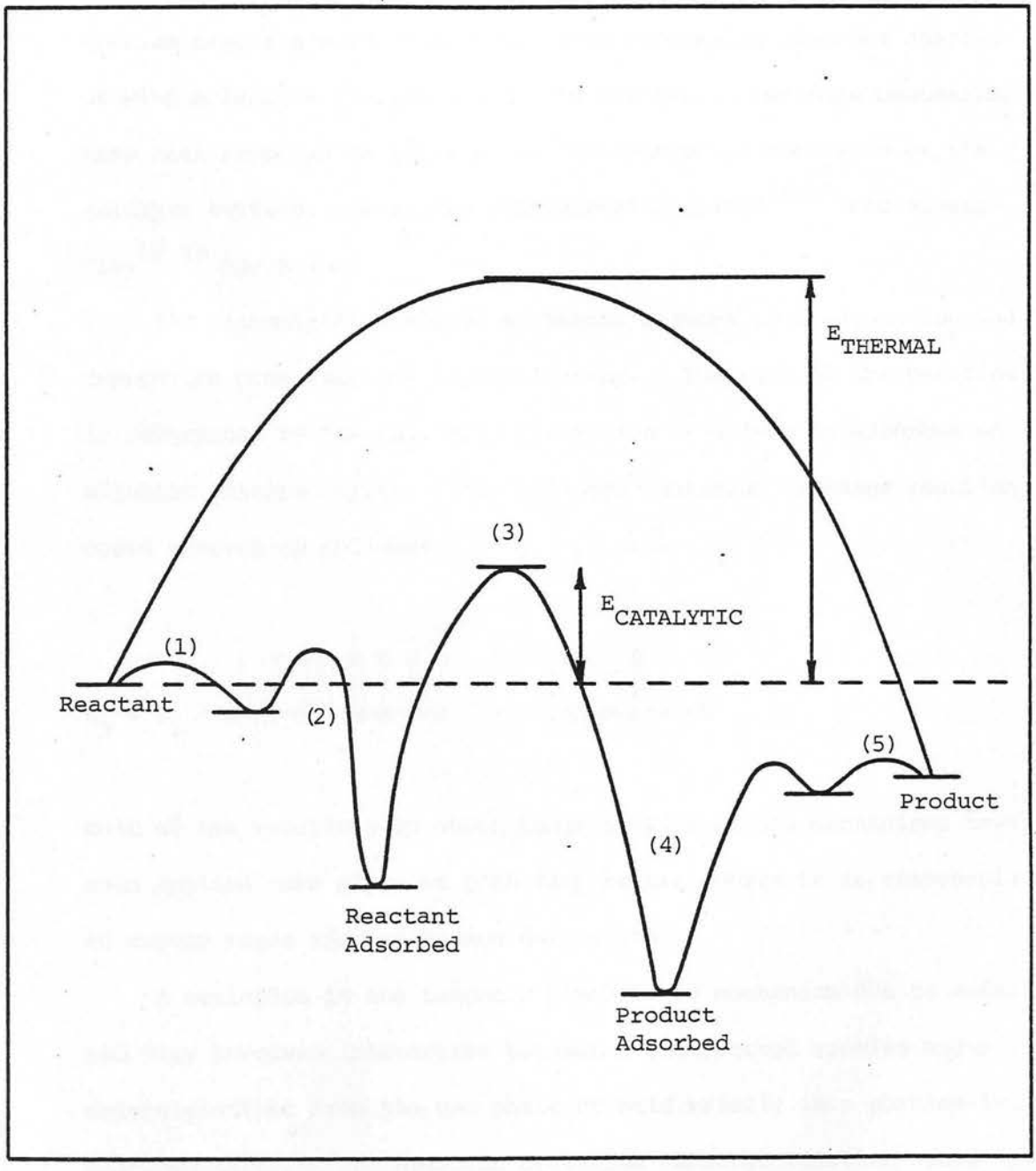


Fig. 1.1. Energy - Reaction Path Diagram for a Simple Unimolecular Reaction ($X \rightarrow Y$) (Steps (1) - (5) are as described in text)

The barriers to chemical reaction with and without a catalyst are shown. It can be seen that the overall energy requirement is much less in the catalysed reaction than in the thermal reaction. The catalytic reaction is therefore faster than the thermal reaction at a given temperature and conversely a lower temperature is required for the catalytic reaction at a given rate.

In the surface reaction it is possible to envisage chemisorbed species reacting with themselves, with physically adsorbed species or with molecules colliding with the surface. Two main mechanisms have been proposed to explain the combination of reactants at the catalyst surface, namely the Langmuir-Hinshelwood[16,17] and Rideal-Eley[18,19] mechanisms.

The Langmuir-Hinshelwood mechanism assumes that adsorption and desorption processes are in equilibrium. The rate of the reaction is determined by the chemical interaction of molecules adsorbed on adjacent catalyst sites. The hydrogen-deuterium exchange reaction would proceed as follows:

$$H_2 + D_2 + 4M \rightarrow \begin{matrix} H & H & D & D \\ | & | & | & | \\ M & - & M & - & M & - & M \end{matrix} \rightarrow \begin{matrix} H & & D \\ | & & | \\ M & - & M & - & M & - & M \end{matrix} + HD$$

Most of the reactions to which Langmuir-Hinshelwood mechanisms have been applied take place at high temperatures where it is reasonable to expect rapid adsorption and desorption.

A variation in the Langmuir-Hinshelwood mechanism due to Rideal and Eley involves interaction between a chemisorbed species and a molecule either from the gas phase or held briefly in a physically adsorbed layer. The hydrogen-deuterium exchange reaction would proceed as follows:

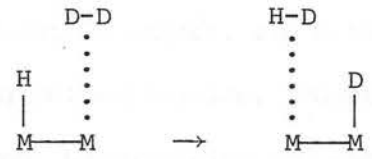


A full line represents chemisorption and a dotted line physical adsorption.

The exact nature of the surface reaction is difficult to determine since the nature, properties and concentrations of various chemical species cannot be easily derived from the kinetics of a catalytic reaction. Direct information on the nature of surface species can be gained using spectroscopic techniques but the results are often difficult to interpret. Nevertheless, indirect experimental methods using deuterium and tracer elements have been found useful in elucidation of surface mechanisms[20].

## 1.6. Catalyst Classification

A wide range of chemicals, represented by both elements and compounds, exhibit catalytic action. Heterogeneous catalysts may be divided into two distinct groups: 1) metals and 2) non-metals. The former group is comprised largely of the metals of Groups VIII and 1B, the latter of metal oxides, sulphides, salts and acids. The non-metallic catalysts may be further classified according to their electrical conductivities into a) semi-conductors and b) insulators.

These three classes of catalyst possess characteristic individual functions. The metals are, in general, active for hydrogenation and dehydrogenation reactions. The semi-conducting oxides and sulphides are good catalysts for oxidation-reduction processes, cyclisation and to a lesser extent, hydrogenation. The insulators, which include

salts and stoichiometric oxides, are active for a wide variety of reactions including polymerisation, isomerisation, cracking, dehydration, alkylation, halogenation and dehalogenation. They possess very little ability to catalyse hydrogenation or oxidation. These catalysts are thought to function through acid sites.

The reactive properties of different catalyst types may be usefully combined in the formation of dual function catalysts. For example, platinum on alumina provides a catalyst active for hydrogenation/dehydrogenation reactions and alkene isomerisation.

This thesis is concerned with catalysts known as zeolites or molecular sieves, which may be regarded as highly ordered crystalline aluminosilicates. These are active for reactions catalysed by insulators and are considered to function through similar acid sites. A large number of naturally occurring and synthetic zeolites are known and their structures and properties are discussed in detail in Chapters 2 and 3.

# CHAPTER 2

## General Introduction to Zeolites

### 2.1. Definition and Occurrence

With the discovery of stilbite in 1756, Cronstedt[21] recognised a new group of minerals consisting of crystalline, hydrated aluminosilicates of the alkaline earth and alkali metals. As a consequence of their intumescent properties these materials were called zeolites (Greek; 'zeein' to boil, 'lithos' a stone).

In 1937, Hey[22] defined the zeolites as "a group of crystalline solids, hydrated aluminosilicates of mono- and divalent bases, in which the ratio (R", $R_2$)O : $Al_2O_3$ is unity, which are capable of losing a part or the whole of their water without change of crystal structure, and of absorbing other compounds in place of the water removed, and which are capable of undergoing base-exchange". This definition is descriptive and still applicable.

Zeolite minerals were first obtained from vesicles and fractures in basaltic rocks, their formation resulting from precipitation from fluids which permeated the basalts. In some occurrences, more than one episode of zeolite crystallisation occurred, as at Sasbach, Kaiserstuhl, Germany, where faujasite lined the cavities prior to growths of tuffs of phillipsite[23]. In general, the bulk composition of the host rock correlates with that of the zeolite. Thus mordenite and other silica rich zeolites occur in rocks supersaturated in silica whereas faujasite, chabazite and gmelinite occur preferentially in rocks deficient in silica.

In recent years zeolites have been found in massive amounts in sedimentary deposits. These deposits appear to have been produced by the alteration of volcanic ash and other pyroclastic material by the action of alkaline lake waters. The variable proportions of

minerals observed in the different deposits are a result of sporadic volcanic activity, specific geographical location and the chemistry of ephemeral lakes.

All the zeolite minerals known have been found in igneous rock but only six commonly occur in sedimentary deposits. These are analcime, chabazite, clinoptilolite, erionite, mordenite and phillipsite.

## 2.2. Synthesis

Although the syntheses of certain zeolites had been reported[24] as early as the nineteenth century, positive identification of the products was not possible until the advent of X-ray diffraction.

Barrer[25,26] studied zeolite synthesis and, by 1948, had prepared several zeolites using a high pressure hydrothermal technique. At about this time, a study of zeolite synthesis demonstrated that high temperatures and pressures were not necessary in the hydrothermal process and that many species of zeolites may be synthesised under mild temperature conditions[27-29].

Synthetic zeolites are formed by crystallisation of freshly prepared metal aluminosilicate gels in the temperature range 298 K to about 448 K. The gel is prepared from soluble salts of alkali metals by a copolymerisation of individual silicate and aluminate species. Depolymerisation by the hydroxyl ions present, followed by the rearrangement of the metal ions and the silicate and aluminate species yields large numbers of crystalline nuclei. The product is a white powder usually consisting of two or more zeolite phases.

Synthesis of different zeolites is achieved by variation of the initial gel composition and the crystallisation temperature. The role played by the cation in zeolite formation is demonstrated by the fact that many zeolites, which crystallise from a sodium

aluminosilicate gel do not crystallise from a similar potassium gel. For example, the substitution of $K_2O$ for $Na_2O$ in an aluminosilicate reaction mixture results in the formation of zeolite L instead of zeolite Y[30].

Zeolites have been prepared in which aluminium and silicon have been replaced by other atoms. The substitution of gallium and germanium for aluminium and silicon in the A, X and P zeolites was reported by Barrer et al[31] using gels prepared from aqueous solutions of sodium gallate, sodium germanate and aqueous silica sol. Several zeolites containing significant amounts of phosphorus incorporated in their crystal framework have also been prepared[32]. In a similar manner, iron, $Fe^{3+}$, has been substituted for aluminium in the aluminosilicate structure[33].

Although there are no known ammonium or alkylammonium zeolite minerals, synthetic zeolites have been prepared from systems containing quaternary ammonium ions[34], in particular the tetramethylammonium (TMA) cation. The crystallisation of such zeolites requires at least two bases, the alkylammonium base together with alkali metal hydroxide. For example, the gel systems incorporating the mixed bases, TMA, sodium and potassium hydroxides produce nitrogeneous zeolite phases including zeolite omega, and zeolites of the offretite- and erionite-type[35].

In general, zeolites produced synthetically are more uniform in chemical composition and properties than their natural counterparts, most synthetic zeolites containing only one or two different cation species. In contrast, the mineral zeolites exhibit considerable compositional variation. This is a result of their genesis and subsequent alteration by cation exchange and/or recrystallisation dependent upon their history.

## 2.3. Structure and Classification

Although recognised in the eighteenth century as being a unique mineral group, the elucidation of the complex structure of zeolites did not occur until much later. In 1930, using X-ray crystallography, Taylor[36] reported the first analysis of the crystal structure of a zeolite, analcime. In the years that followed many more zeolite structures were characterised[37-39]. X-ray diffractional analysis was the major source of information although additional data was obtained from other techniques including infrared absorption, nuclear magnetic resonance, electron spin resonance and Mössbauer spectroscopy.

The zeolite structure is based on fundamental units in which a $Si^{4+}$ or $Al^{3+}$ ion is tetrahedrally coordinated to four oxygen atoms. These tetrahedral units are linked in three-dimensions by oxygen bridges to form rings, the size of which are analagous to the size of the anions[40] thought to be responsible for zeolite growth during synthesis. According to Loewenstein[41] the alumina tetrahedra only link to silica tetrahedra so that no Al-O-Al bonding occurs and consequently the Si/Al ratio is never less than unity.

Within the zeolite framework, the presence of aluminium atoms tetrahedrally coordinated to four oxygen atoms results in a net negative charge which must be compensated for by cations located within the interstices of the structure. In natural zeolites the cations present are generally the alkali metal ($R^{+}$) or alkaline earth ($R^{2+}$) type.

Classification of the many zeolitic topologies into groups has been accomplished according to common features of the aluminosilicate framework structure. In the classification proposed by Breck[42], zeolites have been divided into seven structural groups according to the presence of specific arrangements of $(Si,Al)O_4$ tetrahedra.

These arrangements have been called secondary building units by Meier[43] and are illustrated in Fig. 2.1. Linkage of these secondary building units into chains, layers and polyhedra results in the characteristic framework structures of different zeolites. The seven groups, with representative zeolite structures, are listed in Table 2.1.

| Group | Secondary Building Unit | Examples |
|---|---|---|
| 1 | Single 4-ring S4R | Analcime, Phillipsite |
| 2 | Single 6-ring S6R | Erionite, Offretite, Omega |
| 3 | Double 4-ring D4R | A |
| 4 | Double 6-ring D6R | X, Y, Faujasite, Chabazite |
| 5 | Complex 4-1, $T_5O_{10}$ unit | Thomsonite |
| 6 | Complex 5-1, $T_8O_{16}$ unit | Mordenite |
| 7 | Complex 4-4-1, $T_{10}O_{20}$ unit | Clinoptilolite, Stilbite |

Table 2.1. Classification of Zeolites ($T = (Si,Al)O_4$)

A number of cage-like, polyhedral units, such as the truncated octahedron, can be recognised within certain zeolite framework structures. These cage-like units are designated by Greek letters: $\alpha$, $\beta$, $\gamma$, etc. The $\beta$-cage or truncated octahedron which is illustrated in Fig. 2.2. can be described in terms of four- and six-membered single rings.

The framework structures of zeolites A and X are shown schematically in Fig. 2.3. In zeolite A the $\beta$-cages are linked by double four-rings to form a cubic structure. The cavity enclosed by such an arrangement is a truncated cubo-octahedron ($\alpha$-cage). In contrast

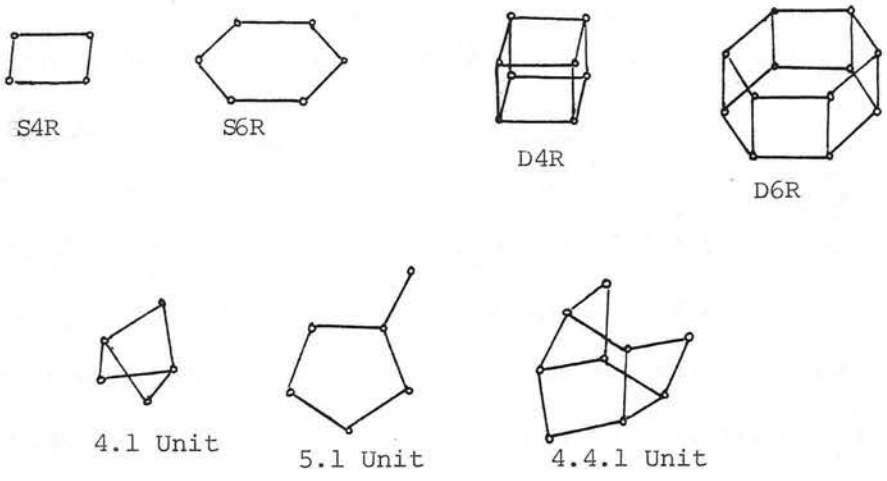


Fig. 2.1. The Secondary Building Units Found in Zeolite Frameworks

Fig. 2.2 The β-Cage or Truncated Octahedron

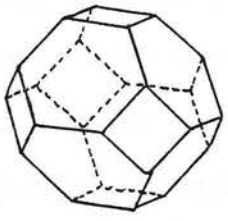

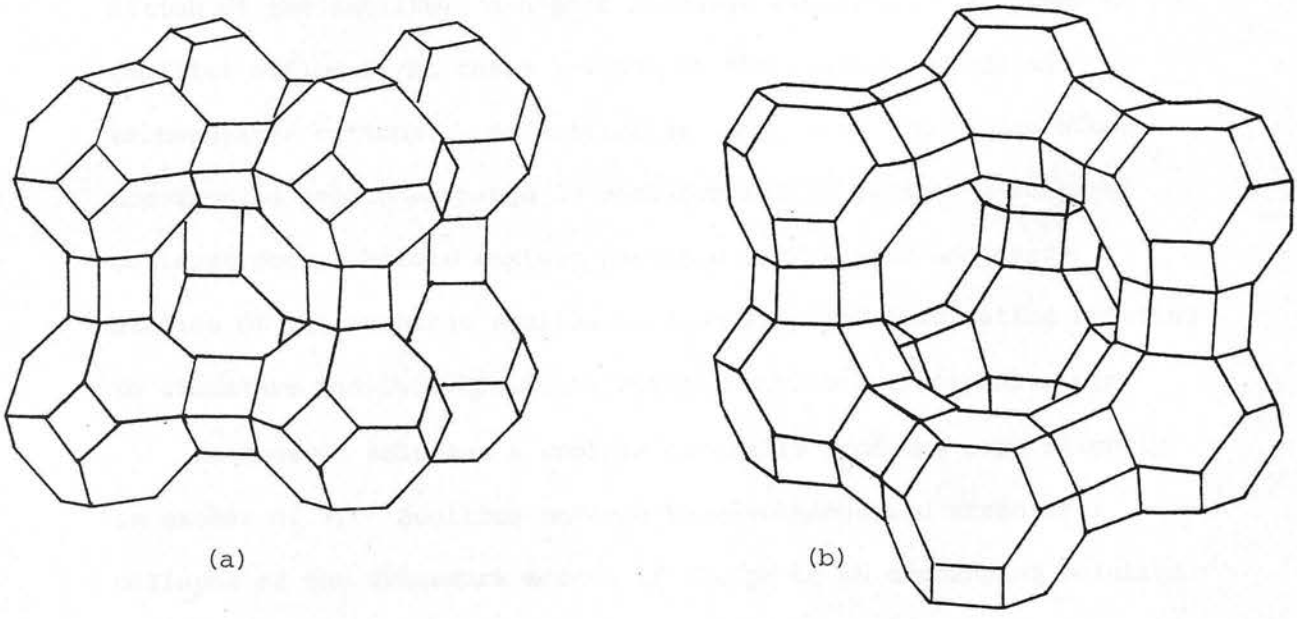


Fig. 2.3. Framework Structures of (a) Zeolite A and (b) Zeolite X.

the β-cages in zeolite X are linked tetrahedrally by double six-ring units in a diamond-like array.

Obviously a large number of zeolite framework structures are possible depending on the component secondary building units and their position and orientation relative to one another.

The work described in this thesis is concerned with the Group 2 zeolites, omega and erionite, the structures and properties of which are described in detail in Chapter 3.

## 2.4. Ion Exchange Properties

One of the earliest properties of zeolites to be recognised was their ability to effect cation exchange in aqueous solutions, leading to an interest in these materials as water-softening agents. The cation exchange behaviour of zeolites depends on a number of factors including the nature of the cation and the structural characteristics of the zeolite. These and other factors are described in a qualitative manner by Barrer[44].

The cation exchange capacity is dependent on the chemical composition of the zeolite; a higher exchange capacity is observed in zeolites of low Si/Al ratio because of the greater number of exchangeable cations. An alteration in lattice dimensions often accompanies cation exchange in zeolites and in general structural collapse occurs before maximum possible exchange is achieved. Studies of ion exchange equilibria have supplied information relating to structure and the population and distribution of cation sites.

In aqueous solution a zeolite generally produces a pH slightly in excess of 7. Zeolites undergo base-exchange and structural collapse of the framework occurs if the pH of an exchanging solution

falls below 5. Consequently, in the majority of cases, exchange of zeolite cations for protons cannot be achieved by treatment with acid. The silica-rich zeolites, mordenite and clinoptilolite are exceptions to this, "hydrogen" forms of these zeolites having been prepared by acid treatment[45,46].

Replacement of zeolite cations by protons is, in general, achieved by firstly exchanging with ammonium ions. Thermal treatment of the ammonium-exchanged zeolite at about 673 K liberates ammonia and leaves protons situated on oxygens in the lattice. The extent to which this decationisation can occur is dependent on the Si/Al ratio of the zeolite. A crystalline zeolite completely free of cations can be obtained by treating silica-rich Y zeolite in this manner but attempts to achieve complete hydrogen exchange of A and X result in structural collapse[47].

If temperatures higher than about 673 K are used to expel ammonia, water is lost from two nearby hydroxyl groups in a process termed dehydroxylation. The stability of a zeolite against dehydroxylation depends on the extent of decationisation[48], the decationised zeolites being less heat resistant than the sodium forms.

Decationisation has been shown by Uytterhoeven et al[48] and Ward[49] to result in the formation of structural hydroxyl groups which act as Brönsted acid centres. Dehydroxylation results in the loss of hydrogens and framework oxygen atoms as water with the consequent formation of tri-coordinated aluminium oxide Lewis acid sites[49].

## 2.5. Dehydration and Stability

Nuclear magnetic resonance provides information on the state of water molecules in hydrated zeolites. Water molecules in the larger zeolite cavities exhibit the same pattern as the isolated

liquid indicating that molecules in the centres of the large cavities do not occupy definite lattice sites. In smaller cavities, however, water is known to form hydrated complexes with the exchangeable cations[50]. The presence of water even in small amounts, has been shown to influence the cation distribution[51]. Mikheikin et al[52,53] have reported the migration of $Cu^{2+}$ and $Cr^{3+}$ ions, from the large cavities of zeolite Y to the sodalite pores, on the removal of water. On rehydration the cations migrate back to the large cavities.

Most zeolites can be dehydrated to some extent (by heating and/or evacuation) without any major alteration to the crystal framework. Zeolites with monovalent cations normally dehydrate more readily than the multivalent forms for which the bonding in the hydrated complex is stronger. The dehydrated zeolites exhibit a high degree of thermal stability. A temperature of about 973 K is required to decompose the crystal structure of zeolite X although structural collapse occurs in the presence of water at lower temperatures[30]. It has also been shown that the stability of X and Y zeolites to water vapour depends on the Si/Al ratio[30] and on the nature and extent of cation exchange. Barrer and Bratt[54] found strontium- and cobalt-exchanged forms of zeolite X to be thermally less stable than other monovalent and divalent forms.

In 1967, McDaniel and Maher[55] reported a highly stable material obtained by calcining ammonium zeolite Y. The crystal structure of this material, termed 'ultrastable' faujasite is retained after heating to temperatures in excess of 1273 K. In a series of papers[56-60] Kerr has investigated the thermal and hydrothermal stabilities of sodium and hydrogen Y zeolites. He reported that removal of about one-third of the aluminium caused considerable enhancement of stability. Furthermore, he demonstrated that the atmosphere

surrounding the ammonium-exchanged zeolite during the thermal treatment altered the stability of the product[60]. Calcination conditions which impeded removal of gaseous products resulted in a product similar to the ultrastable faujasite of McDaniel and Maher[55]. The enhanced stability of ultrastable faujasites appears to be a consequence of the removal of aluminium from tetrahedral sites by hydrolysis at elevated temperatures.

The enhanced stability at high temperatures and under hydrothermal conditions is of considerable significance since these materials may be used as a foundation for preparing ultrastable zeolite catalysts.

## 2.6. Sorption and Diffusion

After dehydration the zeolite is a crystalline solid permeated by micropores. This intracrystalline pore system readily occludes and releases small molecules, the entire crystal adsorbing and desorbing on a large scale. The adsorption of a gas or vapour depends on the equilibrium pressure, the temperature, the nature of the gas or vapour and the nature of the pores within the zeolite crystal. When exposed to a gas or vapour, the zeolite cavities will adsorb readily until the pore volume is filled; such behaviour gives a rectangular-shaped adsorption isotherm.

The selective adsorption properties of chabazite were discovered in 1925 by Weigel and Steinhoff[61]. Water, ethanol and methanol were rapidly adsorbed by the zeolite whereas acetone, benzene and ether were excluded. To describe the phenomenon of selective adsorption McBain[62] originated the term "molecular sieve".

The molecular sieving phenomenon demonstrated by zeolites is caused by differences in size and/or shape between the pore apertures and the adsorbate molecules. The calculated molecular dimensions were originally based on the equilibrium diameter. This was found to be unsatisfactory and an improved treatment[63] utilised the collision or kinetic diameter. This was defined to be the distance of closest approach for two molecules colliding with zero initial kinetic energy. For long molecules, such as hydrocarbons, the critical dimension is the diameter of the smallest cylinder which may encompass the molecule when in its most favourable conformation. The van der Waals radii of the hydrogen atoms must be included. Values of the critical diameters of some molecules are listed in Table 2.2.

| Molecule | | Critical Diameter/nm |
|---|---|---|
| Methane | $CH_4$ | .408 |
| Ethane | $C_2H_6$ | .436 |
| Propane | $C_3H_8$ | .51 |
| Butane | $C_4H_{10}$ | .51 |
| Ethylene | $C_2H_4$ | .407 |
| Propene | $C_3H_6$ | .495 |
| Cyclopropane | $C_3H_6$ | .52 |
| But-1-ene | $C_4H_8$ | .495 |
| Trans But-2-ene | $C_4H_8$ | .495 |
| Cis But-2-ene | $C_4H_8$ | .558 |

Table 2.2. Critical Diameters of Some Hydrocarbons[64]

The pore apertures are bounded by oxygen atoms of connected tetrahedra and, to a first approximation, the limiting size of the pore aperture is governed by the size of the ring. In general these rings involve six, eight or twelve oxygen atoms. As the free diameters of the six-membered rings are too small(0.28 nm) to allow most molecules to pass through them, sorption in zeolites occurs primarily through the eight- and twelve-membered rings. These rings may assume various configurations according to the structure in which they occur[65]. Hence the free dimensions of the apertures and the molecular sieving character vary considerably from zeolite to zeolite.

The sorption properties of zeolites are strongly dependent on the nature and number of cations within the structure. In zeolite A, replacement of sodium ions by larger potassium ions effectively reduces the pore size, the reduction occurring gradually with increasing extent of potassium exchange[66]. In contrast calcium exchange for sodium increases the effective pore size so that molecules not normally adsorbed by zeolite A are reaily occluded in the calcium-enriched zeolite.

The mechanism by which a molecule passes through the aperture and enters a zeolite cavity is a very complex one. In addition to the structure of the molecule and the zeolite aperture, forces of attraction and repulsion between the molecules and zeolite framework atoms and cations are involved. These and other factors relating to the molecular seiving effect have been reviewed by Venuto and Landis[67].

Adsorption of a molecule with dimensions close to the diameter of the zeolite aperture requires additional energy to surmount the potential energy barrier. The deformation of a molecule containing

two or more atoms can, within narrow limits, allow the adsorption of a molecule somewhat larger than the aperture. Passage is assisted by thermal pulsation of the crystal lattice. At a certain characteristic temperature for an adsorbate the energy of the molecules is just sufficient to overcome the energy barrier. Below this temperature the material is not adsorbed.

The theoretical basis for zeolite diffusion is complex due to the existence of zeolite pores, the dimensions of which are close to those of the diffusing molecules. Since zeolite particles contain both a microporous and macroporous network either, or both, system(s) can control the diffusion rate under a given set of conditions. Intracrystalline diffusion was shown to be controlling for ethane on Linde 4A[68], both in powder and pellet form, whereas both types of diffusion were significant on Linde 5A[69].

True zeolitic diffusion occurs within the micropore structure. It depends strongly on the properties of the molecule, size and shape of the intracrystalline pore, pressure and temperature and on the chemical nature of the pore walls. One of the most striking characteristics of zeolitic diffusion is its strong dependence on temperature. It generally increases exponentially with temperature and can be expressed by the Arrhenius type of relationship,

$$D = D_* e^{-E/RT} \qquad \text{Eqn.2.1.}$$

where

D = Diffusivity

$D_*$ = Constant

E = Activation energy

T = Temperature

R = Gas constant.

Activation energies in the range 2 to 80 kJ $mol^{-1}$ have been reported[70].

A hydrocarbon molecule occluded within a zeolite cavity is in a region of low potential energy and has considerable freedom of movement within that cavity. Diffusion involves the passage of the occluded molecule through the windows between adjacent cavities. While passing through the windows the freedom of movement of the zeolites is severely constrained. There may also be an appreciable energy barrier due to repulsive forces.

Activated diffusion through the intracrystalline channels may be the rate controlling process in the adsorption of a gas by a zeolite. Under diffusion limiting conditions the process may be described by Eqn. 2.2.

$$Q_t - Q_o = Bt^{\frac{1}{2}} + C \qquad \text{Eqn. 2.2.}$$

where

$Q_t$ = Amount adsorbed at time t.

$Q_o$ = Amount adsorbed at t = o.

B and C are constants.

A plot of the amount adsorbed versus $t^{\frac{1}{2}}$ should yield a straight line, although a foot, resulting from rapid initial adsorption at the external surface, may occur near the start of the adsorption.

Since the process of adsorption involves the liberation of heat, the temperature within the zeolite may be substantially higher than the surroundings. These temperature effects were considered by Eagen et al[71] during adsorption of nitrogen on zeolite 4A and propane on zeolite 5A at 195 K. Increases of 15 K and 60 K respectively were recorded. However, in spite of these temperature differences, the observed rates of adsorption did not differ appreciably from the calculated isothermal case. This was attributed

to two compensating effects; as the temperature within the zeolite increases, decrease in sorption capacity is accompanied by an increase in diffusion rate.

The diffusion characteristics of zeolites are easily altered by ion exchange. Substitution of large cations in the lattice reduces diffusivity and may increase the diffusional activation energy. This has been demonstrated over several zeolites. In a study[72] of diffusivity of hydrocarbons in NaY and HY, faster rates of diffusion over HY were reported for all hydrocarbons except 2,4,6 trimethyl-aniline. The slow diffusion of this molecule was attributed to the strong acid-base interaction. Exchanged forms of mordenite exhibited a general trend of increasing diffusivity; Ca < K < Ba < Na < Li. This trend prompted Barrer and Brook[73] to suggest a role of cation deformability in determination of diffusivities.

Although the critical diameter of the adsorbate molecule is important in zeolitic diffusion other molecular parameters must be considered. All n-alkanes with more than three carbon atoms have the same critical diameter. Nevertheless, in zeolite A, diffusivity decreases and diffusional activation energy increases with increasing carbon number[64,74,75]. Diffusivities of n-alkanes in zeolite T were also demonstrated[76] to be dependent on hydrocarbon chain length but in a much more complex manner. A more detailed discussion may be found in Section 3.1.2.

Also of importance is the chemical nature of the diffusing molecule. Molecules possessing permanent dipoles diffuse more slowly through zeolites than non polar molecules of similar size and shape[73]. Interactions between dipoles and cations, present in the zeolite channels, lead to hindered diffusion and result in an increase in activation energy with the polarity of the molecule.

Similarly the presence of unsaturation in a molecule reduces the adsorption rate[77]. Rates of adsorption of 1-hexene and 2-octene in zeolite 5A are only about 1/20 those of the corresponding saturated molecules. This is a result of the greater ion-induced dipole interaction between the zeolite surface and the π-electrons of the double bond.

## 2.7. Surface Investigations

Structural hydroxyl groups are not included in the formal description of zeolite crystal structure. Hydroxyl groups are necessary to terminate the faces of a zeolite crystal at positions where bonding would normally occur with adjacent tetrahedral silicon or aluminium atoms within the crystal. In addition to these the surface may contain hydroxyl groups in place of the usual metal cations. The presence of these structural hydroxyl groups has been recognised for many years and their nature studied by infrared and nuclear magnetic resonance spectroscopy.

Investigations utilising infra-red spectroscopy have been the subject of reviews by Yates[78] and Ward[79]. For X and Y type zeolites, three infrared bands are usually observed. The highest frequency band has been assigned to silanol groups either terminating the zeolitic lattice or present in amorphous material. The other two bands have been attributed to protons bonded to framework oxygens at different geometrical locations in the zeolite supercages[49]. The latter hydroxyl groups have been suggested to arise from cation hydrolysis[80] or deammoniation[81]. Corresponding bands, observed in a study of ammonium exchanged erionite, were assigned in a similar manner[82]. The existence of two types of hydroxyl group on

H-mordenite has been demonstrated. The disappearance of the lower frequency group on dealuminisation prompted Eberly et al[83] to suggest its association with a structural feature of the mordenite induced by the alumina tetrahedra.

The nature of hydroxyl groups and the presence of Lewis acid sites on zeolites has been investigated using the infrared spectra of adsorbed molecules. Adsorption of pyridine has been used on many occasions to differentiate between Brönsted and Lewis acid sites. Using this technique three types of acidic sites were distinguished[84] on cation exchanged mordenite. Lewis sites, Brönsted sites and a third type which were attributed to a strong interaction between the cation and the pyridine molecule.

Hattori and Shiba[85] have reported the existence of different types of acidic sites on exchanged forms of zeolite X although only weak Lewis sites were reported on sodium X. In a subsequent study of X zeolites, Ward[86] demonstrated that the Brönsted acidity of calcium and magnesium exchanged X increased with the silica/alumina ratio of the zeolite. Ultra-violet spectroscopy of anthraquinone and triphenyl carbinol adsorbed on zeolites has also demonstrated the existence of protonic and aprotonic sites[87]. Both Brönsted and Lewis acid sites were evident on calcium exchanged X and on hydrogen forms of X and Y zeolites. An increase in proton donating properties of these zeolites on addition of small amounts of water was observed[88]. Zhandov and Kotov[89], using optical electron spectroscopy, showed that the concentrations of protonic and aprotonic sites in decationised faujasites were altered by thermal treatment at different temperatures.

Wu et al[90] have used infrared spectroscopy to investigate the organic transformations and associated structural changes during

thermal decomposition of a tetramethylammonium offretite. The infrared spectra revealed that lattice associated hydroxyl groups, confirmed as protonic in nature by their interaction with ammonia, were generated from the tetramethylammonium cations. Dissimilarities in the environments of the hydroxyl groups were indicated by differences in their absorption frequencies. Differences in their retention of ammonia demonstrated a variation in acidic strength. Dehydroxylation occurred at approximately 773 K resulting in Lewis acid sites.

A comparison of the adsorption of pyridine and ammonia on H-clinoptilolite demonstrated the location of about ten per cent of the lattice hydroxyl groups on the external surface. Furthermore, Detreköy et al[91] were able to attribute catalytic activity of the zeolite to the external surface hydroxyls. In a similar study[92] over exchanged mordenites the active sites were located in the channels. Exchange with relatively large cations restrained the diffusion of pyridine to these sites.

Proton mobility of structural hydroxyl groups is necessary for their Brönsted acidity and for dehydroxylation of zeolites. Relaxation and line width studies[93,94] in nuclear magnetic resonance spectroscopy have been used to characterise proton mobility in zeolites.

Investigation of adsorbed species in connection with zeolite acidic properties has already been discussed. The nature of several other adsorbed species has been studied. An investigation of adsorption of benzene and toluene on a cobalt exchanged zeolite Y[95] revealed changes in the spectra from that of the liquid. These were attributed to the interaction of the cations and surface oxygens of the zeolite with the $\pi$-orbital of the benzene ring, orientated parallel to the internal surface. Eberly[96] reported loss of double

bond character when hex-1-ene was adsorbed on faujasites. Studies[97] of adsorption of butenes on a sodium hydrogen Y zeolite also showed the formation of a saturated species by reaction with a hydroxyl group. Ethylene formed no adsorbed species capable of detection[96]. $^{23}Na$ nuclear magnetic resonance spectroscopy of small molecules adsorbed on an A type zeolite, demonstrated that the eight-membered rings were the preferential centres of adsorption[98].

The presence of reactive intermediates on zeolites has been investigated by electron spin resonance techniques. Hirschler et al[99] reported that benzene, methyl-substituted benzenes and alkenes, adsorbed on cation exchanged X and Y zeolites, exhibited electron spin resonance signals. Similar signals were observed for benzene and its methyl-substituted derivatives adsorbed on hydrogen mordenite[100]. In a further study[101] investigating the alkenes, 2,2 dimethyl but-2-ene and cyclopentene, the spectra observed were attributed to cation radicals.

## 2.8. Catalytic Properties

### 2.8.1 Catalysed Reactions

A large number of studies using zeolites as catalysts have been carried out. For many reactions, especially those of the carbonium ion type, the zeolites and amorphous silica aluminas have common properties. Activation energies of reactions with the two types of catalyst are similar and they respond to promoters and poisons in the same way[102]. Zeolites, however, demonstrate greatly enhanced activity for certain reactions when compared with amorphous silica alumina catalysts[103]. This enhanced activity may be explained in terms of a greater active site concentration[104], there being a greater number of highly acidic centres in zeolites than in silica

alumina catalysts[105]. The number and strength of acid sites in zeolites depends on the extent of cation exchange and the Si/Al ratio[105,106].

The catalytic behaviour of zeolite has been the subject of several reviews[67,107-110] and numerous papers. Zeolites catalyse a broad spectrum of reactions ranging from double bond isomerisation to fragmentation of benzene rings. Venuto[111] has listed some fifty important organic reactions in which zeolites exhibit some type of catalytic effect. It is impracticable to include all these reactions here and hence aspects of a few selected types will be considered.

a) Cracking Reactions

Many workers have studied the activity of zeolites for the catalytic cracking of n-alkanes and cumene. The results are summarised in a review by Rabo and Poutsma[112]. Activity is dependent on nature and extent of cation exchange. The most active catalysts are those which have been ion exchanged with a consequent reduction in their alkali metal content. Rare earth exchanged and hydrogen zeolites are more active than other cracking catalysts for the cracking of n-hexane[103].

Product patterns typical of acidic type catalysts have been reported[103,114] over multivalent cation exchanged forms. Hydrocarbon cracking is generally accepted as passing through a carbonium ion intermediate. The necessity of protons was demonstrated by Benesi[115] who showed that removal of hydroxyl groups, by activation at progressively higher temperatures, reduced the n-alkane cracking activity. Activity was restored by the readdition of water to the zeolite. Ward[49] confirmed the correlation between acidity pattern and Brönsted acid concentration.

Product patterns from n-alkane cracking reactions over alkali metal zeolites have been suggested to be indicative of a radical type mechanism[116]. From catalytic results of n-hexane cracking over lanthanum X zeolites, Aldridge et al[117] proposed that both carbonium ion and radical type mechanisms could occur concurrently, the relative importance of these depending on pretreatment and exchange. A completely exchanged lanthanum X outgassed at less than 770 K uses the former and sodium X and a sixty per cent exchanged lanthanum X the latter. A product pattern between these two extremes was observed with a seventy eight per cent exchanged zeolite although the radical type mechanism was approached as the outgassing temperature was increased. A similar trend with outgassing temperature was observed for the completely exchanged lanthanum X zeolite.

b) Alkene Forming Eliminations

Alkene forming eliminations are among the most characteristic reactions observed over zeolite catalysts. The alkene is formed by loss of a proton from one of two adjacent carbon atoms in a ring or chain and loss of a nucleophile from the other.

The dehydration of alcohols over zeolites has been extensively studied. The reaction rate and selectivity of dehydration are strongly influenced by zeolite type and the nature of the exchanged cation[118]. The water produced influences zeolite cations and promotes carbonium ion type mechanisms. The activity of calcium X for tertiary butanol dehydration increased after pretreatment of the catalyst with small amounts of water[119]. A study[120] of the elimination reactions of 1-chlorobutane and 2-chlorobutane over X zeolites revealed a nearly linear relationship between the strength of the electrostatic field of the cation in the cages and the activity.

For divalent exchanged zeolites the eliminations were found to occur by the carbonium ion (E1) type mechanism. This is a two step mechanism involving initial fission of the carbon-chlorine bond forming an intermediate carbonium ion. Over sodium X zeolite the concerted (E2) mechanism was preferred although a change to E1 was observed with increasing temperature. The mechanism operative depends on the relative strengths of interaction between reactant and catalyst.

For many zeolite catalyst systems the substrate reactivity parallels the increasing stability of the carbonium ion formed by loss of the nucleophile; tertiary alcohols react faster than secondary alcohols which react faster than primary alcohols. Polar or ionic intermediates are generally considered to be involved in reactions of this type. It has been suggested[67] that the function of the zeolite is to give assistance to the ionisation or heterolytic bond cleavage in the adsorbed substrate (alcohol or halide). The nucleophile is rendered a better leaving group by interaction with protons in hydrogen zeolites, metal cation fields, lattice defect sites or other electron deficient sites.

c) Reactions of Alkenes

Zeolite catalysed reactions of alkenes include double bond and cis-trans isomerisation, polymerisation and isotopic exchange. Activity is again dependent on the nature and extent of cation exchange. Sodium X is relatively inactive for the isomerization of butene but an increased activity is noted following cation exchange[121-123]. For most zeolites studied, products were indicative of a carbonium ion type mechanism although a radical type mechanism was suggested over copper[123] and nickel[124] exchanged zeolites.

A correlation has been observed between Brönsted acid site concentration and o-xylene isomeriation activity over exchanged forms of zeolite Y[104,125]. The isomerisation of cyclopropane over sodium and ammonium Y zeolites has also been related to Brönsted acidity[126].

Cis-trans isomerisation was enhanced relative to double bond shift when the calcium ion content (acidity) of zeolites was increased[127]. The loading of zeolites with alkali metals has been reported[107] to produce catalysts which are active for double bond shift but inactive for skeletal isomerisation.

The isomerisations of butene and cyclopropane over zeolites are discussed more fully in Sections 4.1.3 and 4.2.4.

Investigation of olefin polymerisation over synthetic zeolites X and A revealed the following order of olefin reactivities; isobutene > propene >ethylene[128]. The calcium exchanged zeolite exhibited a higher activity than the sodium form. Products observed were consistent with those predicted from an acid catalysed polymerisation. The presence of branched chain alkenes as products over all active catalysts prompted Norton to suggest, from size considerations, that at least the majority of reactions over sodium and calcium A zeolites must occur outside the pores.

The reaction of ethylene over rare earth exchanged zeolites at 486 K produced only low molecular weight alkanes as gaseous products although a complex mixture of alkylated aromatics was found to be trapped within the pores. Venuto et al[129] suggested the occurrence of a complex series of transformations initially involving the acid catalysed polymerisation of ethylene to low molecular weight aliphatic polymers. Subsequent intermolecular hydrogen transfer and dehydrogenation-cyclisation reactions, accompanied by skeletal isomerisation, result in the observed products. Decreasing

activity with time of a nickel exchanged zeolite for ethylene polymerisation was attributed to the formation of a similar intracrystalline polymeric material[67].

Occluded polyalkenes, as large as $C_{30}H_{60}$, are formed from isomerisation and polymerisation reactions of hex-1-ene over rare earth exchanged X zeolites at 333 K[129]. Addition of deuterium oxide to these catalysts, followed by mass spectroscopic analysis, indicated that substantial transfer of deuterium, from catalyst deuteroxy groups to the alkene, had occurred. A carbonium ion type mechanism was proposed. An infrared investigation[96] of the transformations of hex-1-ene over HY zeolite demonstrated the initiation of polymerisation and dehydrogenation processes at 423 K to form a conjugated polyene. Upon heating to 533 K cyclisation occurs resulting in an unsaturated ring structure.

A study of reactions of low molecular weight alkenes over a deuterated decationised Y zeolite revealed that no exchange with ethylene occurred at low temperatures[130]. The observed exchange between deuterated ethylene and catalyst hydroxyl groups above 423 K was suggestive of the involvement of a primary carbonium ion-like species i.e. $CD_2H\text{-}CD_2^{\oplus}$. The occurrence of isotopic exchange and polymerisation of propene at room temperature is in agreement with this type of mechanism.

d) Hydrogenation, Dehydrogenation and Related Reactions

Most crystalline aluminosilicates have very little intrinsic catalytic activity for hydrogenation/dehydrogenation type reactions. Metal loaded zeolites, prepared by ion exchange and subsequent reduction in situ, have been reported to catalyse hydrogenation[131], hydroisomerisation[132] and hydrocracking reactions[133-135].

Correlation of the catalytic activity with the metal surface was demonstrated by Penchev et al[135] who concluded that the zeolite aluminosilicate framework mainly influenced the formation of the metal surface which determined the activity.

Sodium and calcium X zeolites exhibited little activity for dehydrogenation of n-alkanes. Moderate activity was observed over nickel, cobalt, iron or chromium exchanged zeolites[136]. Enhanced activity for dehydrogenation of alkenes to dienes is shown by zinc and cobalt exchanged zeolites in the presence of ammonia. The large excess of ammonia has been suggested to partially poison acid sites and thus inhibit coke formation.

Many other reactions are known to be catalysed by zeolites including condensation and cyclisation, acetal and ketal formation, epoxide transformations, electrophilic aromatic substitution, Beckmann re-arrangement and amination reactions.

### 2.8.2 Shape Selective Catalysis

Molecular shape selective catalysis by zeolites was first recognised in 1960[114]. By contrasting the behaviour of small pore sodium and calcium A zeolites with corresponding forms of zeolite X, Weisz et al[131] were able to demonstrate both reactant and product selectivity. Reactant selectivity occurs when entry to the zeolite cavities is afforded to one class of reactant molecules and denied to another on the basis of molecular shape and dimensions. Product selectivity is observed when, among all the products formed within the cavities, only those with the proper dimensions can diffuse through the windows and appear as products. Bulky molecules, if formed, are either converted to smaller molecules or they eventually deactivate the catalyst by blocking the pores. A third type of shape

selectivity, restricted transition-state selectivity, occurs when certain reactions are prevented because the corresponding transition state would require more space than is available in the cavities. Neither reactant nor potential product are prevented from diffusing through the pores and reactions which proceed through less bulky transition states occur without hindrance.

Reactant and product shape selectivity can be predicted by comparison of the molecular dimensions with the pore window diameter. It is controlled by the same factors as selective sorption. Diffusion is a very important factor in shape selective catalysis. In general one type of molecule will react preferentially in a shape selective zeolite if its diffusivity is at least one or two orders of magnitude higher than that of competing molecular types. The diffusivity of molecules completely excluded from the zeolite pores is zero. Catalytically active sites are present both in the internal pore structure and on the external surface in a ratio of about 100 : 1. Internal diffusion could make the interior sites less effective resulting in catalysis by the non shape selective external sites becoming much more important than warranted by their small number.

Many examples of product and reactant selectivity have been demonstrated with erionite, mordenite and zeolite A. Zeolite CaA[131] and erionite[103] have pores large enough to enable n-alkanes, but not branched alkanes, to pass through. Hence both these zeolites demonstrate selective cracking of n-alkanes in the presence of branched alkanes, the products containing essentially no branched hydrocarbons. Chen and Weisz[137] have extended shape selectivity to distinguish between trans and cis alkenes. At 371 K the hydrogenation rate constant of trans but-2-ene over a platinum-containing

calcium A zeolite is seven times that of cis but-2-ene.

Cation exchange may alter the shape selective characteristics of zeolites. Yashima and Hara[138] have shown that toluene disproportionates and o-xylene isomerises readily over H-mordenite and Be-mordenite but only very slowly over Ca- or Ce- mordenites. The large calcium and cerium cations reduce the effective pore radii and hinder the diffusion of the toluene or xylene molecules. The pores are even more restricted in Na-mordenite. Chen and Weisz[137] used this property to hydrogenate ethylene selectively in the presence of propene as only ethane was able to escape from the pores.

### 2.8.3 Mechanism of Zeolite Catalysis

The majority of reactions over zeolites are thought to involve a carbonium ion intermediate. However, a number of theories regarding the nature of active sites over zeolites have been proposed. Ward[49] demonstrated the existence of both Brönsted and Lewis sites and concluded that the acidic hydroxyl groups were the active sites. Turkevich et al[139] observed a corrleation between catalytic activity and Lewis acid site concentration and proposed that the tri-coordinated aluminium atoms were the active sites. The cations were considered to be the active sites by Pickert et al[140]. They postulated that the electrostatic fields, set up by the cations, polarised the hydrocarbon molecule to a carbonium ion-like species. Current thinking, however generally attributes the catalytic activity of zeolites to their Brönsted acid sites, the hydroxyl groups. Correlation between catalytic activity and surface hydroxyl groups has been established in a number of studies[49,91,141]. The large number of possible environments for the hydroxyl group leads to a wide distribution in zeolite acid strength. Only a small number of the hydroxyl groups are sufficiently

acidic to be active in catalysis as demonstrated in a study of cumene cracking over a deammoniated ammonium exchanged Y zeolite[141]. In a further publication[142], Jacobs et al reported that sites of different acid strength were required for the disproportionation of toluene and the cracking of cumene.

The catalytic activity depends markedly on the nature and location of the cation. Ward[143] found the catalytic activity of a series of exchanged zeolites to be a function of the calculated electrostatic field. He concluded that the polarity of the acid site and hence the acidity of the hydroxyl group is influenced by the cations. Other workers[144], studying the reactions of chlorobenzene and benzaldehyde with ammonia, established a correlation between the catalytic activity and the electronegativity or amine complex formation constant of the cation.

Very few examples of zeolite catalysis are known which imply basic sites. Nevertheless, basic centres have been suggested[145] in the alkylation of toluene with methanol and formaldehyde over X and Y zeolites. Although the alkylation of the benzene ring exhibited acid catalysed characteristics, the side chain reaction was depressed by addition of an acidic reagent and unaffected by aniline. The ring and side chain reactions were suggested to depend on the catalyst acidity and basicity respectively. Basic sites have also been implied[146] in the dehydrogenation of 2-propanol over potassium, rubidium and caesium exchanged zeolites. This reaction was poisoned by addition of phenol whereas the dehydration reaction observed over all alkali cation exchanged zeolites was poisoned by addition of pyridine. Potassium, rubidium and caesium exchanged X zeolites were endowed with acidic and basic sites.

The complexity of zeolite catalysis has been succinctly summarised by Smith[147]; "Catalysis by zeolite molecular sieves can be regarded as the combined effect of electrostatic fields, reversible proton and electron transfer and both spatial and temporal factors. All of these contribute to the combined processes of chemisorption and bond weakening which constitute the heart of heterogeneous catalysis".

# CHAPTER 3

## Erionite and Zeolite Omega

The work in this thesis is concerned specifically with the zeolites erionite and omega (Ω). The structure and properties of these zeolites are discussed in the following sections.

### 3.1. Erionite

#### 3.1.1. Structure

Erionite, a fibrous zeolite was discovered in Oregon in 1898[148]. The crinkly, white appearance of the mineral fibres led to the derivation of the name erionite from the Greek word for wool. Several other occurrences of the mineral have since been reported[149,150].

The aluminosilicate framework structure of erionite, as proposed by Staples and Gard[151], is illustrated schematically in Fig. 3.1.1.a. The hexagonal lattice is composed of columnar arrays of cancrinite cages linked top and bottom by double six-ring units. Rotation of alternate cancrinite units by $60^{\circ}$ gives an ACBCAC sequence to the structure. The elongated erionite cavities, having a free length of 1.30 nm and a free diameter of 0.63 nm at the mid-girth pinch, are stacked along the c-direction. Each erionite cavity is enclosed by six eight-membered rings (B,C), two planar six-membered rings (A,A'), three assymmetrix six-membered rings (D) and twelve four-membered rings (E). (Fig. 3.1.2.a.)

Direct movement of molecules through the erionite cavities in the c-direction is impossible because of the small free diameter (0.25 nm) of the six-membered rings at the top and bottom of each cavity. Diffusion, however, can occur through the eight-membered ring windows, the stereochemistry and free dimensions of which are shown in Figs. 3.1.2.b and c. These rings are common to two

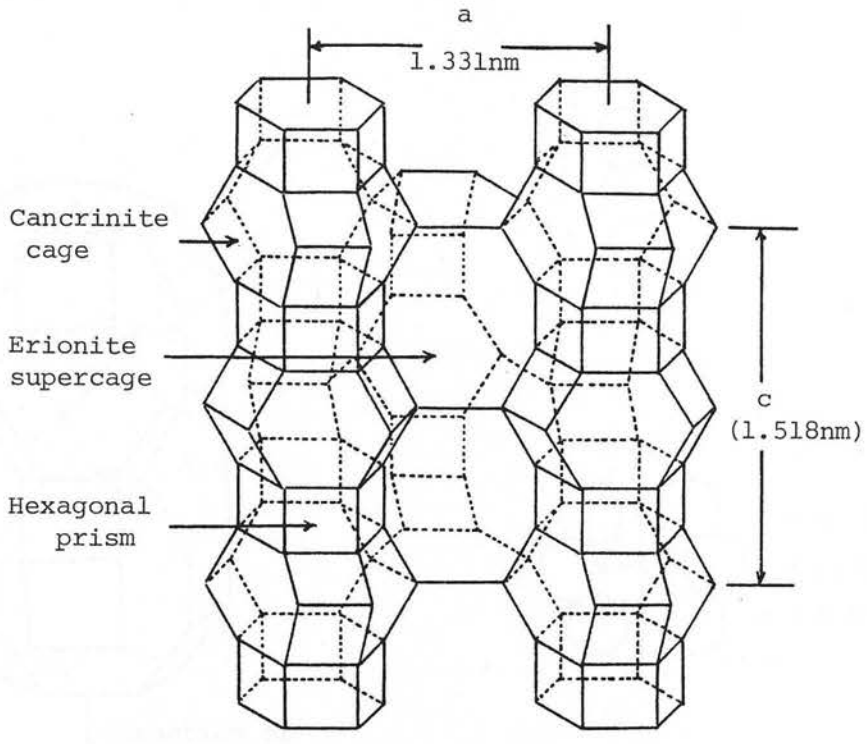


Fig. 3.1.1. (a) Line drawing of erionite showing the crystallographic parameters

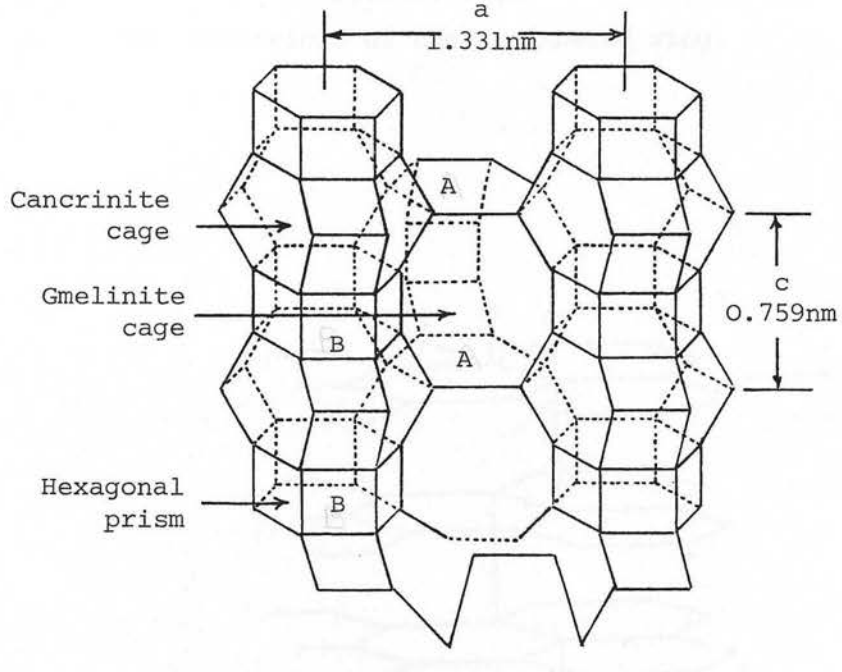


Fig. 3.1.1. (b) Line drawing of offretite. Stacking sequence is indicated by capital letters

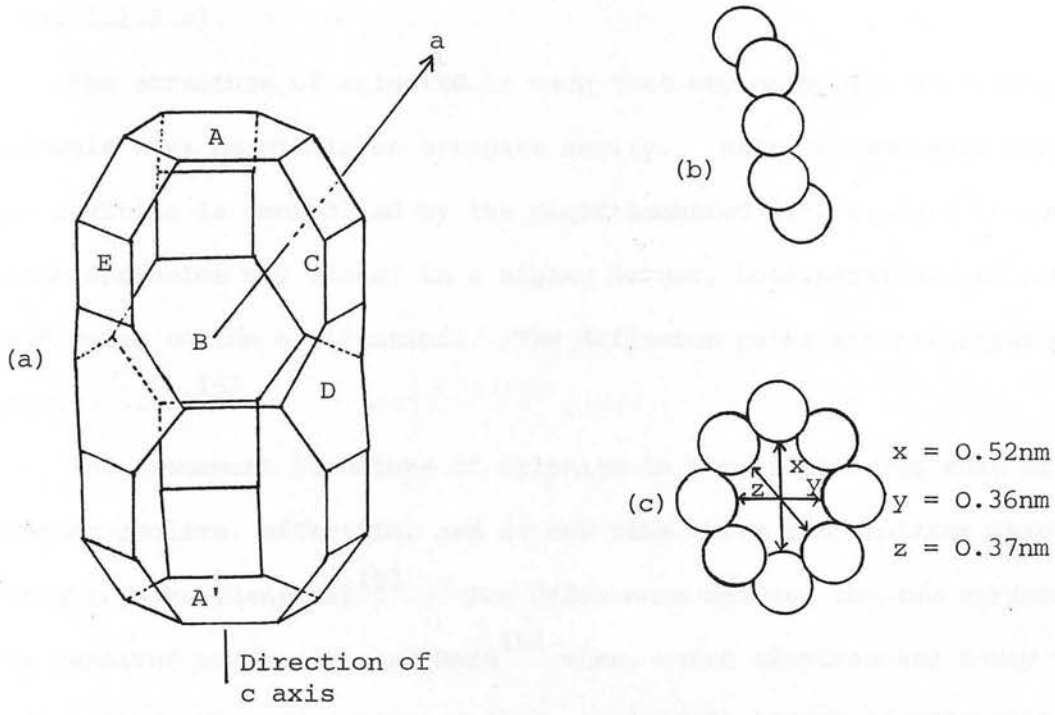


Fig. 3.1.2. (a) An erionite cavity (Al and Si atoms occupy each corner but oxygen atoms are not shown)

(b) Stereochemistry of an 8-membered ring of an erionite cage

(c) Dimensions of the 8-membered ring.

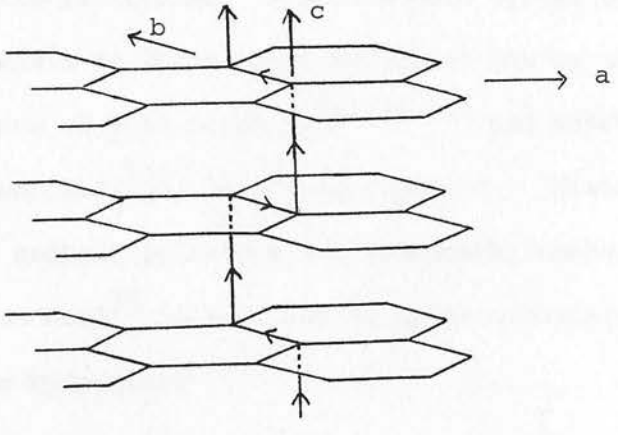


Fig. 3.1.3. The arrangement of diffusion paths in erionite showing the way in which the molecules may move along the c-direction and normal to it.[152]

erionite cavities and result in the formation of a long column of windows spaced about 0.7 nm apart and angled at 30° to the a-axis. (Fig. 3.1.2.a).

The structure of erionite is such that any part of a diffusing molecule must be within an erionite cavity. Entry to and exit from the cavities is controlled by the eight-membered ring windows through which diffusion may occur, in a zigzag manner, both parallel and perpendicular to the c-direction. The diffusion paths are illustrated in Fig. 3.1.3[152].

The framework structure of erionite is very similar to that of another zeolite, offretite, and at one time these two zeolites were thought to be identical[153]. The difference between the two structures was resolved by Bennett and Gard[154] when, using electron and X-ray diffraction, they demonstrated that a unit cell length of offretite was half that of erionite. Both zeolites are composed of the same secondary building units. The difference in unit cell length arises as a consequence of the uniform stacking of the cancrinite units giving an ABABAB sequence to the structure, as illustrated in Fig. 3.1.1.b. This results in the formation of large channels, of free diameter 0.63 nm, parallel to the c-axis, permitting the sorption of larger molecules than is possible in the erionite structure. A second pore system composed of the gmelinite cages exists in which small molecules can be sorbed.

Synthetic preparations of both erionite[35,133,155] and offretite[35] and their intergrowth, zeolite T[156], have been reported. Mixed based systems containing sodium, potassium and tetramethylammonium (TMA) hydroxides have been used[35] in addition to systems containing only sodium and potassium hydroxides[133,155].

Analyses of specimens of natural erionite have revealed a complex chemical composition, variable even within a single deposit[157]. In addition to sodium, appreciable amounts of potassium and calcium ions together with small amounts of magnesium, iron, titanium and calcium ions have been detected. Sheppard and Gude[157] found rather more than two potassium ions per unit cell in all but one of eleven samples analysed. Analysis[158] of an erionite from Rome, Oregon, indicated iron substitution for up to fifteen per cent of the framework aluminium.

Cation exchange studies[158,159] performed on natural erionite have indicated that two potassium ions per unit cell are not exchangeable at temperatures below 573 K and that their removal at higher temperatures results in a partial disruption of the framework structure. These potassium ions must be located within the lattice in positions such that they are unable to move during ion exchange. Using X-ray diffraction Kawahara and Curien[160] located a cation in each cancrinite cage. The identification of these cations as unexchangeable potassium ions was reported by Gard and Tait[161]. Although the position of the other cations is uncertain, various sites within the erionite cavity have been proposed incorporating bonding to both water and framework oxygens.

The presence of an unexchangeable potassium ion in each cancrinite cage of natural offretite has also been demonstrated[161]. Magnesium ions have been located in the gmelinite cages and calcium ions in the wide channels. The hexagonal prisms of offretite contain some calcium ions whereas in erionite they appear to be empty.

An exchange study[35] of synthetic erionite revealed that three tetramethylammonium (TMA) ions per unit cell did not exchange at 353 K. These must be located in the erionite 23-hedral cages since the structure has no other cavity large enough to accommodate them.

One unexchangeable TMA ion per unit cell was located in the gmelinite cages of synthetic offretite[35,162].

The templating action of tetramethylammonium (TMA) and potassium ions in the synthesis of these zeolites has been suggested[35]. As precursors to crystallisation gmelinite and erionite cages collect round TMA ions and cancrinite cages round potassium ions. The zeolite framework is subsequently formed by condensation of these units.

An infrared investigation of ammonium exchanged erionite[82] revealed that calcination at 673 K for one hour removed all the water but temperatures of about 873 K had to be employed to remove ammonia. This contrasts with ammonium exchanged Y zeolite where the ammonium bands were removed at 653 K[49]. Erionite also exhibits a higher thermal stability to dehydroxylation than the Y zeolite. The hydroxyl bands observed have been assigned to a siliceous impurity and to hydroxyls on two crystallographically different oxygens, one group pointing towards the large channel, the other pointing to the inside of a six-ring.

### 3.1.2. Sorption and Diffusion

The sorption and diffusion of various hydrocarbons in erionite and zeolite T have been investigated[74,76,133,158,163,164]. Eberly[158] observed that the sorption properties of natural erionite were profoundly affected by ion exchange. Molecular sieving was exhibited by the original erionite in that n-alkanes were sorbed while branched and cyclic alkanes and aromatics were excluded. Exchange with potassium ions prevented even the sorption of n- alkanes whereas exchange with calcium ions permitted more n-alkanes to be sorbed. The larger potassium ions (0.133 nm for $K^+$, 0.095 nm for $Na^+$) decreased the

effective pore diameter while exchange with calcium reduced the total number of cations and opened up the channels. Hence erionites from various natural deposits would be expected to exhibit different sorption properties dependent on their chemical composition.

In a comparison of n-hexane sorption on natural and synthetic erionites Robson et al[133] demonstrated considerable differences in rate. The higher rate observed on the synthetic zeolite was attributed to intergrowths of offretite in the erionite crystals allowing more rapid distribution of sorbate.

The sorption of $C_5$-$C_8$ n-alkanes in erionite has been reported to decrease with increasing molecular weight[163]. Sorption was not completely reversible and the desorption rate was slower than that of sorption, the rates of desorption of n-heptane and n-octane being virtually imperceptible. In a comparative study of diffusion in natural erionite and synthetic zeolite A, the diffusional activation energy of ethane in erionite was greater than in zeolite A whereas for ethylene the two values were approximately the same. This was explained qualitatively by the difference in shape of the windows. The planar ethylene molecule can pass through the oval erionite window with about the same ease as through the symmetrical A window but the smaller erionite window offers greater resistance to the three-dimensional ethane molecule. This theory has been substantiated by Barrer and Peterson[164] who investigated the role of aperture size in chabazite, erionite and calcium A by calculating the interaction energy between the eight-membered ring windows and an n-alkane chain. Erionite was shown to have the greatest interaction energy and calcium A the smallest. The variation in interaction energy with changes in oxygen positions of the ring, as caused by alteration of the Si/Al ratio, was also demonstrated.

A study of the diffusion of n-alkanes in zeolite T revealed an interesting and complex variation of diffusivity with hydrocarbon chain length[76]. N-octane diffused much more slowly than either shorter ($C_2$-$C_7$) or longer ($C_9$-$C_{14}$) n-alkanes and n-dodecane demonstrated the maximum diffusity of any of the n-alkanes excepting ethane. The authors attributed this diffusivity pattern to the "window effect"[103]. The length of the n-octane molecule is such that it will just fit in the erionite cage when orientated along the c-direction. Molecules larger than n-octane must assume a configuration with part of the molecule extending through an eight-membered ring. This is considered to result in a partial surmounting of the energy barrier. There is also increased mobility due to partial orientation of the molecule in the direction required for migration (the a-direction). A diffusivity maximum is obtained at n-dodecane because the length of this molecule is such that it can just extend to the extremes of the two eight-membered rings defining the unit cell. This results in the total orientation of the molecule in the direction of migration.

A recent investigation[165] of the chromatographic properties of erionite revealed a pronounced effect of the cation on the separation of a mixture of methane, ethane, ethylene and propane. Although propane and ethylene are not separated by the natural erionite, sodium enrichment or lithium exchange improves the separation properties. The order of elution is methane, ethane, ethylene, propane. On the potassium enriched erionite, however, propane is eluted before the other hydrocarbons. This has been attributed to a decrease in the size of the apertures brought about by the relatively large potassium ions forcing propane to diffuse along the outside surface of the erionite.

3.1.3. Catalytic Properties

Studies of the catalytic properties of erionite have been more or less confined to cracking and hydrocracking reactions. The shape selective nature of the zeolite was demonstrated in a study of cracking of n-hexane, 2 methyl pentane and methylcyclopentane over a hydrogen form[103]. High cracking activity was observed for n-hexane but very low activity for the other isomers. The products obtained from n-hexane were consistent with the operation of a carbonium ion mechanism but, contrary to the majority of zeolites, only straight chain hydrocarbons were formed. Any branched molecules produced within the intracrystalline structure would be unable to pass out through the pores into the bulk phase.

A further publication[166] reported the cracking of n-alkanes of various chain lengths over erionite. An unusual product distribution compared to that over wide pore zeolites such as zeolite X was observed. The product pattern for the cracking of n-docosane ($_nC_{22}H_{46}$) exhibited peaks at $C_{11}$, $C_6$ and $C_{3-4}$ while hydrocarbons in the carbon number ranges $C_1$-$C_2$, $C_7$-$C_9$ and $>C_{12}$ were absent. Similar patterns were observed for the other n-alkanes. In explanation of these results the authors suggested the existence of the "window effect", a phenomenon caused by the relative dimensions of cages and sorbed reacting molecules. In erionite the apertures controlling passage into or out of the erionite cages are the eight-membered ring windows at a distance of 1.54 nm or 1.82 nm apart, depending on whether the terminal oxygens are included or not. The lengths of $C_{10}$-$C_{12}$ molecules (1.53 nm, 1.66 nm and 1.79 nm) nearly equals this distance enabling these fragments to bridge across two windows and consequently to preferentially pass through the crystal unchanged. Fragments in the $C_7$-$C_9$ range undergo secondary reactions and do not appear as products. Chen and Garwood[134] observed a similar

pattern for hydrocracking rates of various n-alkanes over a dual functional erionite catalyst. The plot of relative rate constants against carbon chain length exhibited two maxima, at $C_6$ and at $C_{10}$-$C_{11}$ respectively, and a minimum at $C_8$.

The diffusivity maximum at $C_{12}$ and minimum at $C_8$, reported by Gorring[76] over zeolite T, correspond well with these catalytic data. It can therefore be concluded that the diffusivities of the n-alkanes in erionite determine the reaction rates and the product patterns of cracking and hydrocracking reactions. Long chain hydrocarbons are initially cracked to a mixture of shorter chain hydrocarbons similar to that over large pore zeolites. As a consequence of the erionite structure n-$C_7$,-$C_8$ and -$C_9$ are effectively trapped in the cages. As they diffuse more slowly than shorter or longer product molecules they spend more time within the zeolite and hence react further to $C_3$ and $C_4$ fragments. N-$C_{11}$ and n-$C_{12}$ diffuse out of the erionite rapidly and hence escape secondary reaction.

Diffusion control of reactions may be revealed by comparison of activation energies. From diffusion and reaction analysis the observed activation energy is expected to be one-half the sum of the activation energy for the reaction and that for diffusion. In normal catalysts the activation energy for diffusion is significantly lower than that for reaction and consequently the observed activation energy may be approximated to one-half that of reaction. Hence an apparent activation energy of 60 kJ $mol^{-1}$ for n-hexane cracking over H-erionite compared to that of 120 kJ $mol^{-1}$ over silica alumina catalysts was considered to be indicative of a diffusion limited reaction over H-erionite[103]. Furthermore, over H-erionite, the apparent activation energy for n-hexane cracking is about one-half that for 2-methyl pentane[167]. Chen suggested that the intracrystalline reaction was

diffusion controlled and that the small amount of cracking of 2-methyl pentane occurred on the external surface. These arguments indicating diffusion control must be used with caution in zeolite systems where the activation energy of counterdiffusion may be quite high. For example, if the activation energy for counterdiffusion were 80 kJ $mol^{-1}$, compared to 10 kJ $mol^{-1}$ for diffusion, and 120 kJ $mol^{-1}$ for reaction, the observed activation energy would be $(80 + 120)/2 = 100$ kJ $mol^{-1}$, not 65. Therefore when activation energies for counterdiffusion are high the one-half argument is invalid.

Recently, Rollman[168] has investigated the behaviour of common acid zeolites using a five component mixture. The shape selective zeolites examined, erionite and ferrierite, exhibited low coking and aging tendencies in comparison with the wide pore zeolites. It was suggested that this was a consequence of the inability of the cycloalkane coke precursor to form within the restricted pore system of the shape selective zeolites.

The treatment of both natural and synthetic erionites to yield improved catalysts has been the subject of several patents. Chen et al[169] claim to have produced a zeolite with improved shape selective properties by treatment of an erionite-type zeolite with sulphur or a sulphur-containing compound, followed by aqueous exchange with a Group VIII transition metal. Other workers[170] have patented a method of reducing the potassium content and hence increasing the cracking activity of erionite by calcination followed by ion exchange. Calcination apparently causes the removal of potassium from the small cages by migration of calcium within the crystal. Subsequent ion exchange removes the potassium ions from the large cages. According to the authors reduction in potassium content does not detrimentally affect the structure of the crystal lattice and a

hydrogenation-dehydrogenation component may be incorporated to yield a useful dual functional catalyst. Activation of erionite by ammonium exchange and steam calcination results[171] in catalysts active for hydrocracking reactions in the presence of a hydrogen atmosphere but in the absence of any hydrogenating component.

H-erionite prepared from a natural erionite has recently been used in conjunction with rare-earth exchanged HY zeolite in the preparation of a highly active, selective and stable hydrocarbon conversion catalyst[172]. Improved activity and selectivity compared to rare-earth exchanged Y zeolites were demonstrated.

## 3.2. Zeolite Omega

Zeolite omega (Ω) is a synthetic molecular sieve with, as yet, no known natural analogue.

### 3.2.1 Structure

The structure of the aluminosilicate framework of zeolite Ω, as proposed by Barrer and Villiger[173] from X-ray powder data, is illustrated in Fig. 3.2.1. The hexagonal type structure is composed of gmelinite cages (14-hedra) linked both laterally and longitudinally. Small cavities are produced by the lateral joining of these units by oxygen bridges. Longitudinal linkage occurs by sharing six-membered ring faces and results in the formation of long columns of gmelinite cages parallel to the c-axis. The lateral joining of six such columns leads to the formation of the main channels, running parallel to the c-axis and circumscribed by 12-membered ring windows. (Fig.3.2.2.). The free diameter of these channels (∿0.75 nm) is such that large molecules like cyclohexane are readily sorbed. A second two-dimensional channel system, running in planes perpendicular to the

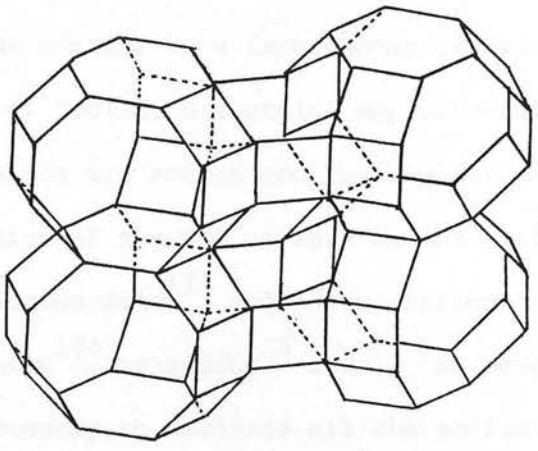

Fig. 3.2.1. Framework structure of zeolite Ω (Al or Si is positioned at each corner and oxygens lie about halfway between adjacent corners).

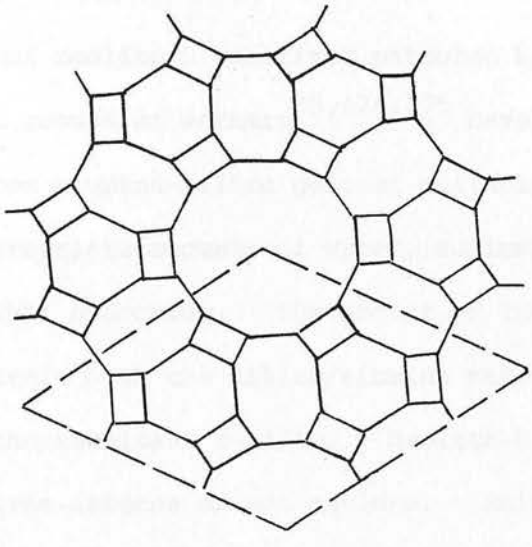

Fig. 3.2.2. Projection of the structure of zeolite Ω in the plane normal to the c axis showing the linking of 6 gmelinite cages to form the wide central channel.

c-axis, is formed by linkage of the gmelinite cages through distorted 8-membered rings. Access to this system is only possible at the surface and there is no easy passage from any of these layers of channels, normal to the c-axis, to a layer above or below.

A typical sample of zeolite Ω contains approximately eight cations per unit cell of which six are sodium and two are tetramethylammonium (TMA) cations. Location of the TMA cations in the gmelinite cages was postulated from diffraction data[173] and later confirmed by their inability to exchange with ammonium[174] or sodium[35] ions. As several exchanges with ammonium ions were necessary to exchange all the sodium ions it was concluded that these ions were not located in the main channels as this would facilitate easy exchange. Sites in the gmelinite cages or in the small cavities between them have been suggested.

### 3.2.2. Synthesis

The synthesis of zeolite Ω was first patented by Flanigen and Kellberg[175]. Several groups of workers[35,174,176] have since reported its crystallisation from alumina-silica gels of suitable composition in the presence of appropriate amounts of water, sodium hydroxide and tetramethylammonium (TMA) hydroxide. The amount of TMA ions present in the parent gel controls both the silica/alumina ratio and the proportion of TMA in the resultant zeolite. Zeolite Ω has not, as yet, been prepared in the absence of TMA cations. Suitable gel cation fractions of TMA (0.05-0.25) result in silica alumina ratios between 6.9 and 7.9 and a TMA cation content of 1.55 to 2.05 per unit cell. The maximum number of about two TMA ions per unit cell indicates a strong selectivity of those ions for the gmelinite cages, only a small fraction being located in the main channels. This fact, together with

the inability of zeolite Ω to form in the absence of TMA cations, suggests a templating action of these ions in the crystallisation of zeolite Ω. Other small ions, such as sodium, which occupy the smaller cavities are necessary to neutralise the charge and allow zeolitisation to proceed.

3.2.3. Pyrolysis

Evidence for two different TMA cationic sites in zeolite Ω was acquired from a pyrolytic study[174]. Differential thermal analysis and differential thermogravimetric analysis of zeolite Ω indicated that decomposition of the TMA cations occurred at two different temperatures. Furthermore the vacuum pyrolysis products at these temperatures were indicative of TMA cations in both restricted (gmelinite cages) and unrestricted (main channels) locations. The major products of pyrolysis at the lower temperature are methanol and trimethylamine corresponding to decomposition of TMA ions in the non-restricted main channel. These decomposition products are unable to escape from the gmelinite cages and must undergo further degradations until small molecules have formed which can escape by activated diffusion. These high temperature pyrolysis products include hydrogen, methane, carbon monoxide, acetylene and ethylene. The small amount of oxygenated product detected was attributed to some dehydroxylation of the framework. The TMA cations in the gmelinite cages can only be removed by thermal treatment at 773-873 K both in oxidising and inert environments. Using X-ray diffraction, Aiello and Barrer[35] reported zeolite Ω to be stable to about 973 K at which temperature the structure collapsed to an amorphous product. Cole and Kouwenhoven[174], using the same technique, detected a loss of crystallinity between 1023 and 1083 K.

Calcination of ammonium exchanged TMA Ω resulted in decomposition of both ammonium and TMA cations[176]. Differential thermal analysis and differential thermogravimetric analysis indicated overlap between cation loss and dehydroxylation. Infrared spectroscopy and X-ray diffraction patterns of samples calcined in air at different temperatures, showed that although the intensity of zeolitic hydroxyl groups was greatest at 873 K the zeolite appeared amorphous at that temperature. Weeks et al[176] concluded that loss of TMA cations apparently results in crystal collapse prior to dehydroxylation. The stability of the ammonium exchanged zeolite Ω appeared to be less than the original sodium zeolite.

The decomposition products of TMA cations in TMA-Ω[174] and TMA-offretite[90] have been analysed and reaction pathways postulated[90]. In both zeolites most of the TMA cations are encapsulated and must be broken down into smaller fragments before they can be removed. Studies over TMA-offretite[90] demonstrated the role of the TMA cation as a proton precursor, hydroxyl groups being generated as a direct consequence of the TMA cation decomposition. These hydroxyl groups decrease in number with further calcination, complete dehydroxylation being achieved by evacuation at 873 K.

### 3.2.4. Sorption

After outgassing zeolite Ω sorbs cyclohexane[173], isobutane, neopentane, $(C_4F_9)_3N$[177] and benzene[174]. Shape selective sorption of n-hexane and 2,3 dimethylbutane was not observed[35].

### 3.2.5. Catalytic Properties

Very little work concerning the catalytic properties of zeolite Ω has been reported. Cole and Kouwenhoven[174] investigated the isomerisation and hydrocracking activity of the hydrogen form of zeolite Ω containing some platinum or palladium and reported moderate alkane isomerisation activity for catalysts containing less than 0.05 wt % sodium.

# CHAPTER 4

## Isomerisation Reactions

In this thesis isomerisation of n-butenes, substituted cyclopropanes and specifically labelled propene over erionite and zeolite Ω have been investigated to enable elucidation of the reaction mechanisms. This chapter provides a general introduction to these isomerisation reactions and the information which may be gleaned from their study.

### 4.1 The Isomerisation of n-Butenes

The thermal and catalytic isomerisation of the n-butenes has been a subject of study for many years. A considerable amount of information concerning this reaction has been accumulated and a great deal known about possible mechanisms. Measurement of initial product ratio may provide a useful guide to the type of mechanism involved as will be shown in the following sections.

#### 4.1.1. State of Adsorbed Alkene

In a study of hydrogenation of unsaturated hydrocarbons on transition metal catalysts Bond and Wells[178] postulated the existence of two fundamental types of adsorbed alkene; 1) σ-adsorbed and 2) π-adsorbed.

The σ-adsorbed alkene involves a rehydbridisation of the double bond carbon atoms from $sp^2$ to $sp^3$ hybridisation followed by formation of two σ-bonds with the surface:

$$RHC = CHR' + 2* \longrightarrow \begin{matrix} RHC & - & CHR' \\ | & & | \\ * & & * \end{matrix}$$

Two forms of π-adsorbed alkenes are possible,

1) involving the formation of a π-donor bond with the surface and retaining $sp^2$ hybridisation:

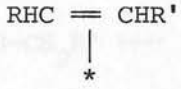

and 2) involving a π-allyl adsorbed species and possible only with alkenes possessing one or more α methylenic hydrogen atom(s):

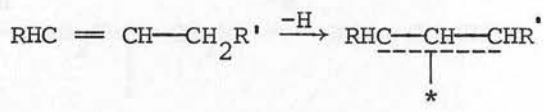

In the π-allyl adsorbed species all the atoms and groups R and R' are coplanar, in a plane parallel to the surface. Therefore, the π-methyl radical formed from a butene molecule will exist in syn and anti conformations:

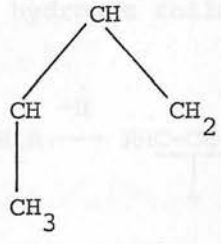

anti

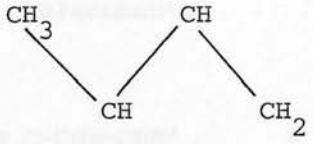

syn

Free rotation of π-allyl adsorbed species is prohibited.

4.1.2. Types of Mechanism

Considering the types of adsorbed species described in the previous section two possible mechanisms of alkene isomerisation have been defined[178].

1) Involving either σ-diadsorbed or π-adsorbed species, in which isomerisation would occur by addition of hydrogen followed by subsequent elimination.

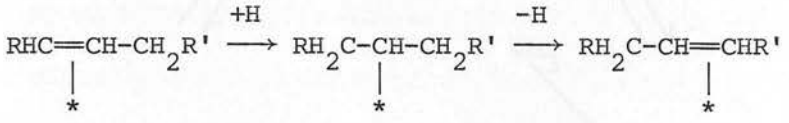

i.e. double bond migration

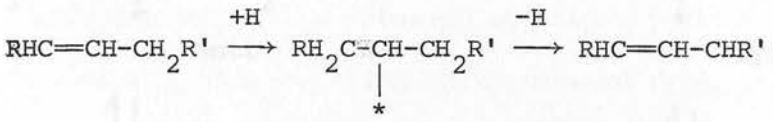

i.e. cis-trans isomerisation

It is apparent that both double bond shift and cis-trans isomerisation involve the same freely rotatable intermediate.

2) Involving a π-allyl adsorbed species, isomerisation occurring by elimination of hydrogen followed by its replacement.

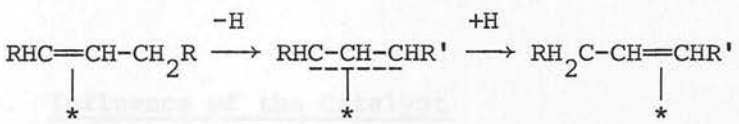

As a consequence of the hindered rotation of the π allyl adsorbed species cis-trans isomerisation must occur through the double bond shift as shown. (Fig. 4.1.1.).

Fig. 4.1.1.

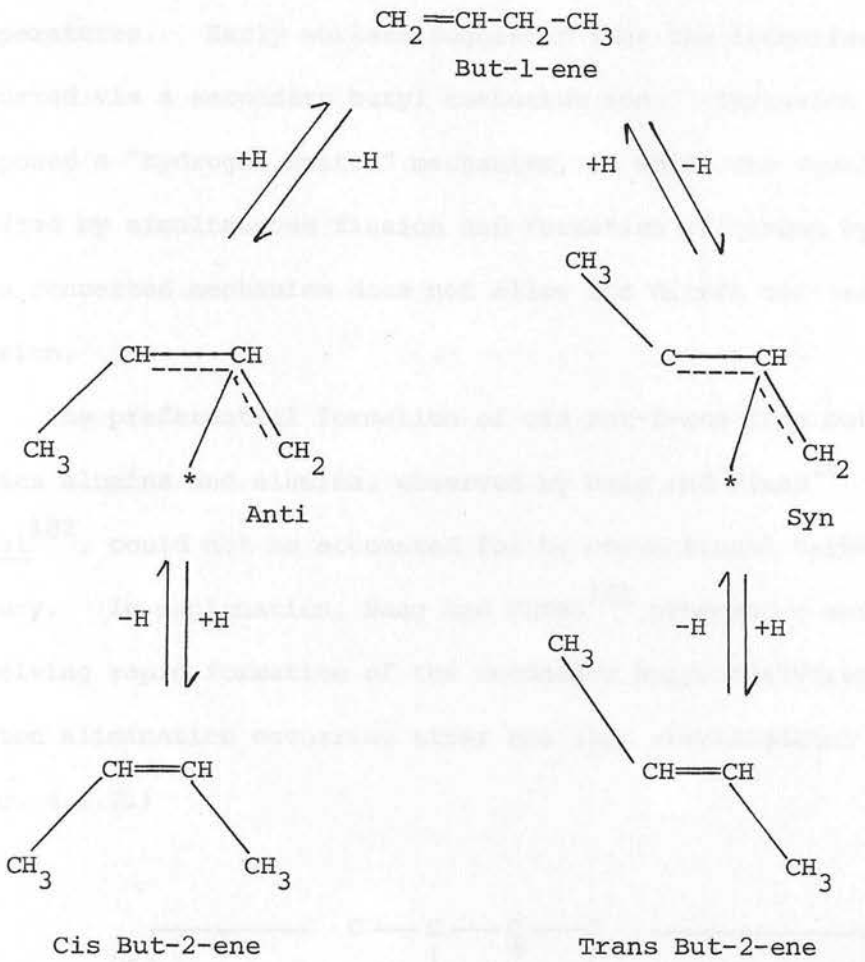


Cis But-2-ene

Trans But-2-ene

4.1.3. Influence of the Catalyst

The initial product ratio of the reaction can supply information on the mechanism and nature of the catalyst. This has been demonstrated by Cvetanovic and Foster[179], who, in an attempt to correlate selectivity with catalyst type, compared product ratios for a series of basic and acidic catalysts. They concluded that in general the isomerisation of butenes occurred in a selective manner and that, although a complete range of selectivity existed between the extreme cases, it was possible to divide the basic and acidic catalysts into two groups.

a) Acidic Catalysts

It is generally accepted that the double bond isomerisation of n-butenes is catalysed by acidic catalysts at comparatively low

temperatures. Early workers suggested that the isomerisation occurred via a secondary butyl carbonium ion. Turkevich and Smith[180] proposed a "hydrogen switch" mechanism, in which the double bond is shifted by simultaneous fission and formation of carbon hydrogen bonds. This concerted mechanism does not allow for direct cis-trans interconversion.

The preferential formation of cis but-2-ene from but-1-ene over silica alumina and alumina, observed by Haag and Pines[181] and Lucchesi et al[182], could not be accounted for by conventional carbonium ion theory. In explanation, Haag and Pines[181] proposed a mechanism involving rapid formation of the secondary butyl carbonium ion with proton elimination occurring after the slow rearrangement to a π-complex. (Fig. 4.1.2.)

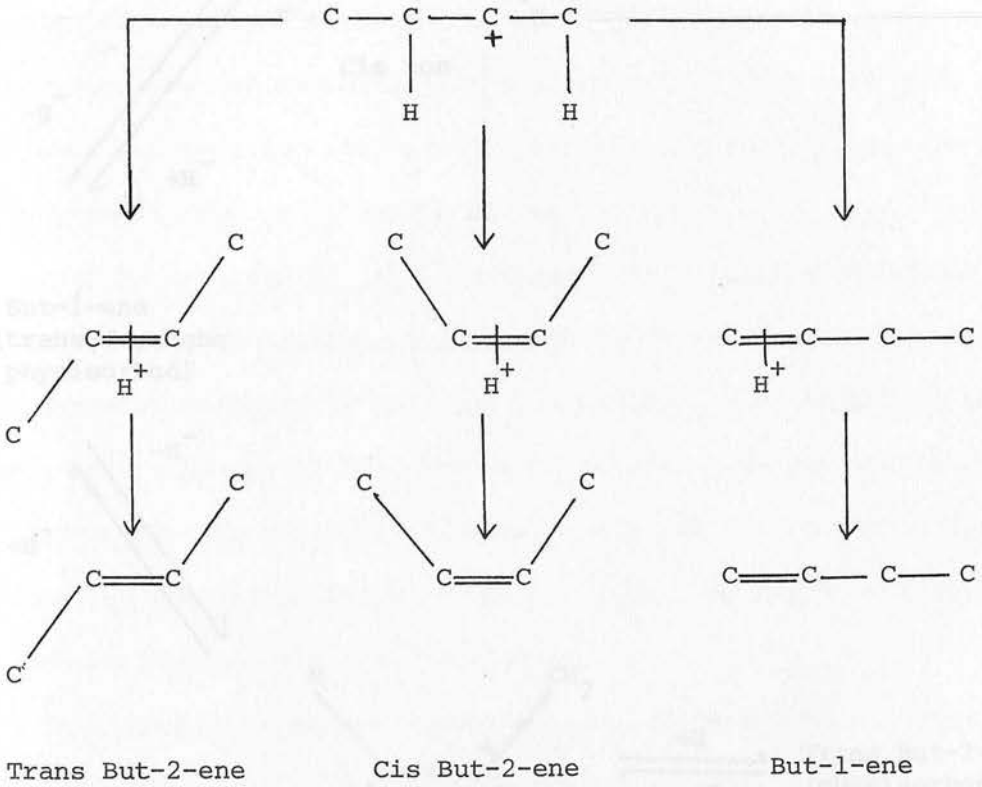


Fig. 4.1.2.

The energies of the π-complexes are cis < trans ≃ but-1-ene accounting for observed product ratios. Conversely Lucchesi et al[182] postulated a mechanism in which the trans alkene is formed from the corresponding cis isomer via a non-classical carbonium ion:

But-1-ene ⇌ Cis But-2-ene ⇌ Trans But-2-ene.

Leftin and Hermana[183] also suggested that direct cis-trans interconversion did not take place over a silica alumina catalyst. The mechanism postulated by these workers involved formation of an allylic carbonium ion by hydride abstraction. (Fig. 4.1.3.)

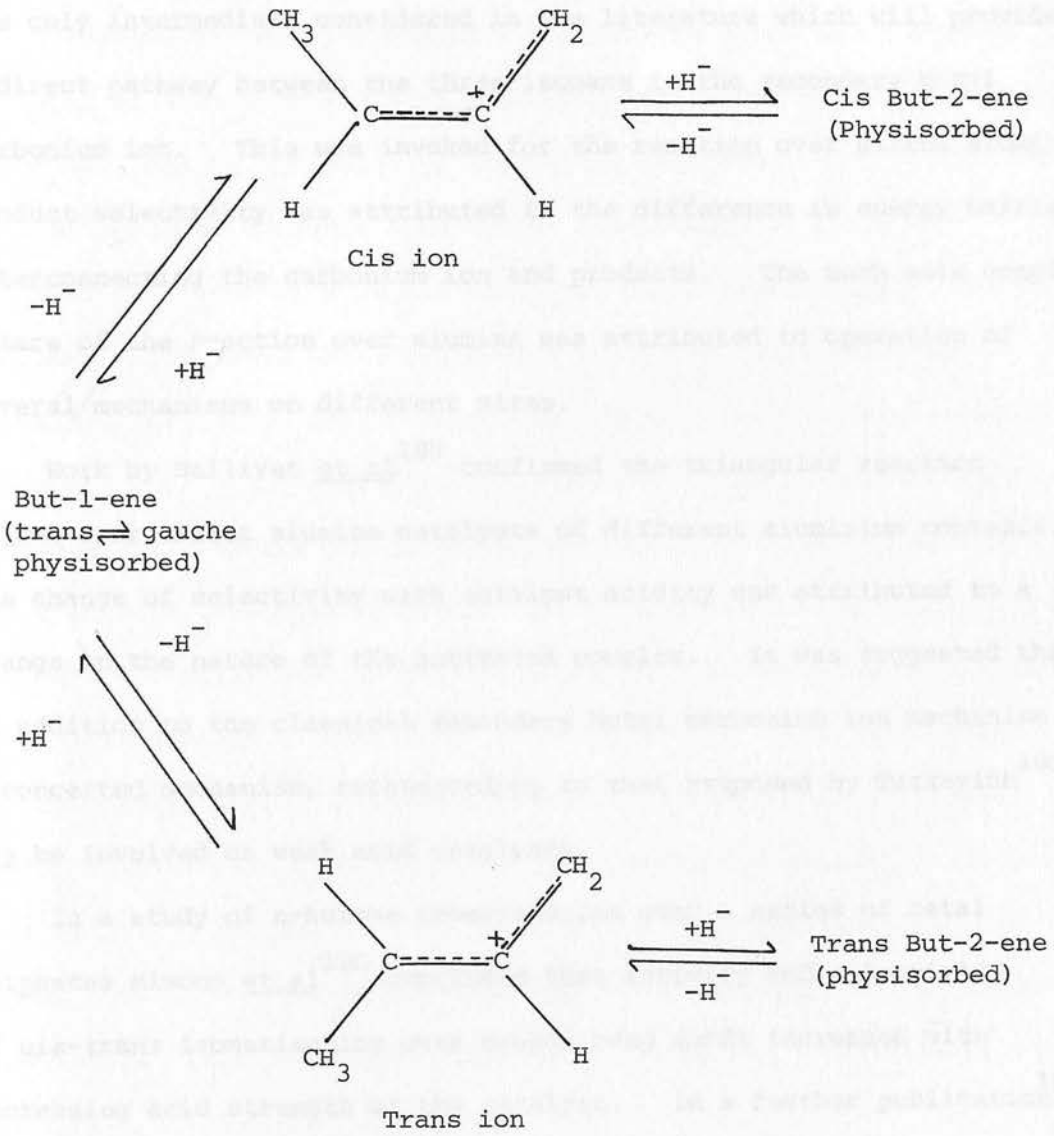


Fig. 4.1.3.

In an extensive study of the isomerisation of n-butenes over silica alumina and alumina[184-188] all reaction rates in the triangular scheme illustrated in Fig. 4.1.4. were found to be significant.

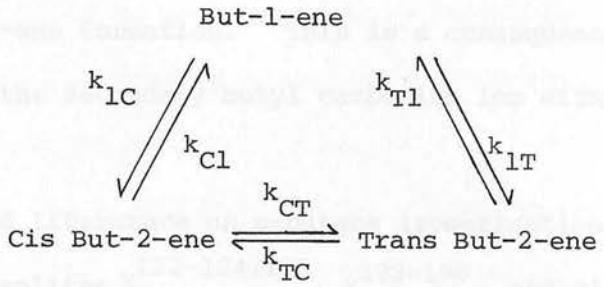


Fig. 4.1.4.

The only intermediate considered in the literature which will provide a direct pathway between the three isomers is the secondary butyl carbonium ion. This was invoked for the reaction over silica alumina. Product selectivity was attributed to the difference in energy barriers interconnecting the carbonium ion and products. The much more complex nature of the reaction over alumina was attributed to operation of several mechanisms on different sites.

Work by Ballivet et al[189] confirmed the triangular reaction scheme over silica alumina catalysts of different aluminium contents. The change of selectivity with catalyst acidity was attributed to a change in the nature of the activated complex. It was suggested that in addition to the classical secondary butyl carbonium ion mechanism a concerted mechanism, corresponding to that proposed by Turkevich[180], may be involved on weak acid catalysts.

In a study of n-butene isomerisation over a series of metal sulphates Misono et al[190] concluded that activity and selectivity of cis-trans isomerisation over double bond shift increased with increasing acid strength of the catalyst. In a further publication[191]

they reported that activity and selectivity were determined principally by the differences in energy barriers. The increase in but-2-ene/but-1-ene ratio with increasing acidity was ascribed to the decrease in height of the energy barrier of but-2-ene formation relative to that of but-1-ene formation. This is a consequence of the increased stability of the secondary butyl carbonium ion with increasing catalyst acidity.

Published literature on n-butene isomerisation over zeolites is confined to zeolites X[122-124,192], Y[193-196] and clinoptilolite[91]. The triangular reaction scheme has been demonstrated together with the first order nature of all six reaction paths.

Investigations using sodium Y zeolite, in which the extent of exchange of sodium by hydrogen correlated well with the isomerisation activity, implied operation of a Brönsted acid mechanism. This was substantiated by evidence from tracer experiments in which one hydrogen or deuterium atom was exchanged per isomerisation. Other studies[194] indicated that pure sodium Y zeolite, containing no impurities or cation deficiencies, is inactive for n-butene isomerisation. Small amounts of divalent cation exchange or decationisation increase the activity and alter the product selectivity. Both of these effects have been attributed to an increase in the acidity of the zeolite. Similar results were obtained over an ammonium-exchanged Y zeolite pretreated at different temperatures[195]. The selectivity has been suggested[195] to stem from a true carbonium ion catalysed reaction (cis-trans isomerisation) and a concerted mechanism (double bond shift). As the catalyst acidity decreases the reaction will appear more concerted, proton addition becoming slower and elimination more rapid. The supercage hydroxyls of hydrogen Y zeolite have been

demonstrated to be the active sites for n-butene isomerisation although there is some evidence of the surface residue playing an active role.

Isomerisation of the n-butenes has been investigated over various cation exchanged forms of zeolite X[122-124,192]. The parent zeolite, sodium X, was found to be catalytically active in the temperature range 473-573 K. Exchange of sodium for a variety of cations caused significant increase in activity and in some cases altered product selectivity. The majority of zeolites studied showed cis/trans ratios close to unity which is indicative of a carbonium ion mechanism. In substantiation of this, enhancement of activity by addition of deuterium oxide was observed. Both copper and nickel exchanged samples exhibited cis/trans ratios significantly less than one which suggests a radical type mechanism[123,124]. Moreover, addition of deuterium enhanced the activity whereas deuterium oxide had no such effect.

Virtually no n-butene isomerisation activity is demonstrated by K-clinoptilolite[91]. The activity of the ammonium exchanged zeolite increases rapidly with pretreatment temperature until all the ammonia is removed, then remains constant until the structure begins to collapse. The selectivity also alters with pretreatment conditions. The cis/trans ratio (< 1) decreases, remains constant, then increases sharply at the point of structural collapse. Poisoning experiments with ammonia and pyridine have led to the catalytic activity being attributed to the hydroxyl groups on the external surface. Once again activity and selectivity were shown to be a function of catalyst acidity.

b) Basic Catalysts

Double bond isomerisation of simple alkenes requires strong basic catalysts which are able to abstract the allylic proton. The reversible triangular reaction scheme for the interconversion of the three n-butenes

has been demonstrated[197]. The following mechanism has been proposed for basic catalysts[198];

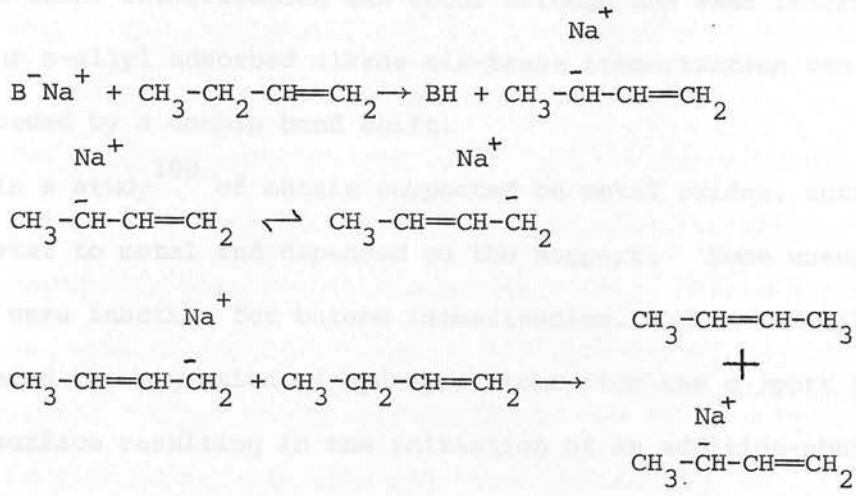

The chain nature of the reaction is consistent with the rapid isomerisation observed.

In a study of butene isomerisation over sodium on alumina, Haag and Pines[199] reported the preferential formation of the less stable cis isomer from but-1-ene. This has been attributed to the hindered rotation of the carbanion $C_2$-$C_3$ bond, resulting in the existence of syn and anti conformations[179,197]. The observed product ratio is considered to be a consequence of the greater abundance of the anti form[197]. Hindered rotation of the carbanion also correlates with the observed preference for double bond shift over cis-trans isomerisation. The allylic carbanion is likely to retain the steric configuration of the reactant but-2-ene and the formation of the other isomer would require its rearrangement.

c) Metal Catalysts

The isomerisation of n-butenes over various metals supported on alumina has been reviewed by Bond and Wells[178]. Two mechanisms were discussed involving different intermediates; 1) an alkyl radical and 2) a π-allyl adsorbed alkene. Free rotation about the carbon-metal

bond of the alkyl radical is possible hence both double bond shift and cis-trans isomerisation can occur through the same intermediate. With the π-allyl adsorbed alkene cis-trans isomerisation can only occur if preceded by a double bond shift.

In a study[199] of metals supported on metal oxides, activity varied from metal to metal and depended on the support. Some unsupported metals were inactive for butene isomerisation. Wells and Wilson[199] postulated the migration of hydrogen atoms from the support to the metal surface resulting in the initiation of an addition-abstraction mechanism.

$$\text{But-1-ene (ads)} \xrightarrow{+H} \text{2-butyl radical} \xrightarrow{-H} \text{But-2-ene (ads)}$$

Butene isomerisation was therefore proposed to be a self-sustaining chain reaction.

## 4.2. Isomerisation of Cyclopropanes

Cyclopropane and its methyl-substituted derivatives are stable molecules which can thermally and catalytically isomerise resulting in a variety of products. These molecules are of considerable importance as materials to test mechanistic theories as types and ratios of products observed are characteristic of the operation of specific mechanisms.

### 4.2.1. General Properties of Cyclopropane

The cyclopropane ring possesses a considerable amount of angle strain. The ring carbon atoms have more 'p' character than $sp^3$ hybridised carbon atoms. Consequently the orbital overlap and hence the bond strength is less than in normal carbon-carbon bonds.

The electron density is not symmetrical about an axis joining the two nuclei, as in normal carbon-carbon bonds, but is directed away from the ring. The resultant bonds are intermediate in character between σ- and π-bonds and are called bent or banana bonds.

The cyclopropane ring possesses many of the properties associated with the ethylenic double bond[200]. Hydrogenation yields propane derivatives and electrophilic reagents such as halogens and hydrogen halides readily attack the ring. Addition of hydrogen halides to substituted cyclopropanes is governed by the Markovnikov Rule resulting in ring fission between most and least substituted carbon atoms[201].

The ring-opening of cyclopropane by acid treatment has been kinetically studied[202]. It appears to involve the opening of the protonated cyclopropane ring to give a more or less solvated propyl cation which then adds to the anion. Ring opening with Lewis acids has also been demonstrated, resulting in a propane derivative[203].

4.2.2. State of Adsorbed Species

In a review of hydrogenolysis of cyclopropanes, Newham[204] defined three modes of adsorption of cyclopropane:

Type A - adsorbed radicals, which may be mono-, 1,2 di-, or 1,2,3 triadsorbed, resulting from the interaction of gas phase or physically adsorbed cyclopropane with the surface.

Type B - a 1,3 diadsorbed species formed by chemisorption with simultaneous ring cleavage.

Type C - a π-adsorbed species involving bond formation between delocalised electrons of the ring and the d orbitals of surface metal atoms. Because of the small amount of delocalisation in cyclopropane this bond would be relatively weak compared to that formed by an alkene.

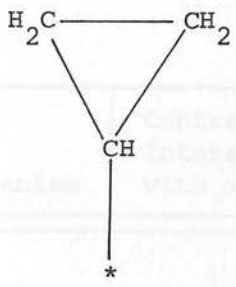

Type A

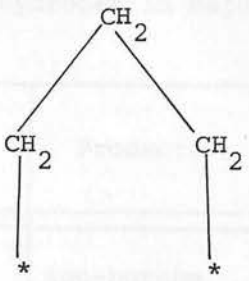

Type B

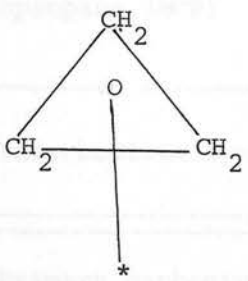

Type C

In addition alkylcyclopropanes may adsorb at the side chain rather than at the ring atoms.

4.2.3. Reaction Mechanisms

In the absence of catalytic effects, the isomerisation of the cyclopropanes may be represented by the simplified general scheme:

Reactant $\rightleftharpoons$ Intermediate $\rightleftharpoons$ Product

Three types of intermediate may be involved, carbonium ion, carbanion and radical. The ionic intermediates would be formed by gain or loss of a proton or hydride at various positions in the cyclopropane molecule. Radicals would result from interaction of hydrogen atoms.

Attack or loss of hydrogen results in ring opening and the formation of a non-cyclic intermediate, the stability of which determines the product distribution. The order of stability for carbonium ions and radicals is tertiary > secondary > primary whereas for carbanions this order is reversed. The products formed from isomerisation of methylcyclopropane, 1,1 dimethylcyclopropane and 1,2 dimethylcyclopropane and the intermediates involved in each mechanism are summarised in Tables 4.1, 4.2 and 4.3. The mechanisms are outlined in detail in Appendix 1. These demonstrate that the type of mechanism involved has an important bearing on the type and relative amounts of products.

Table 4.1. Analysis of Possible Products Arising from Gain/Loss of Hydrogen in Methyl cyclopropane (MCP)

| Type of Mechanism | Centre of Interaction with MCP | Products | Intermediate Type |
|---|---|---|---|
| $H^-$ Loss | 1 | iso-butene | Primary carbonium ion |
| | 2 | n-butenes | Resonance stabilised carbonium ion |
| | Methyl carbon | but-1-ene and/or cyclobutane | Primary carbonium ion and/or Bicyclobutonium ion |
| $H^+$ Loss | 1 | iso-butene | Primary carbanion |
| | 2 | n-butenes | π-allyl type species |
| | Methyl carbon | but-1-ene | Primary carbanion |
| $H^-$ Gain | 1 | but-1-ene | Primary carbanion |
| | 2 | n-butenes | Secondary carbanion |
| | | iso-butene | Primary carbanion |
| $H^+$ Gain | 1 | but-1-ene | Primary carbonium ion |
| | 2 | n-butenes | Secondary carbonium ion |
| | | iso-butene | Primary carbonium ion |
| $H^\cdot$ Loss | 1 | but-1-ene | Primary radical |
| | 2 | n-butenes | Secondary radical |
| | | iso-butene | Primary radical |
| $H^\cdot$ Gain | 1 | but-1-ene | Primary radical |
| | 2 | n-butenes | Secondary radical |
| | | iso-butene | Primary radical |

Table 4.2. Analysis of Possible Products Arising from Gain/Loss of Hydrogen in 1,1 Dimethylcyclopropane (1,1 DMCP)

| Type of Mechanism | Centre of Interaction in 1,1 DMCP | Products | Intermediate Type |
|---|---|---|---|
| $H^-$ Loss | 2 | 3 methyl but-1-ene<br>2 methyl but-2-ene | Resonance-stabilised carbonium ion |
| | Methyl carbon | 2 methyl but-1-ene | Primary carbonium ion |
| $H^+$ Loss | 2 | 3 methyl but-1-ene<br>2 methyl but-2-ene | π-allyl species |
| | Methyl carbon | 2 methyl but-1-ene | Primary carbanion |
| $H^-$ Gain | 1 | 3 methyl but-1-ene | |
| | 2 | 2 methyl but-2-ene<br>2 methyl but-1-ene | Tertiary carbanion |
| $H^+$ Gain | 1 | 3 methyl but-1-ene | Primary carbonium ion |
| | 2 | 2 methyl but-2-ene<br>2 methyl but-1-ene | Tertiary carbonium ion |
| $H^\cdot$ Loss | 2 | 2 methyl but-1-ene<br>2 methyl but-2-ene | Tertiary radical |
| $H^\cdot$ Gain | 1 | 3 methyl but-1-ene | Primary radical |
| | 2 | 2 methyl but-2-ene<br>2 methyl but-1-ene | Tertiary radical |

Table 4.3. Analysis of Possible Products Arising from Gain/Loss of Hydrogen in 1,2 Dimethylcyclopropane (1,2 DMCP)

A. 1-3 Scission

| Type of Mechanism | Centre of Interaction in 1,2 DMCP | Product | Intermediate Type |
|---|---|---|---|
| $H^-$ Loss | 1 | 2 methyl but-2-ene<br>2 methyl but-1-ene | Resonance stabilised carbonium ion |
| | Methyl carbon | 3 methyl but-1-ene | Primary carbonium ion |
| $H^+$ Loss | 1 or 3 | 2 methyl but-2-ene<br>2 methyl but-1-ene | Allyl species |
| | Methyl carbon | 3 methyl but-1-ene | Allyl species |
| $H^-$ Gain | 1 | 2 methyl but-1-ene | Primary carbanion |
| | 3 | 2 methyl but-2-ene<br>3 methyl but-1-ene | Secondary carbonium ion |
| $H^+$ Gain | 1 | 2 methyl but-1-ene | Primary carbonium ion |
| | 3 | 2 methyl but-2-ene<br>3 methyl but-1-ene | Secondary carbonium ion |
| $H^\cdot$ Loss | 1 | methyl butenes | Primary radical |
| | 3 | methyl butenes | Secondary radical |
| $H^\cdot$ Gain | 1 | 2 methyl but-1-ene | Primary radical |
| | 3 | 2 methyl but-2-ene<br>3 methyl but-1-ene | Secondary radical |

Table 4.3 (contd.)

Analysis of Possible Products Arising from Gain/Loss of Hydrogen in 1,2 Dimethylcyclopropane (1,2 DMCP)

B. 1-2 Scission

| Type of Mechanism | Centre of Interaction in 1,2 DMCP | Products | Intermediate Type |
|---|---|---|---|
| $H^-$ Loss | 1 or 3 | cis and trans pent-2-ene | Resonance stabilised carbonium ion |
| | Methyl carbon | pent-1-ene | Secondary carbonium ion |
| $H^+$ Loss | 3 | cis and trans pent-2-ene | Resonance stabilised secondary carbanion |
| | Methyl carbon | pent-1-ene | Secondary carbanion |
| $H^-$ Gain | 1 | n-pentenes | Secondary carbanion |
| $H^+$ Gain | 1 | n-pentenes | Secondary carbonium ion |
| $H^\cdot$ Loss | 1 | n-pentenes | Secondary radical |
| $H^\cdot$ Gain | 1 | n-pentenes | Secondary radical |

4.2.4. Influence of the Catalyst

Various metals and oxides are effective catalysts for the reactions of cyclopropane and its derivatives.

a) Metals

Most of the published literature on metal-catalysed reactions of cyclopropanes is concerned with hydrogenolysis. Investigation of deuterolysis of cyclopropane over metals indicated the formation of hydrocarbon radicals as primary products[204]. The observed exchange could occur via a mono-, di- or triadsorbed species or by a π-bonded species utilising delocalised ring electrons and orbitals of metal atoms on the catalyst surface. From studies using cyclopropane and methyl-cyclopropane. Anderson and Avery[205] concluded that cyclopropane adsorption occurred to give a π-bonded precursor which ring opened to yield a 1,3 diadsorbed species:

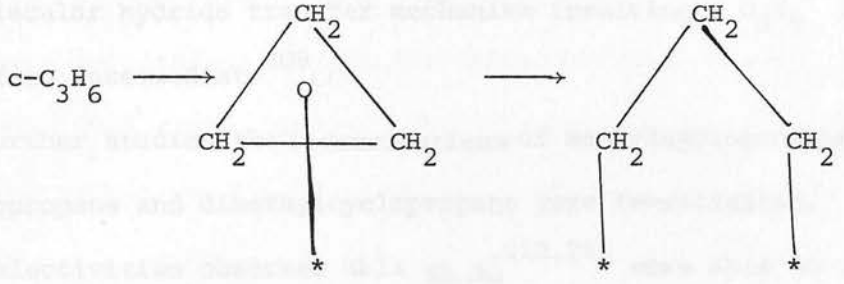


Further evidence for involvement of 1,3 diadsorbed species in ring opening of substituted cyclopropanes over palladium has been reported[206].

Metal catalysed isomerisation of cyclopropane to propene only takes place at elevated temperatures in the absence of hydrogen[207]. A mechanism involving chemisorption with simultaneous ring cleavage to form a 1,3 diadsorbed species has been suggested[204].

b) Acidic Catalysts

Roberts[208] has reported the isomerisation of cyclpropane to propene over various acidic catalysts. Since basic molecules were found to

poison the reaction, the isomerisation was proposed to occur via an n-propyl carbonium ion formed by attachment of a catalyst proton to a ring carbon atom:

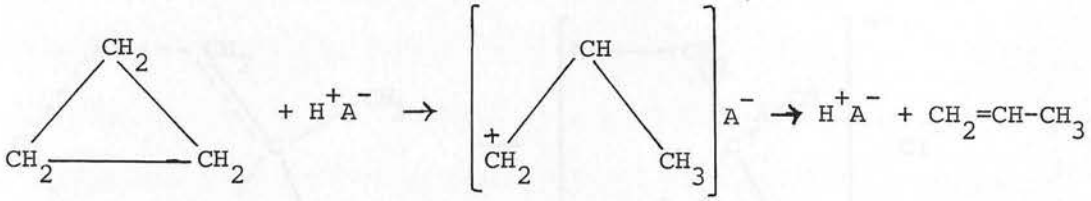

Isomerisation is completed by loss of another proton to the catalyst surface.

The use of tracer techniques has demonstrated the intermolecular exchange of one hydrogen atom during cyclopropane isomerisation to propene over silica alumina[209]. This is consistent with the operation of either of two mechanisms:-

1) the protonic mechanism, proposed by Roberts[208], which requires a $C_3H_7^+$ (Brönsted site) surface intermediate.

2) a bimolecular hydride transfer mechanism involving a $C_3H_5^+$ (Lewis type) surface intermediate[209].

In further studies the isomerisations of methylcyclopropane, ethylcyclopropane and dimethylcyclopropane were investigated. From product selectivities observed Hall et al[210,211] were able to conclude that a protonic type of mechanism was operative. The non-classical cyclopropyl carbonium ion[212] was invoked as the surface complex, ring opening to propene proceeding via a primary propyl cation.

To explain the product selectivity observed in a study of hydrogen chloride catalysed isomerisation of 1,1 dimethylcyclopropane, Bullivant et al[213] postulated the occurrence of two concurrent processes:-

1) a unimolecular isomerisation to 2 methyl but-2-ene and 3 methyl but-1-ene

2) a bimolecular HCl catalysed isomerisation to 2 methyl but-1-ene. They proposed that the formation of 2 methyl but-1-ene proceeded via a six-centred transition state

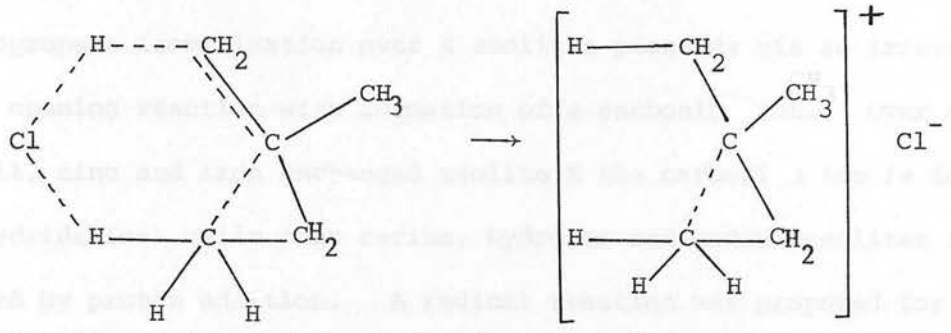

Kinetic studies of isomerisation of cyclopropane to propene over zeolites X and Y at temperatures above 473 K have been reported. First order kinetics with no side reactions were observed over various exchanged forms of X and Y zeolites[214,215]. Studies using deuterated catalysts have indicated that both exchange and isomerisation of cyclopropane proceed via the non-classical cyclopropyl carbonium ion which yields a primary carbonium ion on ring opening[126,216].

A recent publication reports the formation of isobutene as the major product when cyclopropane is passed over hydrogen Y zeolite[217]. A mechanism, involving the non-classical carbonium ion, has been postulated.

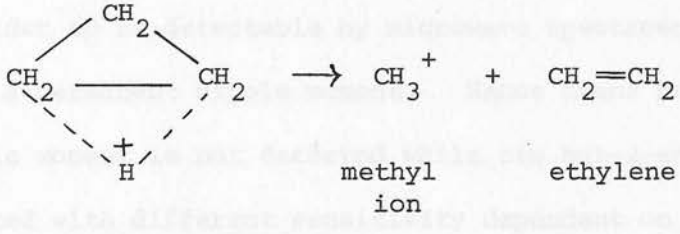


The methyl ion attacks another cyclopropane molecule resulting in the formation of a methylcyclopropane ion which rearranges to form isobutane.

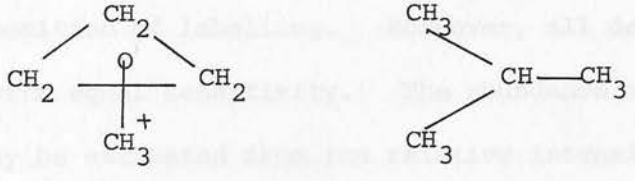

In a study of alkylcyclopropane isomerisation over various exchanged forms of zeolite X activity and product selectivity were dependent on the cation present. Coutts[218] concluded that alkylcyclopropane isomerisation over X zeolites proceeds via an irreversible ring opening reaction with formation of a carbonium ion. Over copper, cobalt, zinc and iron exchanged zeolite X the carbonium ion is formed by hydride loss while over cerium, hydrogen and sodium zeolites it is formed by proton addition. A radical reaction was proposed for nickel exchanged zeolites.

Flockhart et al[219] have demonstrated that in addition to the Brönsted acid mechanism, a second mechanism, possibly involving a Lewis acid site, may be operative, depending on the activation temperature of the zeolite catalyst.

## 4.3. Isomerisation of Propene

Microwave spectroscopy has proved to be a useful technique in the elucidation of the mechanism of exchange reactions of molecules such as propene. It enables detailed analysis of the amount and location of deuterium in the products.

In order to be detectable by microwave spectroscopy, a molecule must have a permanent dipole moment. Hence trans but-2-ene with a zero dipole moment is not detected while cis but-2-ene and but-1-ene are detected with different sensitivity dependent on the magnitude of their respective moments. Labelled propene is an ideal molecule for microwave investigation of double bond shift. Migration of the double bond in isomerisation does not alter the identity of the molecule only the position of labelling. Moreover, all deuteropropenes are detected with equal sensitivity. The abundance of the various species may be estimated from the relative intensities of the corresponding $1_{01} \rightarrow 2_{02}$ rotational transitions[220,221].

### 4.3.1. Influence of the Catalyst

Microwave spectroscopy has been used to investigate the isomerisation of alkenes on alumina and the exchange of propene with deuterium over a range of oxide catalysts[222,223]. On the basis of these studies, a range of intermediates, including carbonium ions, propenyl, π-allyl and σ-allyl species, have been postulated as reaction intermediates of propene on oxide surfaces. A study of specifically labelled propene has confirmed the involvement of an allylic intermediate in exchange reactions over magnesia and rutile[224].

From a microwave investigation of the catalytic reactions between propene and deuterium over zinc oxide, Naito et al[225] concluded that hydrogenation and isomerisation proceed through different reaction intermediates. Propane is produced by addition of hydrogen or deuterium to the double bond whereas isomerisation occurs via a π-allyl intermediate.

### 4.3.2. Mechanism of Isomerisation

As discussed in Section 4.1.2 three mechanisms are possible for the double bond shift of alkenes:-

1) Associative mechanism - the gain of a proton by the alkene resulting in formation of a carbonium ion.
2) Dissociative mechanism - loss of either a proton or a hydride ion from the alkene to generate a π-allylic species.
3) Concerted mechanism - simultaneous loss of hydrogen from a methyl group with hydrogen gain at the methylenic carbon involving a cyclic type of surface intermediate.

These mechanisms can be distinguished on the basis of product distribution from isomerisation of a specifically labelled propene, $CD_2=CH-CH_3$. Each mechanism redistributes the labelling atoms in a characteristic manner.

Associative Mechanism

The associative mechanism for double bond shift is shown in Fig. 4.3.1.

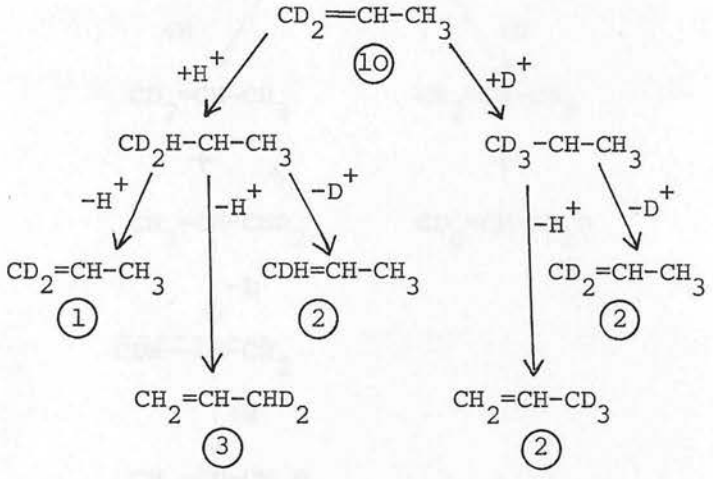


Fig. 4.3.1 - Associative mechanism for double bond shift of $CD_2$=CH-$CH_3$. The circled numbers show the concentrations of products from ten molecules of reactant, predicted purely from statistical considerations.

Addition of a surface proton to propene produces a carbonium ion. This can either lose a proton or deuteron resulting in the formation of $CH_2$=CH-$CHD_2$ and CDH=CH-$CH_3$ as primary products. The reactant is also regenerated. Loss of a deuteron from the carbonium ion provides $D^+$ on the surface from the start of the reaction. This can interact with the reactant resulting in the production of $CH_2$=CH-$CD_3$ as a third primary product. If hydrocarbon deuterium content is conserved the ratios of the amounts of the three primary products are fixed as shown in Fig. 4.3.1.

Dissociative Mechanism

The dissociative mechanism is shown in Fig. 4.3.2. Electronic charges have been omitted for generality.

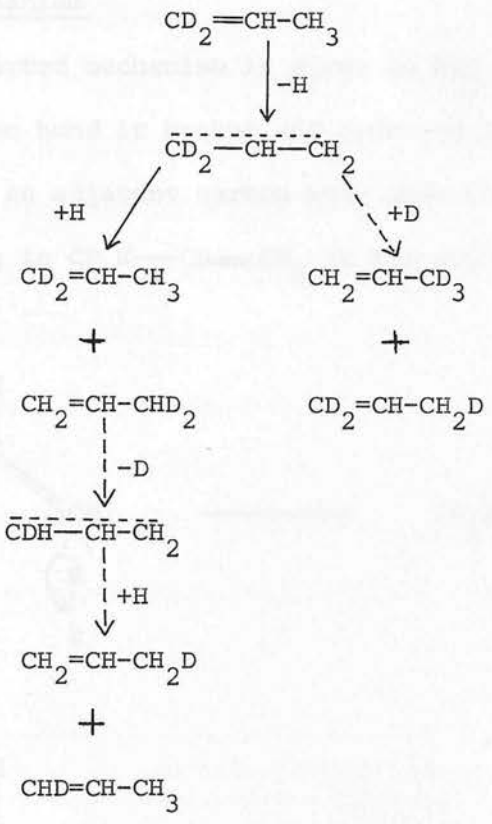


Fig. 4.3.2. - Dissociative mechanism for double bond shift of $CD_2=CH-CH_3$.

⟶ reaction path to primary products

⇢ reaction path to secondary products.

Dissociation of a methyl carbon-hydrogen bond produces a π allylic species which can initially only pick up hydrogen to regenerate the reactant or produce $CHD_2-CH=CH_2$ as the only primary product. In a subsequent reaction this can lose hydrogen or deuterium. Loss of deuterium and gain of hydrogen results in the production of the $[^2H_1]$ species, $CH_2=CH-CH_2D$ and $CHD=CH-CH_3$ in equal amounts, assuming random addition of hydrogen to either side of the symmetrical π-allyl species. Similarly equal amounts of the $[^2H_3]$ species, $CD_3-CH=CH_2$ and $CDH_2-CH=CD_2$, are produced by addition of deuterium to the $CD_2-CH-CH_2$ species. The $[^2H_1]$ and $[^2H_3]$ propenes are secondary products, having been produced by subsequent reaction of the primary product, $CHD_2-CH=CH_2$.

Concerted Mechanism

The concerted mechanism is given in Fig. 4.3.3. As a methyl carbon-hydrogen bond is broken and hydrogen lost to a surface site, hydrogen from an adjacent carbon atom adds to the methylenic carbon atom resulting in $CD_2H—CH=CH_2$ as the only primary product.

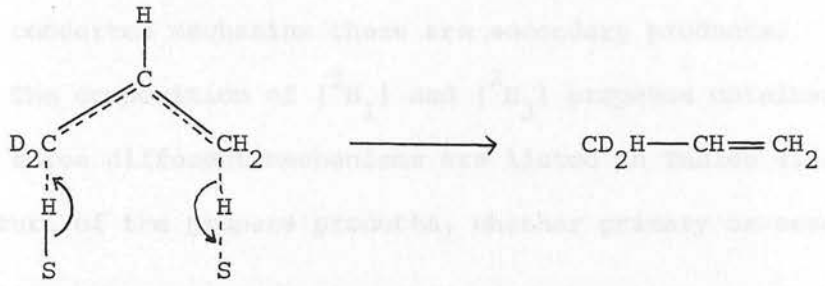


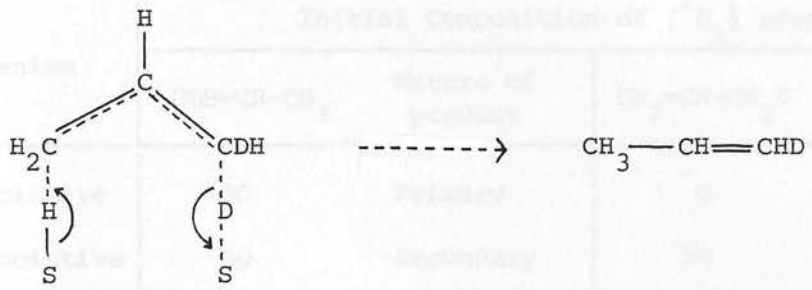


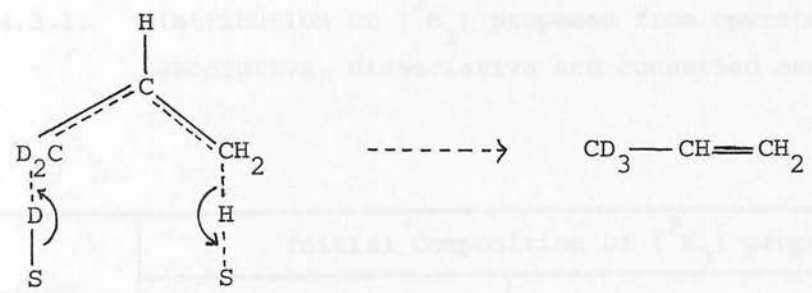


Fig. 4.3.3. Concerted mechanism for double bond shift of $CD_2=CH—CH_3$; ⟶ reaction path to primary products, ---→ reaction path to secondary products. S is a surface site.

Subsequent reaction regenerates the reactant and produces $CH_3—CH=CHD$ as the only $[^2H_1]$ propene. Deuterated surface sites are also produced. These will interact principally with the predominant deuteropropenes present, initially $CD_2=CH—CH_3$, to produce $CD_3—CH=CH_2$ as the only $[^2H_3]$ propene. The $[^2H_1]$ and $[^2H_3]$ propenes produced are the same as those from the associative mechanism. However, in the concerted mechanism these are secondary products.

The composition of $[^2H_1]$ and $[^2H_3]$ propenes obtained from operation of the three different mechanisms are listed in Tables 4.3.1. and 4.3.2. The nature of the propene products, whether primary or secondary, is also listed.

| Mechanism | Initial Composition of $[^2H_1]$ propenes | | | |
|---|---|---|---|---|
| | $CDH=CH-CH_3$ | Nature of product | $CH_2=CH-CH_2D$ | Nature of product |
| Associative | 100 | Primary | 0 | |
| Dissociative | 50 | Secondary | 50 | Secondary |
| Concerted | 100 | Secondary | 0 | |

Table 4.3.1. Distribution of $[^2H_1]$ propenes from operation of associative, dissociative and concerted mechanisms.

| Mechanism | Initial Composition of $[^2H_3]$ propenes | | | | |
|---|---|---|---|---|---|
| | $CH_2=CH-CD_3$ | Nature of Product | $CD_2=CH-CH_2D$ | Nature of Product | $CHD=CH-CHD_2$ |
| Associative | 100 | Primary | 0 | | 0 |
| Dissociative | 50 | Secondary | 50 | Secondary | 0 |
| Concerted | 100 | Secondary | 0 | | 0 |

Table 4.3.2. Distribution of $[^2H_3]$ propenes from operation of associative, dissociative and concerted mechanisms.

It is apparent that the product selectivity exhibited by the associative and concerted mechanisms differs from that of the dissociative mechanism. The occurrence of the $[^2H_1]$ and $[^2H_3]$ propenes as primary products in the associative mechanism and secondary products in the concerted mechanism enables these mechanisms to be distinguished. In the associative mechanism, as primary products, the ratio of $CH_2{=}CH{-}CHD_2$, $CHD{=}CH{-}CH_3$ and $CH_2{=}CH{-}CD_3$ will be constant with time, whereas if the concerted mechanism is operative the ratio of these products will vary.

Application of this scheme, using specifically labelled propene, $CD_2{=}CH{-}CH_3$, has been used in this thesis to investigate the mechanism of double bond shift over erionite and zeolite Ω.

# CHAPTER 5

## Experimental

### 5.1. Materials

#### 5.1.1. Catalysts

The structures and properties of the zeolites, omega and erionite, used in this study, have been discussed in Chapter 3. The zeolites, in powder form, were obtained from the following sources:

Zeolite omega (Ω) from Shell Development Company

Natural erionite (Rome, Oregon) from Professor F.A. Mumpton (State University College of New York)

A commercially treated erionite from Dr. P. Venuto, Mobil Oil Corporation.

Prior to use, the zeolites were stored in sealed glass bottles to avoid atmospheric contamination.

#### 5.1.2. Chemicals

Nitrogen, air and hydrogen were obtained from the British Oxygen Company and used as supplied for gas chromatographic purposes. White spot nitrogen (B.O.C.) was suitable for experiments in which oxygen-free nitrogen was necessary. Drying of nitrogen, when required, was achieved by passage through phosphorus pentoxide and a previously dehydrated molecular sieve (5A). The dried gas was stored in a glass bulb.

But-1-ene, trans but-2-ene, cis but-2-ene, 2-methyl propene, 2 methyl propane and butane were obtained from the Matheson Company as C.P. Grade (99% pure). These materials were purified and outgassed by vacuum distillation and repeated cycles of freezing, pumping and thawing. After purification the gases were stored in glass bulbs on the apparatus until required at which time they were redistilled.

Methylcyclopropane (99% pure), supplied by K. and K. Laboratories, was purified and stored in the same manner as the butenes.

2-methyl but-1-ene, 2-methyl but-2-ene, 3-methyl but-1-ene, pent-1-ene, cis pent-2-ene and trans pent-2-ene were obtained from Koch-Light. After purification, carried out as above, the liquids were stored in cold fingers fitted with Rotaflo teflon taps.

1,1 dimethylcyclopropane (99% pure) and trans 1,2 dimethylcycloprp-pane (99% pure), supplied by Pfaltz and Bauer, were also stored in cold fingers following purification.

Specifically labelled 1,1 $d_2$-propene (minimum isotopic purity 98%) was obtained from Merck, Sharp and Dohme. The amount required for a reaction was admitted to the gas handling apparatus and purified by vacuum distillation and repeated cycles of freezing, pumping and thawing before use.

## 5.2. Isomerisation Reactions of n-Butenes and Methyl-substituted Cyclopropanes

### 5.2.1. Apparatus

a) Gas Handling and Reaction System

The apparatus was constructed from Pyrex glassware and is represented schematically in Fig. 5.1. The cylindrical reaction vessels were attached to the apparatus via water cooled ground glass joints. Silica reaction vessels were used when outgassing temperatures exceeded 773 K. All ground glass joints and taps were lubricated with Apiezon 'L' grease.

Two mercury diffusion pumps backed by rotary vacuum pumps were capable of evacuating the apparatus to approximately 133 $\mu$ $Nm^{-2}$ ($10^{-6}$ torr). Vacuum testing, using a McLeod Gauge was always carried

Fig. 5.1.

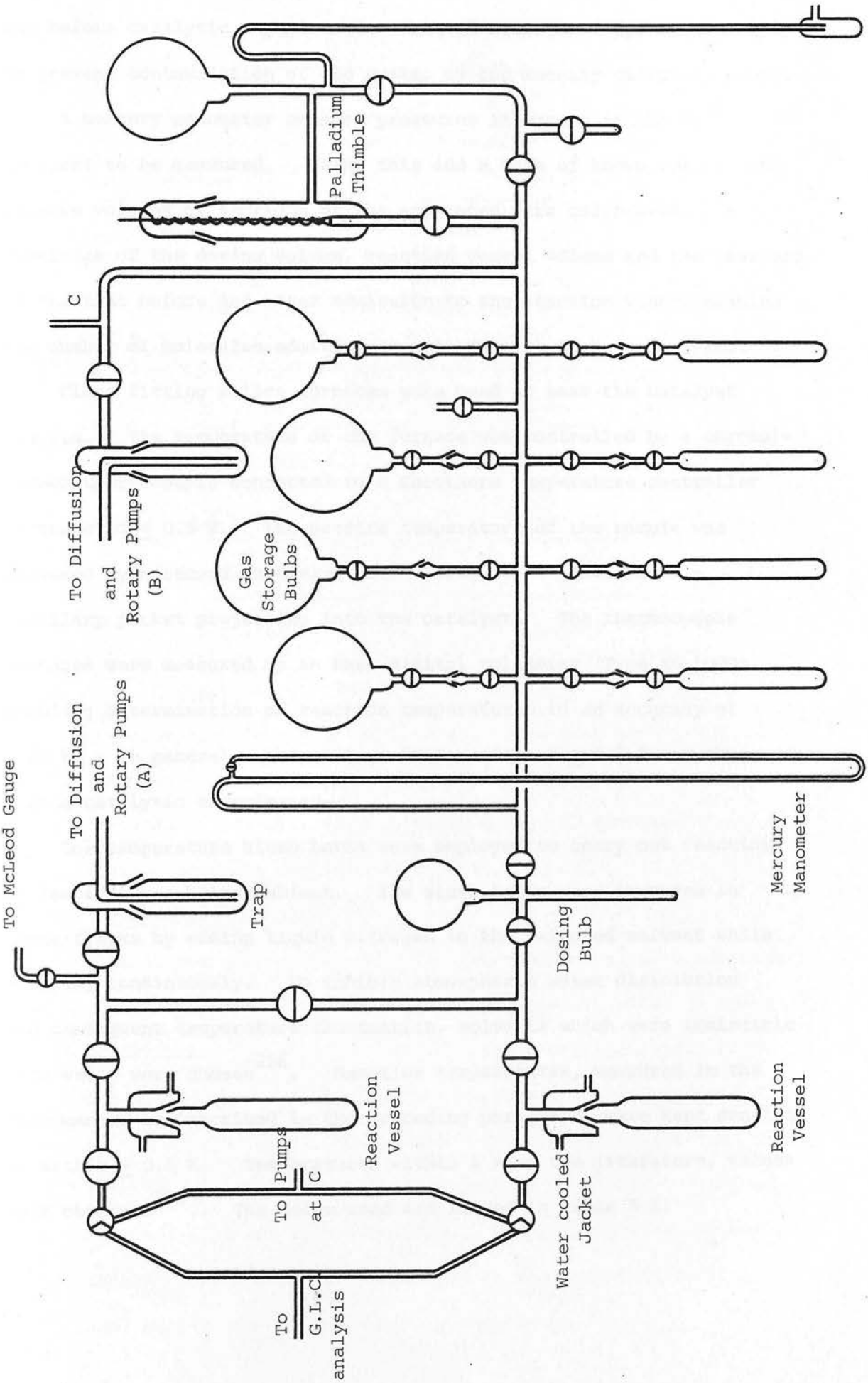


Fig. 5.1. Gas Handling and Reaction System

out before catalytic experiments. Liquid nitrogen traps were used to prevent contamination of the system by the mercury diffusion pumps.

A mercury manometer enabled pressures in excess of 133 $Nm^{-2}$ (1 torr) to be measured. Using this and a bulb of known volume, the gaseous volumes of sections of the apparatus were calibrated. A knowledge of the dosing volume, reaction vessel volume and the pressure of reactant before and after admission to the reaction vessel enabled the number of molecules admitted to the catalyst to be calculated.

Close fitting silica furnaces were used to heat the catalyst samples. The temperature of the furnace was controlled by a chromel-alumel thermocouple connected to a Eurotherm temperature controller accurate to $\pm$ 0.5 K. The precise temperature of the sample was measured by a second chromel-alumel thermocouple placed down a capillary pocket projecting into the catalyst. The thermocouple voltages were measured by an Exel digital voltmeter (Type XL 1000) enabling determination of reaction temperatures to an accuracy of 0.25 K. In general a temperature fluctuation of $\pm$ 0.5 K was observed during catalytic experiments.

Low temperature slush baths were employed to carry out reactions at temperatures below ambient. The slush baths were prepared in Dewar flasks by adding liquid nitrogen to the selected solvent while stirring continuously. To inhibit atmospheric water dissolution and consequent temperature fluctuation, solvents which were immiscible with water were chosen[226]. Reaction temperatures, measured in the same manner as described in the preceding paragraph, were kept constant to within $\pm$ 0.5 K. Temperatures within 1 K of the literature, values were observed[226]. The baths used are listed in Table 5.1.

| Low Temperature Baths | Temperature of Baths/K |
|---|---|
| p-Xylene slush | 286 |
| Cyclohexane slush | 280 |
| Ice/water | 273 |
| Aniline slush | 266 |
| Methyl benzoate slush | 261 |
| Tetrachloromethane slush | 250 |
| Bromobenzene slush | 242.2 |
| Arklone slush | 237 |
| Chlorobenzene slush | 227.4 |
| Trichloromethane slush | 209.5 |

Table 5.1. Low Temperature Baths

Samples of the gas phase (∿2%) were removed from the reaction vessel as required by manipulation of a 3-way tap attached to a Perkin Elmer sampling valve incorporating a 0.2 $cm^3$ evacuable sample loop. Analysis by gas chromatography followed.

b) Gas Chromatographic Apparatus

Samples of the gas removed from the reaction vessel were admitted to the chromatographic column by adjusting the sample valve to bring the loop containing the sample into the carrier gas (nitrogen) flow. The sample was flushed out of the loop and through the chromatographic column by the carrier gas. The columns used to resolve reactant and products in the reactions studied are listed in Table 5.2. Optimum operating conditions are also tabulated. In most reaction systems it was necessary to immerse at least half of the column in an ice or ice/ethanol bath to obtain satisfactory resolution.

| Reactant | Column(s) | Inlet Pressure/k $Nm^{-2}$ | | | Temperature of Column/K |
|---|---|---|---|---|---|
| | | Air | Hydrogen | Nitrogen | |
| n-Butenes | 4 m of ⅛" o.d. stainless steel loaded with bis-2-methoxy ethyl adipate (13.5%) and di-2-ethyl hexyl sebacate on 80/100 mesh Chromasorb P. | 69 | 69 | 69 | 273 |
| MCP | 15 m of ⅛" o.d. copper tube loaded with 35% propylene carbonate on P60:80 Chromosorb | 69 | 69 | 455 | 7½ m at 263<br>7½ m at 273 |
| 1,2 DMCP | 8 m of ⅛" o.d. stainless steel loaded with 20% bis-2 methoxy ethyl adipate on chromosorb P60:80 | 69 | 69 | 455 | 4 m at 273<br>4 m at 298 |
| 1,1 DMCP | 4 m of ⅛" o.d. stainless steel loaded with 20% bis-2 methoxy ethyl adipate on chromosorb P60:80<br>+<br>10 m of ⅛" o.d. polythene tube loaded with 15% silicone oil on 60:80 celite | 69 | 69 | 455 | 298 |

Table 5.2. Chromatographic Columns and Conditions Used in the Analysis of $C_4$ and $C_5$ Hydrocarbons

The resolved components were eluted to a hydrogen/air flame ionisation detector. The resulting signals were amplified by a Perkin Elmer amplifier and parallel amplified signals supplied to a Hewlett Packard integrator and a Servoscribe potentiometric recorder. The integrated peak areas were assigned to components of the gaseous mixture. Sensitivity factors of the columns were determined by the preparation and analysis of standard mixtures of hydrocarbons. Correction of observed peak areas by these factors enabled quantitative analysis to be accomplished.

5.2.2. Procedure

The hydrated zeolite (.13 g) was accurately weighed and transferred to a clean dry reaction vessel (volume 250 $cm^3$) which was attached to the gas line by means of a ground glass joint. Both types of erionite were outgassed by evacuating the reaction vessel and maintaining a temperature of 643 K for 16 hours. The pretreatment conditions of zeolite omega were varied as will be discussed more fully in a later section. Outgassing under vacuum at elevated temperatures and oxygen pretreatment were used. Oxygen treatment involved admission of two doses of oxygen ($5 \times 10^{20}$ molecules) to the catalyst at the outgassing temperature. Each dose was left in the reaction vessel for 30 minutes, and the system was pumped for 15 minutes between doses. Following this the reaction vessel was evacuated for a further hour.

After pretreatment the furnace was removed and the sample allowed to equilibrate to the desired reaction temperature. A known quantity of reactant ($10^{20}$ molecules) was admitted to the reaction vessel by expansion of a measured pressure from the dosing bulb. The reaction was monitored by removing samples

from the gas phase at regular intervals and analysing by gas chromatography. After use the reaction vessels were cleaned with surfactant solution (Decon), copiously rinsed with distilled water and dried in an oven (∿ 420 K).

5.2.3. Treatment of Data

A knowledge of the peak areas for each chromatographic scan and the sensitivity factors for the resolved components enabled the percentage composition of each chromatographic analysis to be determined. A plot of percentage composition against time gives a general picture of the course of the reaction, including initial product ratios.

The rate of disappearance of but-1-ene was calculated assuming first order kinetics, the triangular reaction scheme of

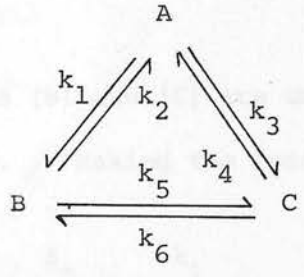


where A = But-1-ene

B = Trans but-2-ene

C = Cis but-2-ene

being considered as

$$\text{But-1-ene} \xrightarrow{k} \text{Products}$$

Data are plotted according to the first order rate equation

$$\ln(x-x_e) = -kt + \ln(a-x_e) \qquad \text{Eqn.(5.1)}$$

where a = Initial concentration of but-1-ene

x = Percentage of but-1-ene at time t

$x_e$ = Percentage of but-1-ene at equilibrium

This equation holds rigorously for a reversible reaction where one reactant becomes a single product, the reaction being first order in both directions.

The relative rate constants for the six possible reactions in the n-butene triangular scheme may be calculated from the initial product ratios and equilibrium ratios[227]. Absolute rate constants are difficult to determine because of the reversibility of the reaction. However, the ratio of products at very low conversions is proportional to the ratio of their rate constants. For example, starting with A, the ratio $k_1/k_3$ may be obtained from the concentrations of B and C formed

$$dB/dt = k_1[A]^n - k_2[B]^{n'} - k_5[B]^{n''} + k_6[C]^{n'''}$$

$$dC/dt = k_3[A]^m - k_4[C]^{m'} - k_6[C]^{m''} + k_5[C]^{m'''}$$

At very low conversions [B] and [C] are small and the corresponding terms can be neglected. Making the reasonable assumption that n = m gives

$$\lim_{t \to o} \left(\frac{B_t}{C_t}\right) = \frac{k_1}{k_3}$$

Thus determination of the ratio B/C at low total conversion and extrapolating back to zero time gives the ratio $k_1/k_3$. Similarly with trans but-2-ene and cis-but-2-ene as reactants $k_2/k_5$ and $k_4/k_6$ may be obtained. Since the forward and reverse rates are equal at equilibrium $k_1/k_2$, $k_3/k_4$ and $k_5/k_6$ can be calculated from equilibrium concentrations. Therefore by equating $k_2$ to 1 the relative rate constants may be evaluated.

Isomerisation of methylcyclopropane and dimethylcyclopropanes involves an irreversible ring-opening step. Data for these reactions are plotted according to the first order rate equation,

$$\ln x = -kt + \ln a \qquad \text{Eqn.(5.2)}$$

where

a = Initial concentration of reactant

x = Concentration of reactant at time t.

The reactions of butenes and cyclopropanes in general exhibited apparent zero or first order kinetics. Values of the rate constant at various reaction temperatures were plotted according to the Arrhenius equation.

$$k = Ae^{-E_A/RT} \qquad \text{Eqn.(5.3)}$$

where

k = Rate constant

A = Frequency factor

$E_A$ = Activation energy

R = Gas constant

T = Temperature/K.

This expression may also be written as,

$$\ln k = \ln A - E_A/RT$$

Hence a plot of ln k against $1/T$ has a gradient of $-E_A/R$ and $E_A$ may be determined. Knowing $E_A$, the number of molecules admitted and the surface area, A can also be evaluated.

The equilibrium data at different temperatures were calculated assuming the triangular reaction schemes:

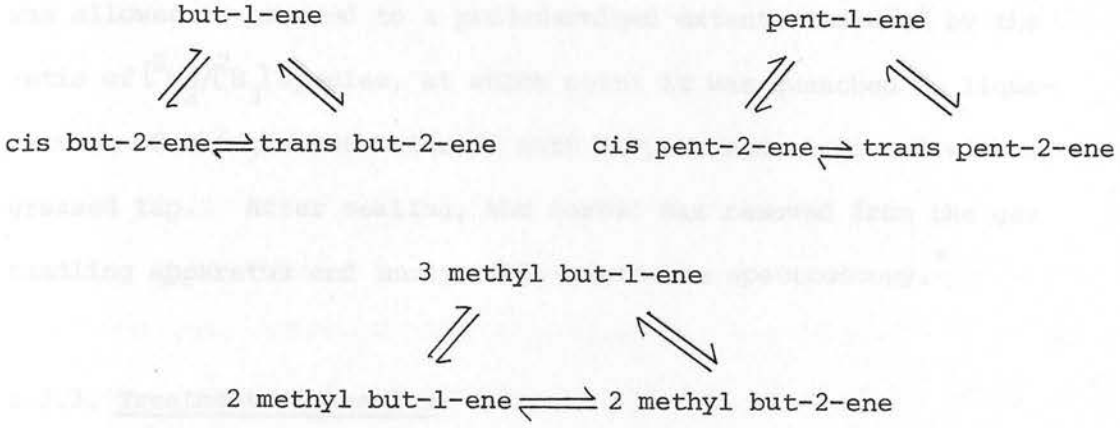


Equilibrium concentrations of the species involved in each triangular reaction scheme were calculated from their equilibrium constants of formation at a series of different temperatures[228]. Graphical representation of this data enabled equilibrium concentrations of species at specific reaction temperatures to be determined.

## 5.3. Double Bond Shift of 1,1 $[^2H_2]$-Propene

### 5.3.1. Apparatus

The gas handling and reaction apparatus was similar to that depicted in Fig. 5.1. The gas line was equipped with a capillary leak enabling a small continuous stream of gas to be drawn into an AEI M.S. 10 mass spectrometer operating at 24 x $10^{-16}$ kJ (15 eV). The mass spectrometer is described in detail elsewhere[229].

### 5.3.2. Procedure

Catalyst samples were pretreated as described in Section 5.2.2. After outgassing the furnace was lowered and the reaction vessel allowed to cool before immersing in a liquid nitrogen bath. A known quantity ($10^{20}$ molecules) of purified reactant was frozen into the reaction vessel and a furnace, at the desired temperature, raised around the vessel. The extent of reaction was monitored by mass spectrometry, scanning from 39 to 48 mass units at regular intervals. The reaction

was allowed to proceed to a predetermined extent, measured by the ratio of $[^2H_2]/[^2H_3]$ species, at which point it was quenched by liquefaction of the gaseous material into a Pyrex vessel fitted with a greased tap. After sealing, the vessel was removed from the gas handling apparatus and analysed by microwave spectroscopy.*

5.3.3. Treatment of Results

Relative abundances of deuteropropenes, propene and fragmented species were determined by measurement of recorder peak heights. Analyses of deuteropropene mixtures were made after correction for background, natural abundances of heavy isotopes, $^{13}C$ and D ($^2H$), and fragmentation. The background spectrum and fragmentation pattern of the parent hydrocarbon were determined before each mass spectral analysis as these varied. The Fortran programme, incorporating these corrections, used for the calculation of the percentage composition of the deuteropropene mixtures is listed in Appendix 2.

Owing to appreciable fragmentation in the mass spectrometer source, the derived percentages of $[^2H_3]$ propenes were much more reliable than those of $[^2H_1]$ propenes. However, due to the overall mass balance, initial rates of $[^2H_1]$ and $[^2H_3]$ formation must have been equal. Hence the most accurate way of calculating the amount of $[^2H_2]$ from the computer output was

$$[^2H_2] = 100 - 2([^2H_3] + [^2H_4]) \qquad \text{Eqn.(5.4)}$$

as

$$[^2H_3] = [^2H_1]$$
$$[^2H_4] = [^2H_0]$$

The disappearance of $[^2H_2]$-propene is plotted according to the first order rate equation.

*Microwave analysis was kindly carried out by R. Dickinson in the Chemistry Department, Glasgow University.

$$\ln([^2H_2] - [^2H_{2e}]) = -kt + C \qquad \text{Eqn. (5.5)}$$

where

$[^2H_2]$ = concentration of $[^2H_2]$-propene at time = t

$[^2H_{2e}]$ = concentration of $[^2H_2]$-propene at equilibrium

C = constant

First order rate constants were determined for a series of temperatures and plotted according to the Arrhenius equation. (Eqn. 5.3.) enabling the activation energy to be calculated.

The possible locations of deuterium atoms in a propene molecule are shown in Fig. 5.2

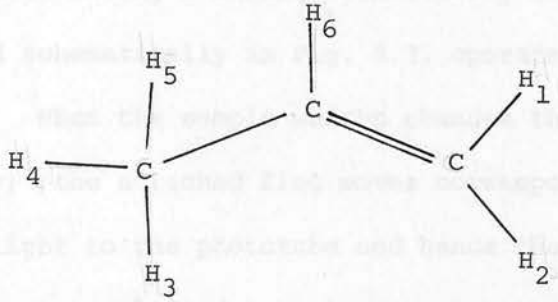


Fig. 5.2. The position of hydrogen atoms in propene.

Microwave analysis enables the positions of deuterium atomsin propene to be exactly located as discussed in Section 4.3. It is possible to differentiate between 5 types of $[^2H_1]$, 11 types of $[^2H_2]$ and 14 types of $[^2H_3]$ species by microwave spectroscopy. However for the purpose of the study of double bond shift, investigated in this thesis, several of these are equivalent. For example the $[^2H_3]$ species labelled (1,2,3), (1,2,4) and (1,2,5) are all $CD_2 = CH-CH_2D$ differing only in the conformational location of the methyl deuterium. Hence the amounts of the isomeric $[^2H_1]$, ($CDH = CH-CH_3$, $CH_2 = CH-CH_2D$) $[^2H_2]$ ($CD_2 = CH-CH_3$, $CDH = CH-CH_2D$, $CH_2 = CH-CHD_2$) and $[^2H_3]$ ($CD_2 = CH-CH_2D$, $CHD = CH-CHD_2$, $CH_2 = CH-CH_3$) propenes are determined by summation of the concentrations of their component species.

## 5.4. Adsorption Experiments

The use of a microbalance to measure the adsorption of gases has been described by several workers.[230,231] Its facility for measuring rapid changes of sample weight directly is of great advantage in adsorption work.

### 5.4.1. Apparatus

#### a) The Balance

The microbalance used in this work was a Cahn RG Automatic Electrobalance having a maximum sensitivity of $\pm$ 1 μg. The balance, represented schematically in Fig. 5.3, operates on the null-balance principle. When the sample weight changes the beam tends to deflect momentarily; the attached flag moves correspondingly altering the amount of light to the phototube and hence the phototube current. This current is amplified in a two-stage servo amplifier and is subsequently applied to a coil attached to the beam. Since the coil is in a magnetic field, it acts like a d.c. motor exerting a force to restore the beam to its original balance position. The restoring force acts so quickly that, to the eye, the beam appears to be locked in position although it is really in a state of dynamic equilibrium.

The restoring current, and the voltage which it develops across the coil are directly proportional to the change in sample weight. To display this accurately on a recorder it is necessary to subtract a known, accurately calibrated voltage across the coil using a potentiometer. A dial (the mass dial) on the potentiometer is calibrated directly in milligrams corresponding to the amount of voltage being subtracted. The excess coil voltage is then applied to a Servoscribe potentiometric recorder. By attenuating this voltage by known ratios it is possible to display various weight ranges on the recorder.

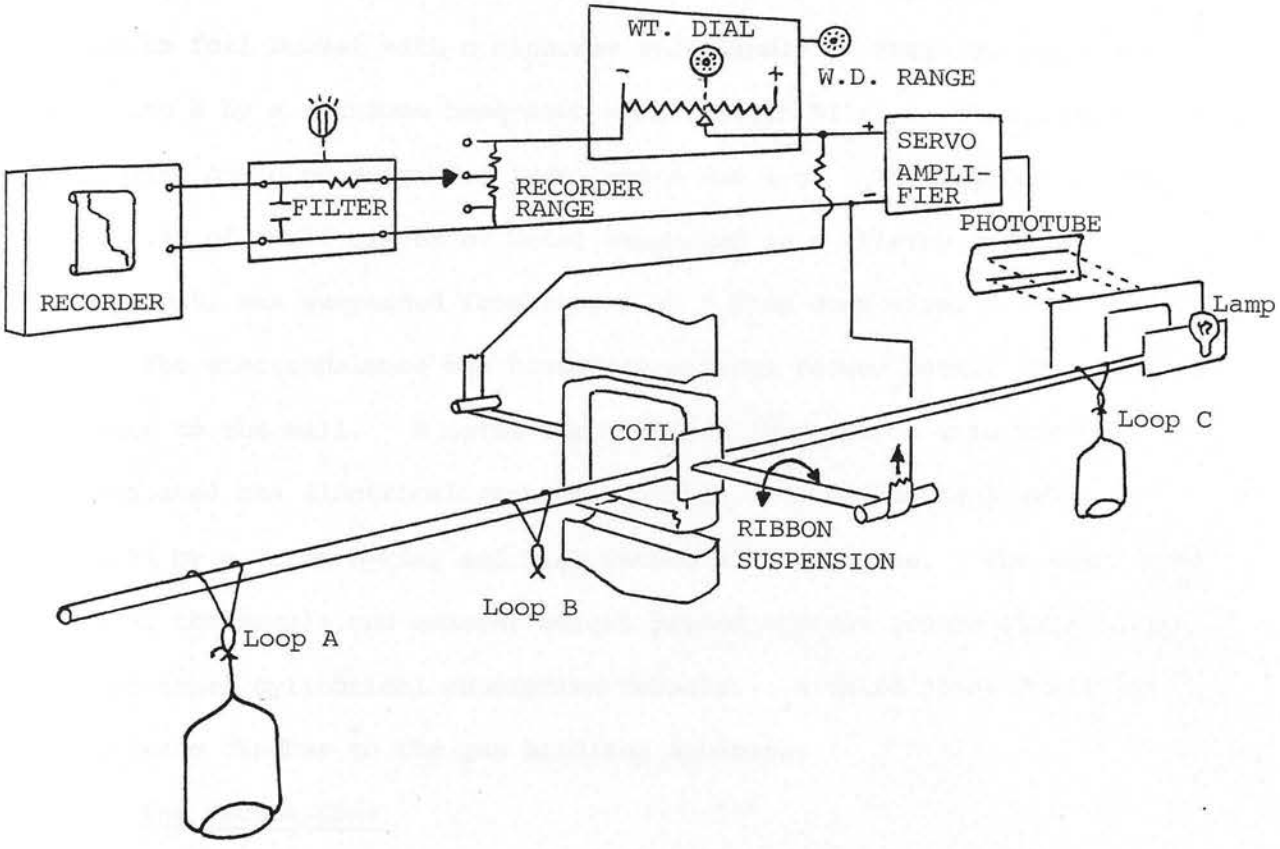


Fig. 5.3. The Cahn Microbalance

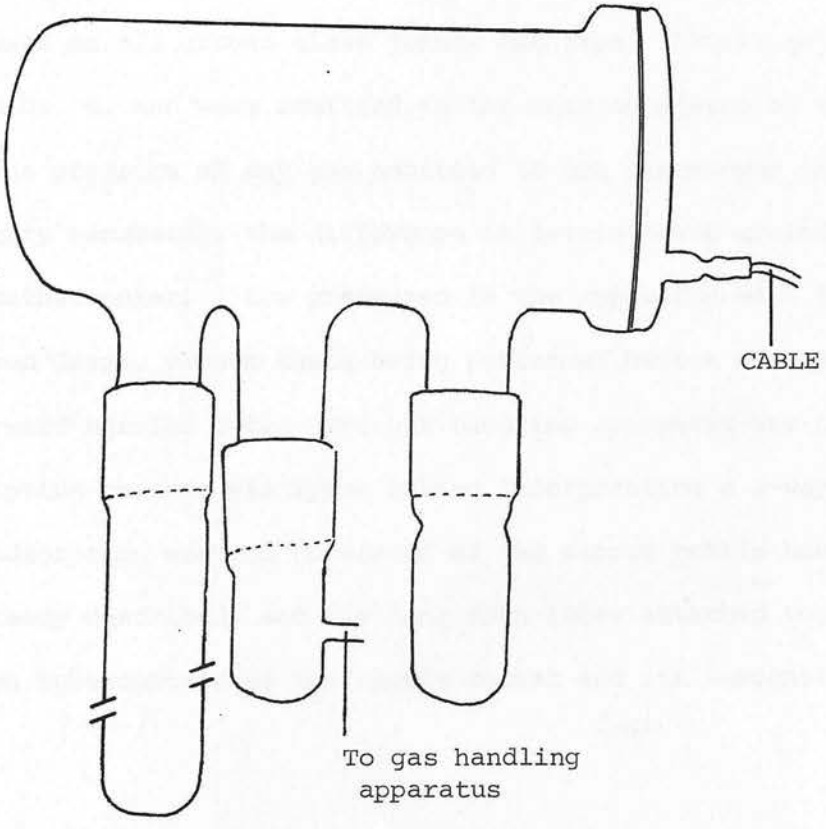


Fig. 5.4. The Vacuum Bottle in which the Balance is placed.

The zeolite samples were contained in a specially fabricated aluminium foil bucket with a nichrome wire handle. This was suspended from loop A by a nichrome hang-down wire (length ∿1 m). The maximum load which could be suspended from loop A was 1 g. The counter weight, comprising of small pieces of metal supported on a stirrup and pan arrangement, was suspended from loop C by a hang down wire.

The electrobalance was housed in a large vacuum bottle (Fig. 5.4) fastened to the wall. A metal cap, clamped in position with springs, accommodated the electrical connecting cable. A vacuum seal was provided by a Viton O-ring and high vacuum silicon grease. The suspension wires of the sample and counter weight passed through ground glass joints into attached cylindrical adsorption vessels. A third joint connected the balance chamber to the gas handling apparatus.

b) The Vacuum Line

The apparatus used comprised of a gas handling section and an adsorption section. The gas handling apparatus, illustrated schematically in Fig. 5.5, was constructed of Pyrex glassware. Apiezon 'L' grease was used on all ground glass joints and taps. Purified gases were stored in bulbs, G, and were admitted to the main apparatus by manipulation of taps. The pressure of any gas admitted to the system was measured using a mercury manometer, the difference in levels being measured by means of a cathetometer. Low pressures in the apparatus were detectable using a McLeod Gauge, vacuum tests being performed before adsorption experiments were carried out. The gas handling apparatus was connected to the adsorption chamber via Pyrex tubing incorporating a 2-way tap.

The adsorption section consisted of the vacuum bottle housing the balance, already described, and the hang down tubes attached to it. The hang down tube containing the sample bucket and its suspension wire

Fig. 5.5 Gas Handling Apparatus for Adsorption Studies

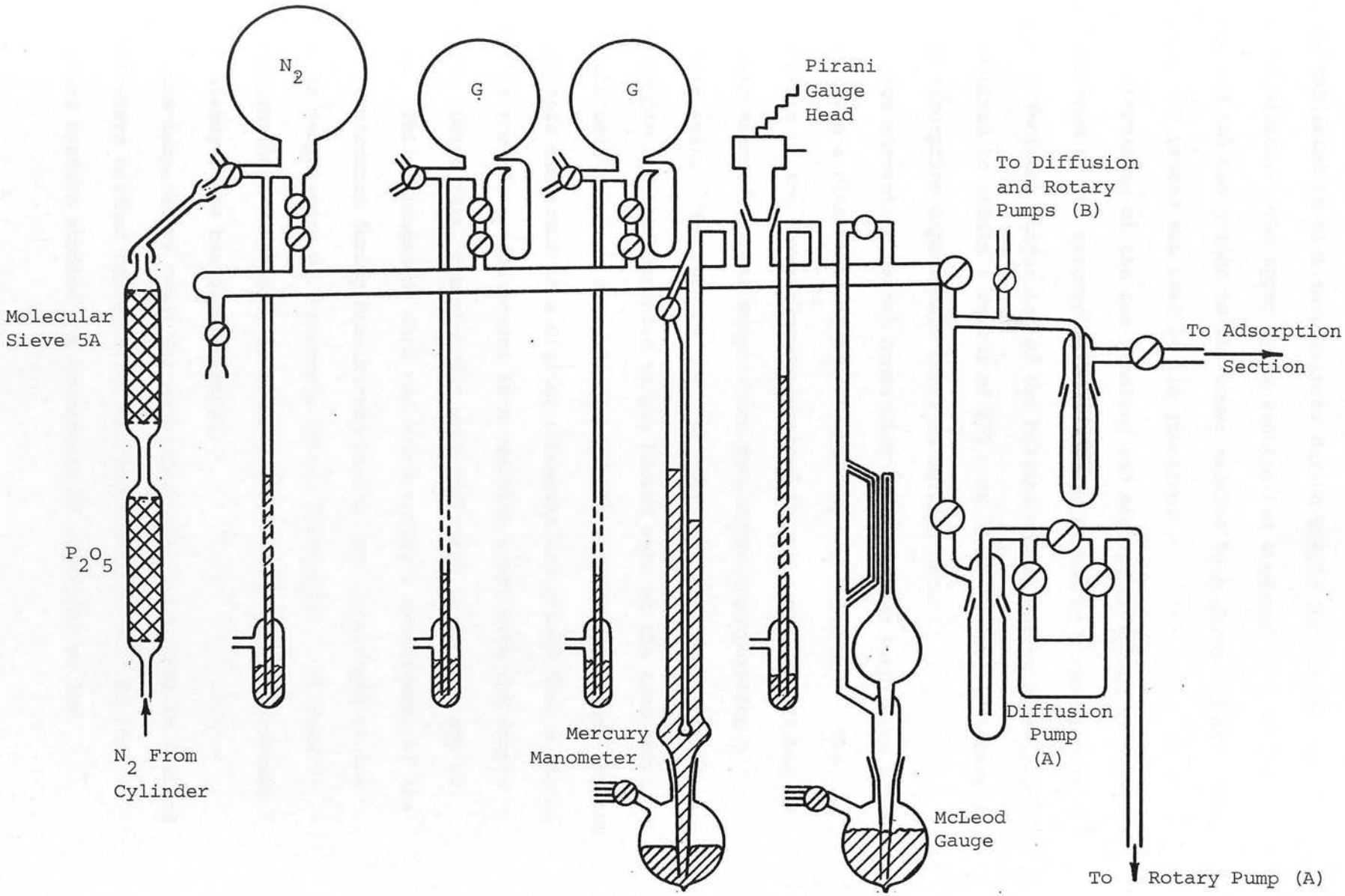


Fig. 5.5

was in two sections to facilitate its removal. The lower section, often subjected to high temperatures during sample outgassing, was made of silica. The upper Pyrex section had a graded seal at its lower end and was joined to the lower section by a ground silica joint. Apiezon 'T' grease was used at the junction.

Evacuation of the gas handling and adsorption apparatus was accomplished by two mercury diffusion pumps backed by vacuum rotary pumps. Thorough outgassing of the balance and extensive glassware was required to obtain a vacuum of 133 $\mu$ $Nm^{-2}$ ($10^{-6}$ torr) necessary before adsorption experiments could be carried out.

The adsorption vessel containing the suspended sample was outgassed using a close-fitting non-inductively wound furnace. The temperature of the furnace was controlled by a thermocouple linked to a Stanton Redcroft linear Temperature Programmer incorporating a Eurotherm unit. The furnace was positioned so that the furnace thermocouple and the suspended sample bucket were at the same level. To enable more accurate determination of the sample temperature another thermocouple connected to a digital voltmeter,was placed down a silica pocket in the adsorption vessel in a position level with the sample bucket. Using this, temperatures were evaluated to an accuracy of 0.25 K. This arrangement does not allow accurate measurement of the sample temperature during heating and cooling nor monitoring of the change in temperature of the sample during adsorption. It does however provide a reasonably accurate measurement of the temperature once a steady state has been attained.

The temperature range for meaningful adsorption data is limited to that where neither condensation nor reaction occurs. In the adsorption systems studied the occurrence of reactions at low

temperatures necessitated the use of slush baths. Suitable slush baths in the limited temperature range are cyclohexane; 280 K, tetrachloromethane; 250 K, and arklone; 236 K. The preparation of these baths is described in Section 5.2.1. Occasional replenishing of the baths was required to maintain a constant temperature over the long duration of the adsorption experiments. The temperature of the sample was taken to be the same as that of the bath after the adsorption vessel has been immersed for periods in excess of one hour. The thermocouple in the side pocket of the adsorption vessel provided a guide to the equilibration of temperatures inside and outside the adsorption vessel.

5.4.2. Procedure

Before use the balance was calibrated according to the manufacturer's instructions using accurately standardised weights. Balance constraints limited the maximum weight loss which could be monitored directly to 100 mg. Since sample weight losses of ∿20% were often observed; a sample weight of 300 mg was chosen, counterbalanced by a suitable substitution weight. The precise weight of the sample was determined by summation of the mass dial value, the recorder deflection and the substitution weight.

The adsorption section of the apparatus was evacuated. It was always necessary to remove and admit gases slowly to minimise disturbance of the balance system and prevent "spurting" of the zeolite. The samples were outgassed at pretreatment temperatures similar to those used in catalytic experiments until no further weight loss was detectable.

During preliminary experiments a considerable increase in sample weight was observed when the furnace was switched off and lowered;

a gain of approximately 300 μg being recorded in the time taken to cool to isotherm temperature. This 'gettering' continued at isotherm temperatures at approximately 0.006 mg $min^{-1}$ although the rate was neither linear with time nor reproducible making control experiments of little use. However, the rate of gettering was reduced by following a procedure used by Day et al.[232] After outgassing, dry nitrogen gas was admitted to the adsorption vessel to a pressure of ∿20 k $Nm^{-2}$ (160 torr). The reaction vessel was allowed to cool to the appropriate isotherm temperature after which the pressure was reduced to $1.3 \times 10^{-3} Nm^{-2}$ ($10^{-5}$ torr) by pumping for approximately 30 minutes. The weight of the sample was recorded at this point and constituted the zero of the isotherm. Successive doses of purified adsorbate were admitted to the adsorption section and for each dose at equilibrium the weight of the sample and the equilibrium pressure were recorded.

Where preliminary work indicated that adsorption and desorption isotherms were concurrent in the partial pressure ranges studied the isotherms were determined by desorption measurements for convenient manipulation of the balance. In addition equilibrium was generally established more rapidly by desorption than by adsorption. This may be a consequence of the significant alteration of the temperature of the adsorption system by the admission of successive doses of adsorbate at room temperature. Re-equilibration to the isotherm temperature would therefore require an appreciable time particularly at low pressures . Conversely alteration of the equilibrium pressure by desorption does not disturb the temperature of the adsorption system to any appreciable extent.

The gravimetric arrangement used facilitated a continuous recording of sample weight both on admission and removal of the adsorbate to and from the adsorption section. However, the initial disturbance caused

by introduction of the gas to the evacuated chamber persisted for about six seconds prohibiting measurements during this period.

The basic pattern used in these experiments involved regeneration of the sample after each adsorption/desorption run by outgassing at elevated temperatures (erionite; 623 K, zeolite omega; 773 K). The original outgassed weight of the sample was attained and good reproducability of adsorption results ($\pm$2%) was observed.

### 5.4.3. Treatment of Results

The problem of gettering makes results impossible to analyse accurately in a quantitative manner particularly for certain sorbates over erionite where the rates of adsorption are slow. However, where possible, quantitative results are presented.

During adsorption or desorption the recorder trace shows the variation of sample weight with time and hence gives a measure of the rate of adsorption and desorption processes. Adsorption on external surface only, rapid sorption into the pores and an apparently diffusion controlled sorption may be distinguished. Diffusion control of sorption may be indicated by plotting increase in sample weight against $t^{\frac{1}{2}}$ according to Eqn. (2. 2 ). A straight line is indicative of diffusion control although a foot due to adsorption on the external surface is often observed at the beginning of the adsorption.

Buoyancy effects in gravimetric studies arise from differences in volume and temperature between the sample and its container on the one hand and the counter weight on the other. In this work the buoyancy effects have been calculated from Eqn. (5.6.) and allowed for in the calculations of the weight adsorbed.

$$\Delta W = \frac{M}{R}\left(\frac{V_C}{T_C} - \frac{V_B}{T_B}\right) .p. \qquad \text{Eqn.(5.6)}$$

where

$\Delta W$ = Difference in upthrust on the two sides.

M = Molecular weight of the adsorbate.

R = Gas constant.

$V_B$ = Volume of bucket and sample.

$T_B$ = Temperature of bucket and sample.

$V_C$ = Volume of counter weight.

$T_C$ = Temperature of counter weight.

p = Pressure of the adsorbate.

Buoyancy corrections are very small at low pressures but become considerable at higher pressures.

## 5.5. Other Techniques

### 5.5.1. X-Ray diffraction

X-ray diffraction traces were obtained using a Phillips instrument utilising Cu Kα radiation. The catalysts were examined before and after pretreatment and catalytic experiments.

### 5.5.2. Surface Area Measurements

The surface areas of zeolite samples studied were determined by nitrogen adsorption at 78 K in a constant volume apparatus. A measured volume of gas is admitted to the sample, after equilibrium has been established the pressure can be measured and the amount of gas remaining in the gas phase calculated. The difference in these two quantities corresponds to the volume of adsorbate adsorbed. Results are plotted according to the B.E.T. equation. (Eqn. 5.7).

$$\frac{P}{x(P_o - P)} = \frac{1}{X_m C} + \frac{C-1}{X_m C} \cdot \frac{P}{P_o} \qquad \text{Eqn. (5.7)}$$

where

$P$ = Equilibrium gas pressure at the isotherm temperature.

$x$ = Volume of gas adsorbed at pressure P.

$P_o$ = Saturated vapour pressure of the adsorbate at the isotherm temperature.

$X_m$ = Volume equivalent to monolayer coverage of the surface.

$C$ = A constant.

According to this when $P/x(P_o-P)$ is plotted against $P/P_o$ a straight line should result, with slope $S = (C-1)/X_m C$ and intercept $I = 1/X_m C$. Rearrangement and elimination of C gives $X_m = \frac{1}{S+I}$. The specific surface $SA(m^2 g^{-1})$ is related to the monolayer capacity $X_m$ by Eqn. (5.8)

$$SA = \frac{X_m}{M} \cdot N \cdot A_m \times 10^{-20} \qquad \text{Eqn. (5.8)}$$

where

$N$ = Avogadro's constant.

$A_m$ = Molecular cross-sectional area of the adsorbate.

$X_m$ is expressed in grams of adsorbate per gram of solid.

Monolayer capacities and hence surface areas were also calculated using the point B method.

### 5.5.3. X-Ray Fluorescence Spectroscopy

The compositions of the zeolite samples used in this thesis were analysed by X-ray fluorescence spectroscopy.* The theory and applications of this technique are described elsewhere.[213]

*X-ray fluorescence analyses were kindly carried out by G. Angell of the Geology Department, University of Edinburgh.

# Chapter 6

## Results and Discussion - Part I

## Characterisation of the Zeolites

### 6.1. Nature of the Catalysts

#### 6.1.1 X-Ray Fluorescence Analysis

The results of the chemical analyses of the zeolites omega and erionite by X-ray fluorescence spectroscopy are given in Table 6.1. In the table and in the ensuing chapters the two types of erionite studied in this thesis are referred to as erionite (N) - natural erionite and erionite (T) - treated erionite.

| | Zeolite Ω | Erionite (N) | Erionite (T) |
|---|---|---|---|
| | % | % | % |
| CaO | 0.2 | 1.7 | 2.7 |
| $K_2O$ | 0.11 | 5.07 | 3.80 |
| $Fe_2O_3$ | 0.10 | 1.2 | 2.8 |
| $TiO_2$ | 0.11 | 0.24 | 0.38 |
| $SiO_2$ | 63.8 | 60.3 | 62.1 |
| $Al_2O_3$ | 15.4 | 14.1 | 14.3 |
| | ppm | ppm | ppm |
| Ba | | 380 | 2540 |
| Zr | 80 | 380 | 520 |
| Sr | | 145 | 1460 |
| Rb | | 100 | 100 |

Table 6.1. Chemical Analyses of Zeolites by X-ray Fluorescence Spectroscopy

The typical oxide formulae of these zeolites, listed in the literature[47], are:

Zeolite Ω:- $(Na,TMA)_2O.Al_2O_3.7\ SiO_2.5H_2O$

Erionite:- $(Ca,Mg,Na_2K_2)O.Al_2O_3.6SiO_2.6H_2O$.

The analytical results of Table 6.1. therefore list the constituent species with the exceptions of $Na_2O$, MgO and $(TMA)_2O$. This is a consequence of the inability of the technique used to detect atoms of atomic weight less than or equal to that of magnesium.

Table 6.2. lists the ionic concentrations in terms of equivalents per gram atom of aluminium.

| Ion | Zeolite Ω | Erionite (N) | Erionite (T) |
|---|---|---|---|
| | Equiv./g.atom Al | Equiv./g.atom Al | Equiv./g.atom Al |
| Ca | .02 | .22 | .34 |
| K | .01 | .39 | .28 |
| Fe | .01 | .15 | .39 |

Table 6.2. Ionic Concentrations of Zeolites

Neutralisation of the charge in the zeolite lattice due to alumina tetrahedra ($AlO_4^-$) requires that the total number of counter-ion charges should equal the number of aluminium ions. In zeolite Ω therefore sodium and TMA ions must total the remaining 0.96 equiv./g.atom Al not accounted for by the species listed in Table 6.2.

It is not possible to reach a similar conclusion for erionite due to the presence of appreciable amounts of iron in both samples studied. Previously, iron impurities in zeolite Y have been reported to exist as $Fe^{3+}$ in the aluminosilicate framework, $Fe^{3+}$ acting as counter-ions and

as $Fe_3O_4$ or some similar compound occluded within the structure. Furthermore, the substitution of $Fe^{3+}$ ions for up to 15% of lattice aluminium in natural erionite has been demonstrated[159]. It is therefore possible that at least a proportion of the iron contained in the erionite samples may be located in lattice tetrahedral sites. In the case of erionite (N), a white zeolite, it would appear probable that the majority of the iron is located in such framework sites since, in general, colour is associated with transition metal ions in interstitial positions. Assuming that all the iron is in this type of site the unlisted ions $Na^+$ and $Mg^{2+}$ total 0.24 equiv./g.atom Al.

In contrast, the commercially treated erionite (T) is a pale orangey-brown colour indicative of the presence of iron in interstitial sites. If all the iron is present as counter-ions the total equiv./g.atom Al of the ions listed in Table 6.2. is 1.01; no $Na^+$ or $Mg^+$ ions would therefore be required to achieve electroneutrality. Although the exact nature of erionite (T) is unknown, reference to the patented literature[169] and analytical evidence suggest that a natural erionite has been ion exchanged with an aqueous Iron(III) solution following treatment with dimethyl sulphoxide. Dimethyl sulphoxide has been reported to remove a substantial amount of occluded iron, previously remaining intact in aqueous solution. Moreover repeated ion exchange would result in the removal of virtually all the $Na^+$ ions while leaving an appreciable number (2 per unit cell) of $K^+$ ions locked within the cancrinite cages of the structure[159]. Assuming the unit cell contents of erionite (T) are similar to typical literature values[47] $((CaMgNa_2K_2)_4(AlO_2)_8(SiO_2)_{26})$ each unit cell may be calculated to contain 2.3 $K^+$ ions. A similar calculation applied to erionite (N) results in a potassium content of 3.1 ions per unit cell. Therefore,

in view of the colour of the zeolite and the above arguments it would not seem unreasonable to conclude that only a small amount, if any, of the iron contained in erionite (T) is located in tetrahedral lattice sites and that the only counter-ionic species present to any appreciable extent are $Ca^{2+}$, $K^{+}$ and $Fe^{3+}$. Consequently there are considerable differences in the chemical compositions of the two types of erionite.

The Si/Al ratios of the zeolites studied were determined from data in Table 6.1. These experimental ratios, together with listed literature values of these and other commonly used zeolites, are shown in Table 6.3.

| Zeolite | Si/Al (Experimental) | Si/Al (Literature)[47] |
|---|---|---|
| Omega | 3.53 | 2.6-6.0 |
| Erionite (N) | 3.64 | 2.9-3.7 |
| Erionite (T) | 3.70 | |
| Zeolite A | | 0.7-1.2 |
| Mordenite | | 4.2-5.0 |
| Zeolite X | | 1.0-1.5 |
| Zeolite Y | | 1.5-3.0 |

Table 6.3. Si/Al Ratios of Some Zeolites

It is evident from the data in Table 6.3. that the zeolites studied in this thesis have similar Si/Al ratios, all of which are significantly higher than those of most commonly used zeolites excepting mordenite.

The tabulated Si/Al ratio of erionite (N) may be slightly higher than the true lattice value due to the probable substitution of $Fe^{3+}$ for lattice $Al^{3+}$ as discussed in the previous paragraphs.

Assuming all the iron contained in erionite (N) is in tetrahedral lattice sites the true lattice ratio, Si/(Al+Fe),would be 3.45. Similarly the lattice ratio of erionite (T) listed in Table 6.3. may be slightly high although as discussed previously only a small amount of iron substitution in the lattice is suggested.

In the synthesis of zeolite Ω, Aiello and Barrer[35] have reported smooth relationships between the cation fraction of TMA in the parent gel, the Si/Al ratio and the cation fraction of TMA in the zeolite. Application of this correlation to the observed Si/Al ratio yields a value of 0.21 for the cation fraction of TMA ions in the sample of zeolite Ω studied. Hence the approximate unit cell contents of this sample are:-

$$Na_{6.3}TMA_{1.7}(AlO_2)_8(S_1O_2)_{28}.21\ H_2O.$$

6.1.2.X-Ray Diffraction

X-ray powder diffraction traces of the zeolites Ω and erionite are depicted in Figs. 6.1. and 6.2. Diffraction analysis of the zeolites before and after pretreatment enabled their crystallinity to be assessed in a qualitative manner.

a) Zeolite Ω

The relative intensities of the peaks and the observed d-spacings (calculated from the diffraction traces using the Bragg equation $2d \sin \theta = \lambda$) were in good agreement with literature values[35]. Samples pretreated at elevated temperatures displayed traces in which all peaks were weaker relative to background noise than those observed for the hydrated sample. The angles however were not altered. This is illustrated in Fig. 6.1. which compares the diffraction traces obtained from hydrated zeolite Ω and a sample outgassed at 948 K for

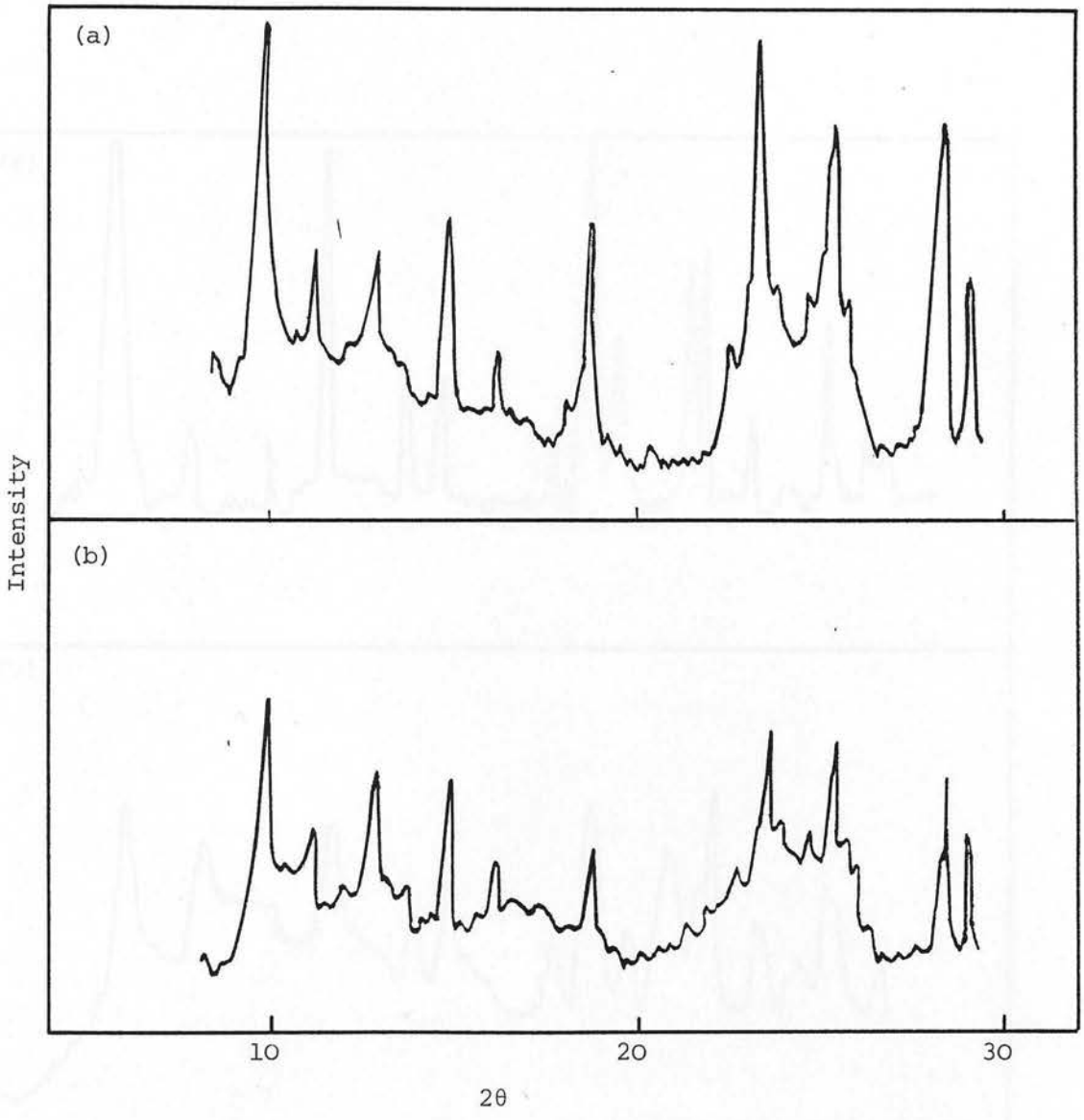


Fig. 6.1. X-ray Diffraction Traces of Zeolite Ω

(a) Hydrated zeolite Ω

(b) Zeolite Ω outgassed at 948 K for 16 hours

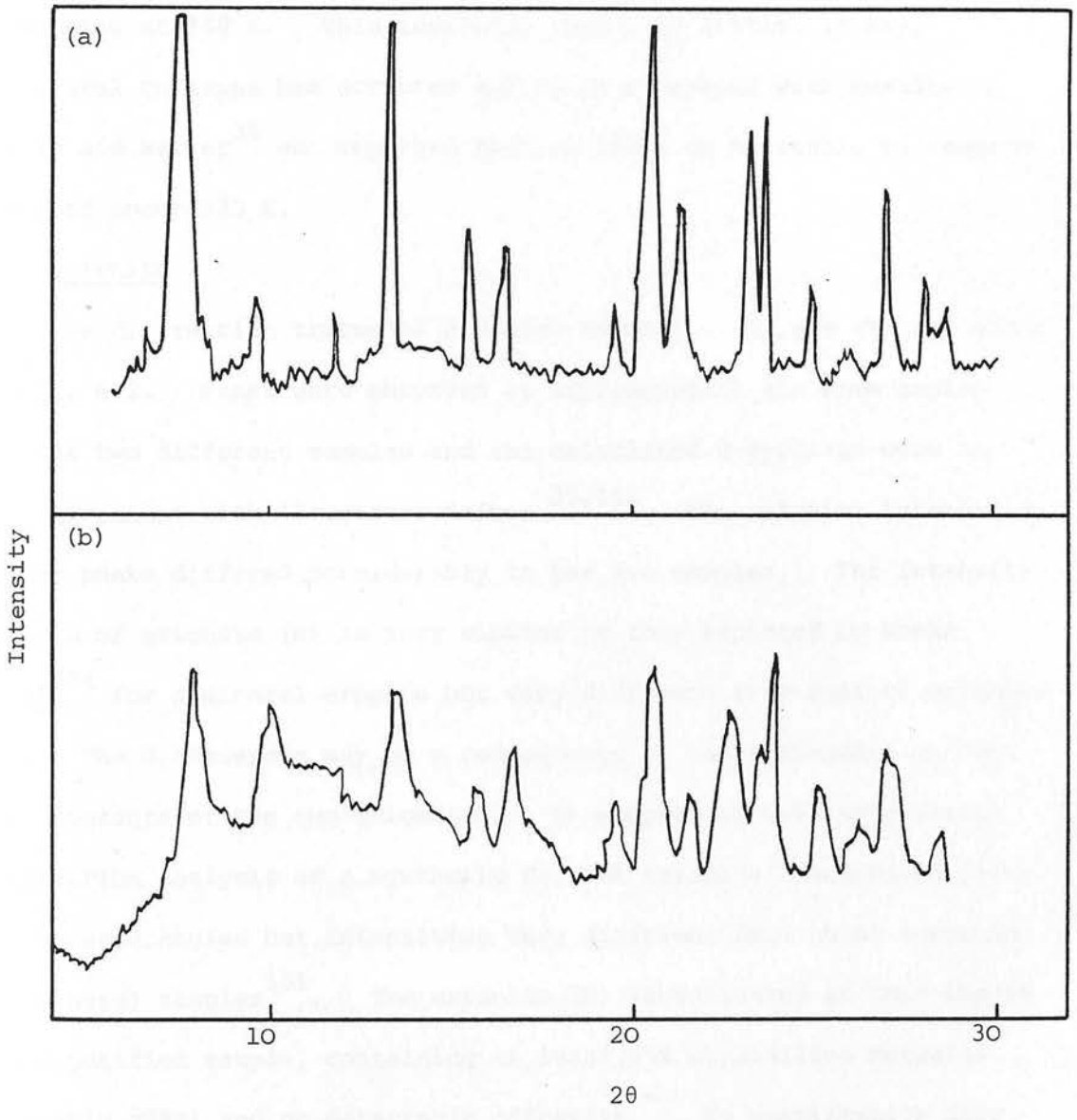


Fig. 6.2. Diffraction Traces of Erionite Samples

(a) Erionite (N)*

(b) Erionite (T)

*Diffraction trace of erionite(N) supplied by Prof. Mumpton

16 hours. In addition to the decrease in overall intensity of the peaks the relative intensities are also altered slightly. Since the angles at which peaks are observed depend only on the size and shape of the unit cell whereas their relative intensities depend on unit cell contents, an alteration in the latter may be expected as a result of removal of water and TMA ions by outgassing. All the peaks detected in the trace from the hydrated sample are still present after outgassing at 948 K. This indicates that very little, if any, structural collapse has occurred and is in agreement with results of Aiello and Barrer[35] who reported zeolite TMA-Ω to be stable to temperatures of about 973 K.

b) Erionite

The diffraction traces of hydrated erionites (N) and (T) are shown in Fig. 6.2. Peaks were observed at approximately the same angles for the two different samples and the calculated d-spacings were in good agreement with literature values.[35,151] The relative intensities of the peaks differed considerably in the two samples. The intensity pattern of erionite (N) is very similar to that reported by Weeks et al[234] for a mineral eronite but very different from that of erionite (T). The differences may be a consequence of the difference in unit cell contents of the two erionites. In support of this suggestion, diffraction analysis of a synthetic Na, TMA erionite[35] exhibited peaks at the same angles but intensities very different from those reported for mineral samples[151]. The erionite (N) investigated in this thesis was a purified sample, containing at least 95% crystalline material (probably >99%) and no detectable offretite.* No quantitative data

*X-ray diffraction, quantitative crystallinity analysis and determination of the absence of offretite were carried out by Prof. Mumpton of New York State University.

concerning the crystallinity of erionite (T) nor the presence of offretite intergrowths are available.

Diffraction traces of erionite (T) obtained after outgassing at catalytic pretreatment temperatures (643 K) showed no significant alteration of peak angles although the total intensity decreased.

### 6.1.3. Surface Areas

The surface areas of zeolites Ω and erionite were determined by nitrogen adsorption, data being plotted according to the BET equation (Eqn.5.7.) A typical plot is illustrated in Fig. 6.3. These measurements enabled the crystallinity of the zeolite samples, pretreated at different temperatures, to be determined in a more quantitative manner than is possible by X-ray diffraction. Moreover surface area measurements provide evidence of partial crystallinity not detectable by X-ray diffraction.

a) Zeolite Ω

The surface areas of samples of zeolite Ω outgassed for 16 hours in the temperature range 654 K - 1033 K vary considerably with outgassing temperature as illustrated in Fig. 6.4. Increased pretreatment temperature results in larger surface area values until a relatively sharp maximum (ca. 287 $m^2 g^{-1}$) is attained at ca. 845-870 K. At outgassing temperatures greater than this the surface area decreases with further increase in the outgassing temperature.

In general, temperatures of 623-673 K are required to dehydrate zeolites. To achieve maximum sample surface area for zeolite Ω elevated outgassing temperatures are necessary to remove the bulky TMA ions from their locations in the gmelinite cages. Evidence of carbon deposition on samples outgassed for 16 hours at temperatures greater than 783 K

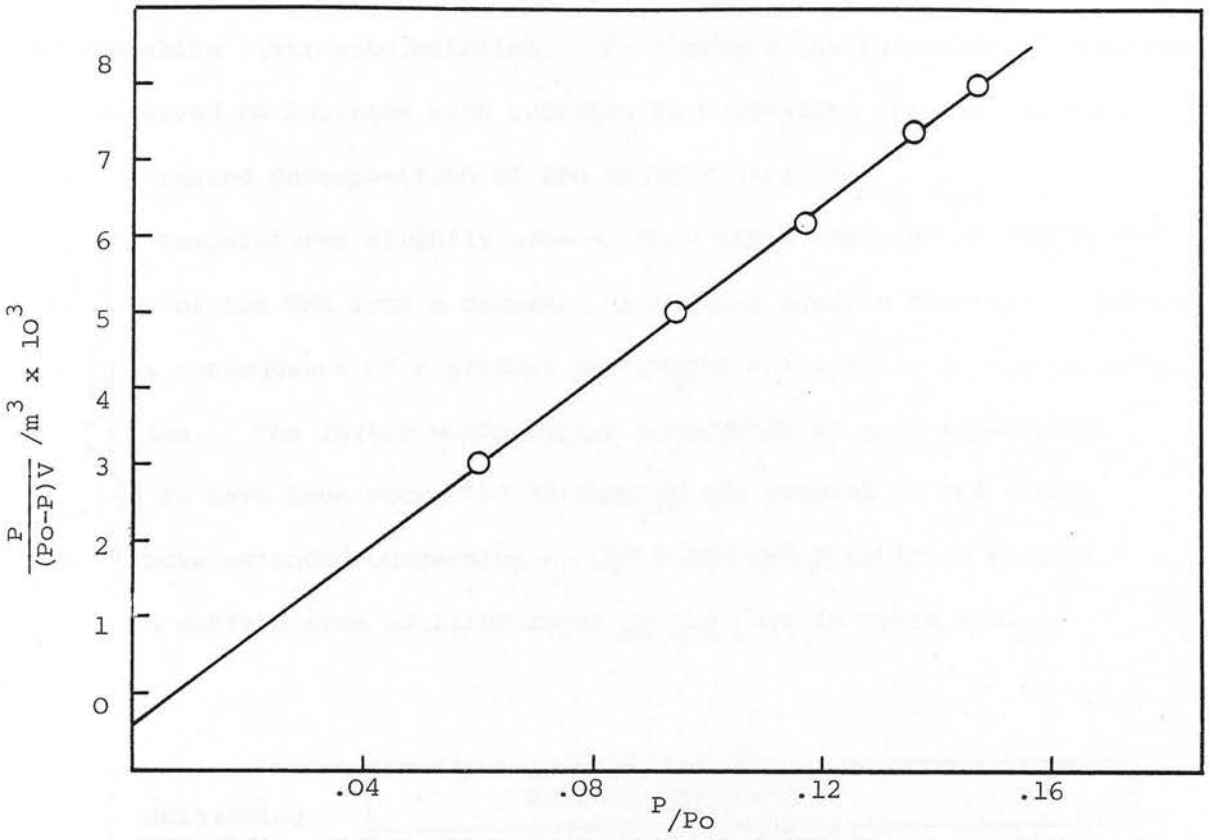


Fig. 6.3. B.E.T. Plot for Zeolite Ω (.2901g) outgassed for 16 hours at 823 K

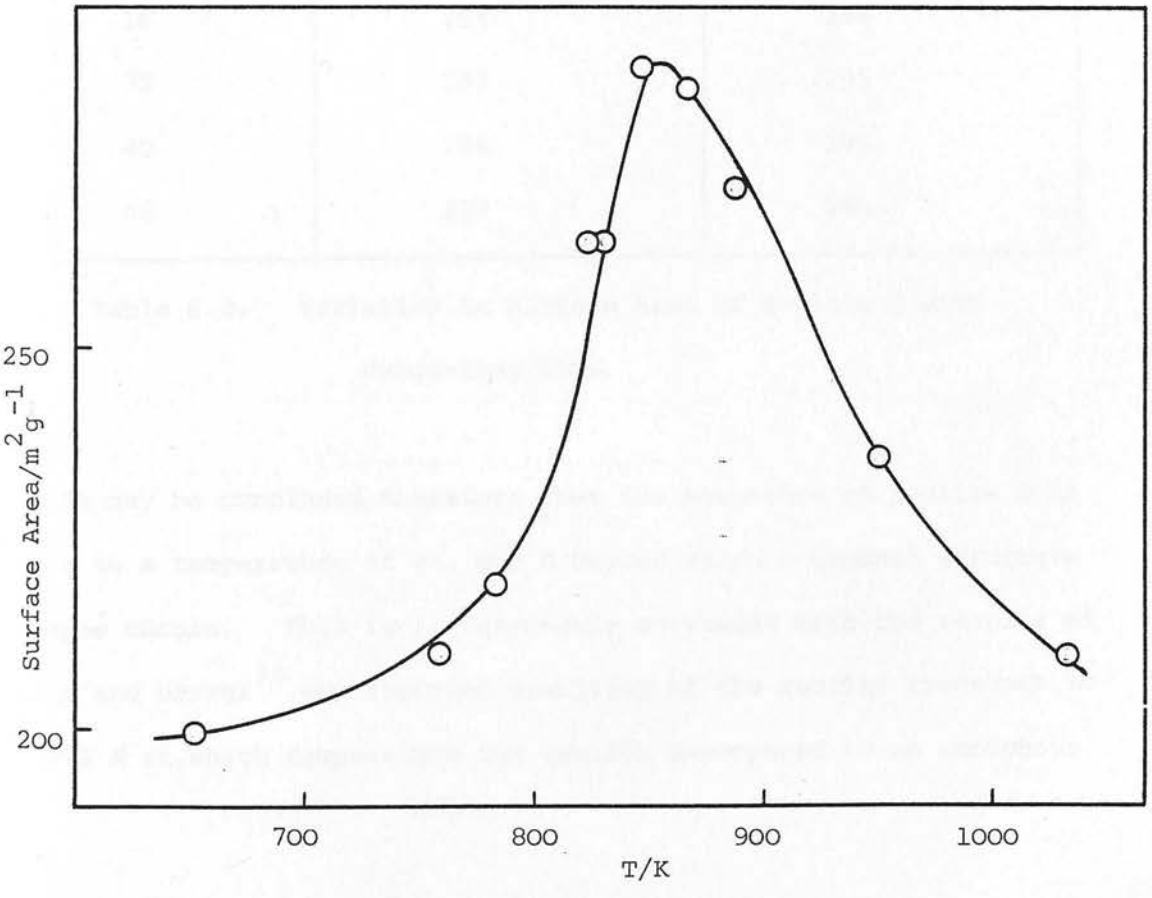


Fig. 6.4. Variation in Surface Area of Zeolite Ω with Outgassing Temperature (16 hours)

was shown by the grey coloration of the outgassed samples in comparison to the white untreated material. Furthermore the intensity of greyness was observed to increase with increase in outgassing temperature i.e. with increased decomposition of the organic cations.

At temperatures slightly greater than those required to remove the majority of the TMA ions a decrease in surface area is observed. This may be a consequence of a gradual structural collapse or be due to carbon deposition. The latter would appear improbable as such deposition appears to have been occurring throughout the removal of TMA ions. Furthermore extended outgassing at 828 K and 868 K exhibits no such decay in surface area as illustrated by the data in Table 6.4.

| Outgassing Time/hr | Surface Area / $m^2 g^{-1}$ | |
|---|---|---|
| | Outgassing Temperature = 828 K | Outgassing Temperature = 868 K |
| 16 | 264 | 284 |
| 32 | 293 | 295 |
| 40 | 296 | 295 |
| 48 | 297 | 296 |

Table 6.4. Variation in Surface Area of Zeolite Ω with Outgassing Time.

It may be concluded therefore that the structure of zeolite Ω is stable to a temperature of ca. 868 K beyond which a gradual structure collapse occurs. This is in reasonable agreement with the results of Aiello and Barrer[35] who reported stability of the zeolite framework to ca. 973 K at which temperature the zeolite decomposed to an amorphous

product. However these workers, using X-ray diffraction were unable to detect any partial loss of crystallinity as reported here. Very different results have been reported[176] for an ammonium exchanged TMA Ω zeolite, substantial loss of crystallinity being observed at 773 K with formation of an amorphous material at 873 K.

Results in Table 6.4. indicate that the maximum surface area of zeolite Ω (ca. 297 $m^2g^{-1}$) may be attained by outgassing at 828 K for periods in excess of 40 hours or at 868 K for slightly shorter periods.

b) Erionite

A similar survey of the effect of pretreatment temperature and time on the surface area of the erionite samples was carried out. The results are listed in Tables 6.5. and 6.6.

| Outgassing Temperature/K | Outgassing Time/hr | Surface Area/$m^2g^{-1}$ |
|---|---|---|
| 601 | 16 | 320 |
| 675 | 16 | 320 |
| 741 | 16 | 321 |
| 868 | 16 | 320 |
| 923 | 16 | 323 |
| 1003 | 16 | 299 |
| 1053 | 16 | 34 |

Table 6.5. Effect of Pretreatment Temperature on Surface Area of Erionite (N)

| Outgassing Temperature/K | Outgassing Time/hr | Surface Area/$m^2g^{-1}$ |
|---|---|---|
| 589 | 16 | 222 |
| 687 | 16 | 226 |
| 687 | 32 | 227 |
| 745 | 16 | 223 |
| 793 | 16 | 222 |
| 958 | 16 | 214 |
| 958 | 32 | 200 |
| 958 | 45 | 182 |

Table 6.6. Effect of Pretreatment Conditions on the Surface Area of Erionite (T)

In agreement with these BET surface area measurements, values of 316 $m^2g^{-1}$ and 220 $m^2g^{-1}$ for erionite (N) and (T) respectively were obtained from gravimetric measurement of nitrogen adsorption, analysing the results by the point B method. Although a small difference in surface area may result as a consequence of the difference in chemical compositions, the large difference observed suggests the presence of different amounts of amorphous material in the two samples. Erionite (N) is a purified sample containing >95% (probably >99%) crystalline material whereas the degree of crystallinity of erionite (T) is unknown.

The lack of variation in surface area at outgassing temperatures between 589 K and 923 K indicates that all the occluded water is easily removed by outgassing for 16 hours at temperatures $\geqslant$ 589 K. A previous thermochemical study[234] of an ammonium exchanged mineral erionite

demonstrated water loss between room temperature and 523 K. The data in Tables 6.5. and 6.6. demonstrate the high thermal stability of erionite, no loss in crystallinity being observed until outgassing temperatures in excess of 923 K are used. At temperatures slightly higher than this a gradual collapse of structure is evident from the small decrease in surface area of erionite (T) with extended outgassing at 958 K. Complete crystal collapse of erionite (N) appears to occur at temperatures between 1003 and 1053 K resulting in a more or less amorphous material. From X-ray diffraction studies of an ammonium exchanged mineral erionite, Weeks et al[234] have reported the occurrence of extensive crystal degradation by 1073 K.

### 6.1.4. Thermogravimetric Analysis

Thermogravimetric analysis of zeolite Ω was carried out using the microbalance. The sample was outgassed at successively higher temperatures, each temperature being maintained until the sample weight remained constant. A plot of zeolite weight loss with outgassing time at 823 K is shown in Fig. 6.5. The weight losses (expressed in milligrams per gram of hydrated zeolite) at the various outgassing temperatures are listed in Table 6.7.

| Outgassing Temperature/K | Weight Loss mg/g | % Weight Loss |
|---|---|---|
| 582 | 138.85 | 13.88 |
| 661 | 143.71 | 14.37 |
| 721 | 148.0 | 14.80 |
| 823 | 192.38 | 19.24 |
| 868 | 192.74 | 19.27 |

Table 6.7. Weight Loss from Zeolite Ω as a Function of Outgassing Temperature

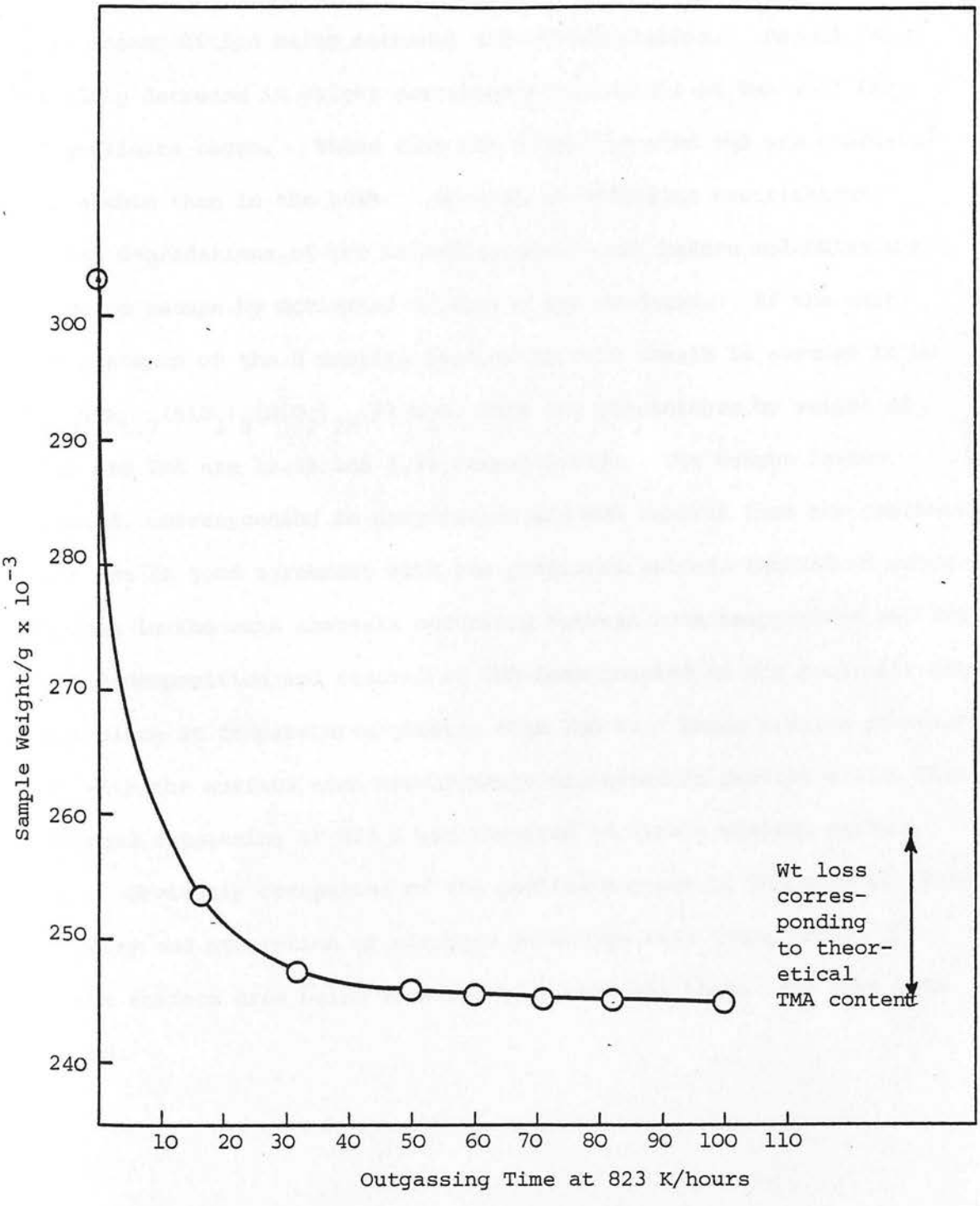


Fig. 6.5. Wt of TMA-Ω Zeolite as a Function of Outgassing Time at 823 K.

The small weight loss evident between 582 K and 721 K could be due to removal of water or TMA ions located in the wide main channels. Cole and Kouwenhoven[174] have previously reported the removal of TMA ions from these sites by evacuation at 623 K, the major products of their decomposition being methanol and trimethylamine. Beyond 720 K the sharp decrease in weight corresponds to removal of TMA ions from the gmelinite cages. These ions are firmly encaged and are thermally more stable than in the bulk. Because of diffusion restrictions further degradations of the molecules must occur before molecules small enough to escape by activated diffusion are produced. If the unit cell contents of the Ω zeolite studied in this thesis is assumed to be $Na_{6.3}{}^{TMA}{}_{1.7}(AlO_2)_8(SiO_2)_{28}.21\ H_2O$. then the percentages by weight of water and TMA are 13.5% and 4.5% respectively. The weight losses observed, corresponding to dehydration and TMA removal from the gmelinite cages are in good agreement with the predicted values, removal of water and TMA ions in the main channels occurring between room temperature and 720 K while decomposition and removal of TMA ions located in the gmelinite cages takes place at temperatures greater than 720 K. These results correlate well with the surface area measurements discussed in Section 6.1.3. where prolonged outgassing at 823 K was required to attain maximum surface area. Obviously occupation of the gmelinite cages by TMA ions prevents the entry and adsorption of nitrogen molecules into these pores, the maximum surface area being measured only when all these ions have been removed.

## 6.2. Adsorption Studies

### 6.2.1. Omega Zeolite

#### a) Adsorption and Desorption of $C_4H_8$ Isomers

The adsorptions of but-1-ene, cis and trans but-2-ene and methylcyclopropane (MCP) on zeolite Ω were investigated after thorough outgassing of the zeolite had removed all the water and tetramethylammonium ions. Rapid adsorption and desorption was observed for all adsorbates, equilibrium being attained more quickly on desorption. This is not unreasonable since admission of a dose of adsorbate at a temperature different from that of the isotherm results in a considerable temperature fluctuation in the adsorbent. Such an effect is not caused by desorption of material from the system. Increase in weight of the zeolite as a result of adsorption of but-1-ene and trans but-2-ene at 243 K as a function of time are illustrated in Figs. 6.6.(a) and (b) respectively. Similar profiles were observed for all adsorbates at all the temperatures studied although the total amount adsorbed after admission of a constant external pressure varied with the adsorbate. The amounts of n-butenes adsorbed at 237 K after admission of 57.2 k $Nm^{-2}$ are listed in Table 6.8. Results are expressed as mg/g of hydrated zeolite.

| Adsorbate | External Pressure Admitted/k $Nm^{-2}$ | Weight Adsorbed mg/g |
|---|---|---|
| But-1-ene | 57.2 | 51.72 |
| Trans but-2-ene | 57.2 | 59.46 |
| Cis but-2-ene | 57.2 | 67.9 |

Table 6.8. Weights of n-butenes adsorbed by Zeolite Ω

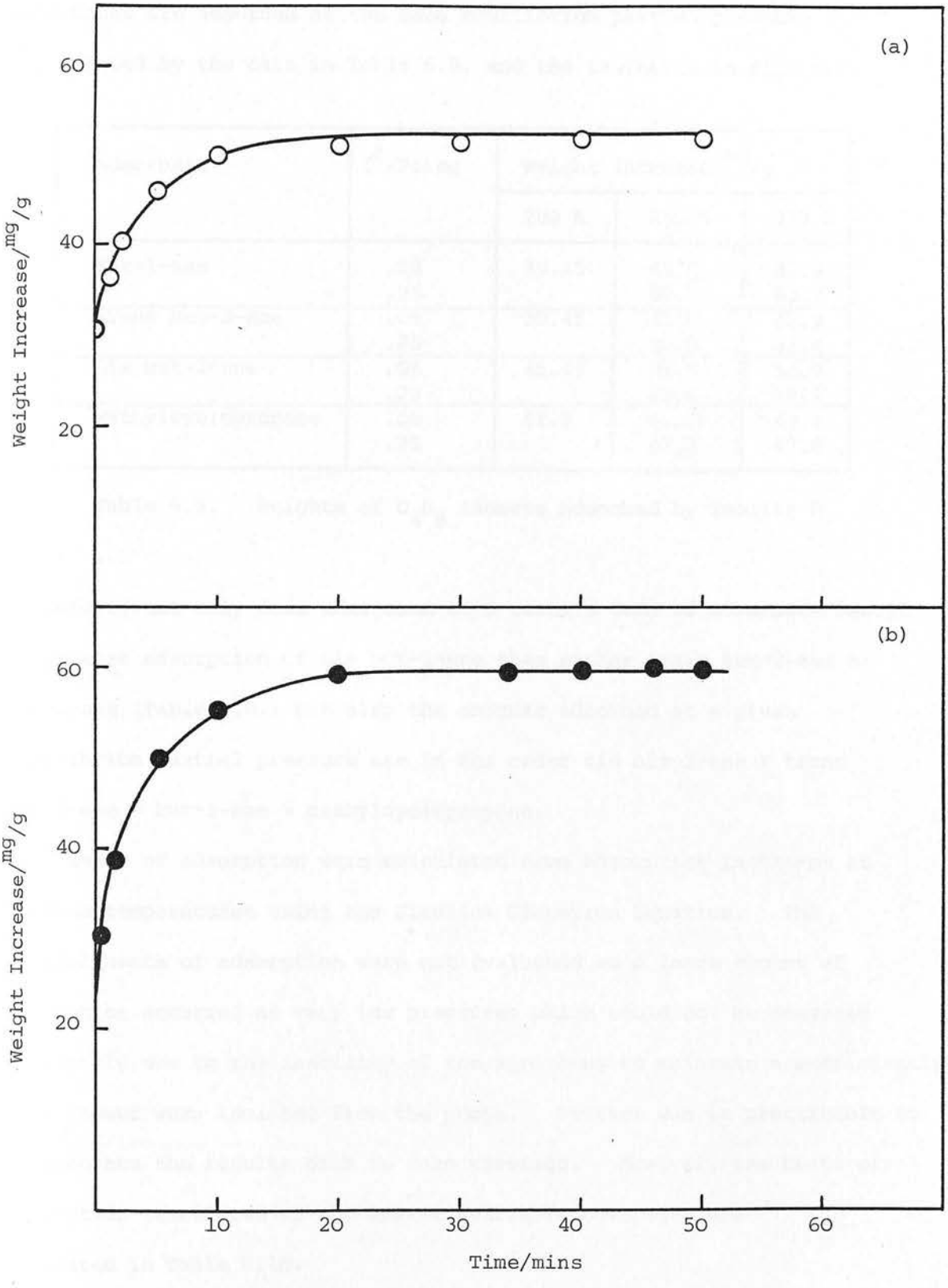


Fig.6.6. Rates of Adsorption on Zeolite Ω at 236 K

(a) But-1-ene )
(b) Trans But-2-ene ) External pressure admitted = 57.2 k $Nm^{-2}$

Adsorption isotherms, of which those in Figs. 6.7. and 6.8. are typical examples, were obtained for the adsorbates at the following temperatures:- 237 K, 250 K and 280 K. Different amounts of adsorbates are adsorbed at the same equilibrium partial pressure as illustrated by the data in Table 6.9. and the isotherms in Fig. 6.8.

| Adsorbate | $(P/Po)_{eq}$ | Weight Increase/mg/g | | |
|---|---|---|---|---|
| | | 280 K | 250 K | 237 K |
| But-1-ene | .06 | 39.45 | 42.5 | 42.9 |
| | .25 | | 49.7 | 50.7 |
| Trans but-2-ene | .06 | 39.45 | 41.6 | 41.9 |
| | .25 | | 50.0 | 51.4 |
| Cis but-2-ene | .06 | 45.45 | 51.8 | 53.9 |
| | .25 | | 62.4 | 67.2 |
| Methylcyclopropane | .06 | 42.9 | 42.9 | 40.3 |
| | .25 | | 47.2 | 47.6 |

Table 6.9. Weights of $C_4H_8$ Isomers Adsorbed by Zeolite Ω

Therefore, not only does admission of a certain dose of adsorbate result in greater adsorption of cis but-2-ene than either trans but-2-ene or but-1-ene (Table 6.8.) but also the amounts adsorbed at a given equilibrium partial pressure are in the order cis but-2-ene > trans but-2-ene ∿ but-1-ene ∿ methylcyclopropane.

Heats of adsorption were calculated from adsorption isotherms at various temperatures using the Clausius Clapeyron Equation. The initial heats of adsorption were not evaluated as a large amount of adsorption occurred at very low pressures which could not be measured accurately due to the inability of the apparatus to maintain a sufficiently good vacuum when isolated from the pumps. Neither was it practicable to extrapolate the results back to zero coverage. However, the heats of adsorption calculated at the lowest available coverages are tabulated in Table 6.10.

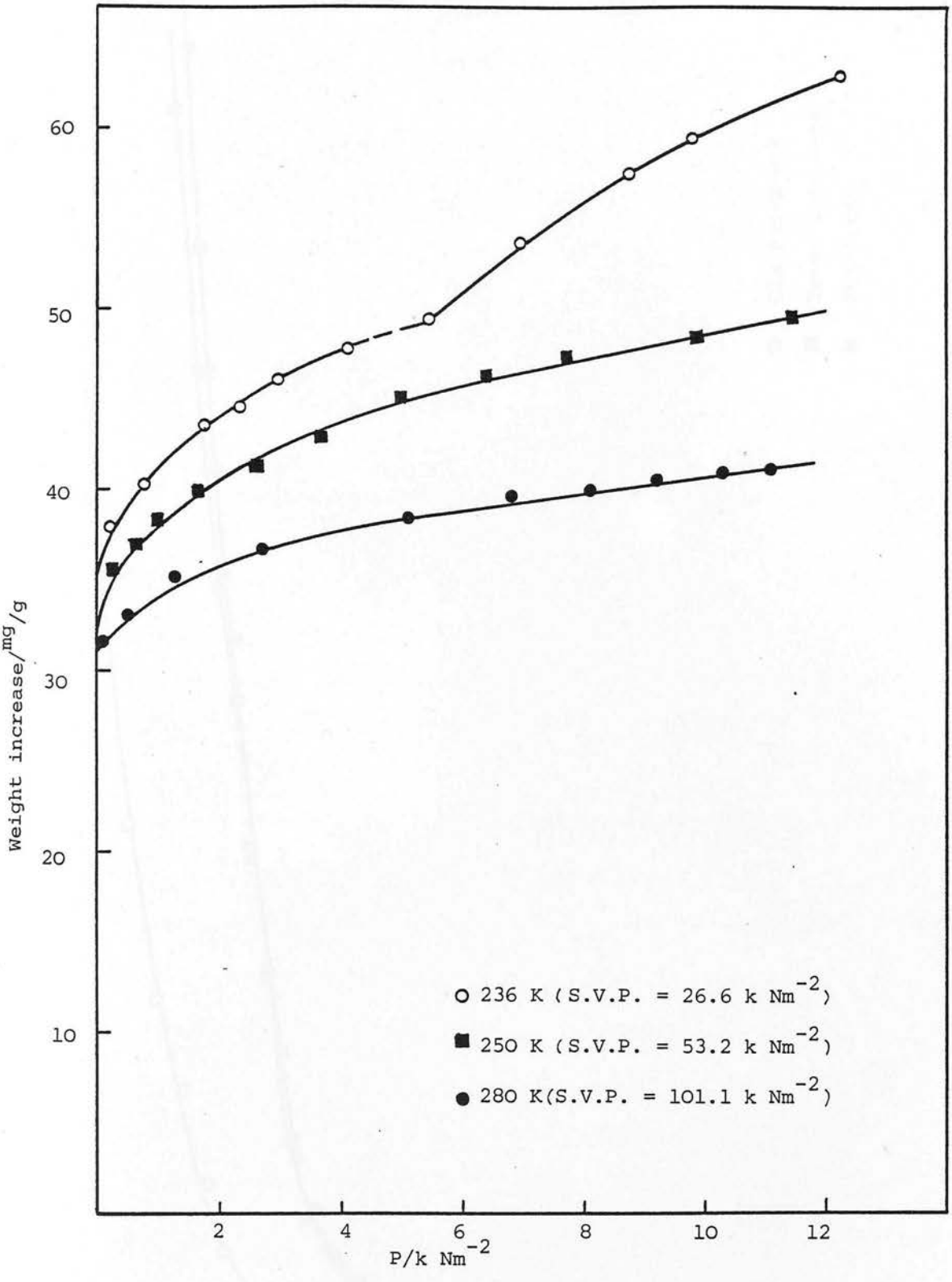


Fig. 6.7. Adsorption Isotherms of But-1-ene

Fig. 6.8. Adsorption Isotherms of the n-Butenes on Zeolite Ω at 280 K

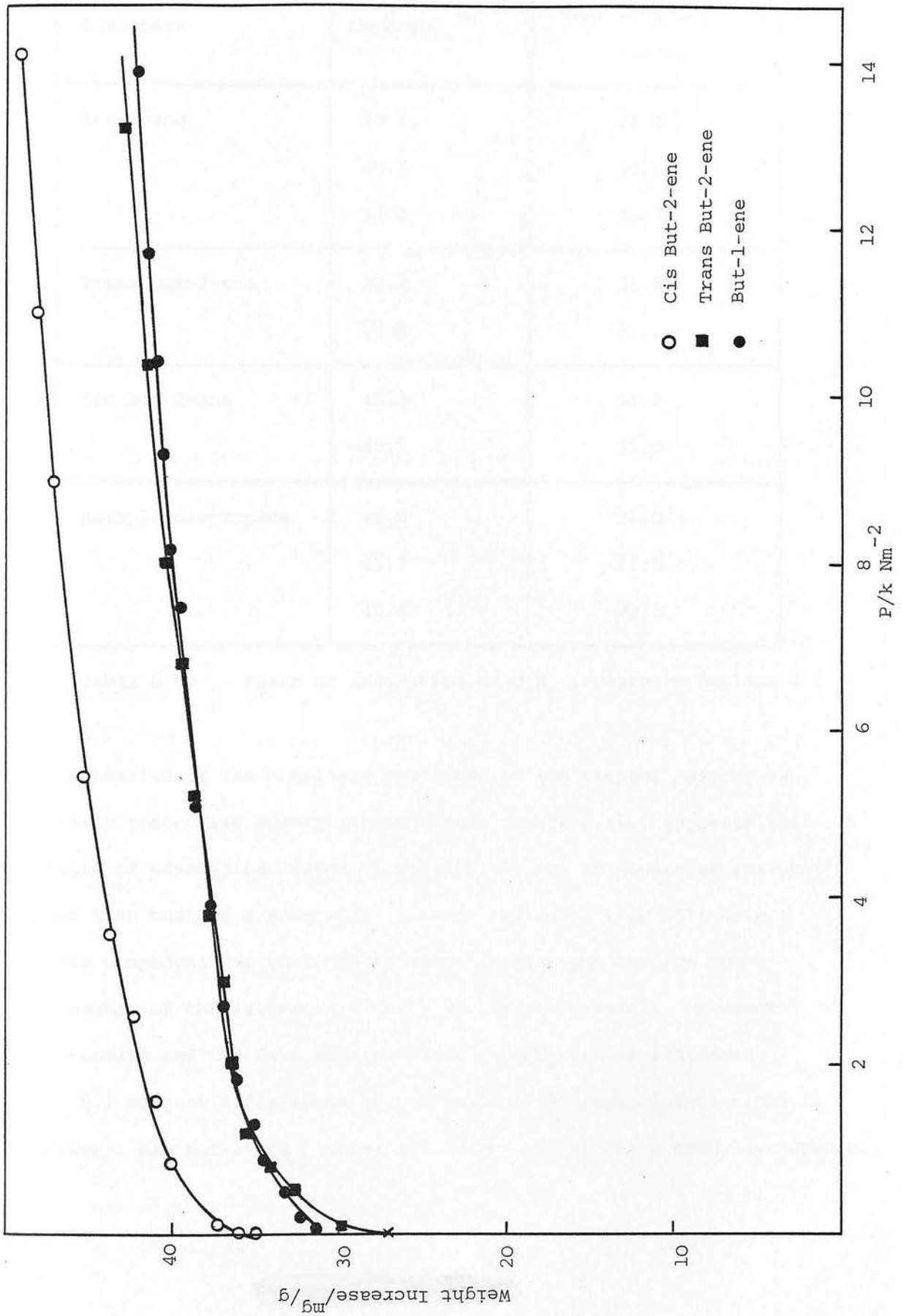

| Adsorbate | Coverage $^{mg}/_{g}$ | Heat of Adsorption kJ/mol |
|---|---|---|
| But-1-ene | 38.4 | 31.2 |
| | 40.5 | 30.6 |
| | 41.9 | 30.75 |
| Trans but-2-ene | 38.4 | 31.9 |
| | 41.9 | 32.1 |
| Cis but-2-ene | 45.3 | 51.2 |
| | 47.1 | 51.0 |
| Methylcyclopropane | 41.9 | 22.0 |
| | 43.7 | 22.5 |
| | 45.4 | 22.5 |

Table 6.10. Heats of Adsorption of $C_4H_8$ Isomers on Zeolite Ω

Estimation of the monolayer coverages of the various adsorbates from their respective adsorption isotherms (Table 6.11.) suggests that the heats of adsorption listed in Table 6.10. are at coverages somewhat greater than that of a monolayer. Hence, as such, they will have a sizeable component due to intermolecular interaction and are not a true measure of the interaction with the zeolite surface. However these results and the data obtained from the adsorption isotherms (Fig.6.8.) suggest differences in the zeolite-adsorbate interactions in the order; cis but-2-ene > trans-but-2-ene ∿ but-1-ene > methylcyclopropane.

Table 6.11. Weights of but-1-enes Corresponding to Monolayer Coverage of Zeolite Ω

| Adsorbate | Monolayer Coverage/$^{mg}/_{g}$ | Area/molecule[235] $nm^2$ | Area of Monolayer $m^2g^{-1}$ |
|---|---|---|---|
| But-1-ene | 35 | 37.8 | 142 |
| Trans but-2-ene | 35 | 33.4 | 153 |
| Cis but-2-ene | 42 | 38.5 | 174 |

Table 6.11. lists the estimated weights of the n-butenes corresponding to monolayer coverage (estimated from the adsorption isotherms by the point B method) together with the area occupied per molecule[235] and hence the calculated area covered. The area covered by a monolayer of n-butene molecules is considerably less than the area measured by nitrogen adsorption (ca. 297 $m^2g^{-1}$). The structure of zeolite Ω, however, is such that some of the internal surface available to nitrogen molecules may be inaccessible to butene or methylcyclopropane molecules, in particular that within the gmelinite cages. If the free dimensions of the eight-ring windows of these cages are similar to those in gmelinite (0.34 nm x 0.37 nm)[65] they will not permit the entry of molecules, such as the butenes, having critical diameters of ca. 0.5 nm. Moreover, although the occurrence of slightly larger apertures may permit the entry of the n-butenes the rate of sorption would be determined by the rate of diffusion through

the apertures, a factor controlled by the critical diameter and polarity of the molecule. Hence if sorption into the gmelinite cages of zeolite Ω was occurring, a diffusion - limited rate dependent on the nature of the adsorbate would be expected. Both the rapid rate of weight increase observed for all adsorbates and the estimated monolayer coverages suggest sorption of n-butenes and MCP in the main channels only. Furthermore the rapid desorption observed is typical of that expected on removal of molecules from easily accessible sites and not through restricted pore openings.

Adsorption isotherms of but-1-ene and MCP at 237 K indicated an apparent condensation at pressures well below the saturated vapour pressures at that temperature; at P/Po of .33 for MCP and .216 for but-1-ene. This effect, illustrated in Fig. 6.7, was not observed at similar relative pressures and temperature for cis and trans but-2-ene nor at higher relative pressures of but-1-ene or MCP at 250 K.

b) Summary of Adsorption Results in Zeolite Ω

The adsorption results over zeolite Ω illustrate rapid adsorption and desorption of the n-butenes and MCP. No diffusional limitations to sorption are apparent suggesting adsorption only within the main channels. Adsorption isotherms and heats of adsorption results suggest different strengths of interaction between the adsorbate and zeolite Ω with cis but-2-ene > trans but-2-ene ∿ but-1-ene > MCP.

6.2.2. Erionite

a) Adsorption of $C_3H_6$ and $C_4H_8$ Isomers on Erionite (N)

Samples of erionite (N) and erionite (T) outgassed at 643 K until steady weights were maintained lost 15.3% and 15.5% of their initial hydrated weights. Reference to the literature formula predicts a weight loss due

to dehydration of ca. 14.3%.

The adsorptions of propene and the n-butenes on erionite (N) at 280 K were investigated gravimetrically. On admission of the same external pressure of different adsorbates to the zeolite, rates of adsorption which were markedly dependent on the nature of the adsorbate were observed. These rates were in the order trans but-2-ene > propene > but-1-ene > cis but-2-ene. The weight increases (mg/g hydrated zeolite) observed as a function of time during adsorption of these molecules are illustrated in Fig. 6.9.

Trans but-2-ene can enter and diffuse through erionite (N) much more easily than the other n-butenes or propene. As trans but-2-ene has the same critical diameter as propene and but-1-ene (0.495 nm) the sorption rate cannot be a function of this parameter alone. However, whereas trans but-2-ene has a zero dipole moment, but-1-ene and propene have dipole moments of 0.34D and 0.37D respectively. The dipole interactions of these molecules with cations in the channels will cause diffusion to become hindered and rates of sorption less. Similar effects were reported for diffusion of $C_3H_8$, $CH_2Cl_2$ and $(CH_3)_2NH$ in chabazite[73] where increase in polarity resulted in increased diffusional activation energy. The higher rate of sorption of propene relative to but-1-ene, both molecules having the same critical diameter and similar dipole moments must be a consequence of its shorter carbon chain length. A regular increase in activation energy with chain length has been reported for diffusion of n-alkanes ($C_1$-$C_7$) in zeolite 5A[74] although a more complex pattern has been observed for zeolite T[76] showing a decrease in diffusional activation energy with increasing chain length from $C_3$ to $C_5$ followed by an increase to $C_7$.

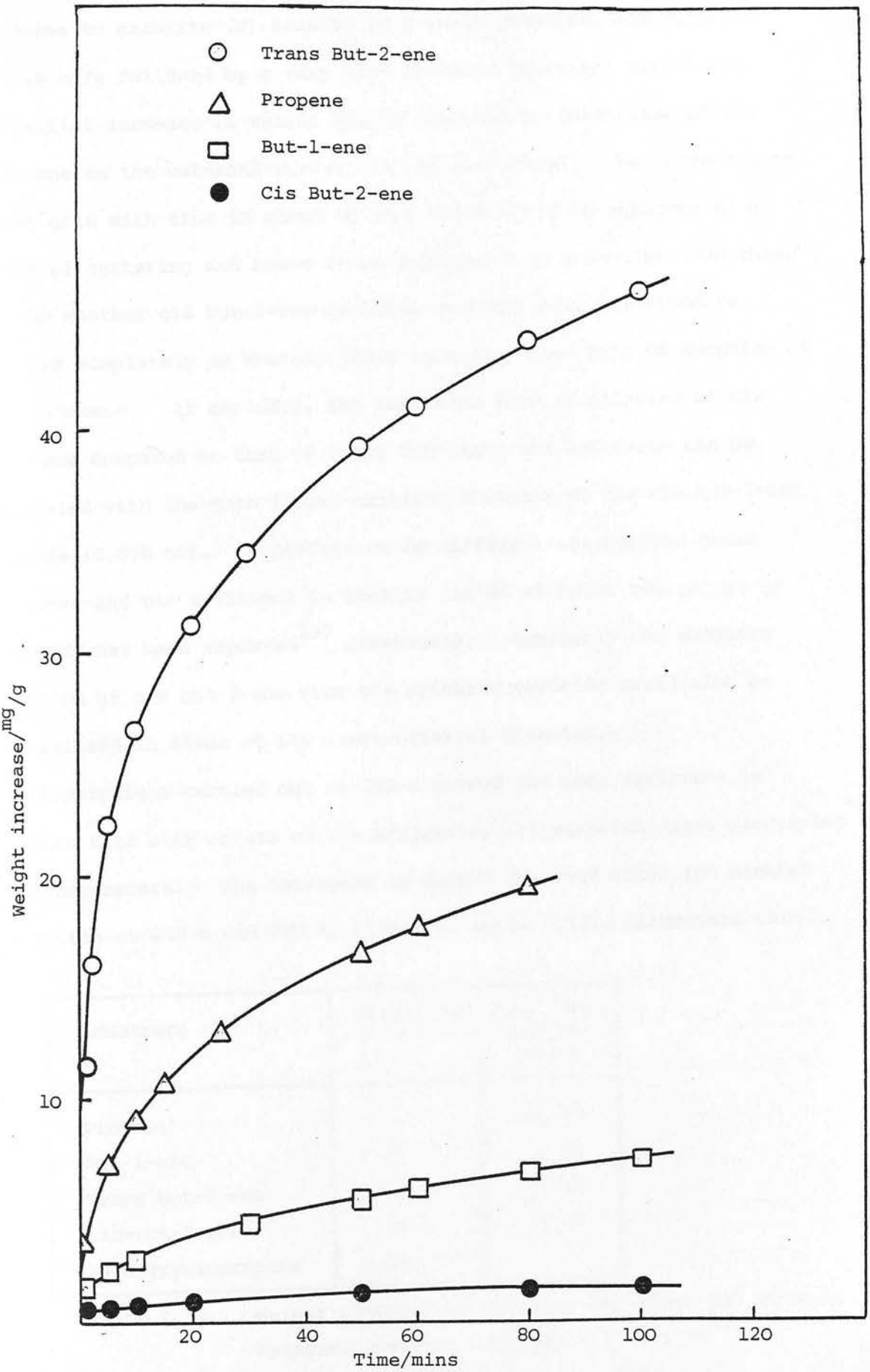


Fig. 6.9. Rates of Adsorption of Propene and n-Butenes on Erionite (N) at 280 K.
(External Pressure = 144 k $Nm^{-2}$)

In contrast to the molecules discussed above admission of cis but-2-ene to erionite (N) results in a sharp immediate adsorption of ca. 0.5 mg/g followed by a very slow increase in weight with time. The initial increase in weight may be assigned to adsorption of cis but-2-ene on the external surface of the particles. The further slow weight gain with time is close to that which would be expected as a result of gettering and hence it is impossible to establish from these results whether cis but-2-ene is being excluded from the erionite cavities completely or whether there is a very slow rate of sorption of this isomer. If occluded, the very slow rate of sorption of cis but-2-ene compared to that of trans but-2-ene and but-1-ene can be correlated with the much larger critical diameter of the cis but-2-ene molecule (0.558 nm). A difference in diffusivities between trans n-alkenes and cis n-alkenes in zeolite CaA of at least two orders of magnitude has been reported[137] previously. Similarly the complete exclusion of cis but-2-ene from the erionite cavities could also be rationalised in terms of its large critical diameter.

Adsorptions carried out at 250 K showed the same variation in sorption rate with nature of the adsorbate, all sorption rates decreasing with temperature. The increases in weight observed after 100 minutes adsorption at 250 K and 280 K, listed in Table 6.12., illustrate this.

| Adsorbate | Weight Adsorbed mg/g | |
|---|---|---|
| | 250 K | 280 K |
| Propene | | 20.73 |
| But-1-ene | 2.72 | 7.29 |
| Trans but-2-ene | 18.95 | 46.35 |
| Cis-but-2-ene | 1.21 | 1.54 |
| Methylcyclopropane | 2.68 | |

Table 6.12. Weight adsorbed by erionite (N) after 100 minutes. External pressure admitted = 1.44 k $Nm^{-2}$.

These results, showing a marked decrease in rate of sorption with decreasing temperature, are indicative of an activated diffusion process. The occurrence of such a process is reasonable in these systems where, once sorbed, the molecules diffuse through the cavities by passing through 8-ring windows identical to those permitting initial entry and hence having similar free dimensions to the critical diameters of the molecules.

In the case of cis but-2-ene if the slow weight gain following the initial adsorption on the surface is a result of gettering alone an increase in weight adsorbed with decreasing temperature would be expected due to both an increase in the gettering effect and to increased adsorption capacity of the external surface. Therefore the results in Table 6.12. tend to suggest a very slow rate of sorption of cis but-2-ene into the erionite cavities at 280 K. This however is a tenuous conclusion due to the irreproducibility of the rate of gettering.

The effect of increasing the temperature on the adsorption of propene is illustrated in Fig. 6.10. In contrast with the n-butenes the temperature at which propene is adsorbed may be increased without introducing complications in the analysis of results due to formation of reaction products substantially different from the initial adsorbate. Fig. 6.10.(a) shows the adsorption of propene at 280 K, after 80 minutes the temperature is increased to 300 K resulting in an increase in adsorption rate. In Fig. 6.10.(b) following an initial adsorption at 300 K the temperature is increased to 373 K at a heating rate of 2K/min. A slight increase in adsorption rate is observed but as this is accompanied by a decrease in the sorption capacity it is not a true measure of the increased rate of sorption and diffusion.

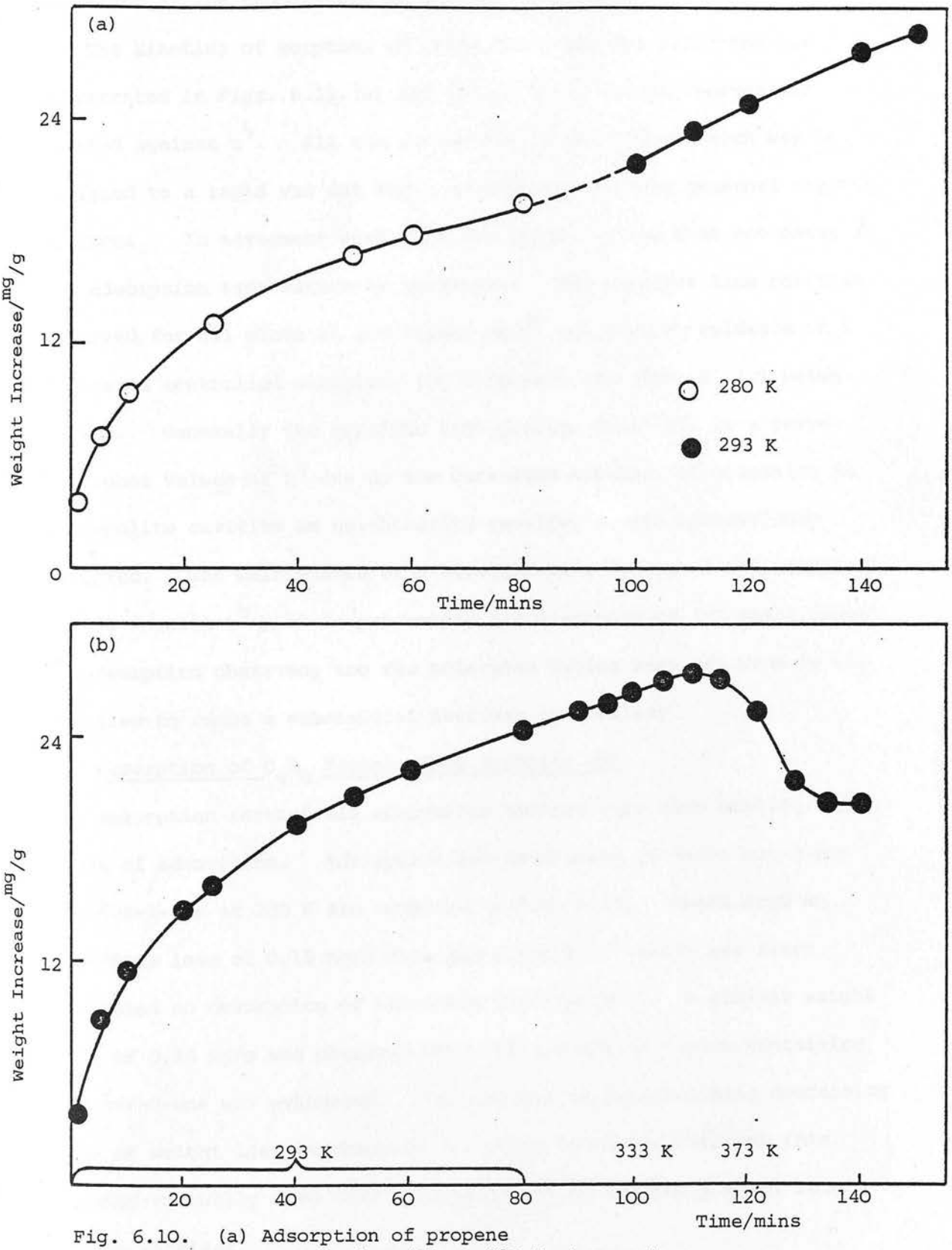


Fig. 6.10. (a) Adsorption of propene on Erionite (N) at 280 K, temperature increased to 293 K after 80 minutes

(b) Adsorption of propene on Erionite (N) at 293 K, temperature increased by 2K/min after 80 minutes.

External pressure = 144 k $Nm^{-2}$)

The decrease in sorption capacity is illustrated by the sharp decrease in weight as the temperature is further increased.

The kinetics of sorption of trans but-2-ene and but-1-ene are illustrated in Figs. 6.11.(a) and (b) in which weight increase is plotted against $t^{\frac{1}{2}}$. All the curves have a small foot which may be assigned to a rapid van der Waals adsorption upon the external crystal surfaces. In agreement with this the height of the foot decreases as the adsorption temperature is increased. The straight line portions observed for all plots at low values of $t^{\frac{1}{2}}$ are further evidence of a diffusion controlled sorption, the diffusion law (Eqn. 2. 2.) being obeyed. Generally the straight line portion tails off to a curve at higher values of $t^{\frac{1}{2}}$ due to the decreased mobility of molecules in the zeolite cavities as neighbouring cavities become increasingly occupied. The maintenance of a straight line for but-1-ene adsorption at 250 K until $t^{\frac{1}{2}} \gg 10$ is presumably a consequence of the small amount of adsorption observed, too few molecules having been admitted to the cavities to cause a substantial decrease in mobility.

b) Desorption of $C_4H_8$ Isomers from Erionite (N)

Desorption rates of all adsorbates studied were much smaller than those of adsorption. Adsorption and desorption of trans but-2-ene and but-1-ene at 280 K are compared in Fig. 6.12. Apart from an immediate loss of 0.15 mg/g when the adsorption vessel was first evacuated no desorption of but-1-ene was apparent. A similar weight loss of 0.14 mg/g was observed when the adsorption system containing cis but-2-ene was evacuated. In contrast an exponentially decreasing rate of weight loss is observed for trans but-2-ene although this becomes virtually zero when a large amount of adsorbate still remains on the catalyst.

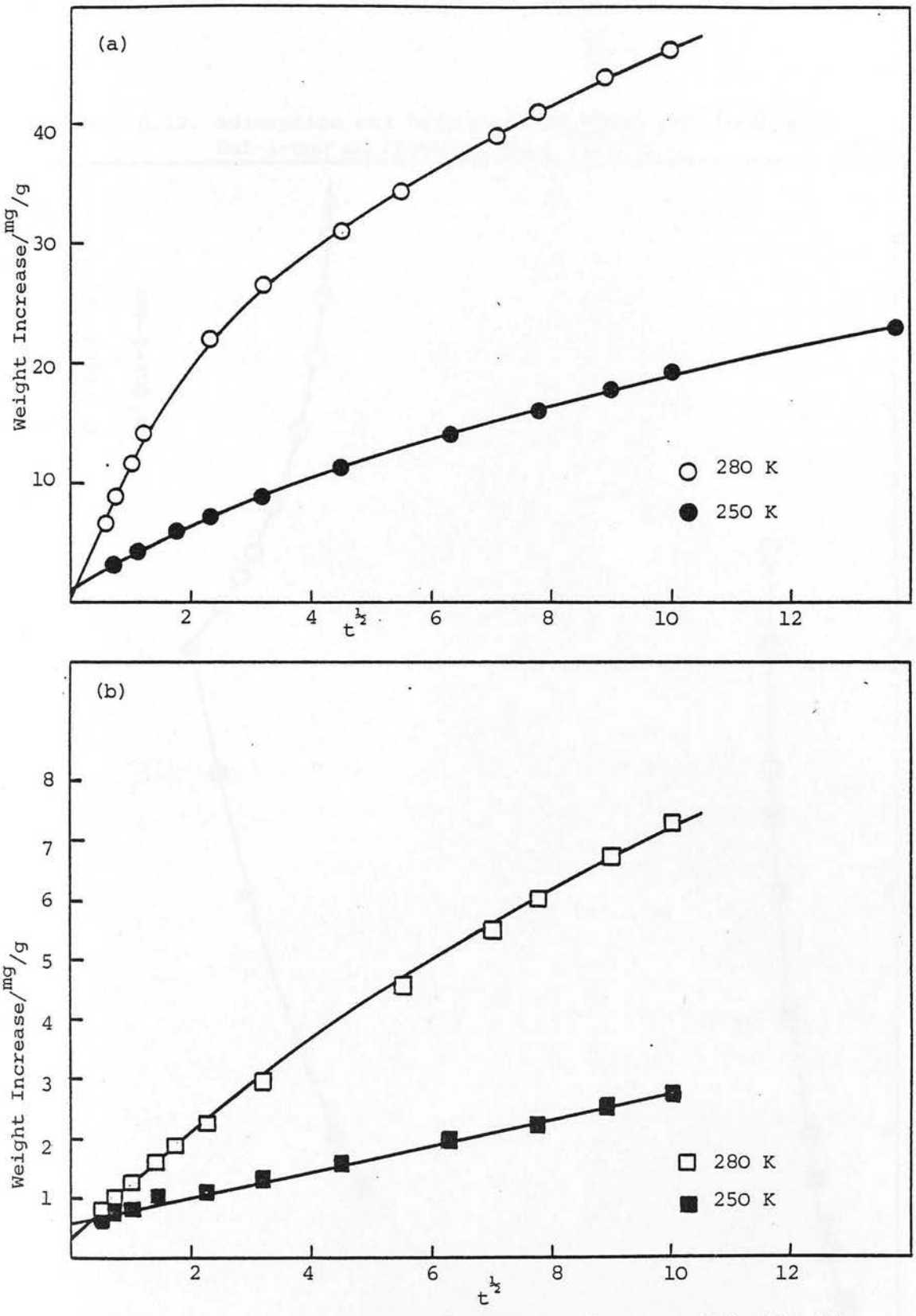


Fig. 6.11. (a) Adsorption of Trans But-2-ene on Erionite (N)

(b) Adsorption of But-1-ene on Erionite (N)

(External Pressure = 1.44 k $Nm^{-2}$)

Fig. 6.12. Adsorption and Desorption of Trans But-2-ene and But-1-ene on Erionite (N) at 280 K

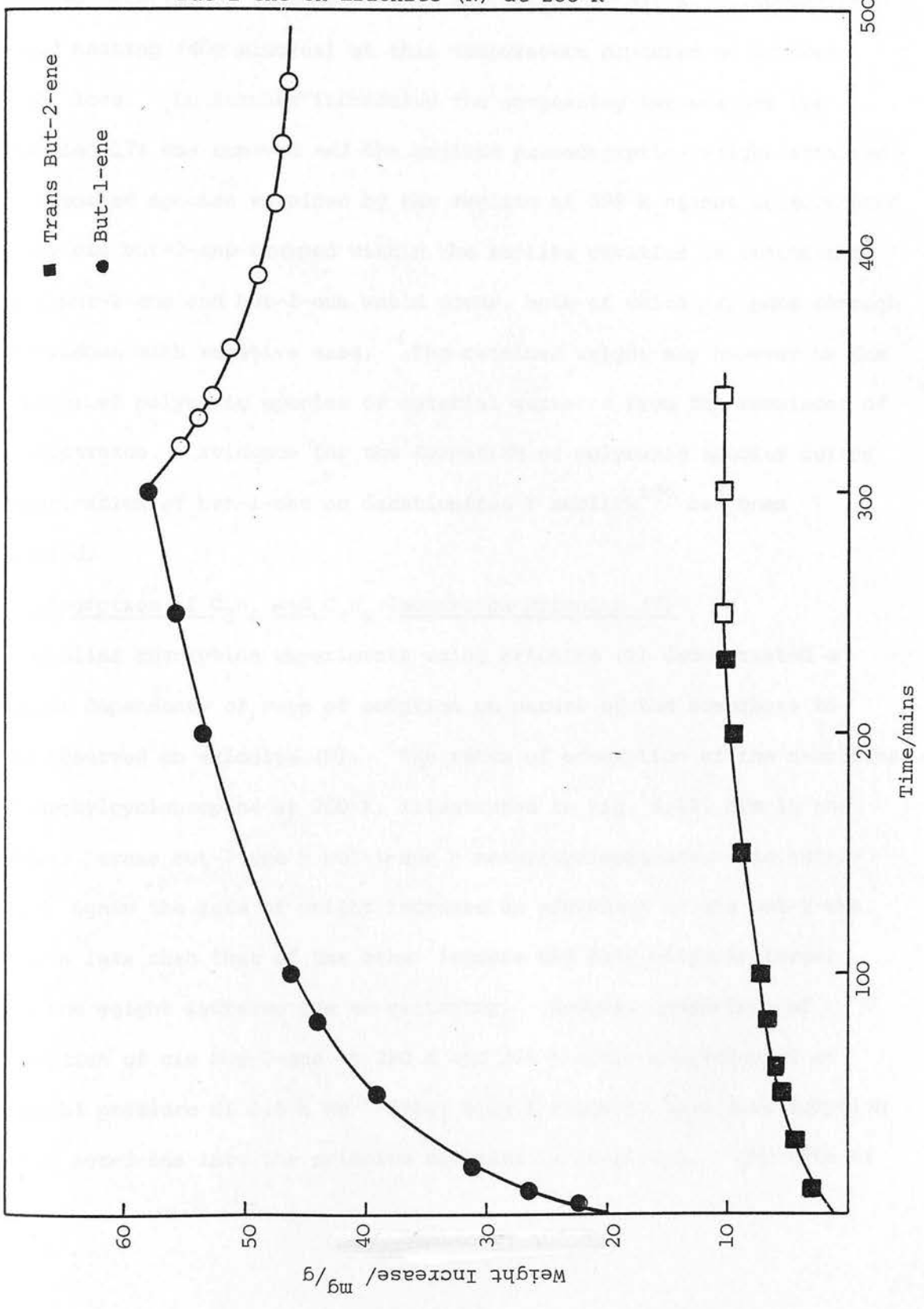

Rates of desorption, like adsorption, are increased by heating although in the case of the butenes results will be complicated by isomerisation reactions. A sample of erionite on which but-1-ene has been adsorbed exhibits a rapid weight loss of ca. 83% of the adsorbed material on increasing the temperature to 398 K. However prolonged heating (400 minutes) at this temperature produced no further weight loss. On further increasing the outgassing temperature the remaining 17% was removed and the zeolite pre-adsorption weight attained. The adsorbed species retained by the zeolite at 398 K cannot be accounted for by cis but-2-ene trapped within the zeolite cavities as reaction to trans but-2-ene and but-1-ene would occur, both of which may pass through the windows with relative ease. The retained weight may however be due to adsorbed polymeric species or material gettered from the remainder of the apparatus. Evidence for the formation of polymeric species during isomerisation of but-1-ene on decationised Y zeolite[196] has been reported.

c) Adsorption of $C_3H_6$ and $C_4H_8$ Isomers on Erionite (T)

Similar adsorption experiments using erionite (T) demonstrated a similar dependency of rate of sorption on nature of the adsorbate to that observed on erionite (N). The rates of adsorption of the n-butenes and methylcyclopropane at 280 K, illustrated in Fig. 6.13, are in the order:- trans but-2-ene > but-1-ene > methylcyclopropane > cis but-2-ene. Again the rate of weight increase on admission of cis but-2-ene is much less than that of the other isomers and only slightly larger than the weight increase due to gettering. However comparison of adsorption of cis but-2-ene at 280 K and 298 K after admission of an external pressure of 1.6 k $Nm^{-2}$ (Fig. 6.14.) suggests that some sorption of cis but-2-ene into the erionite cavities is occurring. The rate of

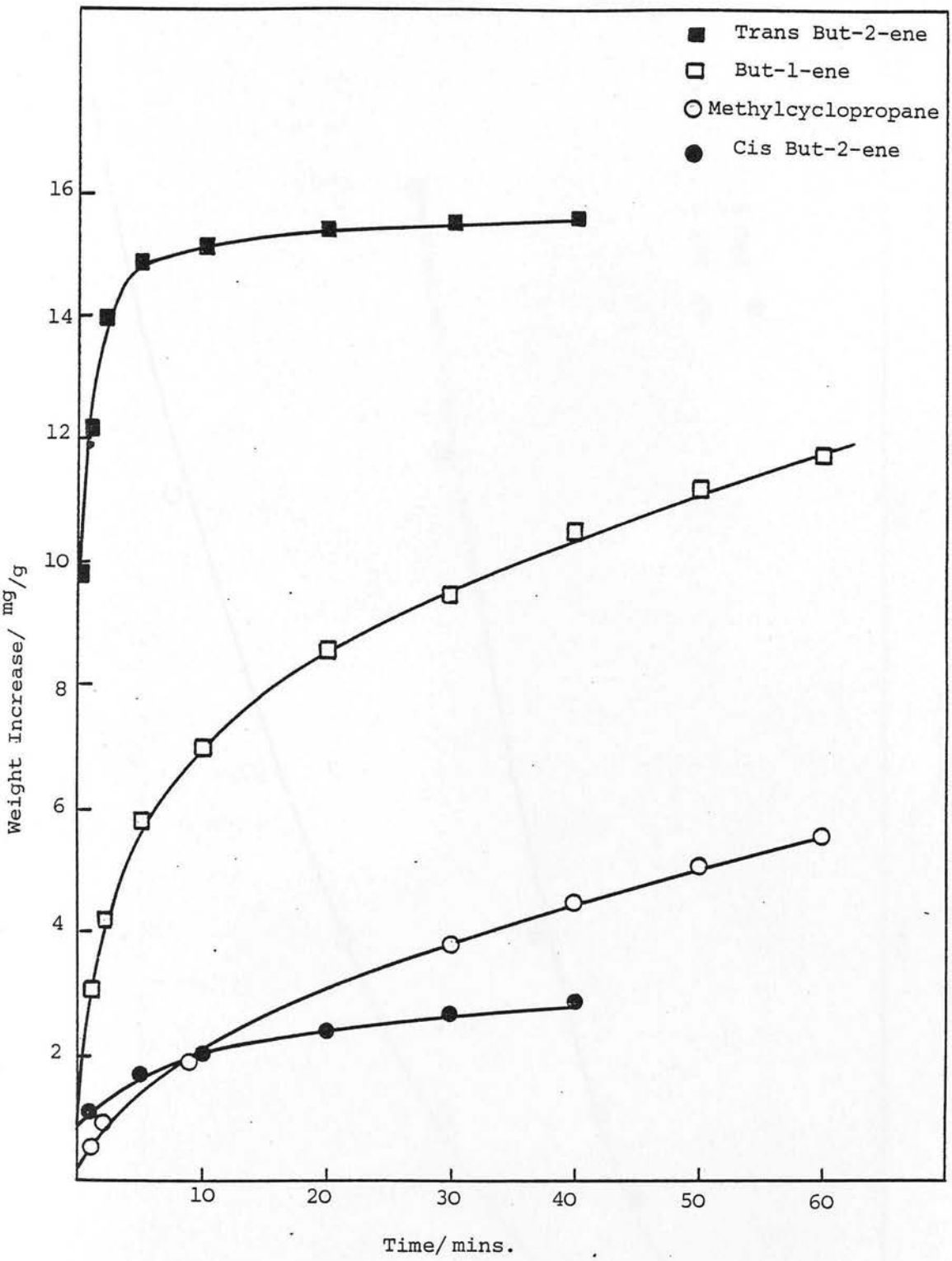


Fig. 6.13. Rates of adsorption of $C_4H_{10}$ Isomers on Erionite (T) at 280 K (External Pressure = .44 kN $m^{-2}$)

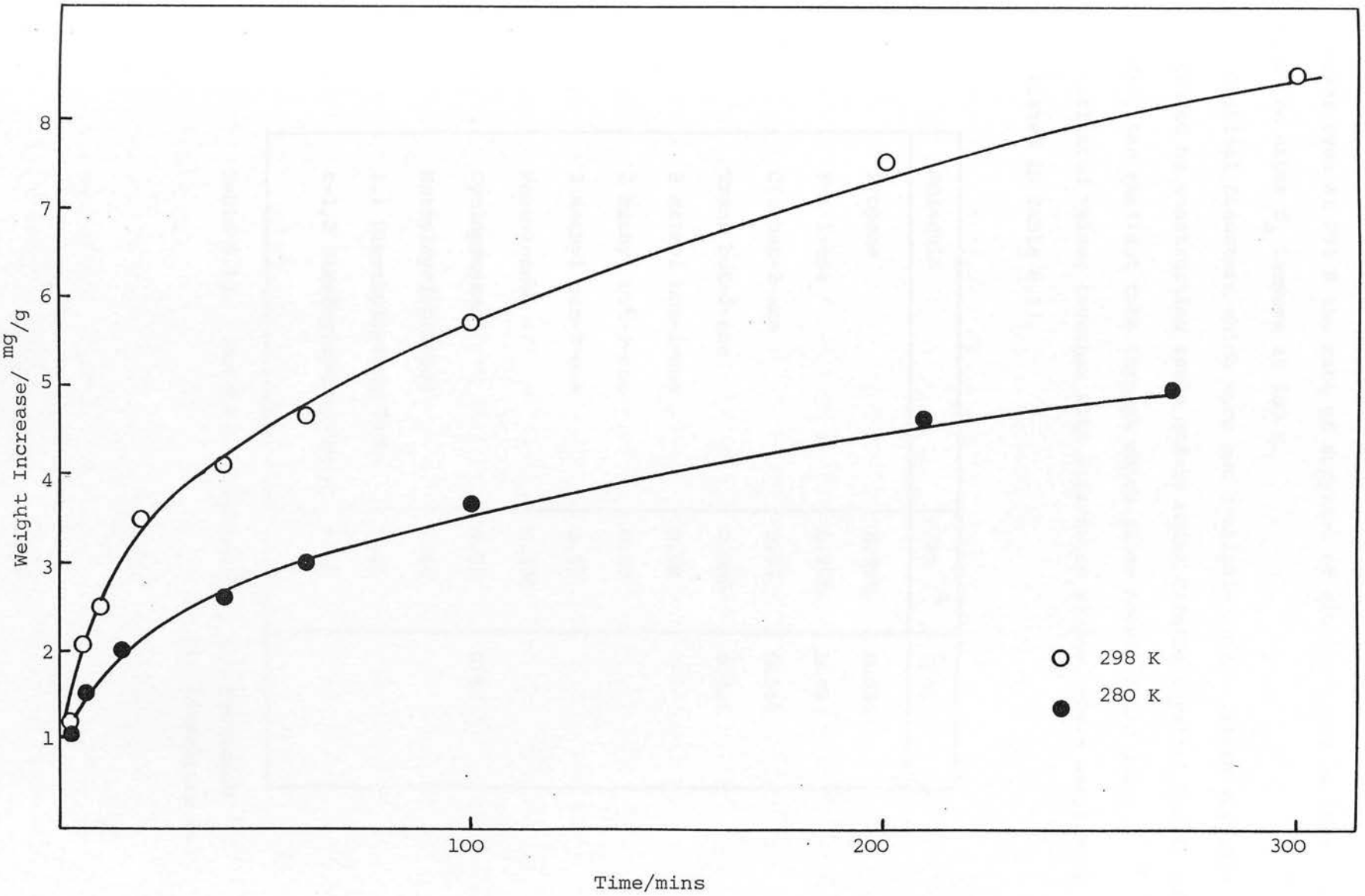


Fig. 6.14

Fig. 6.14 Rates of Adsorption of Cis But-2-ene on Erionite (T). (External pressure = 1.66 kN $m^{-2}$)

weight increase is greater at 298 K than at 280 K, a result not compatible with the weight increase being due solely to gettering. However even at 298 K the rate of sorption of cis but-2-ene is less than the other $C_4$ isomers at 280 K.

Critical diameters which were not available in the literature were estimated by constructing scale models using Catalin Covalent Models and finding the smallest tube through which these models could pass. The estimated values together with literature values, where available, are listed in Table 6.13.

| Molecule | σ/nm [a] | σ/nm [b] |
|---|---|---|
| Propene | 0.495 | 0.495 |
| But-1-ene | 0.495 | 0.495 |
| Cis but-2-ene | 0.53 | 0.558 |
| Trans but-2-ene | 0.495 | 0.495 |
| 3 Methyl but-1-ene | 0.59 | |
| 2 Methyl but-1-ene | 0.59 | |
| 2 Methyl but-2-ene | 0.59 | |
| Pent-1-ene | 0.495 | |
| Cyclopropane | 0.51 | 0.52 |
| Methylcyclopropane | 0.54 | |
| 1,1 Dimethylcyclopropane | 0.61 | |
| t-1,2 Dimethylcyclopropane | 0.56 | |

Table 6.13. Critical diameters σ a = Estimated
b = Literature (64)

With the exception of cis but-2-ene good agreement between estimated and literature values was obtained.

The critical diameter of methylcyclopropane is greater than that of trans but-2-ene and but-1-ene accounting for its slower rate of sorption and diffusion although its dipole moment (ca. 0.16D) also contributes to the diffusion rate. Adsorption of methylcyclopropane does not exhibit the same sharp immediate increase in weight evident in cis but-2-ene adsorption and ascribed to adsorption on the external surface. This is presumably a consequence of a greater interaction between external surface sites and the butenes.

As smaller doses of adsorbate were admitted to erionite (T) Figs. 6.9. and 6.13. cannot be compared directly. However the apparently more rapid attainment of equilibrium on adsorption of trans but-2-ene by erionite (T) suggests the presence of windows which are slightly larger or less hindered than in erionite (N). Further evidence for this is demonstrated by comparison of the rates of adsorption of propene and butene on the two erionites at 280 K following admission of identical doses of adsorbate. (Fig. 6.15.). The rates of adsorption of both propene and but-1-ene are substantially greater in erionite (T) than in erionite (N). Interestingly the ratio of the rates of adsorption of propene and but-1-ene (in terms of molecules adsorbed after 10 minutes adsorption) were almost identical for the two samples, 4.29 for erionite (N) and 4.03 for erionite (T).

After adsorption of 28.65 mg/g of propene at 280 K removal of the low temperature bath resulted in a decrease in weight due to decreased sorption capacity. In contrast erionite (N) displayed a sorption capacity of ca. 28 mg/g at ca. 353 K assuming sample temperature doesn't lag behind furnace temperature substantially (Fig. 6.10.(b)). This smaller sorption capacity of erionite (T) provides further evidence

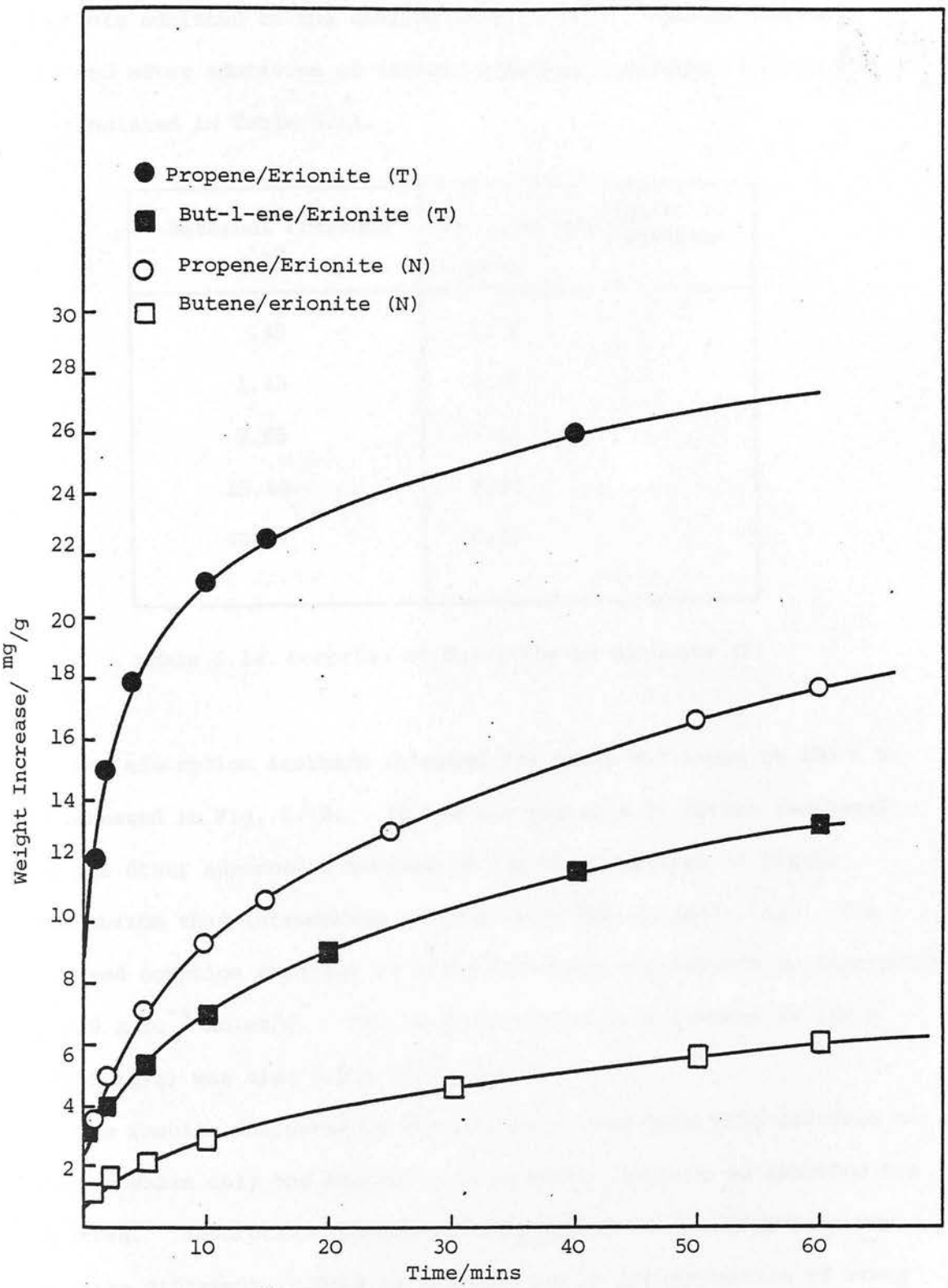


Fig. 6.15. Rates of Adsorption of Propene and But-1-ene on Erionites (N) and (T) at 280 K. (External pressure = 1.44 kN $m^{-2}$.)

for the presence of a substantial amount of amorphous material first suggested by the differences in surface areas of the two samples.

Rates of adsorption increased with increasing external pressure of adsorbate admitted to the zeolite (Fig. 6.16.). Weight increases observed after admission of various external pressures of but-1-ene are tabulated in Table 6.14.

| External Pressure k $Nm^{-2}$ | Wt. Increase (after 10 minutes) mg/g |
|---|---|
| .45 | 7.02 |
| 1.43 | 7.08 |
| 2.55 | 7.43 |
| 15.44 | 8.34 |
| 53.32 | 9.29 |

Table 6.14. Sorption of But-1-ene by Erionite (T)

The adsorption isotherm obtained for trans but-2-ene at 280 K is illustrated in Fig. 6.18. It was not possible to obtain isotherms for the other adsorbates because of the time required to attain equilibrium thus introducing a large error due to gettering. The observed sorption capacity of trans but-2-ene corresponds to adsorption of $6.8 \times 10^{-4}$ moles/g. The sorption capacity of propene at 280 K (28.65 mg/g) was also $6.8 \times 10^{-4}$ moles/g.

The results discussed in the previous paragraphs have referred to systems where only one adsorbate is present, assuming no reaction has occurred. Adsorption results in the presence of other species may be quite different. This is illustrated by the adsorption of trans

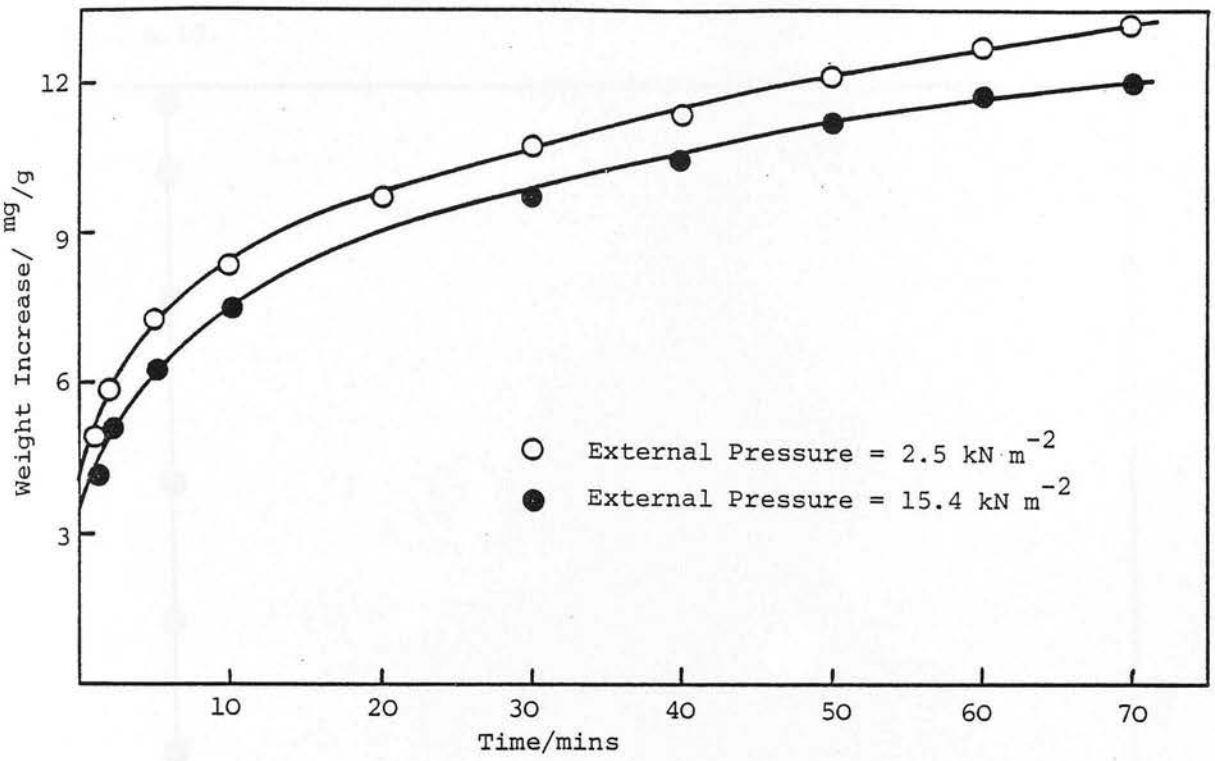


Fig. 6.16 Adsorption of But-1-ene on Erionite (T) at 280 K

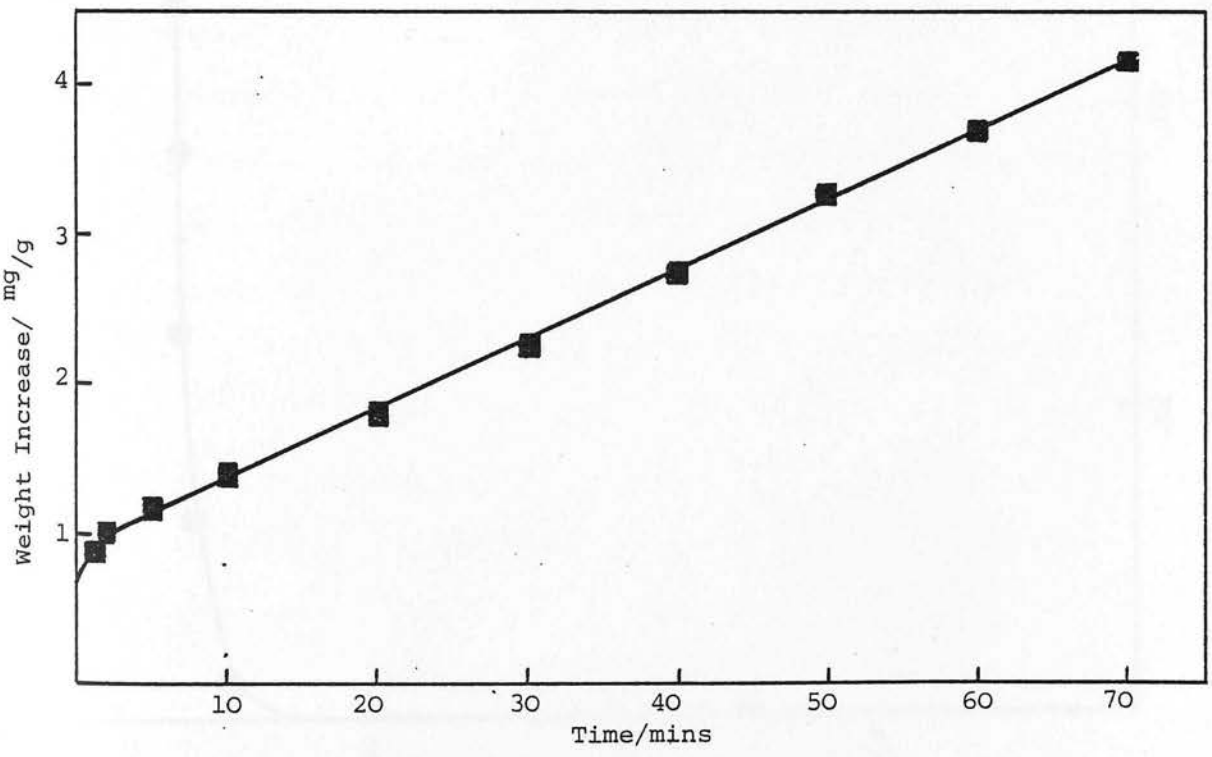


Fig. 6.17. Adsorption of Trans But-2-ene on Erionite (T) at 280 K following adsorption of 10 mg/g But-1-ene (External Pressure of Trans But-2-ene = 24 kN m$^{-2}$)

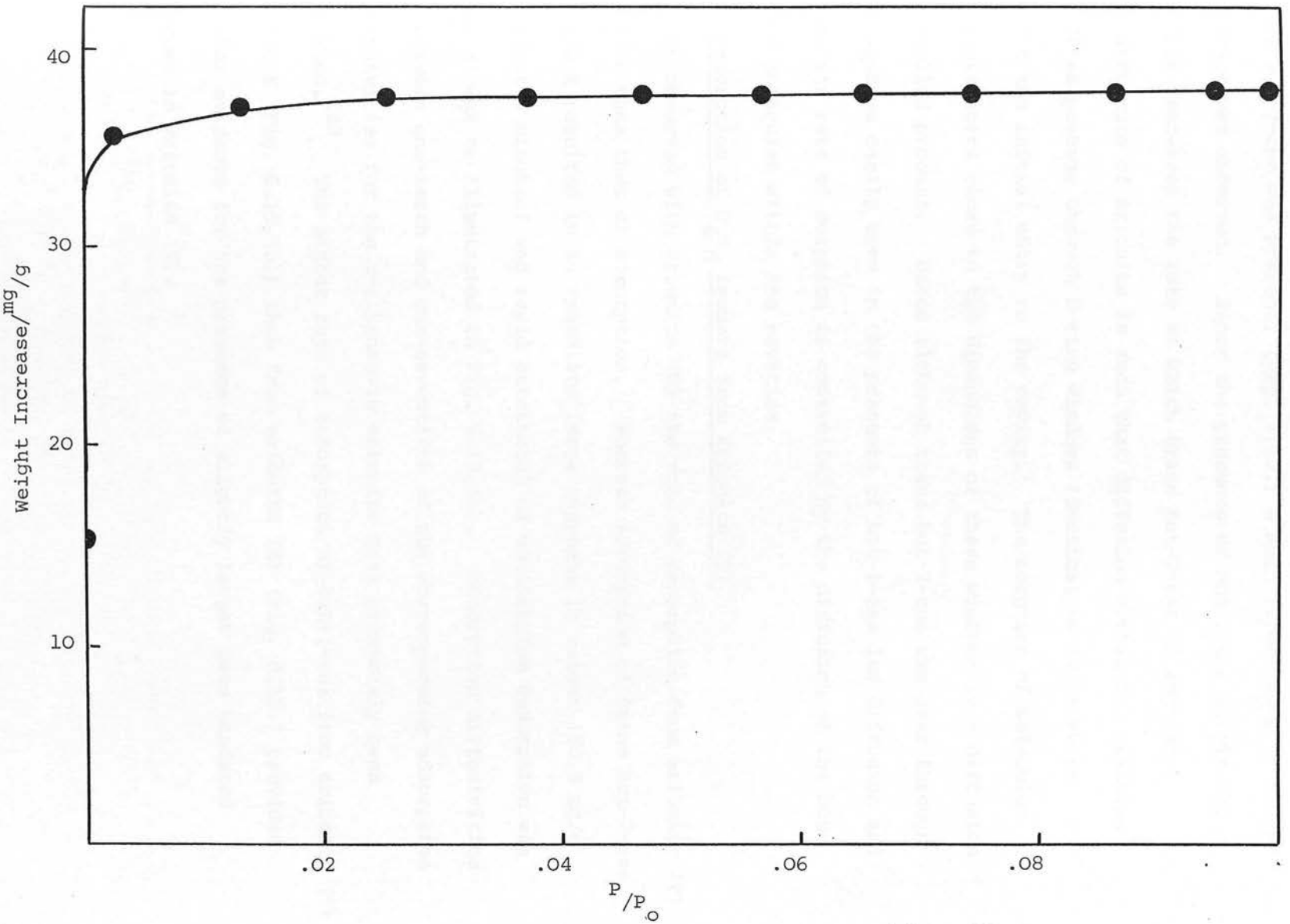


Fig. 6.18.

Fig. 6.18. Adsorption Isotherm; Trans But-2-ene on Erionite (T) at 280 K.

but-2-ene on an erionite (T) sample on which 10.0 mg/g but-1-ene has already been adsorbed. (Fig. 6.17.). Instead of observing rapid entry and diffusion in the erionite cavities, as demonstrated when only trans but-2-ene was present, (Fig. 6.13.) a much slower rate of weight increase was observed. Hence the presence of but-1-ene within the zeolite decreases the rate at which trans but-2-ene is adsorbed. The structure of erionite is such that diffusion within the cavities involves passage through 8-ring windows identical to those which permit the initial entry to the cavity. The sorption of molecules with diameters close to the dimensions of these windows is a diffusion controlled process. Hence although trans but-2-ene can pass through the windows easily even in the presence of but-1-ene its diffusion and hence its rate of sorption is controlled by the diffusion of the but-1-ene molecules within the cavities.

d) Desorption of $C_4H_8$ Isomers from Erionite (T)

As observed with erionite (N) the rate of desorption from erionite (T) is less than that of adsorption. Whereas adsorption of trans but-2-ene at 298 K resulted in an immediate large increase in weight (30.8 mg/g in first 5 minutes) and rapid attainment of equilibrium desorption was much slower as illustrated in Fig. 6.19.(a). Desorption diffusivities of between one-tenth and one-seventieth of the corresponding adsorption diffusivities for the n-alkanes in erionite have previously been reported.[163] The higher rate of desorption of but-1-ene from erionite (T) at 280 K (Fig. 6.19.(b)) than from erionite (N) (Fig. 6.12.) provides further evidence for the presence of slightly larger less hindered windows in erionite (T).

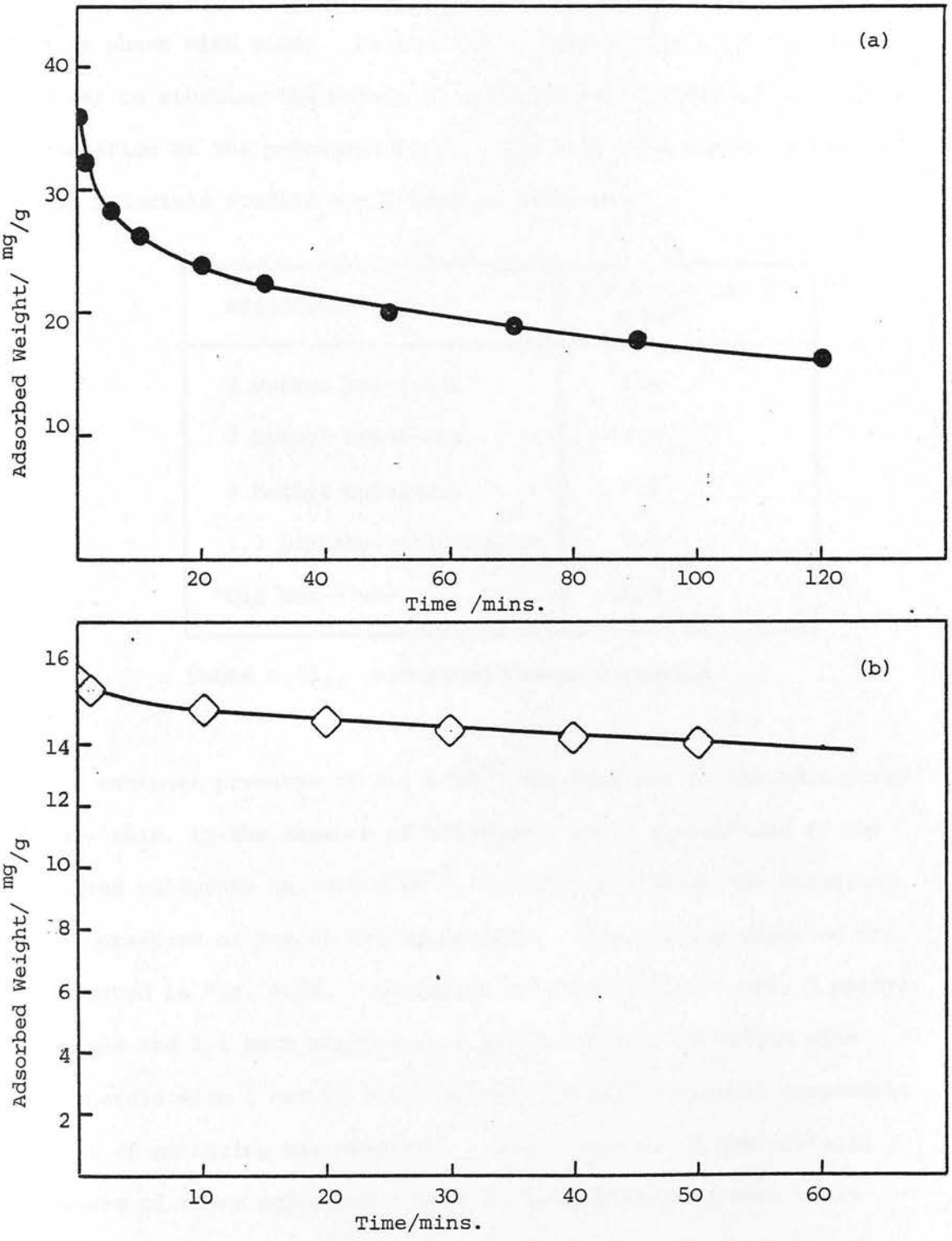


Fig. 6.19. (a) Desorption of Trans But-2-ene from Erionite (T) at 298 K

(b) Desorption of But-1-ene from Erionite (T) at 280 K

e) Adsorption of $C_5H_{10}$ isomers on Erionite (T)

The adsorption of 1,1,dimethylcyclopropane and the methyl butenes on erionite (T) were investigated gravimetrically as preliminary, 1,1 DMCP isomerisation studies had indicated a substantial decrease in the gas phase with time. An adsorption temperature of 237 K was chosen in order to minimise the extent of reaction of 1,1 DMCP and prevent condensation at the pressures used. The saturated vapour pressures of the materials studied are listed in Table 6.15.

| Adsorbate | S.V.P. at 243 K k $Nm^{-2}$ |
|---|---|
| 2 Methyl but-2-ene | 2.8 |
| 2 Methyl but-1-ene | 4.0 |
| 3 Methyl but-1-ene | 7.5 |
| 1,1 Dimethylcyclopropane | 7.5 |
| Cis but-2-ene | 16.0 |

Table 6.15. Saturated Vapour Pressures

An external pressure of 1.4 k $Nm^{-2}$ was admitted to the adsorption vessel, this, in the absence of adsorbent, would equilibrate in the increased volume to ca. 0.5 k $Nm^{-2}$, a value well below the saturated vapour pressure of any of the adsorbates. The results observed are illustrated in Fig. 6.20. Admission of 2 methyl but-1-ene, 2 methyl but-2-ene and 1,1 DMCP results in a rapid increase in weight with time whereas with 3 methyl but-1-ene an increase in weight comparable to that of gettering was observed. Consideration of the critical diameters of these molecules (Table 6.13) demonstrates that these results cannot be due to a selective adsorption. Furthermore,

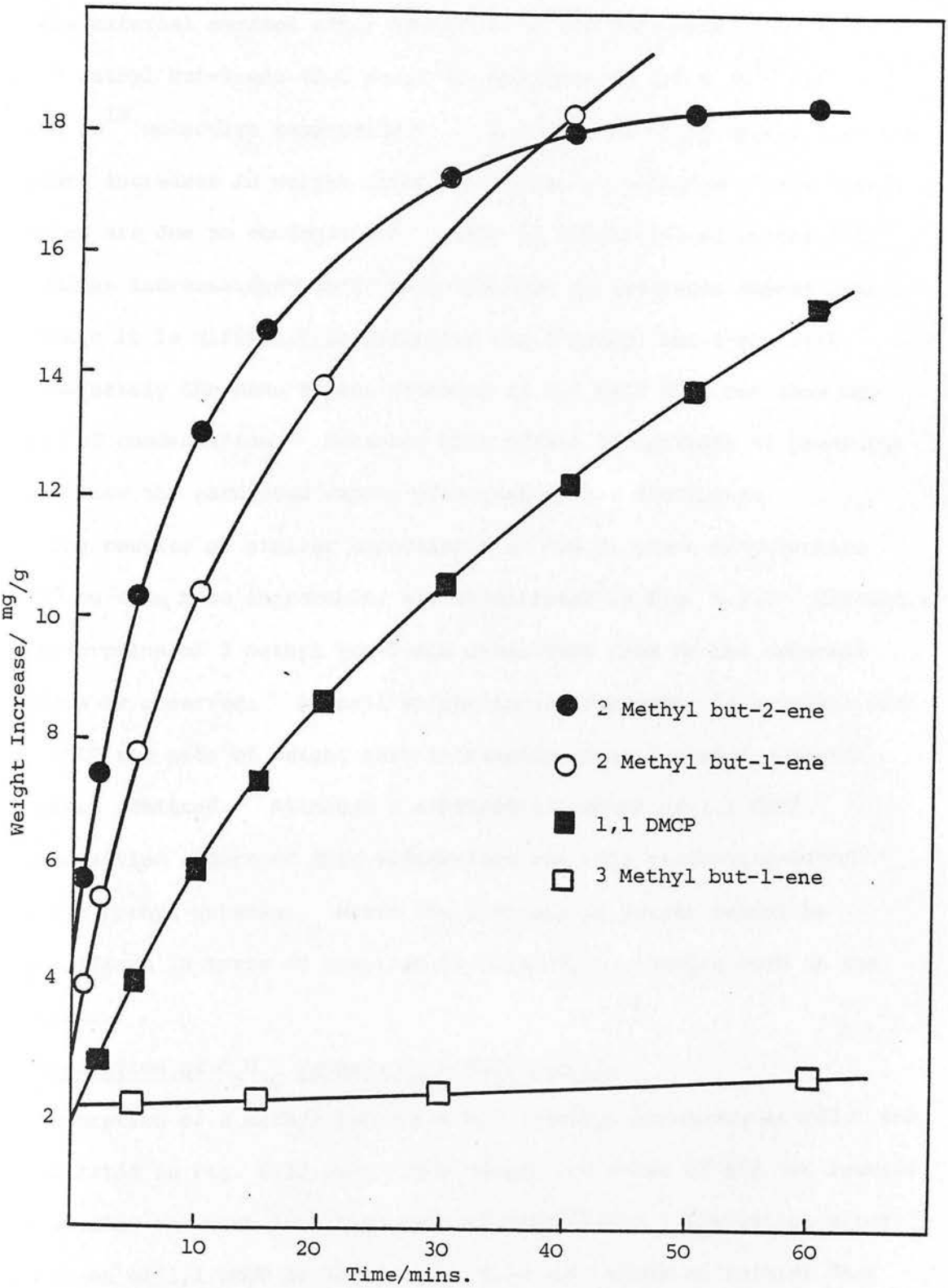


Fig. 6.20. Increase in Weight of Erionite (T) on Adsorption of some $C_5H_{10}$ hydrocarbons at 237 K.

admission of cis but-2-ene to the erionite at 237 K did not result in any increase in weight other than that attributed to the external surface and to gettering. Interestingly, the initial weights adsorbed on the external surface after admission of cis but-2-ene (1.39 mg/g) and 3 methyl but-1-ene (2.0 mg/g) corresponded to $1.5 \times 10^{19}$ and $1.7 \times 10^{19}$ molecules respectively. It would therefore appear that the further increases in weight observed following admission of the methyl butenes are due to condensation. This is substantiated by the rate of weight increase decreasing with increase in saturated vapour pressure although it is difficult to establish why 3 methyl but-1-ene with approximately the same vapour pressure as 1,1 DMCP does not show any signs of condensation. Moreover this effect is apparent at pressures well below the saturated vapour pressures of all adsorbates.

The results of similar experiments at 280 K, where condensation would be even more improbable, are illustrated in Fig. 6.21. Virtually no adsorption of 2 methyl but-2-ene other than that on the external surface is observed. A small weight increase however is apparent with 1,1 DMCP the rate of weight gain increasing with increased external pressure admitted. Although a substantial amount of 1,1 DMCP isomerisation occurs at this temperature the only products observed are the methyl butenes. Hence the increase in weight cannot be rationalised in terms of sorption of other $C_5H_{10}$ isomers such as the pentenes.

f) Desorption of $C_5H_{10}$ Isomers from Erionite (T)

Desorption of 2 methyl but-2-ene and 2 methyl but-1-ene at 243 K are illustrated in Fig. 6.22.(a). The desorption rates of the two isomers are similar but much less than that of adsorption. Evacuation after admission of 1,1 DMCP at 280 K (Fig. 6.24 (b)) shows an initial fast rate of desorption decreasing quite rapidly to zero.

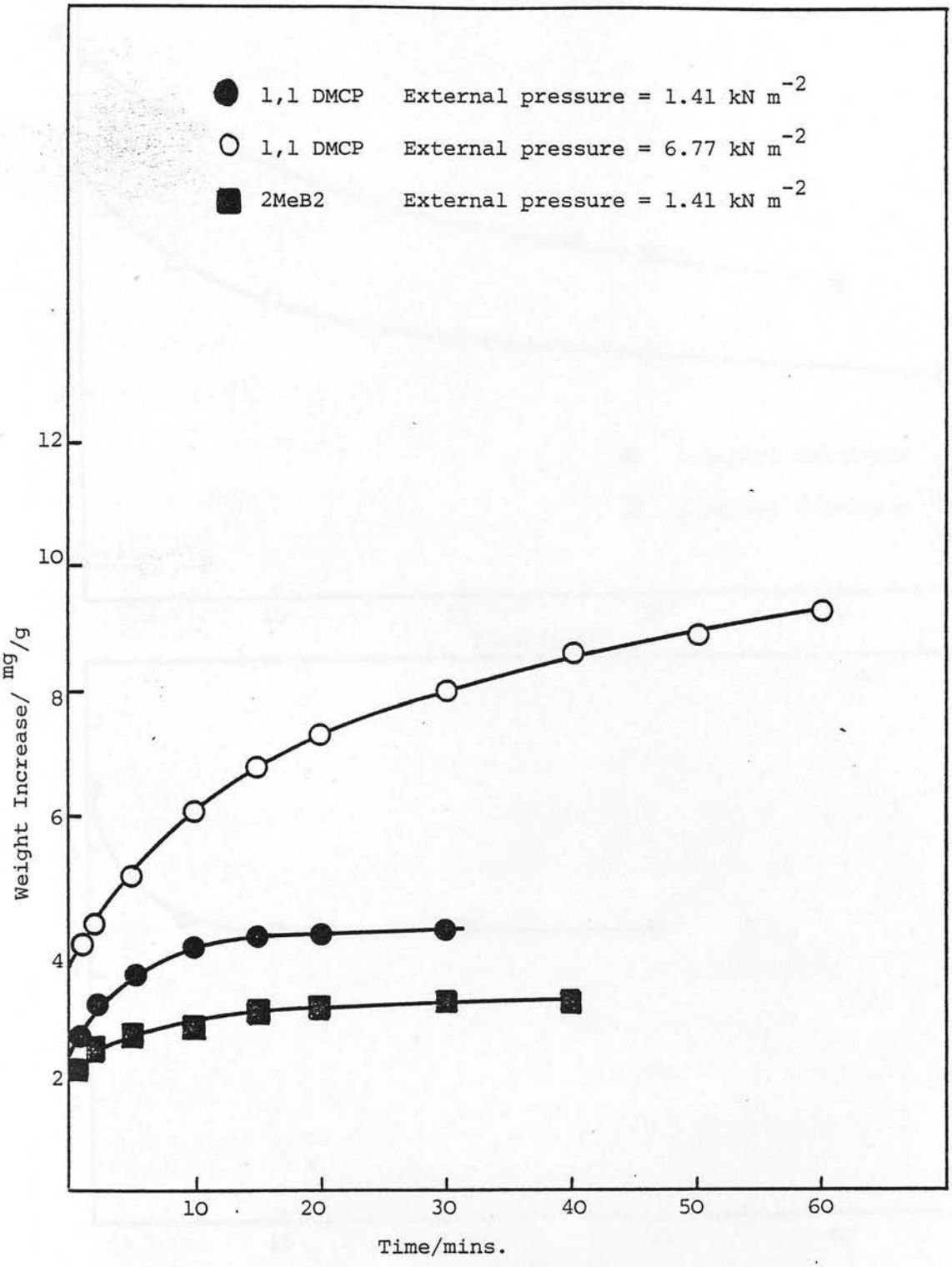


Fig. 6.21. Adsorption of some $C_5H_{10}$ isomers on Erionite (T) at 280 K.

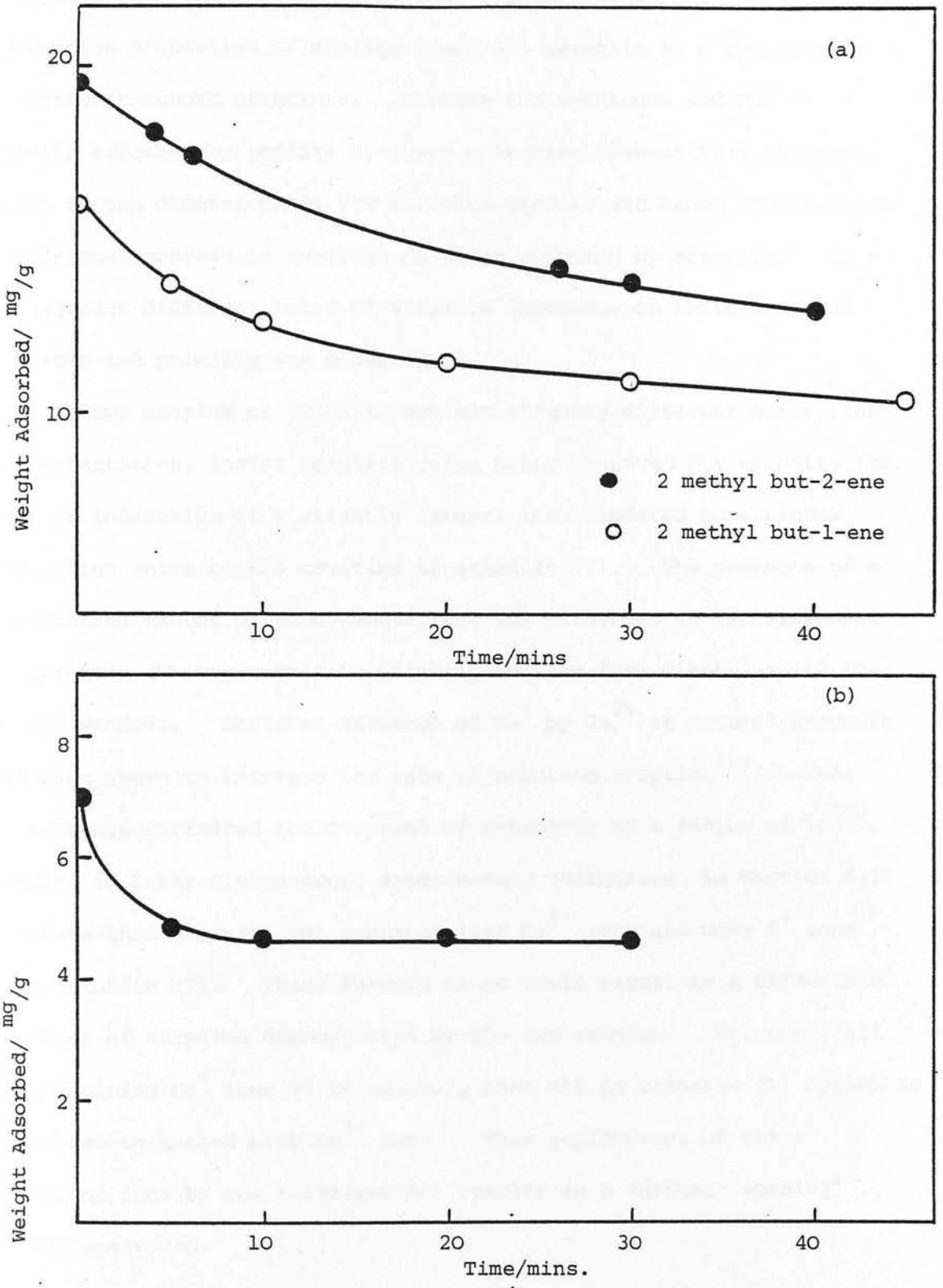


Fig. 6.22. (a) Desorption of 2 methyl but-2-ene and 2 methyl but-1-ene at 237 K from erionite (T)

(b) Desorption of 1,1 DMCP at 280 K from erionite (T).

g) Summary of Adsorption Results over Erionite

Adsorption experiments have shown distinct differences in the adsorption properties of zeolite omega and erionite as a consequence of their framework structure. Whereas the n-butenes and MCP are readily adsorbed by zeolite Ω, these molecules have critical diameters close to the dimensions of the erionite windows and hence an activated diffusional process is involved in their sorption by erionite. As a consequence different rates of sorption dependent on their critical diameter and polarity are observed.

The two samples of erionite exhibit slightly different adsorption characteristics, faster sorption rates being observed for erionite (T). This is indicative of a slightly larger, less hindered pore window permitting entry to the cavities of erionite (T). The presence of a substantial amount of iron substituted for aluminium in the framework of erionite (N) may result in slightly smaller free dimensions of the 8-ring windows. Moreover exchange of $Na^+$ by $Ca^{2+}$ in natural erionite has been shown to increase the rate of n-butane sorption[164] whereas $K^+$ exchange decreased the sorption of n-pentane by a factor of 10[159]. Results of X-ray fluorescence spectroscopy (discussed in Section 6.1) indicate that erionite (N) contains less $Ca^{2+}$ ions and more $K^+$ ions than erionite (T). These factors alone would result in a difference in rates of sorption demonstrated by the two samples. Moreover, all the remaining $Na^+$ ions (0.24 equiv./g atom Al) in erionite (T) appear to have been exchanged with $Fe^{3+}$ ions. This replacement of three univalent ions by one trivalent ion results in a further 'opening' of the apertures.

The differences in ionic composition should also result in different sorption capacities, that of erionite (T) being greater than erionite (N). Adsorption results tend to suggest the opposite. This is not unreasonable because of the strong possibility of some amorphous material in erionite (T) as indicated by surface area measurements.

The methyl butenes and 1,1 DMCP do not appear to enter the erionite cavities but, at low temperatures, condense on the zeolite at pressures well below their saturated vapour pressures at that temperature. In contrast zeolite Ω, able to sorb cyclohexane, would be expected to sorb these molecules within its main channels.

## 6.3. Catalyst Activity

The variation in catalytic activity of the zeolites with pretreatment conditions was investigated before the various reactions described in this thesis were studied in detail.

### 6.3.1. Zeolite Ω

The effect of pretreatment on the catalytic activity of zeolite Ω was investigated using the isomerisations of but-1-ene and methylcyclopropane (MCP) as test reactions. A sample outgassed at 723 K showed no but-1-ene isomerisation activity even at a reaction temperature of 419 K. In contrast, samples outgassed between 763 K and 948 K exhibited considerable activity as shown by the first order rate constants for but-1-ene isomerisation at 328 K listed in Table 6.16.

| Outgassing Temperature/K | Outgassing Time/hr | k x $10^{-4}$ $s^{-1}g^{-1}$ | Surface Area $m^2g^{-1}$ |
|---|---|---|---|
| 763 | 16 | 2.3 | 212 |
| 823 | 16 | 7.7 | 263 |
| 873 | 16 | 14.5 | 278 |
| 948 | 16 | 5.2 | 238 |
| 823 | 45 | 15.9 | 295 |

Table 6.16. Rate Constants for But-1-ene Isomerisation over Zeolite Ω as a Function of Outgassing Conditions.

The variation in catalytic activity with outgassing temperature is illustrated in Fig. 6.23. Isomerisation activity increases rapidly with increasing overnight (16 hr) outgassing temperature to a sharp maximum at ca. 873 K. At outgassing temperatures greater than this the activity decreases quite rapidly with further increase in temperature. Prolonged outgassing (45 hours) at 823 K resulted in a catalyst with substantially higher activity than a sample outgassed at the same temperature overnight (16 hours). The activity of this sample was the maximum observed for but-1-ene isomerisation over zeolite Ω.

The corresponding surface areas of the samples are also listed in Table 6.16. A plot of activity versus surface area (Fig. 6.24) illustrates the similar dependence of activity and surface area on outgassing conditions.

The variation in catalytic activity with outgassing time, indicated in the but-1-ene experiments was investigated in more detail using MCP as reactant. Preliminary experiments showed that subsequent isomerisation of but-1-ene, formed as a product from MCP isomerisation, proceeded at the same rate as but-1-ene originally admitted as reactant. Hence

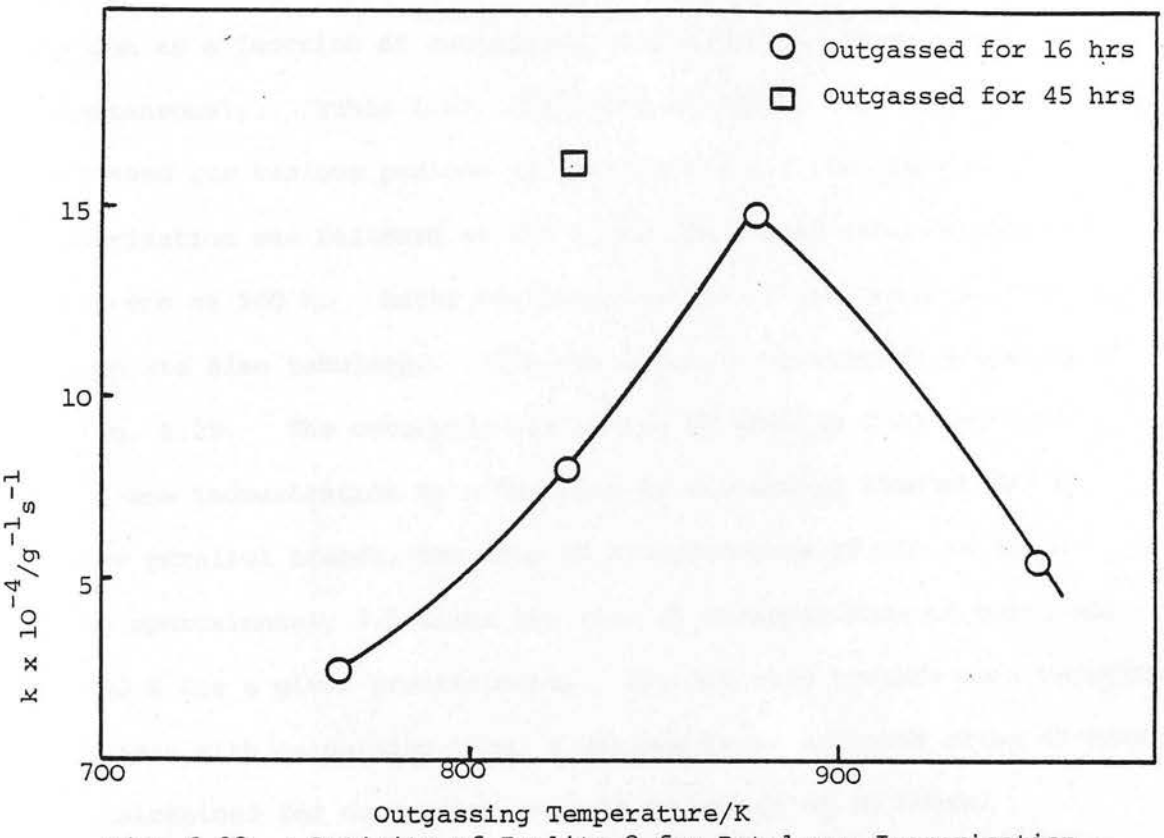


Fig. 6.23. Activity of Zeolite Ω for But-1-ene Isomerisation at 328 K as a Function of Outgassing Conditions

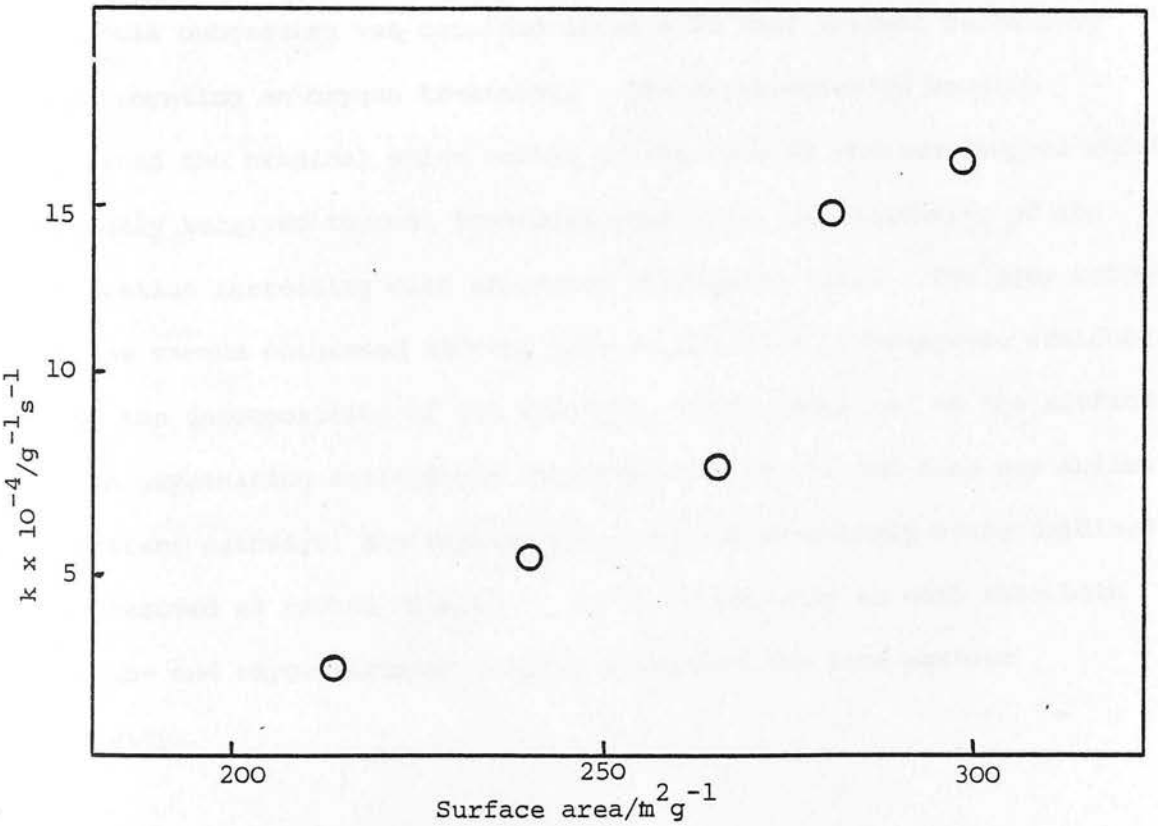


Fig. 6.24. Activity of Zeolite Ω for But-1-ene Isomerisation at 328 K as a Function of Surface Area

variation of activity of zeolite Ω for both MCP and but-1-ene isomerisation as a function of outgassing time could be investigated simultaneously. Table 6.17. lists the 1st order rate constants of samples outgassed for various periods of time at 823 K. The rate of MCP isomerisation was followed at 328 K and the slower isomerisation of but-1-ene at 340 K. Rates of isomerisation of samples pretreated with oxygen are also tabulated. The results are represented graphically in Fig. 6.25. The catalytic activities of zeolite Ω for MCP and but-1-ene isomerisation as a function of outgassing time at 823 K follow parallel trends, the rate of disappearance of MCP at 328 K being approximately 3.5 times the rate of disappearance of but-1-ene at 340 K for a given pretreatment. The activity towards both reactants increases with outgassing time, a maximum being achieved after 40 hours and maintained for outgassing periods in excess of 80 hours.

The enhancement of activity by oxygen pretreatment is illustrated in Figs. 6.26 (a) and (b). The maximum activity achieved after 40 hours outgassing was attained after a 20 hour thermal outgassing incorporating an oxygen treatment. The oxygen-treated samples retained the original white colour of the zeolite whereas samples which had only received thermal treatment were grey, the intensity of the coloration increasing with increased outgassing time. The grey colour of the vacuum outgassed samples must be due to a carbonaceous residue, from the decomposition of the TMA ions, being deposited on the surface. In an oxygenating environment decomposition of the TMA ions may follow different pathways, any carbonaceous residue presumably being oxidised and removed as carbon dioxide. It is interesting to note that both vacuum- and oxygen-treated samples exhibited the same maximum activity.

| Outgassing Time/hr | $k_a/s^{-1}g^{-1} \times 10^{-3}$ | ln $k_a$ | $k_b/s^{-1}g^{-1} \times 10^{-4}$ | ln $k_b$ |
|---|---|---|---|---|
| 4 | .19 | -8.57 | | |
| 6 | .63 | -7.37 | | |
| 12 | 1.46 | -6.53 | 4.67 | -7.67 |
| 16 | 2.08 | -6.18 | | |
| 16 | | | 11.33[C] | -6.78 |
| 17.5 | 3.69 | -5.60 | 11.8 | -6.74 |
| 19.5 | | | 15.92[C] | -6.44 |
| 21 | 5.51 | -5.20 | 18.3 | -6.30 |
| 34.5 | 8.53 | -4.76 | | |
| 40 | 10.1 | -4.60 | 29.3 | -5.83 |
| 65 | 9.8 | -4.63 | 28.2 | -5.87 |
| 86 | 10.5 | -4.56 | 26.0 | -5.95 |
| 87.5 | 9.5 | -4.66 | 29.8 | -5.82 |
| 2 [D] | 3.58 | -5.63 | 6.66 | -7.31 |
| 9.5[D] | 7.50 | -4.89 | 22.0 | -6.12 |
| 20 [D] | 10.05 | -4.60 | 27.4 | -5.90 |
| 40 [D] | 10.28 | -4.58 | 26.1 | -5.95 |

Table 6.17. Rates of Isomerisation of MCP and But-1-ene over Zeolite Ω outgassed at 823 K.

$k_a$ = 1st order rate constants for disappearance of MCP at 328 K.

$k_b$ = 1st order rate constants for disappearance of but-1-ene at 340 K.

C = Results from but-1-ene admitted as reactant in contrast to majority of results which were obtained for the disappearance of but-1-ene, formed as a product from MCP isomerisation.

D = Oxygen treatment of catalyst incorporated in the pretreatment.

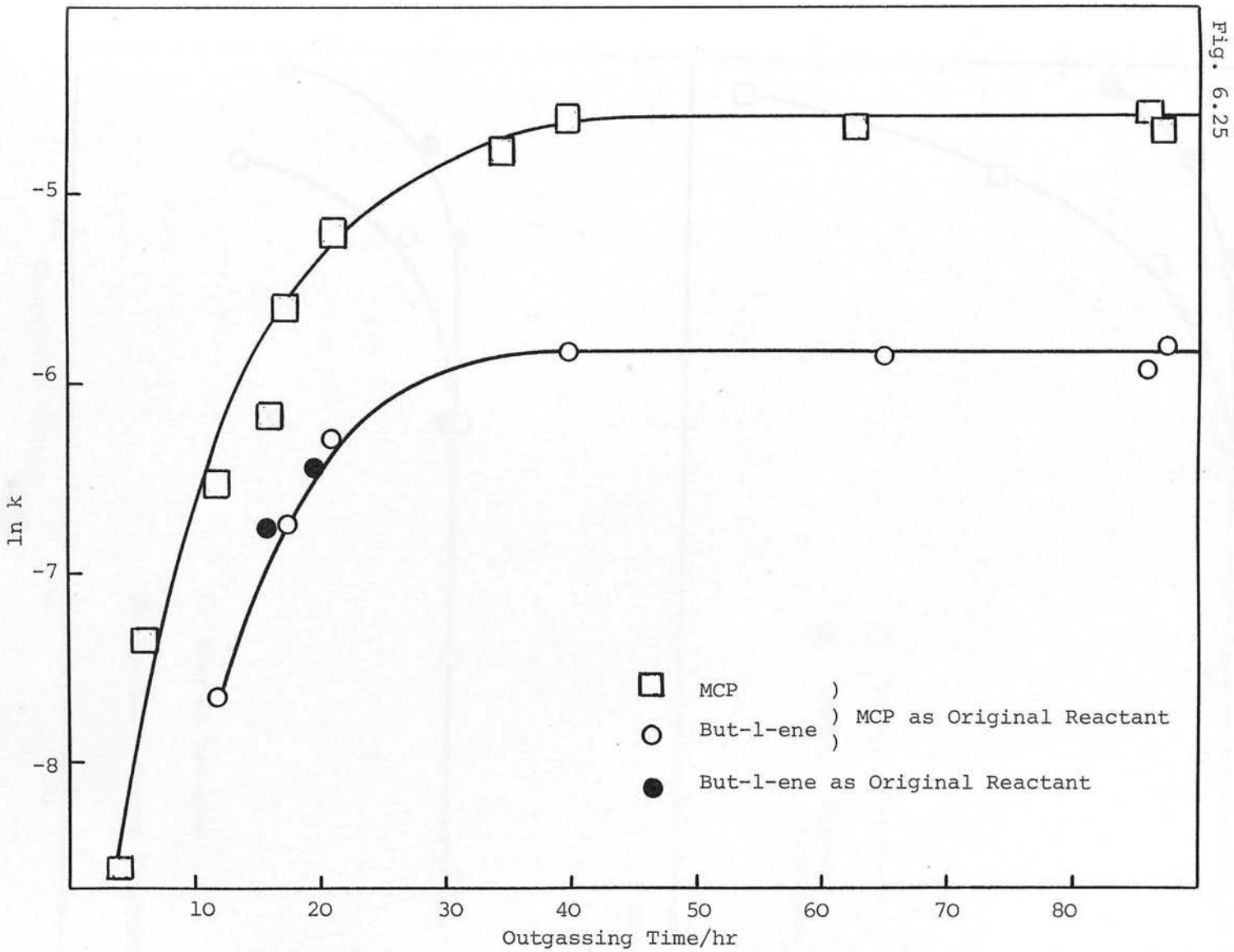


Fig. 6.25. Activity of Zeolite Ω for MCP Isomerisation (328 K) and Butene Isomerisation (340 K) as a Function of Outgassing Time at 823 K.

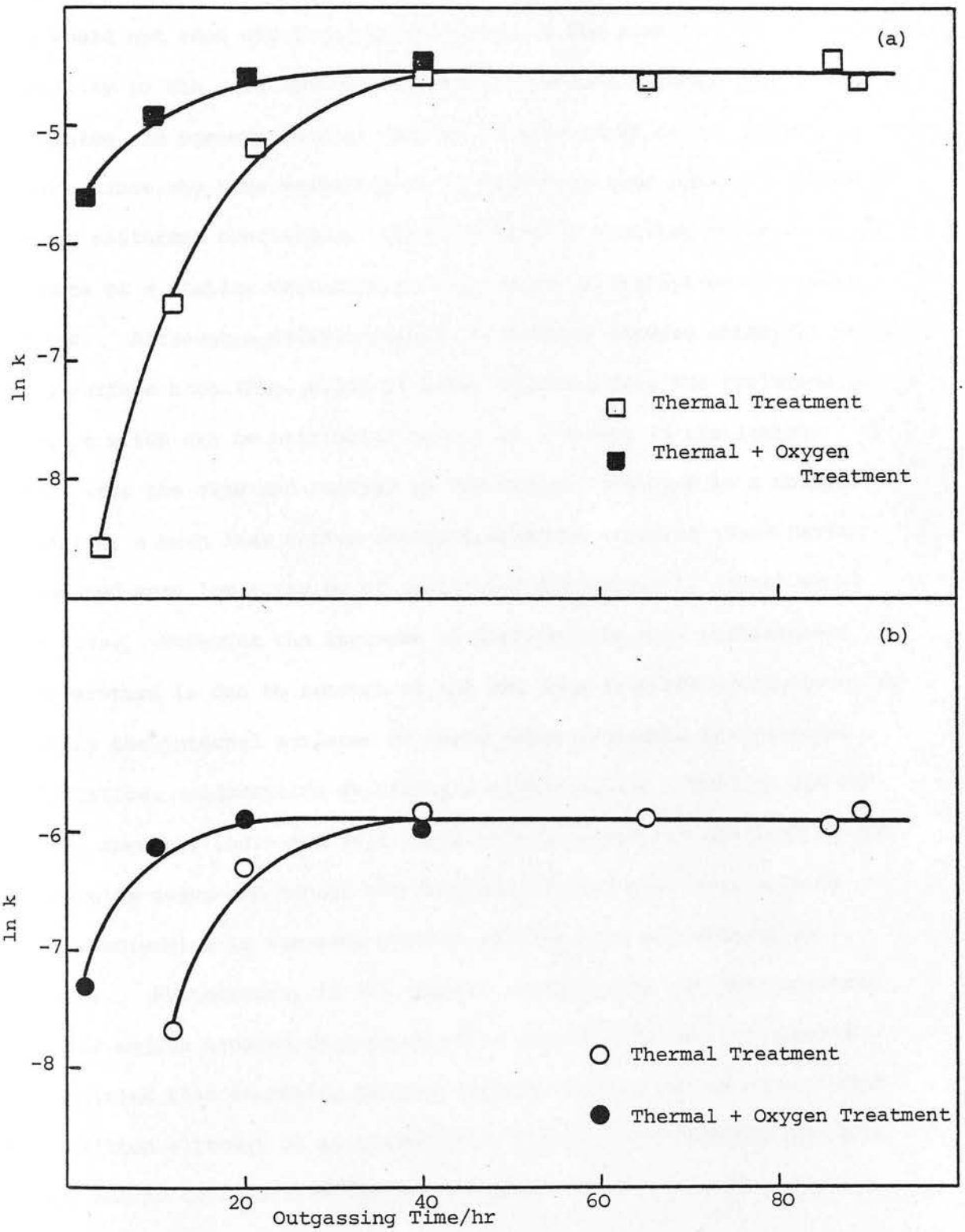


Fig. 6.26. Effect of Oxygen Treatment on Activity of Zeolite Ω

(a) MCP Isomerisation at 328 K
(b) But-1-ene Isomerisation at 340 K

The variation of surface area of zeolite Ω with pretreatment has been attributed to the removal of TMA cations and a collapse of structure. It would not seem unreasonable to attribute the similar trend in catalytic activity to the same sources. Observed product ratios, activation energies and pre-exponential factors, discussed in detail in Chapter 7, demonstrate the same mechanism to be operative over samples pretreated under different conditions; the variation in activity being a consequence of a similar variation in the number of catalytically active sites. Although a definite trend is observed between catalytic activity and surface area (Fig. 6.24) it seems unlikely that the variation in active sites can be attributed merely to a change in the latter. If this were the case and removal of TMA cations resulted in a sodium zeolite, a much less active catalyst would be expected Ward having reported very low activity of zeolites containing only alkali metal cations. Moreover the increase in surface area with pretreatment temperature is due to removal of the TMA ions from the gmelinite cages making the internal surfaces of these cages available for nitrogen adsorption. Adsorption experiments involving the n-butenes and MCP have, however, indicated that these molecules are not admitted to the gmelinite cages and hence, the internal surface area available to these molecules is the same whether the TMA ions are present or absent. Furthermore, if the zeolite surface area was the important factor oxygen treated samples would be expected to exhibit greater activities than thermally treated samples which show definite carbon deposition although it is conceivable that the carbonaceous residues need not be deposited on the active sites.

It therefore seems probable that the variation in activity with removal of the TMA cations is caused by the generation of catalytically active sites during the decomposition of these ions. Wu et al[90] have reported evidence for the generation of acidic structural hydroxyl groups from decomposition of TMA-offretite. These workers have postulated a number of mechanistic pathways which will explain both the complex product distribution and the generation of protonic acid sites. During decomposition of the TMA cations protons are released which interact with lattice oxygens to give rise to hydroxyl species. Weeks et al[176] have reported the appearance of a similar hydroxyl groups after calcination of ammonium exchanged Ω zeolite in air at 673 K. This hydroxyl group achieved maximum intensity at 873 K although X-ray diffraction showed that the zeolite had become amorphous at this temperature. These observations caused the authors to suggest that the hydroxyl group was not part of the zeolite framework but due to a hydroxy-aluminium species. In contrast the correlation between activity and surface area shown in Fig. 6.24 suggests that the hydroxyl groups generated here are part of the zeolite lattice.

It can be concluded therefore that the catalytic activity of zeolite Ω would appear to be a function of the number of acidic hydroxyl groups generated by the decomposition of the TMA ions. Furthermore the observed relationship between activity and removal of TMA (evidenced by surface area measurements) suggests that at least a proportion of these active sites must be generated in positions accessible to reactant molecules i.e. in the main channel.

The foregoing has provided an explanation for the observed increase in activity with pretreatment temperature. However activity, in addition to surface area, attained a sharp maximum beyond which both parameters decreased rapidly with further increase in temperature. Decrease in

activity could therefore be attributed to a decrease in the surface area. Conversely it could be due to dehydroxylation resulting in a decreased number of sites. Dehydroxylation of zeolites at temperatures in excess of 673 K has been reported in a number of instances. Weeks et al[176] have reported crystal collapse of ammonium exchanged Ω zeolite near 773 K prior to dehydroxylation and the hydroxyl groups of offretite generated from TMA decomposition undergo dehydroxylation at 773 K. It therefore seems likely that dehydroxylation of zeolite Ω is occurring at temperatures >873 K resulting in a decreased activity. It is possible that such a process may be accompanied by a slight alteration in structure resulting in the almost parallel decrease in surface area.

### 6.3.2. Erionite

Isomerisation of MCP over samples of erionite (N) and (T) outgassed at 623 K and 673 K exhibited no alteration in rate with outgassing temperature. This correlates with the constant surface area observed over this temperature and suggests that, if hydroxyl groups are the active sites, no dehydroxylation of the surface occurs at temperatures below 673 K.

# Chapter 7

## Results and Discussion - Part II

## Isomerisation Reactions

### 7.1. Reactions of n-Butenes

#### 7.1.1. Reactions over Zeolite Ω

a) But-1-ene Isomerisation

The variation in activity of zeolite Ω for but-1-ene isomerisation as a function of pretreatment has been discussed in Section 6.3. Samples outgassed between 773 K and 984 K exhibited isomerisation activity in the temperature range 291 K - 365 K. Maximum activity was observed for samples outgassed at 823 K for 20 hours and oxygen treated or samples outgassed at this temperature for periods in excess of 40 hours.

A typical reaction plot for but-1-ene isomerisation over zeolite Ω is illustrated in Fig. 7.1(a). The derived first order plot is shown in Fig. 7.1(b). All samples studied, regardless of pretreatment or reaction temperature, exhibited first order plots in which an initial fast rate (lasting for ca. 10-20 minutes) and a slower steady rate, maintained until ca. 90% but-1-ene conversion, were apparent. The results are given in Table 7.1, the first order rate constants quoted being those of the slower steady rate.

The Arrhenius plots, shown in Fig. 7.2, illustrate the variation of activity with pretreatment conditions discussed in Chapter 6. No change in activation energy is apparent, the activity pattern being due to an alteration in the pre-exponential factor with pretreatment. If this factor is taken as a measure of the number of sites available, the data in Table 7.1 agrees well with the proposed formation of sites by TMA ion decomposition and their reduction in number by dehydroxylation and/or collapse of the zeolite structure.

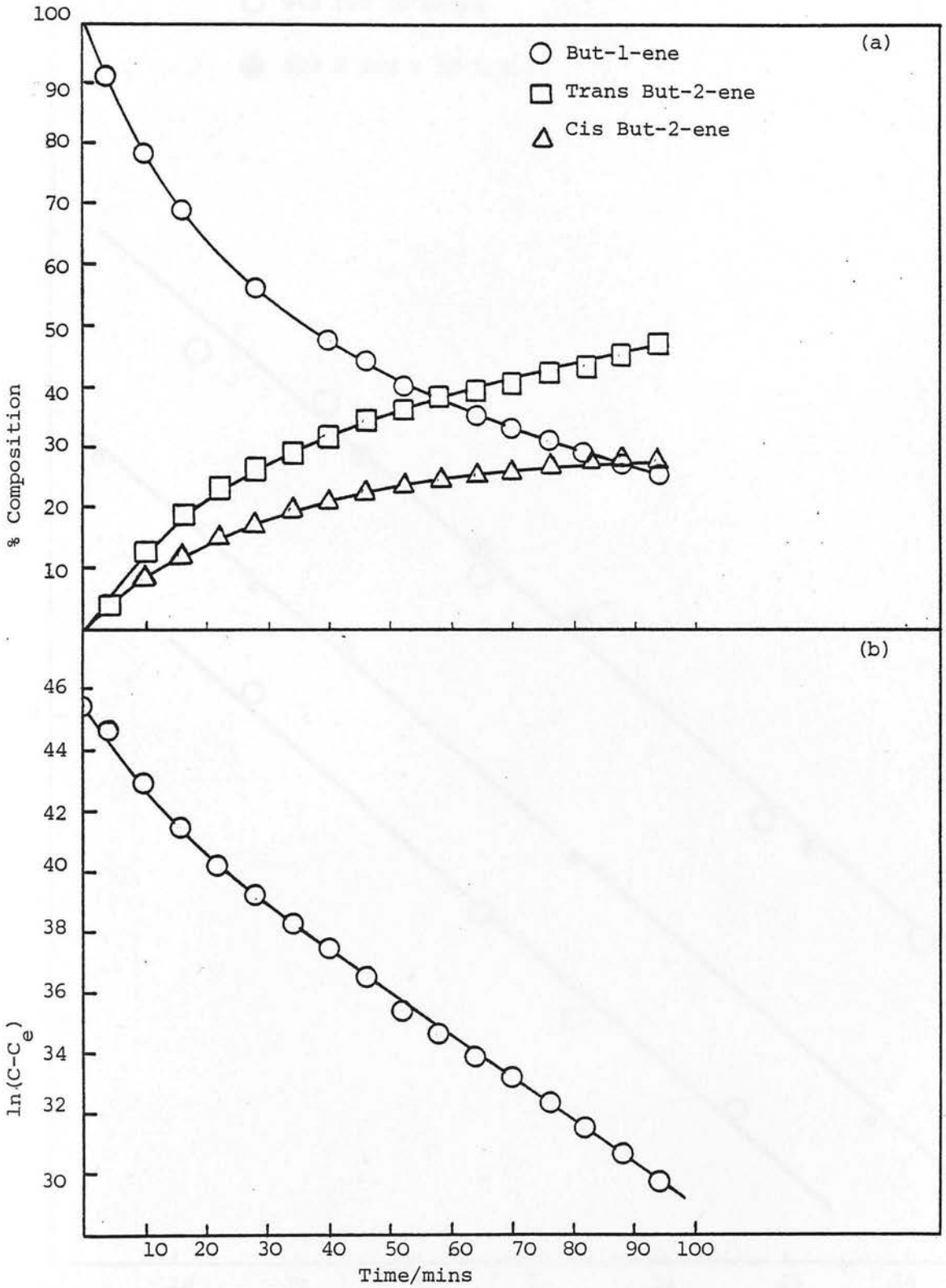


Fig. 7.1 (a) Reaction path for But-1-ene Isomerisation over Zeolite Ω at 349 K
(b) Derived first order plot

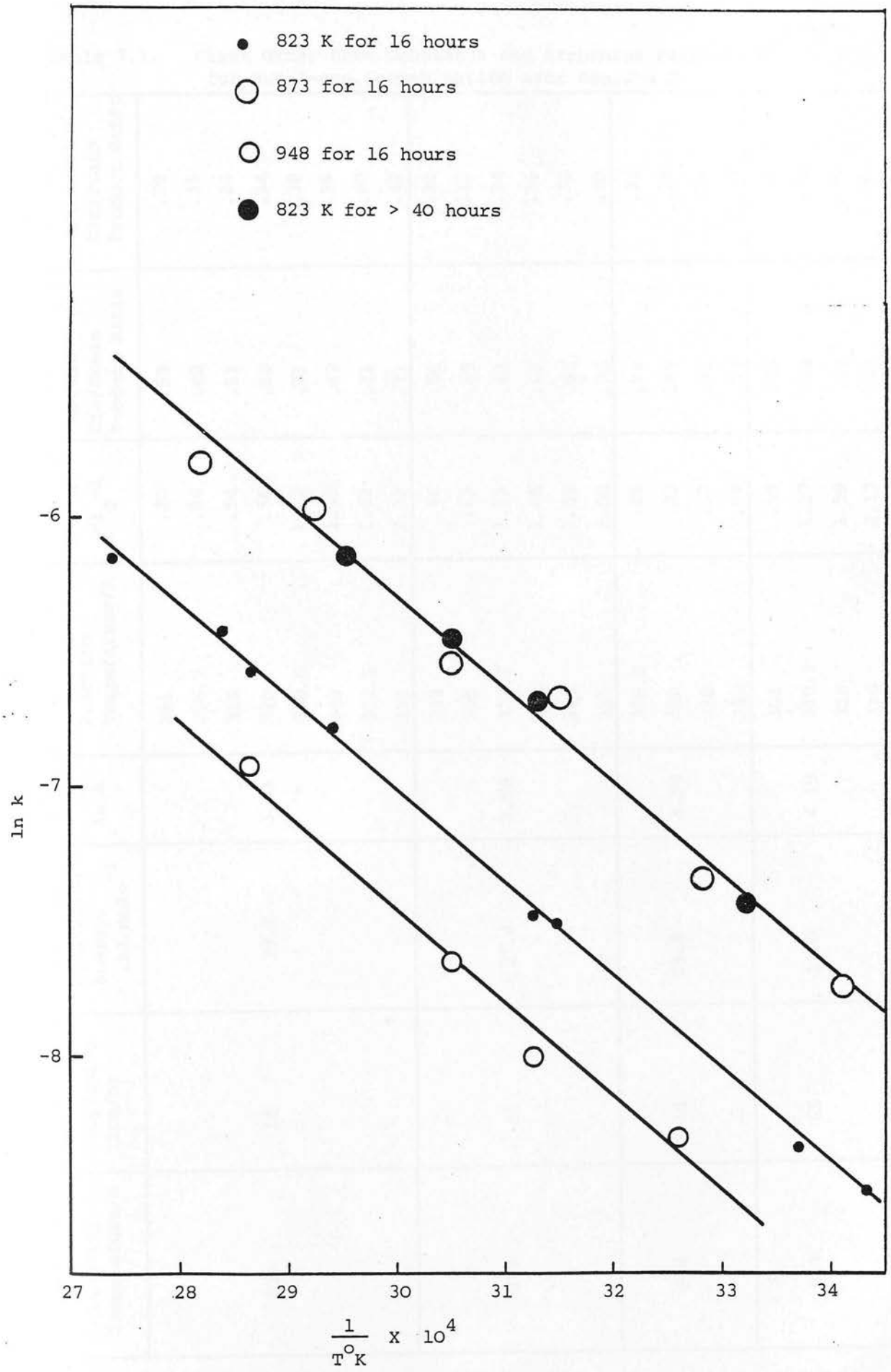


Fig. 7.2. Arrhenius Plots for Disappearance of But-1-ene over Zeolite Ω

Table 7.1. First Order Rate Constants and Arrhenius Parameters for But-1-ene Isomerisation over Zeolite Ω

| Outgassing Temperature/K | Outgassing Time/hr | Activation Energy/ kJ $mole^{-1}$ | ln A | Reaction Temperature/K | k x $10^{-3}$ $s^{-1}$ $g^{-1}$ | Initial Cis/Trans Product Ratio | Equilibrium Cis/Trans Product Ratio |
|---|---|---|---|---|---|---|---|
| 823 | 16 | 29.2 | 3.53 | 291 | .20 | .53 | .29 |
| | | | | 296.5 | .24 | .48 | .31 |
| | | | | 318 | .54 | .51 | .34 |
| | | | | 320 | .56 | .55 | .34 |
| | | | | 340.5 | 1.13 | .71 | .38 |
| | | | | 349 | 1.39 | .67 | .39 |
| | | | | 352.5 | 1.62 | .71 | .40 |
| | | | | 365 | 2.33 | .71 | .42 |
| 873 | 16 | 27.4 | 3.58 | 293 | .44 | .56 | .30 |
| | | | | 305 | .65 | .59 | .32 |
| | | | | 317.5 | 1.26 | .63 | .34 |
| | | | | 328 | 1.45 | .63 | .36 |
| | | | | 342 | 2.55 | .67 | .38 |
| | | | | 355 | 3.00 | .78 | .40 |
| 948 | 16 | 29.8 | 3.34 | 306.5 | .25 | .71 | .32 |
| | | | | 320 | .33 | .67 | .34 |
| | | | | 328 | .52 | .71 | .36 |
| | | | | 349 | .99 | .77 | .39 |
| 823 | 65 | 29.0 | 4.19 | 301 | .59 | .48 | .31 |
| | | | | 319.5 | 1.27 | .58 | .34 |
| | | | | 328 | 1.59 | .67 | .36 |
| | | | | 339 | 2.13 | .67 | .38 |

Product Ratios

Cis and trans but-2-ene were the only products of the reaction, no isobutene being observed. Comparison of the initial product ratios (Table 7.1) with the equilibrium data indicates the stereoselective nature of the isomerisation. In the temperature range studied the cis/trans ratio was always < 1 and showed a general trend with reaction temperature, the cis/trans ratio increasing as the temperature is increased. This variation with temperature is suggestive of a difference in energy between the transition states leading to the respective products, with the barrier to formation of cis being greater than that of trans. The temperature dependence of the initial selectivity ratio, plotted according to the Arrhenius equation (Fig. 7.3) yields a difference in the activation energies of ca. 3 kJ $mol^{-1}$. This is a substantial difference since most acidic catalysts exhibit cis/trans ratios which are near unity and are temperature independent,[179,195] indicative of transition states of similar energy. Furthermore such an energy difference is not reflected in the absolute product ratios which, in the temperature range studied, should lie between .21 and .29 and not .51 to .71 as observed. It is likely that factors other than a difference in energy of the respective transition states are contributing to the observed product ratio. Adsorption studies (Section 6.2.1) have suggested stronger adsorption of cis but-2-ene than the other two isomers, occurrence of which could contribute to the low cis/trans ratios observed. Alternatively the reaction may not be entirely kinetically controlled.

Little change in product ratio with extent of reaction was apparent until the equilibrium concentration of but-1-ene was approached. No significant alteration in selectivity with pretreatment conditions

Fig. 7.3. Arrhenius Plot of Variation in Cis/Trans Product Ratio with Temperature over Zeolite Ω

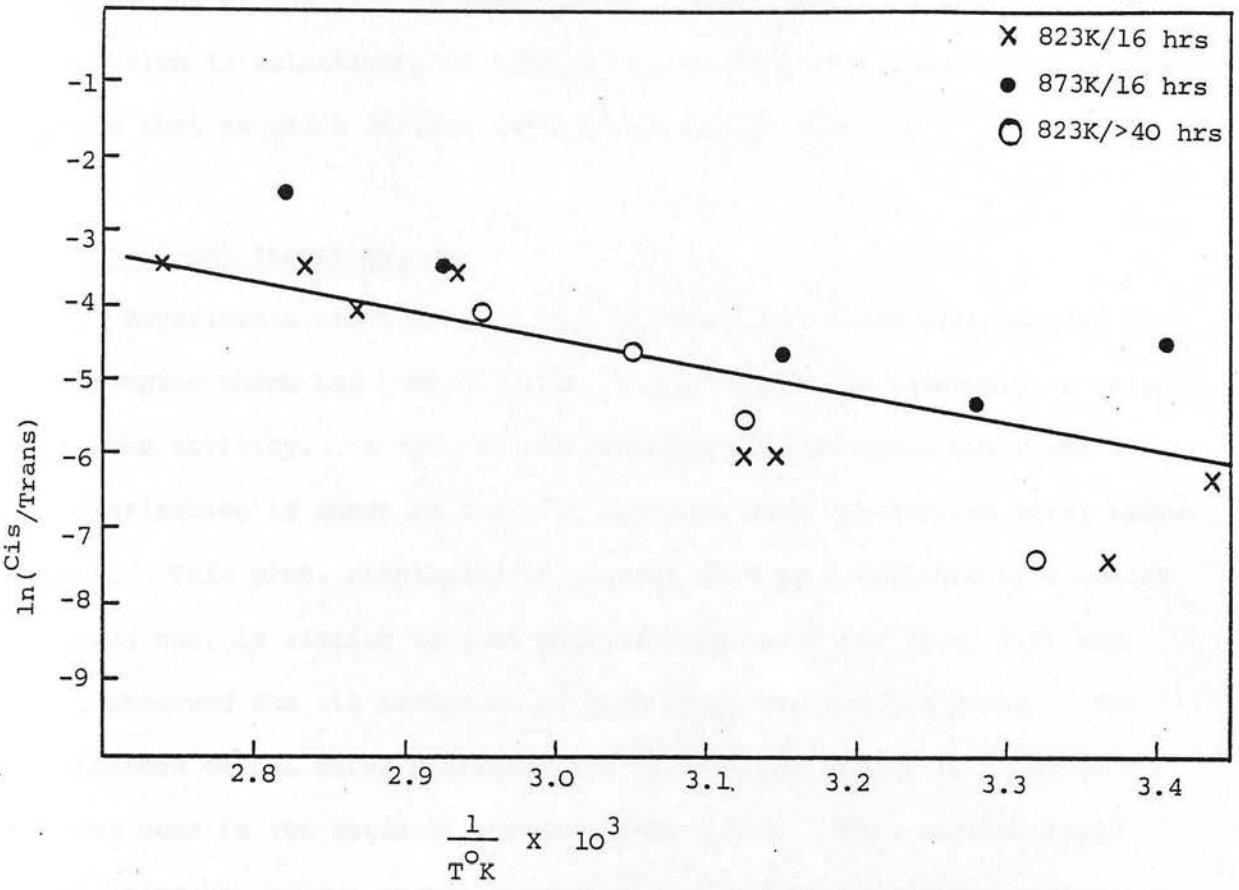


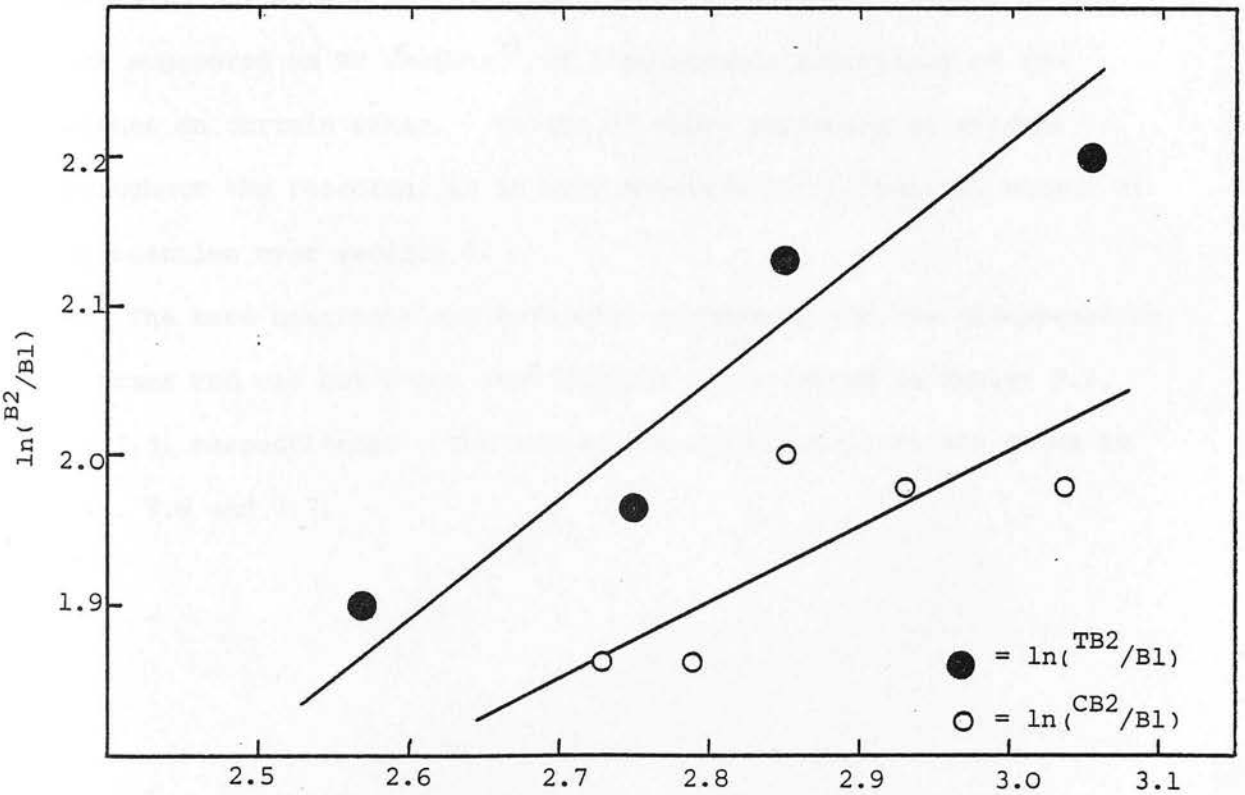


Fig. 7.4. Arrhenius Plots of Variation in Trans But-2-ene/But-1-ene and Cis But-2-ene/But-1-ene Ratio over Zeolite Ω

was observed although slightly higher ratios were apparent after outgassing at 948 K. Detreköy et al[91] have reported a similar reduction in selectivity of clinoptilolite at pretreatment temperatures above that at which lattice destruction starts (873 K).

b) But-2-ene Isomerisation

Experiments starting with cis and trans but-2-ene were carried out on samples which had been outgassed under conditions necessary to achieve maximum activity. A typical reaction profile for trans but-2-ene isomerisation is shown in Fig. 7.5 together with the derived first order plot. This plot, displaying an initial fast rate followed by a slower steady one, is similar to that observed for but-1-ene (Fig. 7.1) and was observed for all reactions of both trans and cis but-2-ene. For reactions of all three n-butenes the initial and steady first order rates were in the ratio of approximately 2.5:1. This initial rapid poisoning may be due to the formation of a polymeric residue as has been suggested on HY zeolite[91] or irreversible adsorption of the butenes on certain sites. Unlike HY where poisoning is evident throughout the reaction, it is only observed in the initial stages of the reaction over zeolite Ω.

The rate constants and Arrhenius parameters for the disappearance of trans and cis but-2-ene over zeolite Ω are listed in Tables 7.2. and 7.3. respectively. The respective Arrhenius plots are shown in Figs. 7.6 and 7.7.

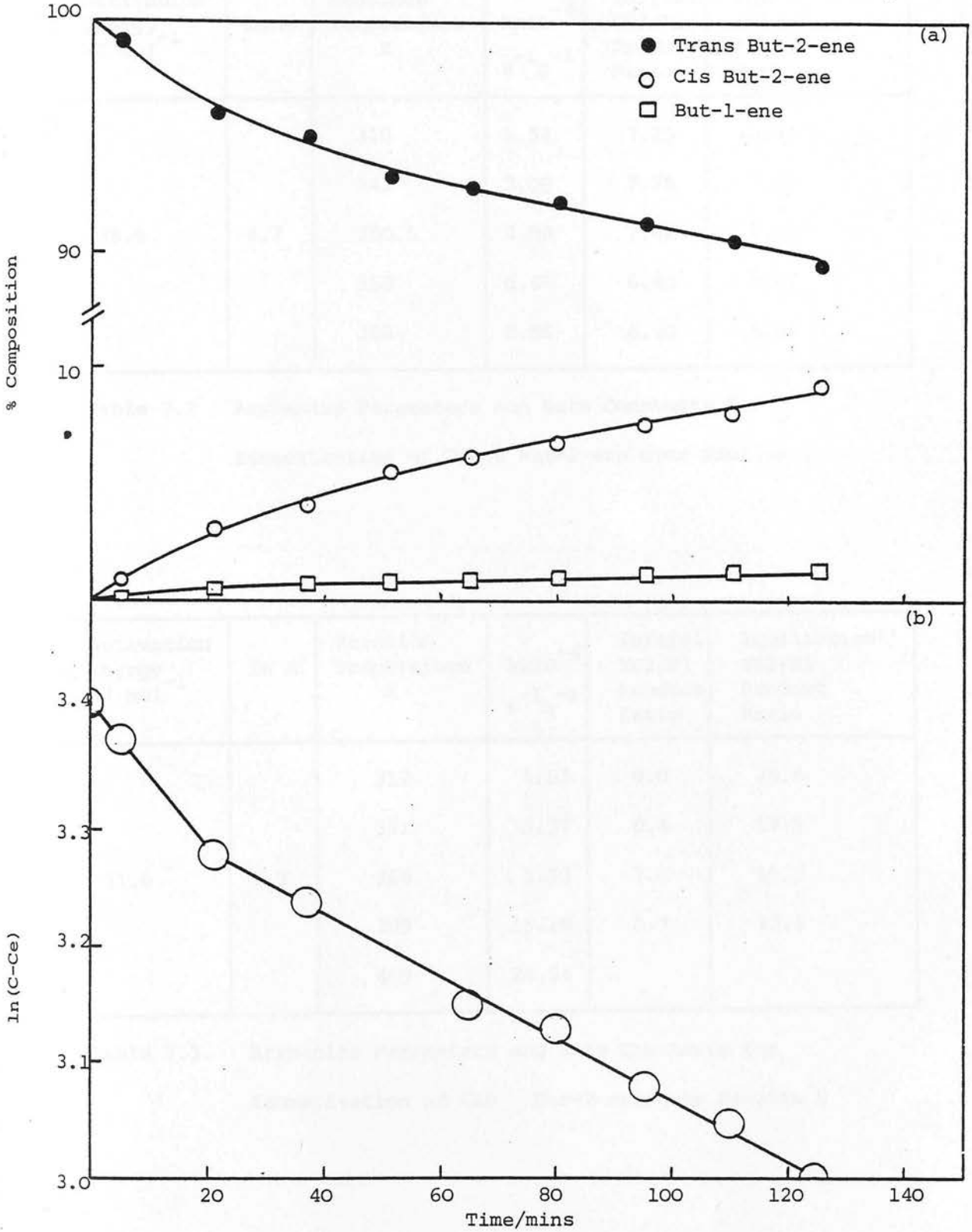


Fig. 7.5 (a) Reaction Profile for Trans But-2-ene Isomerisation over Zeolite Ω at 341 K

(b) Derived First Order Plot

| Activation Energy $_{-1}$ kJ mol | ln A | Reaction Temperature K | kx10$^{-4}$ $s^{-1}g^{-1}$ | Initial CB2/B1 Product Ratio | Equilibrium CB2/B1 Product Ratio |
|---|---|---|---|---|---|
| | | 319 | 1.54 | 7.25 | 8.45 |
| | | 341 | 3.08 | 7.25 | 7.59 |
| 35.9 | 4.7 | 350.5 | 4.98 | 7.42 | 7.11 |
| | | 358 | 6.46 | 6.40 | 6.67 |
| | | 366 | 8.55 | 6.40 | 6.36 |

Table 7.2 Arrhenius Parameters and Rate Constants for Isomerisation of Trans But-2-ene over Zeolite Ω

| Activation Energy $_{-1}$ kJ mol | ln A | Reaction Temperature K | kx10$^{-4}$ $s^{-1}g^{-1}$ | Initial TB2/B1 Product Ratio | Equilibrium TB2/B1 Product Ratio |
|---|---|---|---|---|---|
| | | 317 | 1.63 | 9.0 | 25.6 |
| | | 351 | 5.37 | 8.4 | 17.9 |
| 31.6 | 3.2 | 364 | 5.53 | 7.1 | 15.5 |
| | | 389 | 15.18 | 6.7 | 12.4 |
| | | 409 | 24.54 | | |

Table 7.3. Arrhenius Parameters and Rate Constants for Isomerisation of Cis But-2-ene over Zeolite Ω

Fig. 7.6. Arrhenius Plot for the Disappearance of Trans But-2-ene over Zeolite Ω

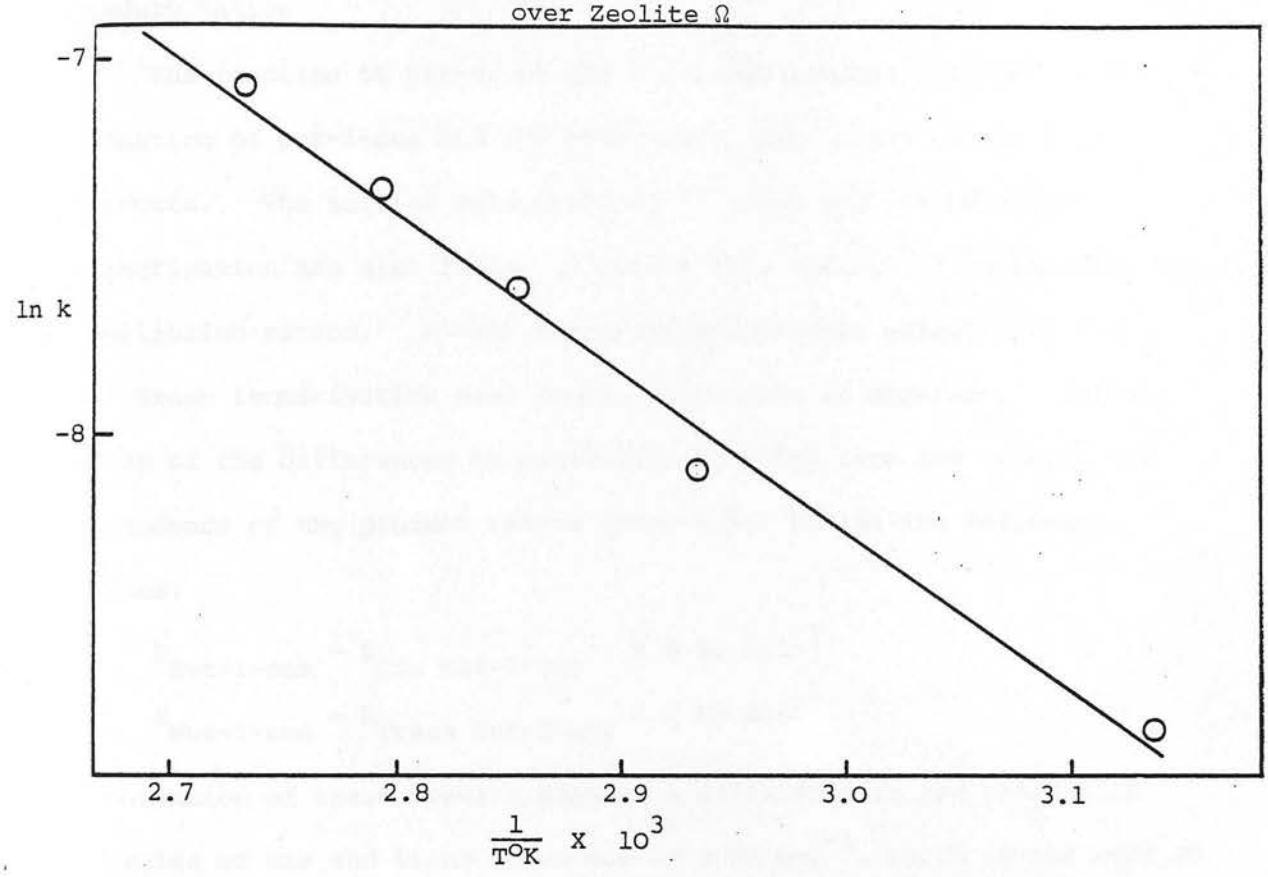


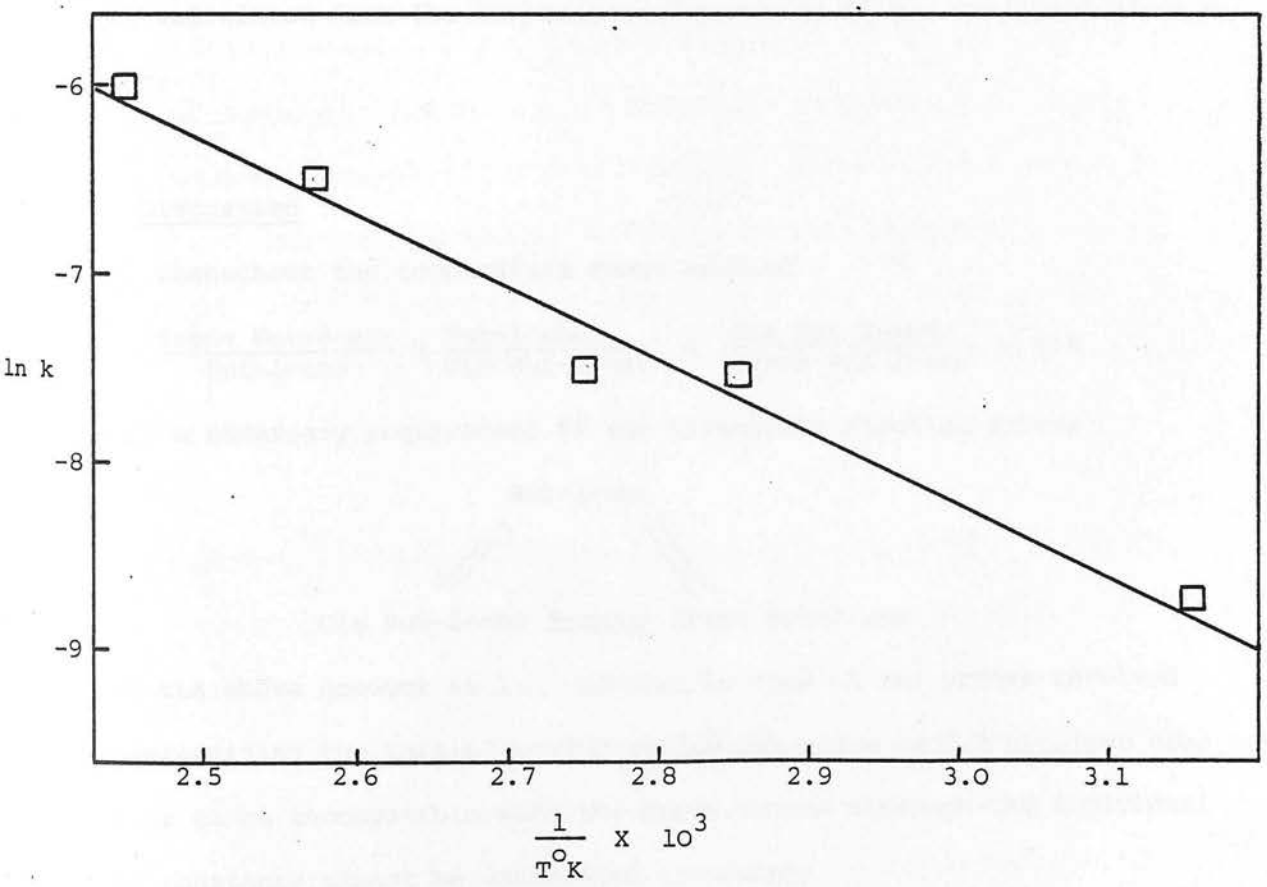


Fig. 7.7. Arrhenius Plot for the Disappearance of Cis But-2-ene over Zeolite Ω

Product Ratios

The reaction of either of the but-2-ene isomers resulted in the formation of but-1-ene and the other but-2-ene isomer as the only products. The initial selectivities of trans and cis but-2-ene isomerisation are also listed in Tables 7.2. and 7.3. together with the equilibrium ratios. A high temperature dependent selectivity for cis-trans isomerisation over double bond shift is apparent. Calculation of the differences in activation energies from the temperature dependence of the product ratios (Fig. 7.4.) yields the following values:

$$E_{\text{But-1-ene}} - E_{\text{Cis But-2-ene}} \simeq 4 \text{ kJ mol}^{-1}$$

$$E_{\text{But-1-ene}} - E_{\text{Trans But-2-ene}} \simeq 7 \text{ kJ mol}^{-1}$$

Combination of these results suggest a difference in the activation energies of cis and trans but-2-ene of 3 kJ $\text{mol}^{-1}$, which is the same as that calculated from the temperature dependency of the cis/trans product ratio.

c) Discussion

Throughout the temperature range studied

$$\frac{\text{Trans But-2-ene}}{\text{But-1-ene}} \times \frac{\text{But-1-ene}}{\text{Cis But-2-ene}} \times \frac{\text{Cis But-2-ene}}{\text{Trans But-2-ene}} \simeq 0.8$$

It is a necessary requirement of the triangular reaction scheme

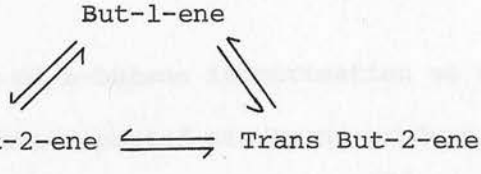


that the above product is 1. However in view of the errors involved in determining the initial productratios the value of 0.8 obtained does not appear to be incompatible with the above scheme although the individual rate constants cannot be calculated accurately.

The available data suggests that all reaction paths interconnecting the three n-butenes exist and contribute to the product ratios. Thus any mechanism which requires that rate constants interconnecting two isomers is zero cannot be solely responsible for the results. The only mechanism considered in the literature which will provide a direct pathway between all three isomers through a common intermediate is that involving the sec-butyl carbonium ion. The isomerisation reaction proceeding through this intermediate must be written as

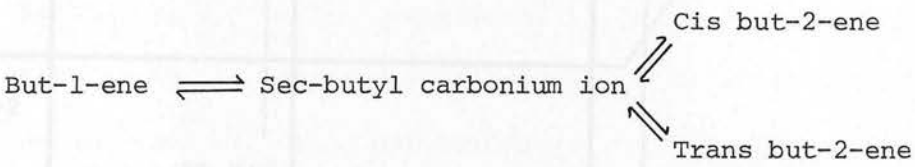


and the energy diagram can be represented as in Fig. 7.8.

Since the overall activation energies calculated for the disappearance of the but-2-enes are the sum of two parallel reactions they are represented in Fig. 7.8. as the energy difference between reactant but-2-ene and a barrier, intermediate between the energies of the transition states for but-1-ene and the other but-2-ene. In view of the greater selectivity for cis-trans isomerisation it would not seem unreasonable for this barrier to be closer to the but-2-ene transition state as shown. The derived activation energies for the disappearances of the but-2-enes is consistent with such a picture.

Previous studies of n-butene isomerisation on acidic catalysts, including zeolites, have reported cis/trans product ratios of 1-2[236] and but-2-ene/but-1-ene ratios of ca.0.5-1.1[187] to be consistent with a mechanism involving the sec-butyl carbonium ion. However Misono and Yoneda[191] have correlated cis-trans isomerisation/double bond shift selectivity with acid strength, their but-2-ene/but-1-ene

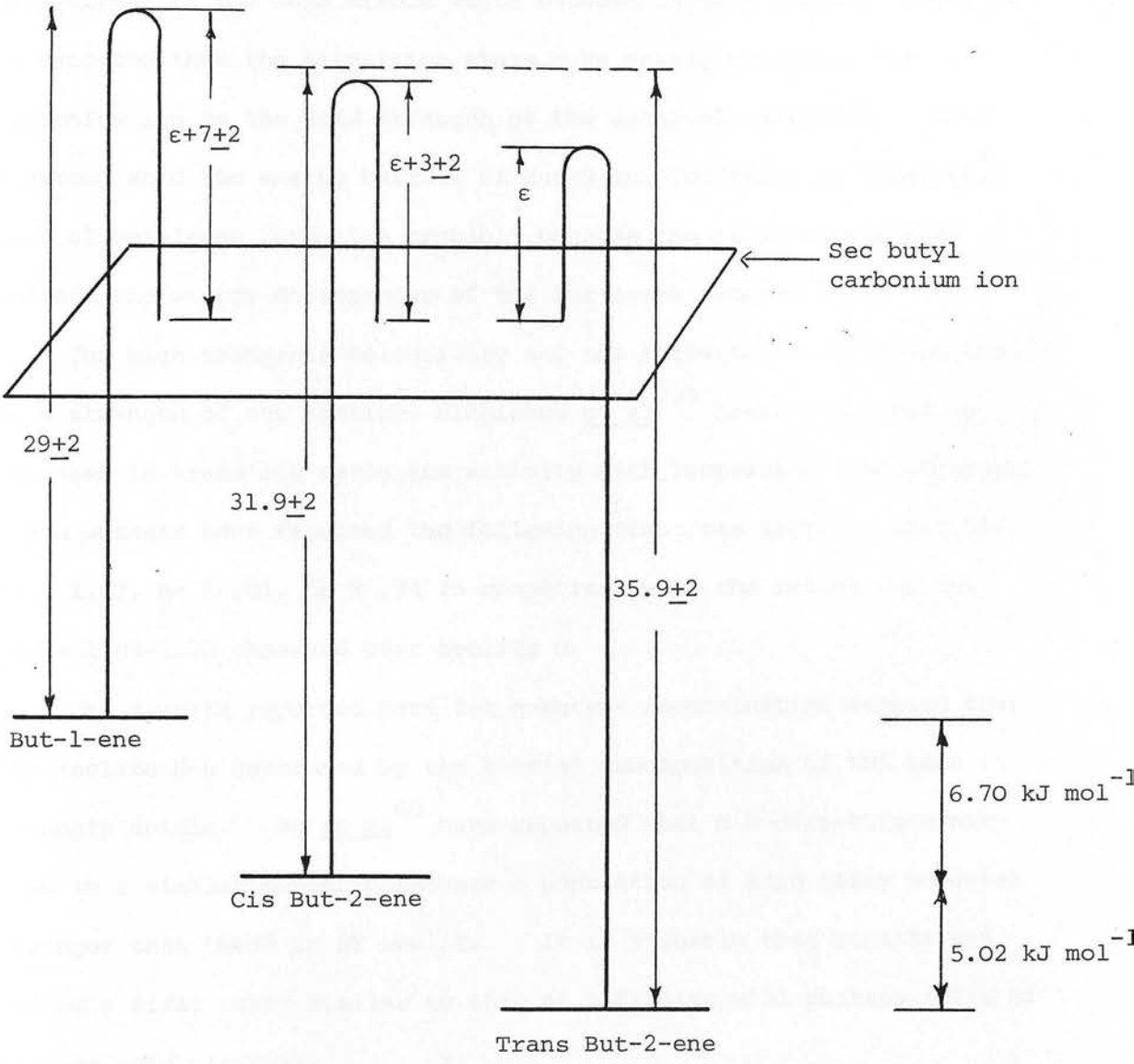


Fig. 7.8. Energy Diagram for Interconversion of n-Butenes over Zeolite Ω showing common intermediate.

selectivity (ca. 6.6) and activation energy difference (ca. 6 kJ $mol^{-1}$) over a strong acid catalyst (AlS) being similar to those reported here. Applying Hammonds[236] postulate that the transition state bears greater resemblance to the less stable state between initial and final ones it is expected that the transition state more nearly resembles the carbonium ion as the acid strength of the catalyst decreases. Over a strong acid the energy barrier of but-2-ene formation is lower than that of but-1-ene formation probably because the transition states reflect the energy differences of the but-1-ene isomers.

The high trans/cis selectivity and the activity also reflect the acid strength of the zeolite, Nishizawa et al[237] having reported an increase in trans/cis ratio and activity with increasing acid strength. These workers have reported the following trans/cis ratios; HX 1.55, Ce X 1.62, Mg X .81, Ca X .74 in comparison with the ratios in the range 1.89-1.28 observed over zeolite Ω.

The results reported here for n-butene isomerisation suggest that the zeolite H-Ω generated by the thermal decomposition of TMA ions is strongly acidic. Wu et al[90] have reported that a H-offretite generated in a similar manner possesses a population of acid sites somewhat stronger than those in HY zeolite. It is probable that zeolite H-Ω having a Si/Al ratio similar to that of offretite will possess sites of similar acid strength.

### 7.1.2. Reactions over Erionite

#### a) But-1-ene Isomerisation

Both samples of erionite (N) and (T) are active catalysts for the isomerisation of but-1-ene although the temperature ranges over which similar rates of isomerisation were observed differed for the two zeolites; erionite (N), 349-422 K and erionite (T), 295-359 K.

This illustrates the difference in activity of the two samples. Typical reaction profiles and first order plots of but-1-ene isomerisation over erionite (N) and (T) are shown in Figs. 7.9. and 7.10. respectively. The noticeable difference in product ratios is principally a function of temperature and will be discussed later. All first order plots of but-1-ene disappearance over erionite (N) exhibited an initial acceleratory period followed by a steady first order rate maintained until but-1-ene concentrations close to the equilibrium value are obtained. In contrast the first order plots over erionite (T) showed an initial decelerating period after which a steady rate was maintained. The rate constants tabulated together with the Arrhenius parameters in Tables 7.4 and 7.5 are those of the steady first order rates for both catalysts. The Arrhenius plots are illustrated in Fig. 7.11. In the temperature range common to studies over both erionites (348-358 K) the rate of isomerisation of but-1-ene over erionite (T) was ca. 15 times greater than that over erionite (N) although this factor alters with reaction temperature because of the difference in activation energy over the two erionites.

Product Ratios

The only products resulting from but-1-ene isomerisation over both erionites were cis and trans but-2-ene. Initial cis/trans product ratios and the equilibrium values are listed in Tables 7.4. and 7.5. The product ratio decreases with extent of reaction, for example isomerisation of but-1-ene at 327 K over erionite (T) exhibits an initial cis/trans selectivity of 1.56 which decreases slowly to a value of 0.99 at 90% conversion.

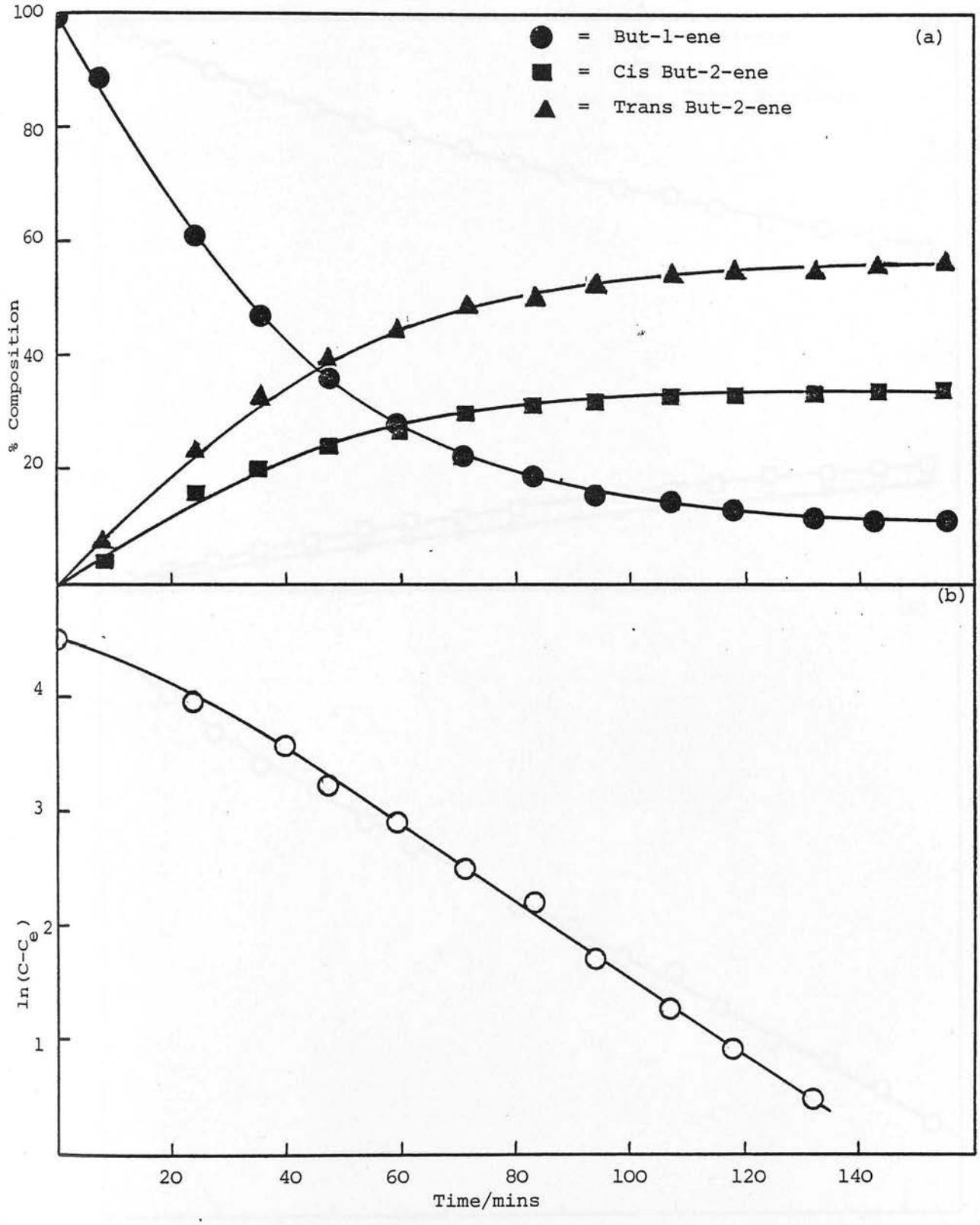


Fig. 7.9. (a) Reaction Profile of Isomerisation of But-1-ene on Erionite (N) at 416 K.

(b) Derived First Order Plot.

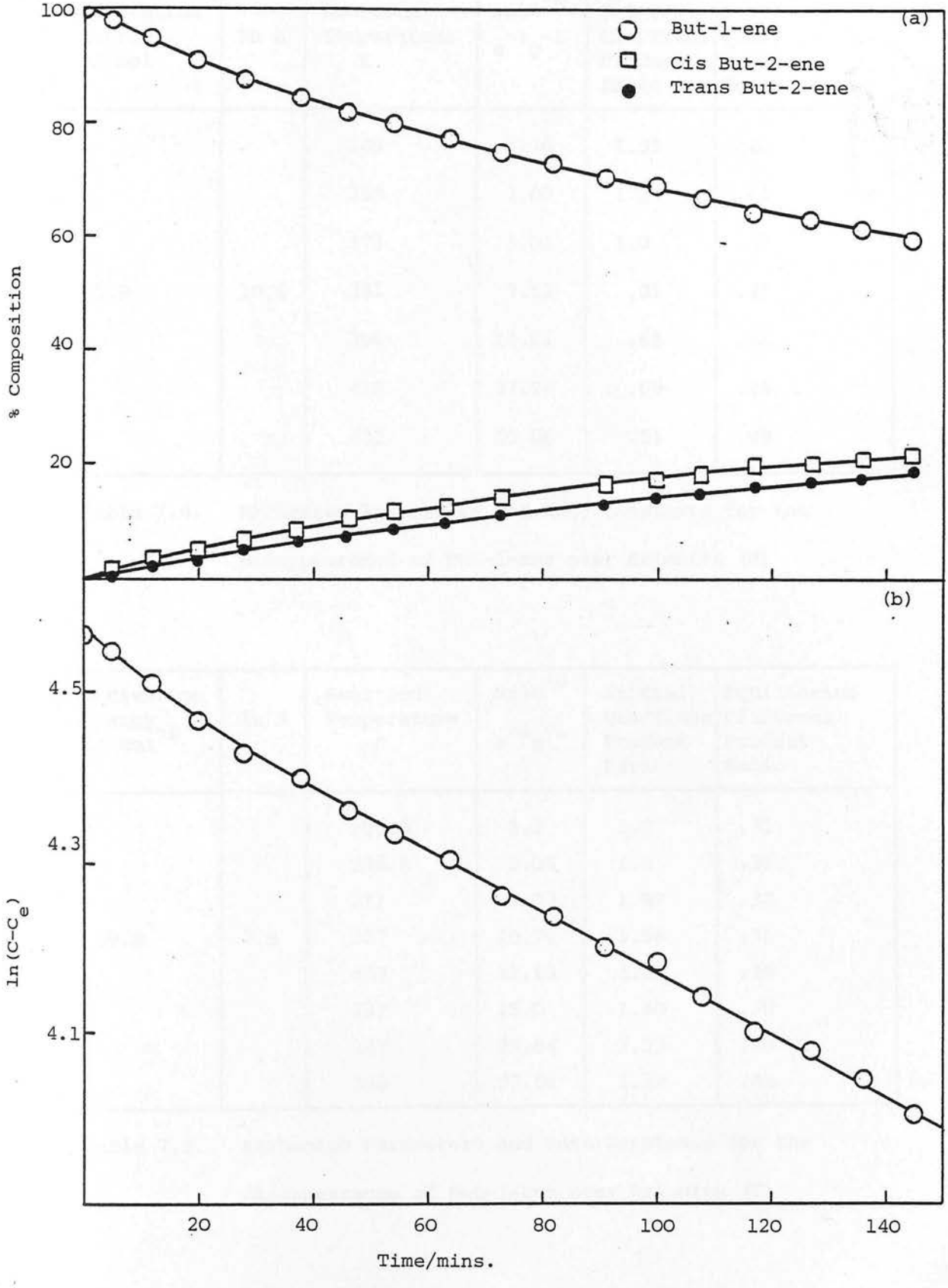


Fig. 7.10. (a) Reaction Profile for Disappearance of But-1-ene over Erionite (T) at 311 K.

(b) Derived First order plot.

| Activation Energy $kJ\ mol^{-1}$ | ln A | Reaction Temperature K | $kx10^{-4}$ $s^{-1}g^{-1}$ | Initial Cis/Trans Product Ratio | Equilibrium Cis/Trans Product Ratio |
|---|---|---|---|---|---|
| | | 349 | 1.76 | 1.35 | .40 |
| | | 359 | 3.07 | 1.24 | .41 |
| | | 373 | 5.01 | 1.0 | .44 |
| 55.9 | 10.6 | 381 | 7.52 | .91 | .45 |
| | | 396 | 14.61 | .85 | .46 |
| | | 416 | 37.94 | .69 | .48 |
| | | 422 | 50.86 | .51 | .49 |

Table 7.4. Arrhenius Parameters and Rate Constants for the Disappearance of But-1-ene over Erionite (N)

| Activation Energy $kJ\ mol^{-1}$ | ln A | Reaction Temperature K | $kx10^{-4}$ $s^{-1}g^{-1}$ | Initial Cis/Trans Product Ratio | Equilibrium Cis/Trans Product Ratio |
|---|---|---|---|---|---|
| | | 295.5 | 2.3 | 1.8 | .31 |
| | | 295.5 | 2.05 | 1.8 | .31 |
| | | 311 | 5.03 | 1.69 | .33 |
| 39.9 | 7.8 | 327 | 10.76 | 1.56 | .35 |
| | | 333 | 12.13 | 1.37 | .36 |
| | | 337 | 15.0 | 1.40 | .38 |
| | | 347 | 25.84 | 1.33 | .40 |
| | | 358 | 37.56 | 1.39 | .41 |

Table 7.5. Arrhenius Parameters and Rate Constants for the Disappearance of But-1-ene over Erionite (T)

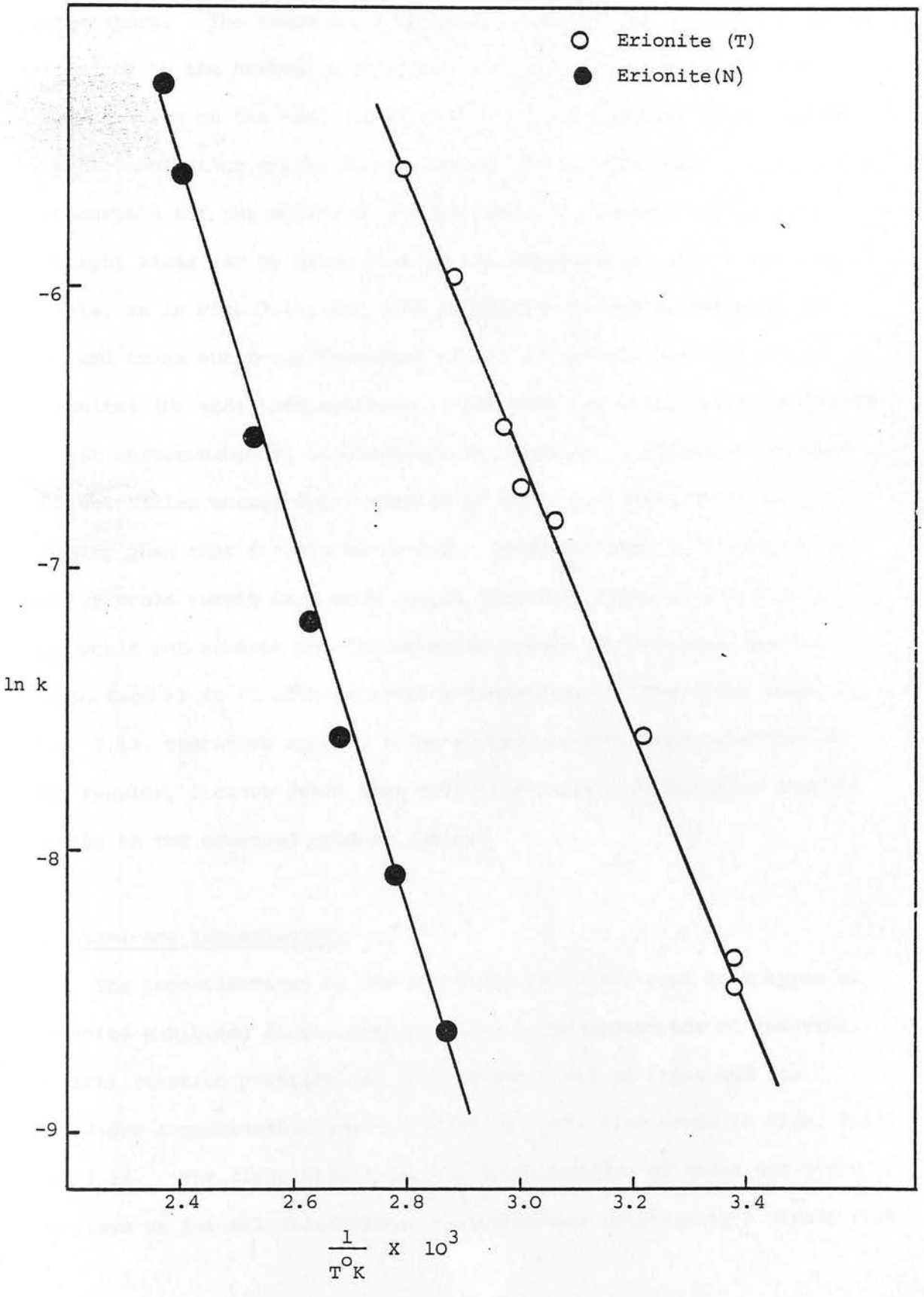


Fig. 7.11. Arrhenius Plots for the Disappearance of But-1-ene over Erionite

The initial cis/trans product ratios of both erionites are markedly dependent on reaction temperature, decreasing with increasing temperature. The temperature dependence of the selectivity is plotted according to the Arrhenius equation in Fig. 7.12., results for both samples lying on the same smooth curve. This suggests that a difference in activation energy for formation of the but-2-enes is not wholly responsible for the observed product ratios. However approximate straight lines may be drawn through the experimental points for each sample, as in Fig. 7.12, yielding activation energy differences for cis and trans but-2-ene formation of ca. 15 and ca. 3 kJ $mol^{-1}$ for erionites (N) and(T)respectively. Although the value for erionite (T) is not unreasonable it is difficult to visualise a situation in which the activation energy for formation of trans but-2-ene is 15 kJ $mol^{-1}$ greater than that for cis but-2-ene. Moreover such a difference in energy would result in a much larger cis/trans ratio than observed and would not account for the observed change in cis/trans product ratio form >1 to <1 with increasing temperature. The curve shown in Fig. 7.12. therefore appears to be a more accurate representation of the results, factors other than activation energy differences contributing to the observed product ratios.

b) But-2-ene Isomerisation

The isomerisations of cis and trans but-2-ene over both types of erionite exhibited first order kinetics in disappearance of reactant. Typical reaction profiles and first order plots of trans and cis but-2-ene isomerisation over erionite (N) are illustrated in Figs. 7.13. and 7.14. The first order plot for disappearance of trans but-2-ene displays an initial decelerating period before maintaining a steady rate

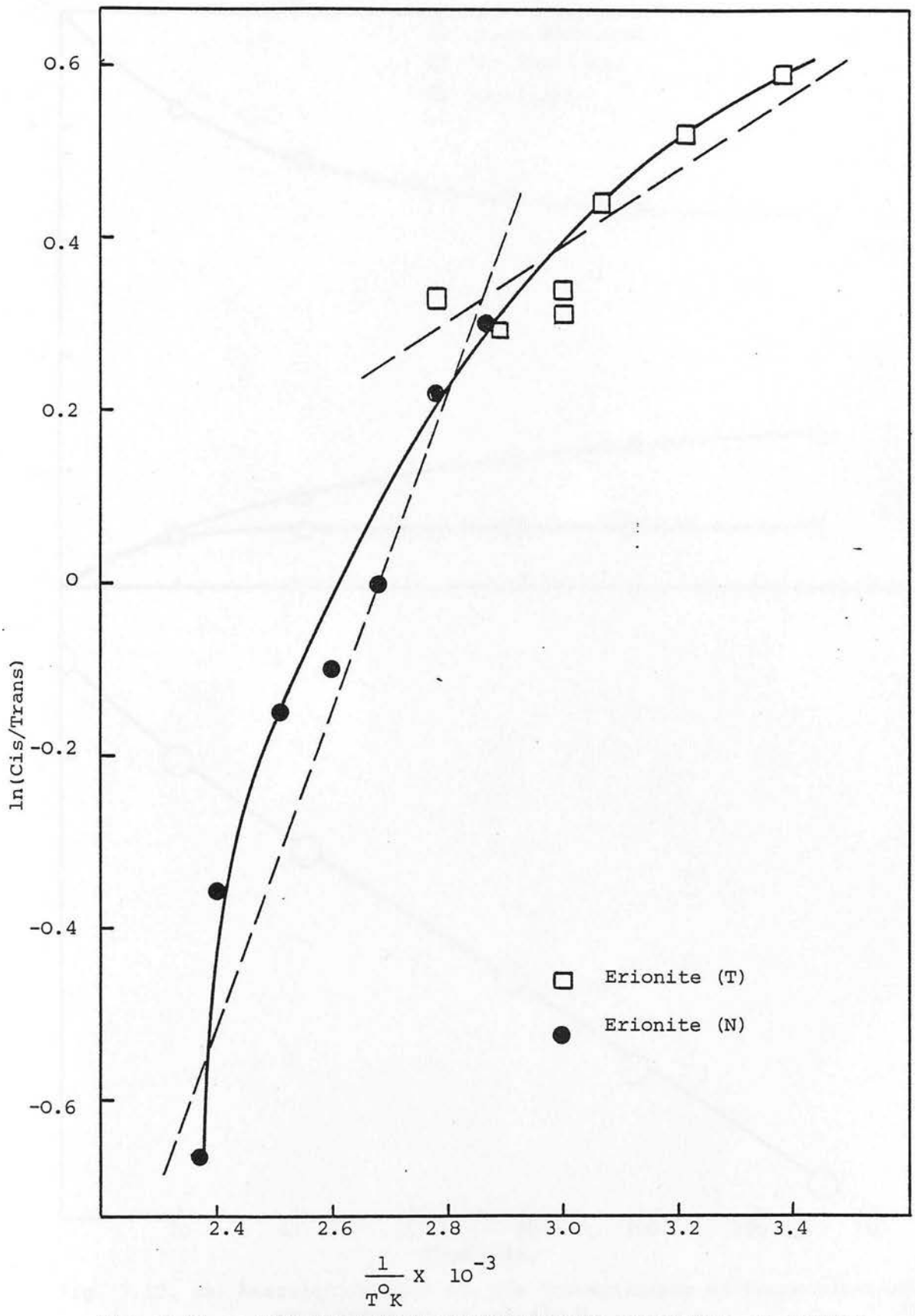


Fig. 7.12. Arrhenius Plot of Temperature Dependence of Initial Cis/Trans Product Ratio

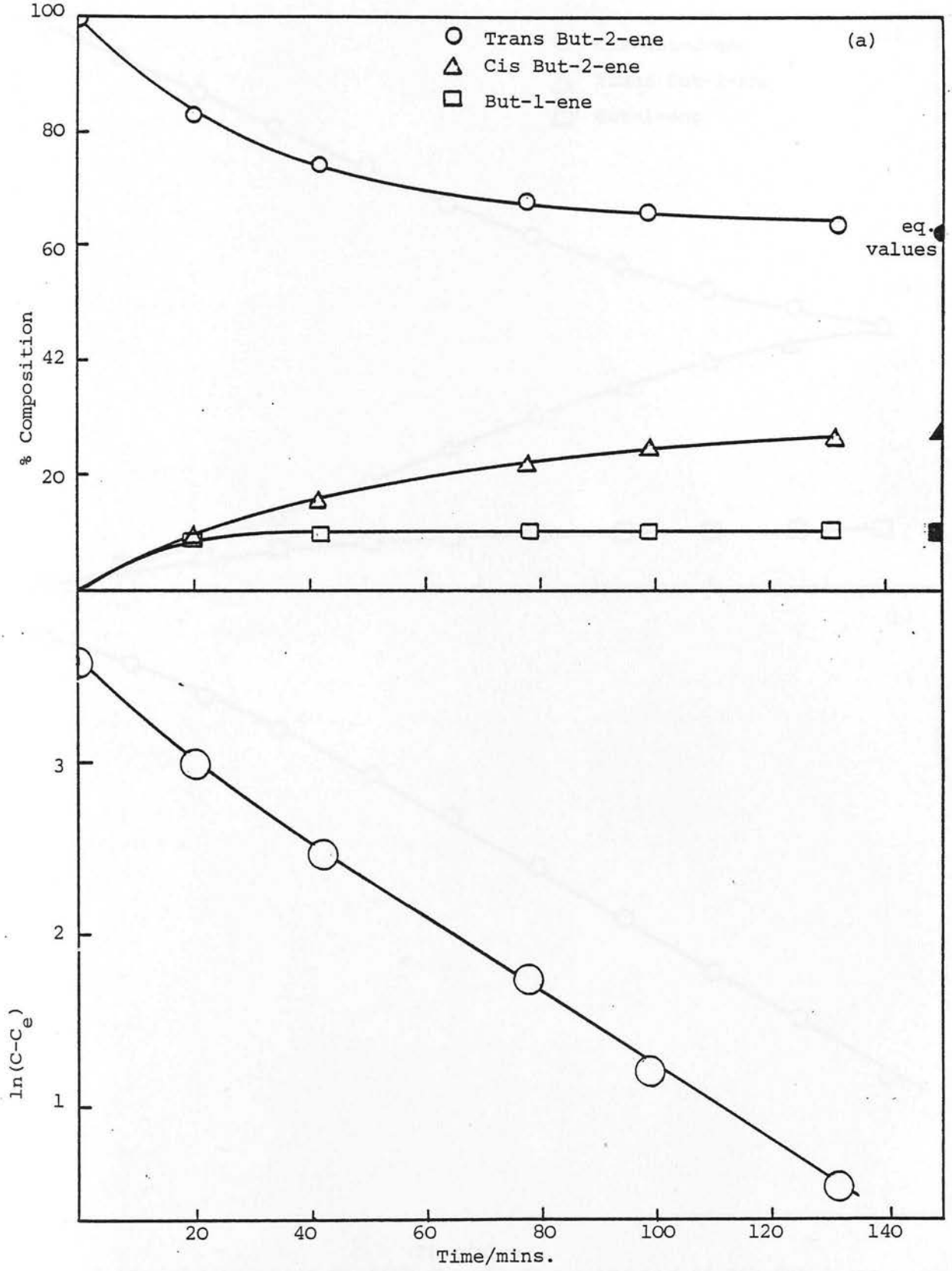


Fig. 7.13. (a) Reaction Profile for the Isomerisation of Trans But-2-ene over Erionite (N) at 420 K

(b) Derived First Order Plot.

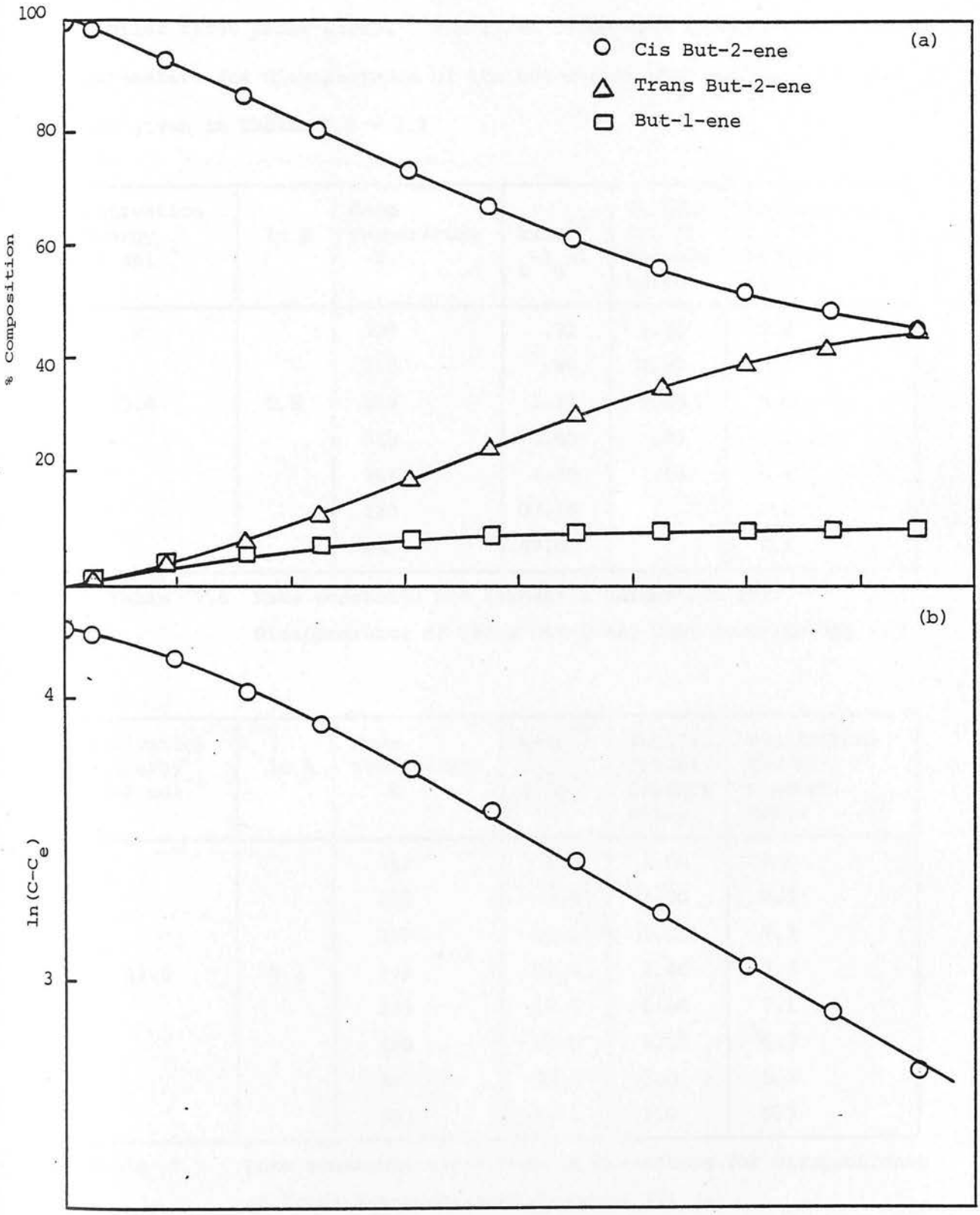


Fig. 7.14: (a) Reaction Profile for the Isomerisation of Cis But-2-ene over Erionite (N) at 431 K.

(b) Derived First Order Plot

whereas that of cis but-2-ene exhibits an initial acceleratory period. The isomerisations of trans and cis but-2-enes over erionite (T) display similar first order plots. The first order rate constants and Arrhenius parameters for disappearance of the but-2-enes over erionite (N) and (T) are given in Tables 7.6 - 7.9

| Activation Energy $kJ\ mol^{-1}$ | ln A | Room Temperature K | $kx10^{-4}$ $s^{-1}g^{-1}$ | Initial CB2/B1 Product Ratio | Equilibrium CB2/B1 Product Ratio |
|---|---|---|---|---|---|
| | | 307 | .72 | 2.92 | 9.4 |
| | | 313 | .86 | 2.47 | 9.2 |
| 39.4 | 5.8 | 322 | 1.11 | 1.46 | 8.5 |
| | | 348 | 4.60 | .87 | 7.1 |
| | | 361 | 4.50 | .58 | 6.6 |
| | | 420 | 37.19 | | 4.8 |
| | | 445 | 87.0 | | 4.2 |

Table 7.6 Rate constants and Arrhenius Parameters for Disappearance of Trans But-2-ene over Erionite (N)

| Activation Energy $kJ\ mol^{-1}$ | ln A | Room Temperature K | $kx10^{-4}$ $s^{-1}g^{-1}$ | Initial CB2/B1 Product Ratio | Equilibrium CB2/B1 Product Ratio |
|---|---|---|---|---|---|
| | | 312 | 2.7 | 3.60 | 9.2 |
| | | 328 | 6.41 | 1.90 | 8.3 |
| | | 337 | 10.1 | 1.95 | 7.7 |
| 42.5 | 8.3 | 343 | 13.7 | 1.40 | 7.3 |
| | | 349 | 18.9 | 1.10 | 7.1 |
| | | 359 | 24.0 | 1.05 | 6.7 |
| | | 385 | 68.4 | 1.0 | 5.7 |
| | | 385 | 64.1 | 1.0 | 5.7 |

Table 7.7 Rate constants and Arrhenius Parameters for Disappearance of Trans But-2-ene over Erionite (T)

| Activation Energy$_{-1}$ kJ mol | ln A | Reaction Temperature K | kx10$^{-4}$ $s^{-1}g^{-1}$ | Initial TB2/B1 Product Ratio | Equilibrium TB2/B1 Product Ratio |
|---|---|---|---|---|---|
| | | 327 | .09 | 2.33 | 23.8 |
| | | 349 | .35 | 1.42 | 17.8 |
| 55.2 | 8.7 | 418 | 7.66 | 1.34 | 9.8 |
| | | 431 | 15.6 | 1.11 | 9.2 |
| | | 437 | 17.0 | 1.50 | 8.5 |
| | | 454 | 28.4 | 1.0 | 7.6 |
| | | 479 | 48.2 | 1.11 | 6.4 |

Table 7.8 Rate constants and Arrhenius parameters for the Disappearance of Cis But-2-ene over Erionite (N)

| Activation Energy$_{-1}$ kJ mol | ln A | Reaction Temperature K | kx10$^{-4}$ $s^{-1}g^{-1}$ | Initial TB2/B1 Product Ratio | Equilibrium TB2/B1 Product Ratio |
|---|---|---|---|---|---|
| | | 311 | 8.33 | 1.20 | 29.6 |
| | | 319 | 1.41 | 1.20 | 26.8 |
| 62.2 | 14.6 | 327 | 2.58 | 1.05 | 23.8 |
| | | 332 | 4.49 | 1.0 | 21.7 |
| | | 343 | 7.69 | 1.05 | 19.6 |
| | | 355 | 15.8 | .90 | 16.9 |

Table 7.9 Rate constants and Arrhenius parameters for the disappearance of Cis But-2-ene over Erionite (T)

The Arrhenius plots are illustrated in Fig. 7.15 Both samples exhibit similar activation energies for the disappearance of cis and trans but-2-ene with that of cis being substantially greater than that of trans. The greater activity of erionite (T) is again apparent but surprisingly at 345 K the rates of disappearance of the trans and cis isomers over erionite (T) are 30 times and 4 times these over erionite (N). The ratio of rates of but-1-ene disappearance over the two catalysts at a similar temperature is ca. 14:1.

Product Ratios

Only but-1-ene and the other but-2-ene isomer are observed as products of the reaction of either cis or trans but-2-ene. The product ratio from either isomer changes considerably with extent of reaction, as illustrated in Fig. 7.16. Moreover a considerable alteration in product ratio in the initial 5% of reaction (Fig. 7.17) makes accurate determination of initial product ratios very difficult. In this period the trans but-2-ene/but-1-ene ratio displays an initial sharp increase followed by a much slower steady increase. Conversely the cis but-2-ene/but-1-ene product ratio appears to increase steadily from the start of the reaction. Although considerable errors are involved, particularly for reactions at higher temperatures, initial product ratios have been estimated and are listed in Tables 7.6-7.9. But-2-ene/but-1-ene selectivities over both erionites are greater than 1 at low temperatures and decrease with increasing temperature.

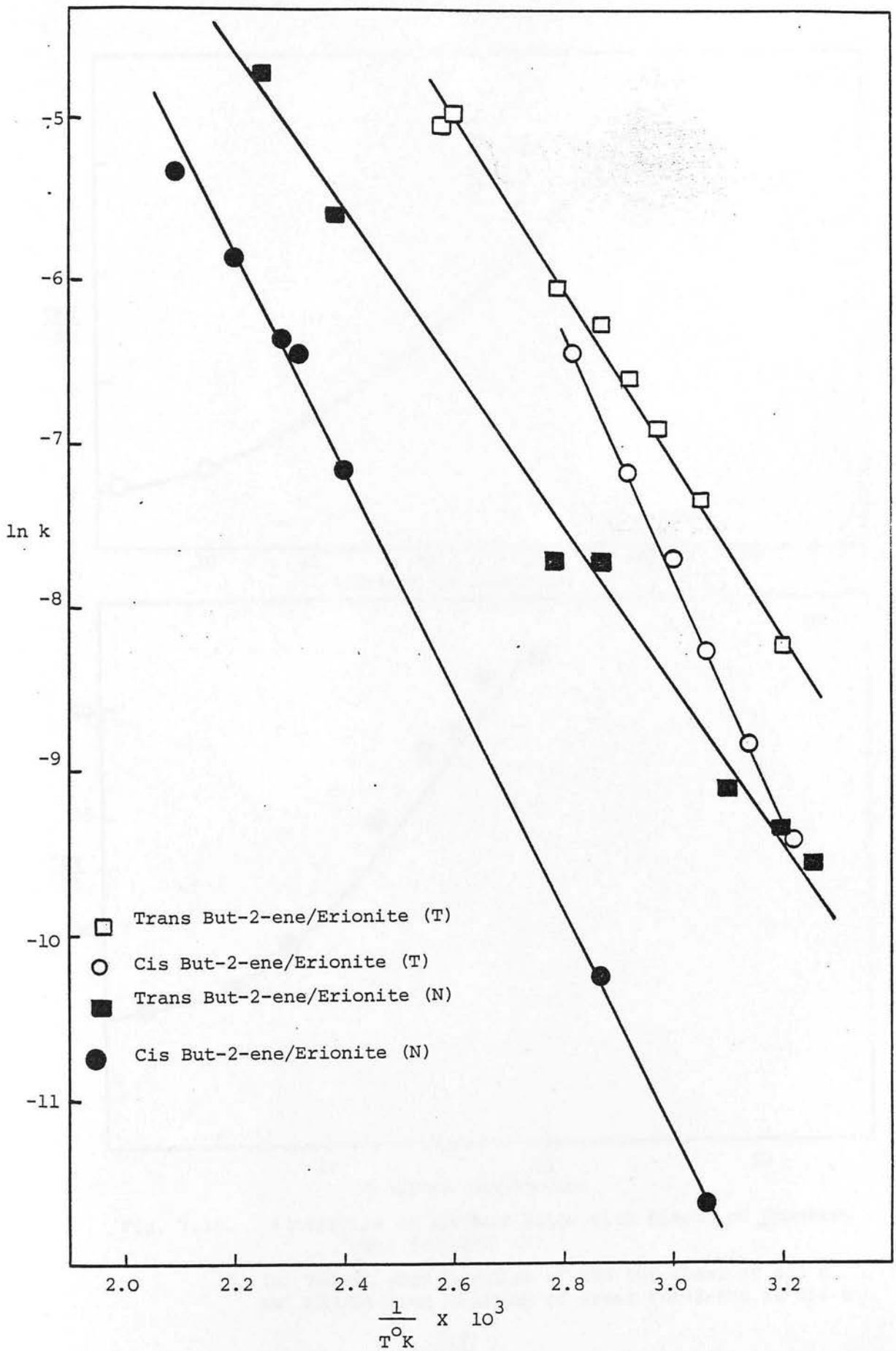


Fig. 7.15. Arrhenius Plots for Disappearance of But-2-enes over Erionites (N) and (T)

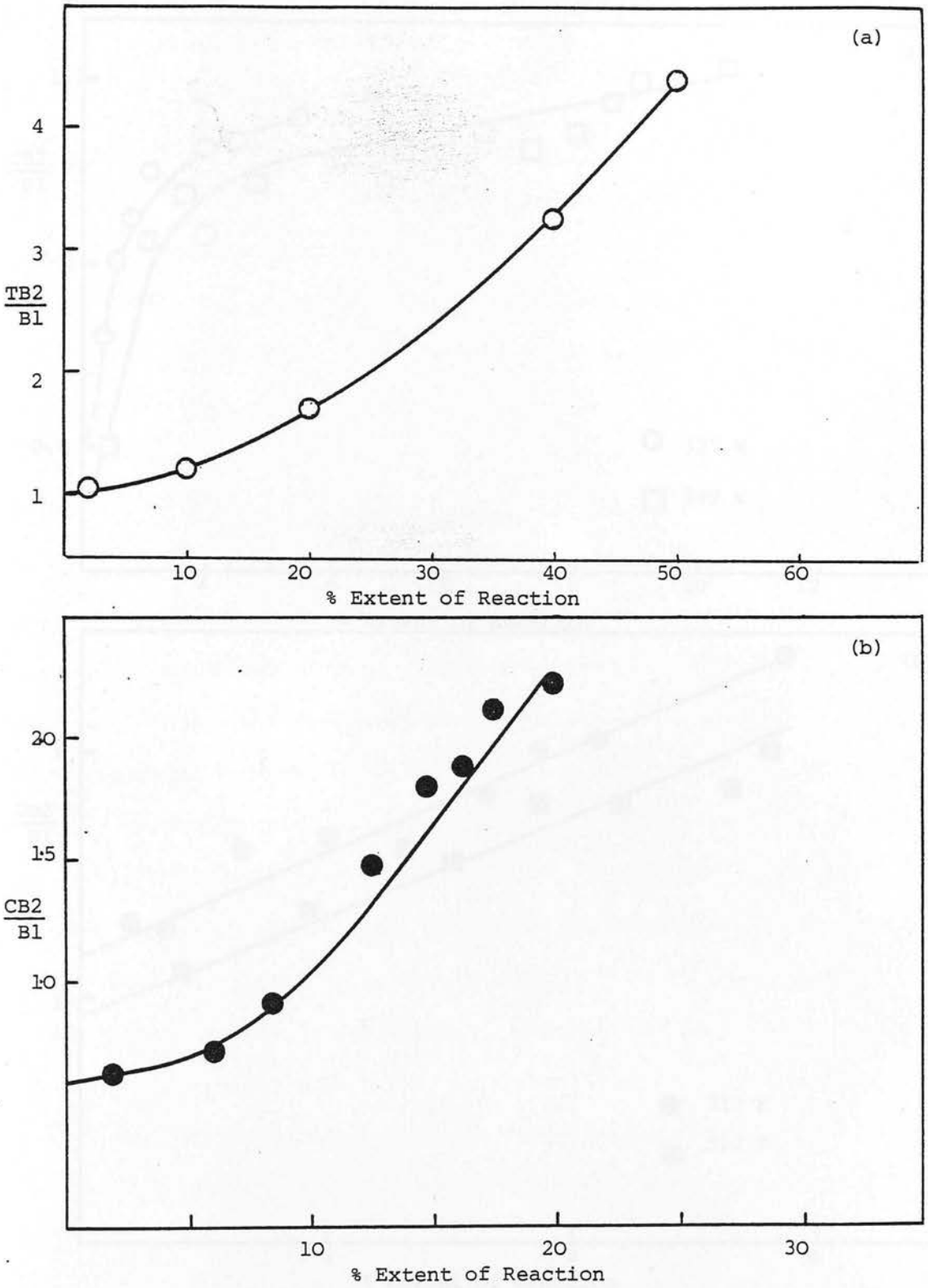


Fig. 7.16. Alteration of Product Ratio with Extent of Reaction over Erionite (N)

(a) TB2/B1 from Reaction of Cis But-2-ene at 431 K
(b) CB2/B1 from Reaction of Trans But-2-ene at 361 K

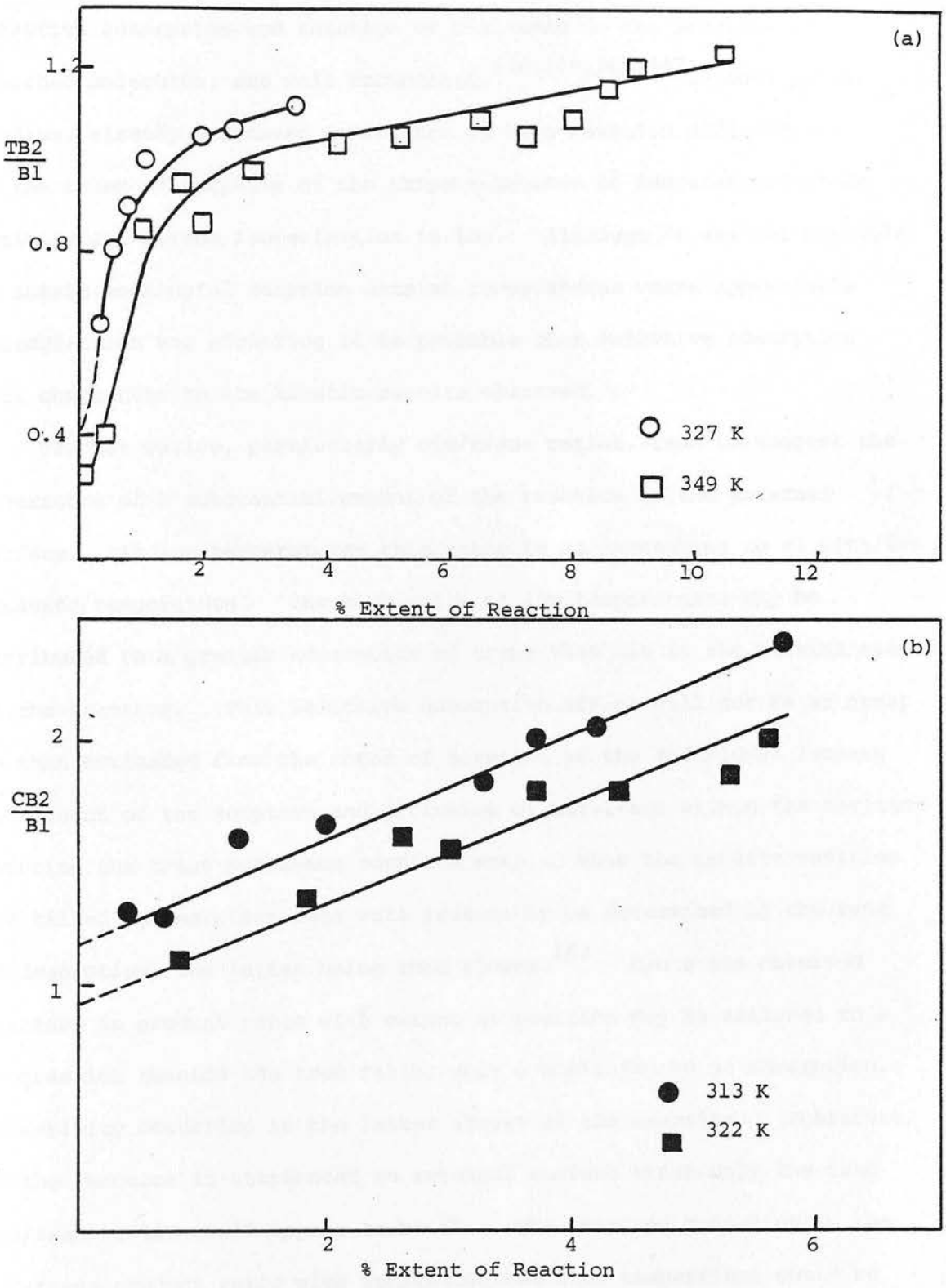


Fig. 7.17. Alteration of Product Ratio in the Initial Stages of the Isomerisation of the But-2-enes over Erionite (N)

(a) Trans But-2-ene/But-1-ene
(b) Cis But-2-ene/But-1-ene

c) Discussion

The shape selective characteristics of erionite, in particular the selective adsorption and reaction of n-alkanes in the presence of branched molecules, are well documented.[134,159,166,167] Adsorption studies, already discussed in Chapter 6, have revealed differences in the rates of sorption of the three n-butenes at temperatures where activity for butene isomerisation is low. Although it was not possible to obtain meaningful sorption data at temperatures where appreciable isomerisation was occurring it is probable that selective adsorption will contribute to the kinetic results observed.

Product ratios, particularly cis/trans ratios, tend to suggest the occurrence of a substantial amount of the reaction on the external surface. At low temperatures this ratio is >1 decreasing to <1 with increasing temperature. The high value at low temperatures may be attributed to a greater adsorption of trans than cis in the initial stages of the reaction. This selective adsorption effect will not be as great as that estimated from the rates of sorption of the individual isomers on account of the sorption and diffusion of but-1-ene within the cavities reducing the trans but-2-ene sorption rate. When the zeolite cavities are filled the sorption rate will presumably be determined by the rate of desorption, the latter being much slower.[163] Hence the observed decrease in product ratio with extent of reaction may be assigned to a progression towards the true ratio, only a small degree of adsorption selectivity occurring in the latter stages of the reaction. Therefore, if the reaction is attributed to external surface sites only the true cis/trans ratio would appear to be $\leq 1$. The observed reduction in the cis/trans product ratio with increasing reaction temperature could be rationalised in terms of a decreased trans/cis adsorption selectivity with temperature.

The cis but-2-ene/but-1-ene and trans but-2-ene/but-1-ene are also >1 at low temperatures and alter with extent of reaction. In particular, the trans but-2-ene/but-1-ene ratio shows a very rapid increase during the first few % of cis but-2-ene conversion. This could be a consequence of an initial preferential adsorption of trans but-2-ene over but-1-ene. After approximately 2% conversion enough cis but-2-ene and/or but-1-ene may have been adsorbed for their diffusion within the zeolite to limit the rate of sorption of trans but-2-ene. Alternatively the slow increase of product ratio after ca. 2% reaction could be regarded as the approach to the true product ratio.

The shapes of the first order plots for the different n-butenes are also compatible with reaction on the external surface. The initial slow disappearance of cis but-2-ene accelerating to a steady rate, could be explained by an initial selective adsorption of the reaction products (but-1-ene and trans but-2-ene) leading to a gas phase concentration of cis but-2-ene greater than the true overall concentration throughout the system. The acceleratory period for but-1-ene disappearance over erionite (N) can be rationalised in a similar manner although with cis but-2-ene as reactant both products are adsorbed more rapidly than the reactant whereas in but-1-ene conversion one product is adsorbed more rapidly and the other more slowly than the reactant. In contrast, the rate of trans but-2-ene disappearance exhibits an initial decelerating period which could arise from a greater initial adsorption of reactant resulting in a gas phase analysis of reactant concentration lower than the true value throughout the system. A similar profile was observed for but-1-ene isomerisation over erionite (T). The difference in but-1-ene profiles over the two systems may be due to their slightly different pore sizes.

All n-butene isomerisations over both erionites exhibit good first order kinetics after the initial acceleratory or decelerating period. If adsorption is assumed to be completed in the initial stages of reaction and desorption is much slower than adsorption, the kinetics of the latter stages of reaction should not be altered significantly by selective adsorption. Selective adsorption may not even be occurring as the presence and diffusion of cis but-2-ene within the cavities may result in the rates of sorption of all 3 n-butenes being approximately the same.

Although the above results appear to suggest the occurrence of a large part of the reaction on the external surface most studies over zeolites have assumed the occurrence of the major part of the reaction within the pores, the increased activity of zeolites over silica alumina catalysts being attributed, in part, to their larger surface area resulting in more active sites. Indeed, in many instances, evidence for reaction within the pores has been provided. However some observed catalytic activities of zeolites have been attributed to reactions occurring on the external surface only. Detreköy et al[91] in a study of but-1-ene isomerisation over H-clinoptilolite concluded that the reaction was only occurring on the external surface sites. Norton[128] arrived at a similar conclusion as a result of the presence of branched chain alkenes as products from polymerisation reactions of alkenes over the small pore zeolites 4A, 5A and 5P. However with erionite (T), in particular, it is difficult to rationalise the occurrence of the majority of reaction on the external sites only in terms of the activity exhibited. Rates of butene isomerisation similar to those observed over zeolite Ω in the same temperature range were observed. As the activity of zeolite Ω was comparable to that of HX and CeX this zeolite was concluded to be a strong acid. Erionite (T) would therefore also

appear to be strongly acidic. The activity and hence acid strength of erionite (N) are somewhat lower. Moreover, the occurrence of the reaction on the external surface alone should be reflected in the values of activation energies, the order expected being E(trans) > E(cis) > E(but-1-ene). This was not so with either of the erionite samples, the orders being E(cis) ∿ E(but-1-ene) > E(trans) for erionite (N) and E(cis) > E(but-1-ene) > E(trans) for erionite (T). Furthermore the ratios of the rates of disappearance of each of the n-butenes over the two erionites should be the same regardless of reactant, trans > but-1-ene > cis was actually observed. These results therefore suggest that reaction is occurring on sites other than those on the external surface.

In comparative studies of reactions of branched and n-alkanes over offretite and erionite, Chen[167] has postulated the occurrence of diffusion-reaction control in erionite leading to apparent activation energies equal to the sum of (the diffusion activation energy/2) and (the reaction activation energy/2). Such control occurs in systems where intraphase diffusion is occurring not in series but simultaneously with reaction. Diffusional activation energies of very few molecules in erionite have been reported. Those available are compared with values in zeolites 5A and KT in Table 7.8.

It would not seem unreasonable to assume activation energies for erionite intermediate between those of zeolites 5A and KT because of the difference in window shape and the presence of large $K^+$ ions. Estimated values for diffusion of but-1-ene, trans and cis but-2-enes might therefore be ca. 25, ca. 25 and ca. 70 kJ $mol^{-1}$ respectively although these values will depend on the exact composition of the erionite sample.

| Sorbate | Diffusional Activation Energy/kJ $mol^{-1}$ | | |
|---|---|---|---|
| | 5A[64] | Erionite[74] | Zeolite KT[76,239] |
| Ethane $C_2H_6$ | 12.7 | 18.1 | |
| Ethylene $C_2H_4$ | 11.55 | 9.8 | |
| Propane $C_3H_8$ | 14.7 | | 46.2 |
| n-Butane $C_4H_{10}$ | 16.8 | | 39.6 |
| n-Pentane $C_5H_{12}$ | 19.3 | 21.0 | 24.8 |
| But-1-ene $C_4H_8$ | 14.5 | | |
| t-But-2-ene $C_4H_8$ | 14.5 | | |
| c-But-2-ene $C_4H_8$ | 38.6 | | |

Table 7.10. Diffusion Activation Energies of Various sorbates in zeolites 5A, KT and erionite

Activation energies for butene isomerisation over acid catalysts in the range 40-50 kJ $mol^{-1}$ have been reported.[187,191] The observed activation energies are in reasonable agreement with the predicted values assuming diffusion-reaction control providing that the diffusion control is that of the reactant. This last prerequisite is difficult to rationalise in that the slowest step should be limiting and that would always seem to be the diffusion of cis but-2-ene whether present as reactant or product. One would therefore expect the diffusional activation energy of cis but-2-ene to contribute to all the observed activation energies.

Over most acidic catalysts the observed order of activity is but-1-ene > cis but-2-ene > trans but-2-ene. Data in Table 7.11 demonstrate that this is not so with erionite as catalyst; in particular the rate of isomerisation of trans is greater than that of cis over both erionite samples.

| | Temperature | $ks^{-1}g^{-1}$ B1 Disappearance | $ks^{-1}g^{-1}$ TB2 Disappearance | $ks^{-1}g^{-1}$ CB2 Disappearance |
|---|---|---|---|---|
| Erionite (N) | 312 | 5.0 | 2.7 | 0.9 |
| | 357 | 37.0 | 24.8 | 16.6 |
| Erionite (T) | 351 | 2.5 | 5.0 | 0.4 |
| | 425 | 49.9 | 49.9 | 11.1 |

Table 7.11. Rate Constants for Disappearance of the n-Butenes on Erionites (N) and (T).

Chen and Weisz[137] have reported a similar result for hydrogenation rates of trans and cis but-2-enes over Pt/CaA catalyst where the relative rates of hydrogenation ranged from 3.3 to 7 in the temperature range 393 K - 371 K. The diffusivity of trans was shown to be ca. 200 times that of cis.

Reaction of but-1-ene within the erionite cavities would be expected to result in an observed initial cis/trans ratio <1 due to initial selective adsorption. Tempere et al[239] have reported the following selectivities for butene isomerisation over CaA at 433 K; trans but-2-ene/but-1-ene = 2.6, but-1-ene/cis but-2-ene = 3.7 and trans but-2-ene/cis but-2-ene = 5.2. These ratios were attributed to reactions occurring within the pores, the electrostatic interactions between the molecules and the zeolite resulting in the easier exclusion of trans but-2-ene. The small amount of reaction on the external surfaces of zeolites NaA, KA and CsA resulted in trans/cis ratios of ca. .5 similar to those observed over wide-pore X and Y zeolites. Furthermore they demonstrated that a crystalline SrA zeolite

exhibited a trans/cis ratio of ca. 5 which reduced to ca. .5 when the crystal structure was destroyed. As sorption experiments of n-alkanes have shown the rates of sorption of molecules in 5A zeolite to be more rapid than in erionite[74] similar selectivity results might have been expected here.

Therefore the available activity and selectivity results do not show conclusively whether the reaction is occurring on the external or internal surface sites. There may in fact be a significant contribution from sites in both locations. The adsorption data has however indicated that the initial product ratios observed are apparent values and hence it is not possible to postulate a reaction mechanism on the basis of these results.

## 7.2. Reactions of Substituted Cyclopropanes

### 7.2.1. Reactions over Zeolite Ω

#### a) Methylcyclopropane Isomerisation

The activity of zeolite Ω for isomerisation of MCP as a function of pretreatment conditions has been discussed in Chapter 6. To derive the activation energy, the reaction was studied in the temperature range 295 K - 335 K following pretreatment at 823 K for 13 hours and 40 hours respectively. A typical reaction profile is shown in Fig. Fig. 7.18.(a). Unlike the n-butenes, the disappearance of MCP appears to follow first order kinetics from the beginning of the reaction as demonstrated by the typical first order plot in Fig. 7.18.(b). Moreover, good first order kinetics are observed for conversions of the order of 90%.

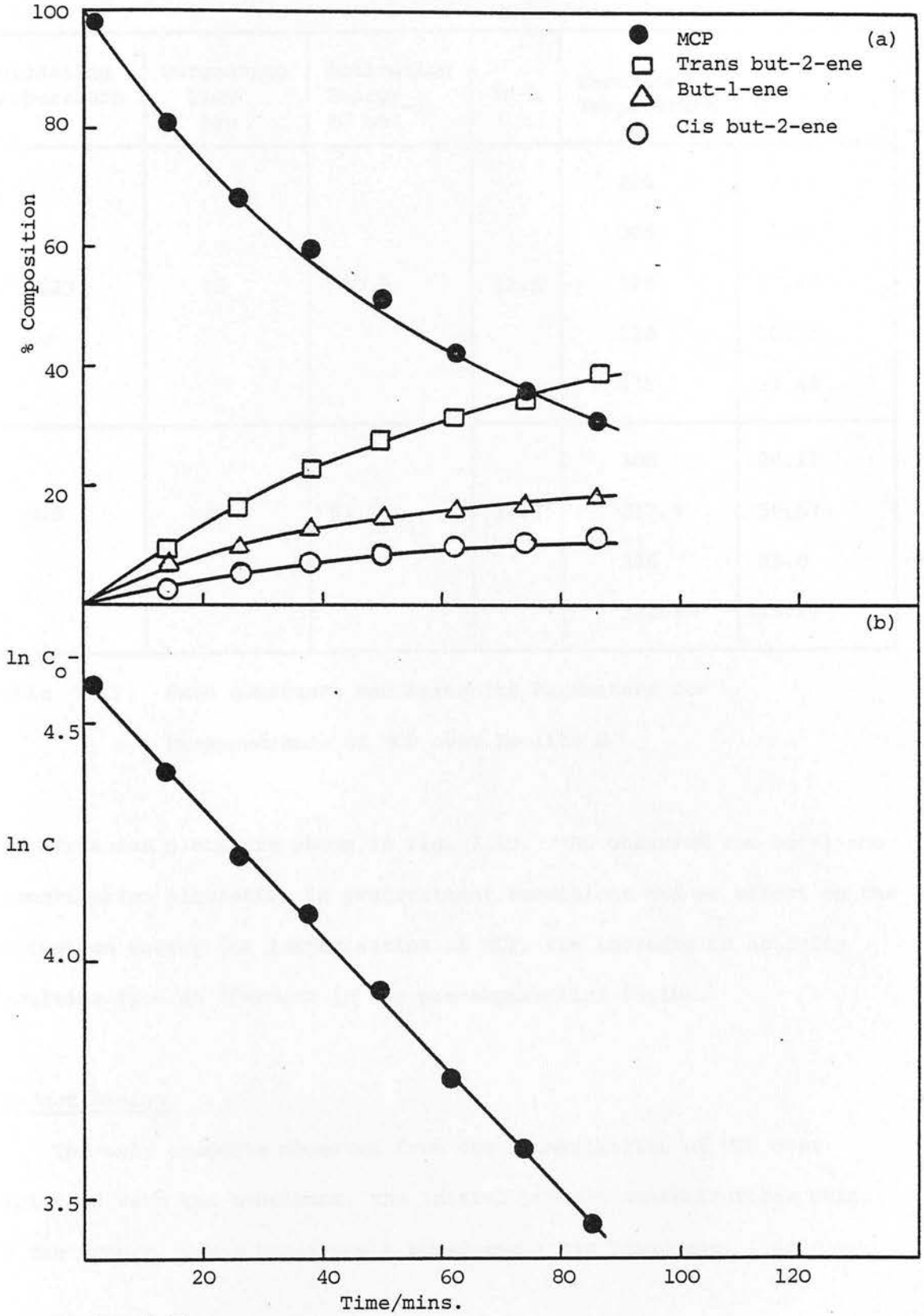


Fig. 7.18. (a) Reaction Profile for MCP Isomerisation at 325 K over Zeolite Ω (outgassed for 13 hours at 823 K)

(b) Derived First Order Plot

The first order rate constants and derived Arrhenius parameters are given in Table 7.12

| Outgassing Temperature K | Outgassing Time hrs | Activation Energy $kJ\ mol^{-1}$ | ln A | Reaction Temperature K | $kx10^{-4}$ $s^{-1}g^{-1}$ |
|---|---|---|---|---|---|
| 823 | 13 | 50.9 | 12.5 | 295 | 2.77 |
| | | | | 308 | 5.85 |
| | | | | 325 | 17.48 |
| | | | | 328 | 20.75 |
| | | | | 335 | 33.42 |
| 823 | >40 | 51.7 | 14.35 | 306 | 24.17 |
| | | | | 317.5 | 59.67 |
| | | | | 328 | 95.0 |
| | | | | 331.5 | 119.17 |

Table 7.12. Rate constants and Arrhenius Parameters for Disappearance of MCP over Zeolite Ω

The Arrhenius plots are shown in Fig. 7.19. As observed for but-1-ene isomerisation alteration in pretreatment conditions had no effect on the activation energy for isomerisation of MCP, the increase in activity resulting from an increase in the pre-exponential factor.

Product Ratios

The only products observed from the isomerisation of MCP over zeolite Ω were the n-butenes, the initial product concentrations being in the order; trans but-2-ene > but-1-ene > cis but-2-ene. No

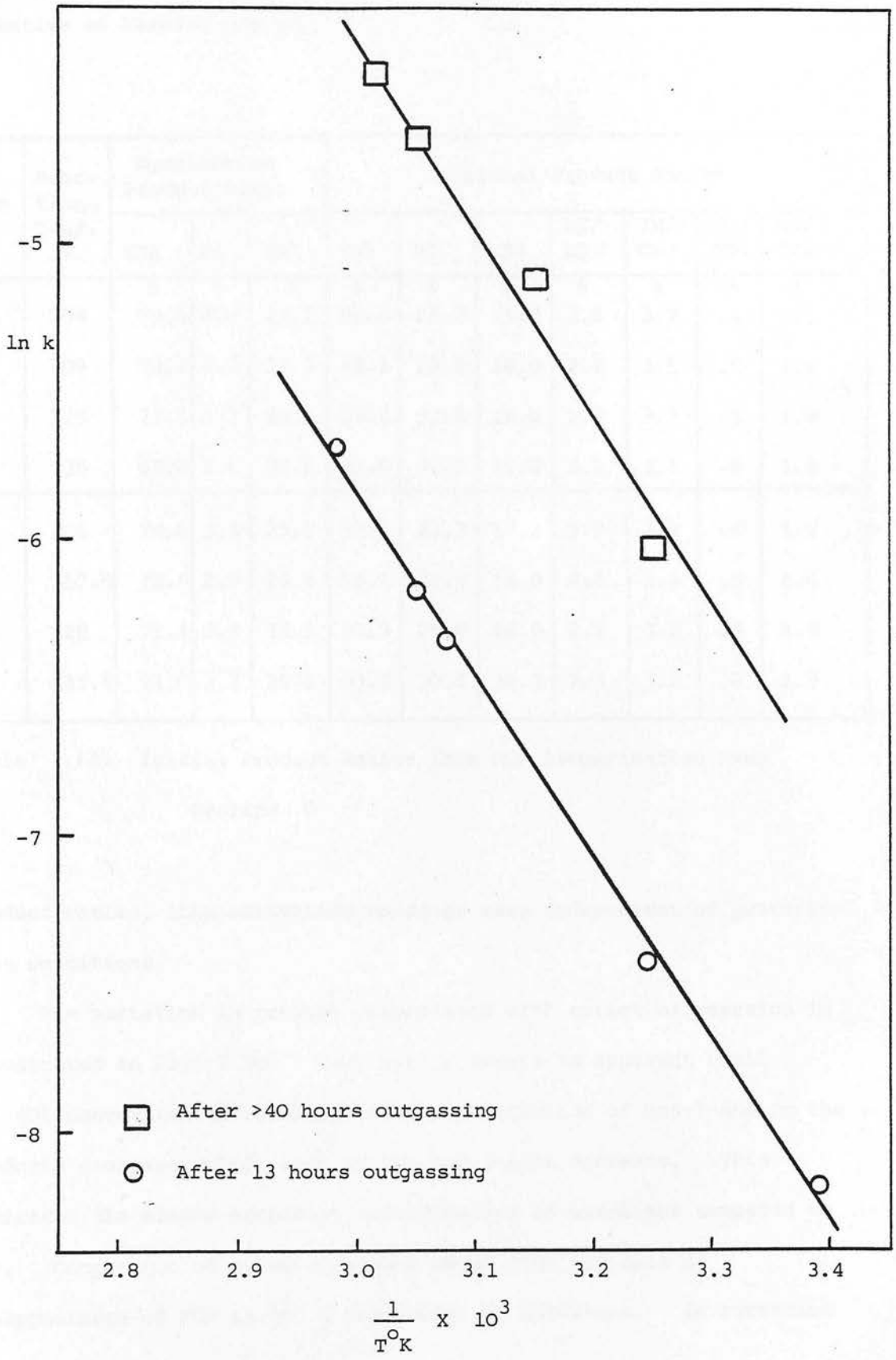


Fig. 7.19. Arrhenius Plots for the Disappearance of MCP over Zeolite Ω

isobutene or cyclobutane were observed. The initial product ratios, given in Table 7.13 are very different from the equilibrium values indicative of kinetic control.

| Out-gassing Time (hrs) | Reaction Temp. K | Equilibrium Product Ratio | | | Initial Product Ratios | | | | | | |
|---|---|---|---|---|---|---|---|---|---|---|---|
| | | TB2 | B1 | CB2 | TB2 | B1 | CB2 | B2/B1 | TB2/CB2 | B1/TB2 | B1/CB2 |
| | | % | % | % | % | % | % | % | % | % | % |
| 13 | 294 | 74.8 | 2.0 | 23.2 | 58.8 | 25.3 | 15.9 | 2.9 | 3.7 | .4 | 1.6 |
| | 309 | 73.4 | 2.3 | 24.3 | 55.2 | 28.8 | 16.0 | 2.5 | 3.5 | .5 | 1.8 |
| | 325 | 71.1 | 3.3 | 25.6 | 53.5 | 30.5 | 16.0 | 2.3 | 3.3 | .5 | 1.9 |
| | 335 | 69.9 | 3.6 | 26.5 | 51.6 | 31.9 | 16.5 | 2.1 | 3.1 | .6 | 1.9 |
| >40 | 306 | 74.0 | 2.3 | 23.7 | 57.1 | 25.7 | 17.2 | 2.9 | 3.3 | .4 | 1.5 |
| | 317.5 | 72.5 | 2.9 | 24.6 | 56.1 | 27.0 | 16.9 | 2.4 | 3.3 | .5 | 1.6 |
| | 328 | 71.1 | 3.3 | 25.5 | 54.3 | 28.8 | 16.9 | 2.5 | 3.2 | .5 | 1.7 |
| | 331.5 | 71.0 | 3.3 | 25.6 | 53.2 | 30.3 | 16.5 | 2.3 | 3.2 | .6 | 1.8 |

Table 7.13. Initial Product Ratios from MCP Isomerisation over Zeolite Ω

Product ratios, like activation energies were independent of pretreatment conditions.

The variation in product composition with extent of reaction is illustrated in Fig. 7.20. Very little change is apparent until ca. 40% conversion after which the % concentration of but-1-ene in the products decreases while that of the but-2-enes decrease. This indicates the slower secondary isomerisation of but-1-ene compared to MCP. Comparison of rates constants shows that the rate of disappearance of MCP is ca. 5 times that of but-1-ene. In agreement

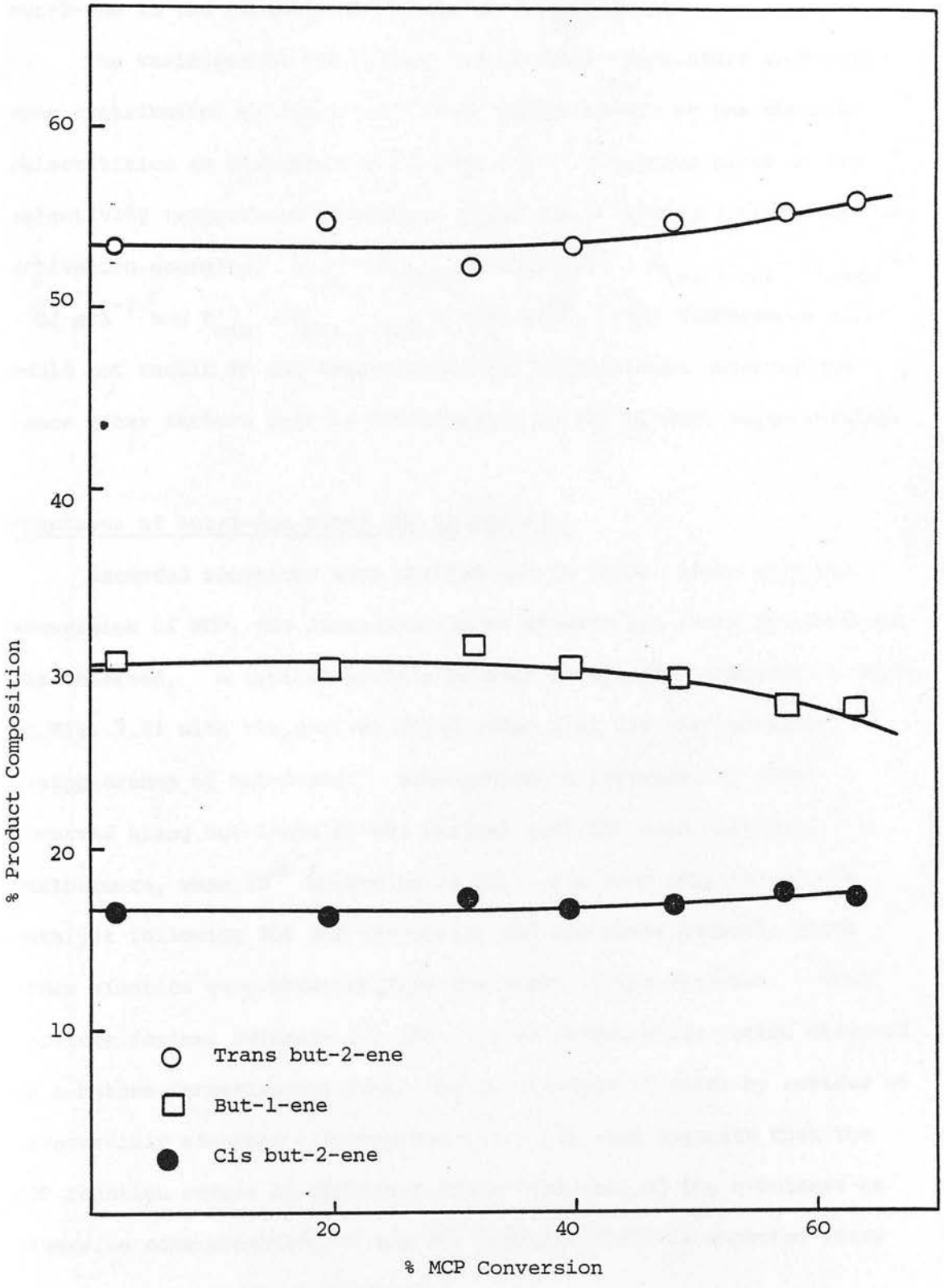


Fig. 7.20 Variation in Product Composition with extent of MCP conversion over Zeolite Ω
(Reaction at 326 K)

with the cis/trans ratios (<1) observed for but-1-ene isomerisation, the secondary reaction causes a greater change in the % of trans but-2-ene in the products than that of cis but-2-ene.

The variation of the product ratios with temperature indicates some contribution of transition state energy levels to the observed selectivities as discussed in Section 7.1. Arrhenius plots of the selectivity temperature dependence yield the following differences in activation energies; $E_{cis} - E_{trans} \simeq 3$ kJ $mol^{-1}$, $E_{but\text{-}1\text{-}ene} - E_{trans} \simeq 5$ kJ $mol^{-1}$ and $E_{cis} - E_{but\text{-}1\text{-}ene} \simeq 3$ kJ $mol^{-1}$. Such differences alone would not result in the absolute product compositions observed and hence other factors must be contributing to the product selectivities.

Reactions of But-1-ene after MCP Isomerisation

Extended reactions were carried out in which, after complete conversion of MCP, the isomerisation of product but-1-ene to but-2-ene was observed. A typical profile of such an extended reaction is shown in Fig. 7.21 with the derived first order plot for the subsequent disappearance of but-1-ene. Rate constants identical to those observed using but-1-ene as the initial reactant were obtained. Furthermore, when $10^{20}$ molecules of but-1-ene were admitted to the catalyst following 90% MCP conversion and gas phase removal, first order kinetics were observed from the start of the reaction. This provides further evidence for the initial decelerating period observed in n-butene isomerisation being due to blockage of sites by residue or irreversibly adsorbed alkene molecules. It also suggests that the MCP reaction occurs on different sites from that of the n-butenes as otherwise some poisoning of the MCP reaction would be expected after some n-butenes had been produced.

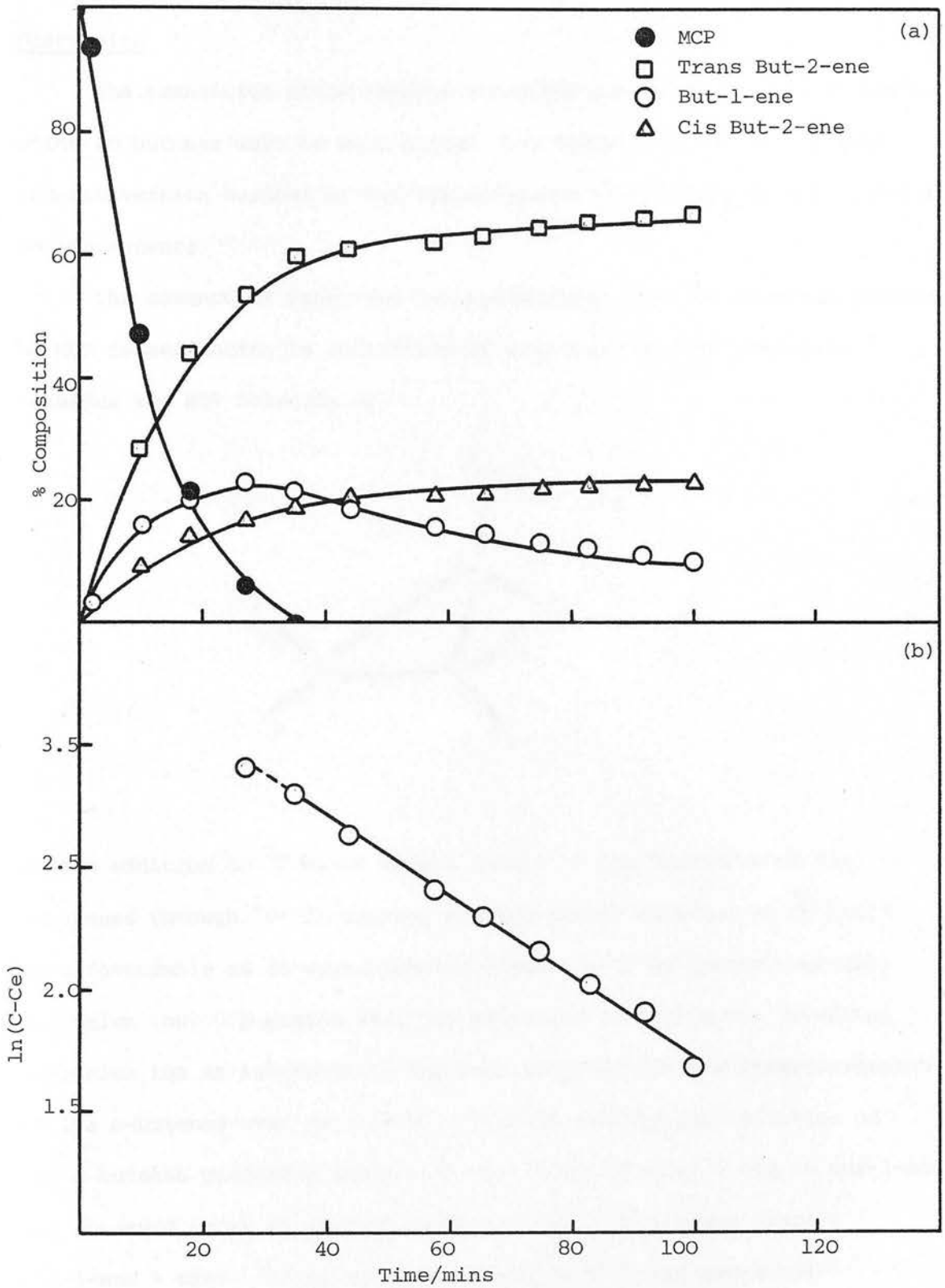


Fig. 7.21. (a) Extended Reaction of MCP over Zeolite Ω
(Reaction Temperature = 339 K)

(b) First Order Plot of Disappearance of But-1-ene.

Discussion

The transition state through which MCP passes during its isomerisation to butenes must be much higher than those involved in n-butene interconversion because of the thermodynamic instability of MCP relative to the butenes.

The absence of isobutene and cyclobutane from the observed products of MCP isomerisation is indicative of a proton addition mechanism. Consider the MCP molecule as

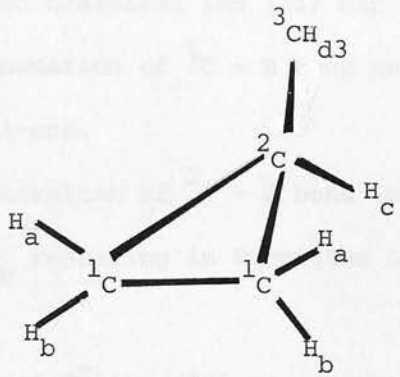


Proton addition to $^{1}C$ would always result in the formation of the n-butenes through $^{1}C$-$^{2}C$ cleavage whereas proton addition to $^{3}C$ would be unfavourable as it would involve formation of an unstable primary carbonium ion. A proton addition mechanism involving the sec-butyl carbonium ion as intermediate has been proposed for the interconversion of the n-butenes over zeolite Ω. However whereas isomerisation of the n-butenes yielded a product distribution of trans > cis >> but-1-ene, the observed order of product concentration from MCP was trans > but-1-ene > cis. It is unlikely therefore that the sec-butyl

carbonium ion can be involved in the isomerisation of MCP over zeolite Ω. Similar differences in product distribution from n-butene and MCP isomerisation have been reported over silica alumina[211], and the non-classical cyclopropyl carbonium ion has been postulated as reaction intermediate for the isomerisation of MCP. The observed product selectivities from isomerisation of MCP over zeolite Ω suggest the involvement of this non classical ion. A possible reaction mechanism is illustrated in Fig. 7.22. It is apparent that cleavage of $C_1$-$C_2$ in the non classical ion (II) can occur in two ways,

1) resulting in formation of $^1C$ - H bond and cleavage of $^1C$ - $H_c$ resulting in but-1-ene.

2) resulting in formation of $^2C$ - H bond and cleavage of either $^2C$ - $H_a$ or $^2C$ - $H_b$ resulting in formation of cis and trans but-2-ene respectively.

If the non-classical $C^+$ ion (II) is adsorbed in a plane parallel to the cyclopropane ring; production of trans but-2-ene and but-1-ene would be favoured from steric considerations, their formation requiring the abstraction of a proton ($H_b$ or $H_c$) orientated towards the surface. In contrast the formation of cis but-2-ene results from loss of $H_a$ which is orientated away from the surface and hence not so easily abstracted by the surface. The preferred formation of trans but-2-ene over but-1-ene may be partially due to energetic considerations, although steric factors, in particular the greater crowding of $^1C$ over $^2C$, amy also contribute to the observed selectivity. The agreement between this mechanism and the results assumes that the ion

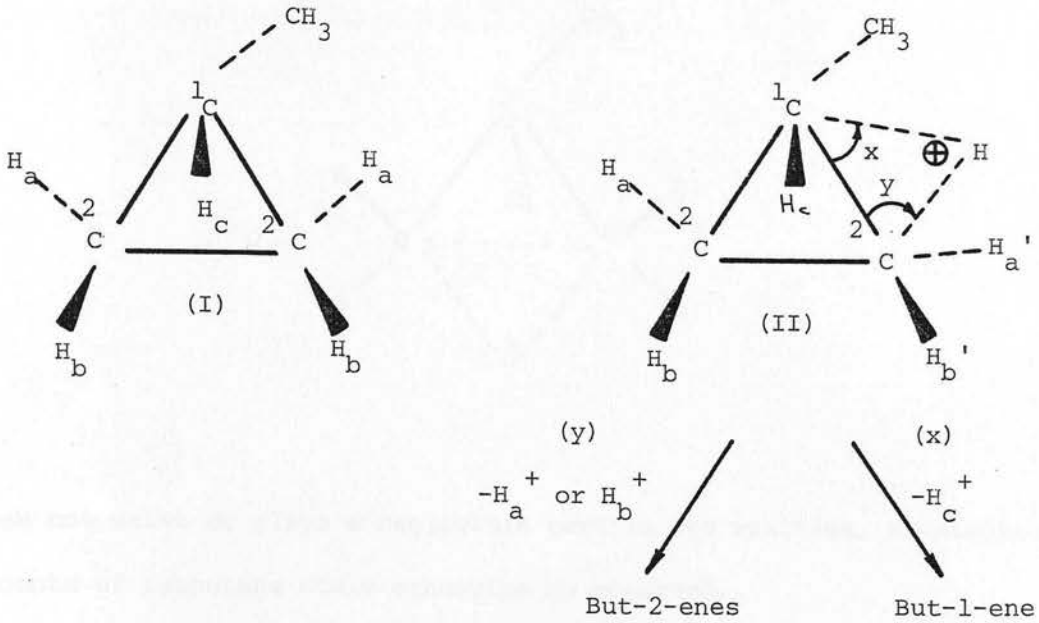


Fig. 7.22. Possible Mechanism for Isomerisation of MCP over Zeolite Ω

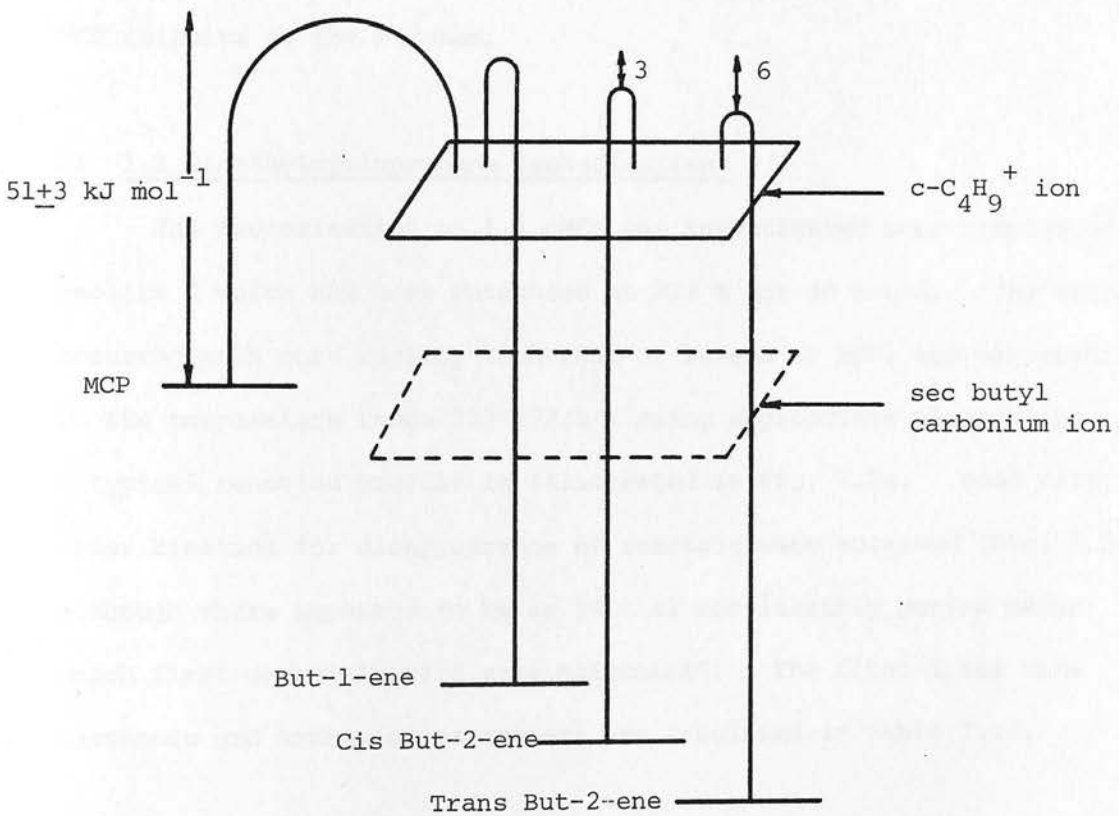


Fig. 7.23. Energy Profile for Isomerisation of MCP over Zeolite Ω

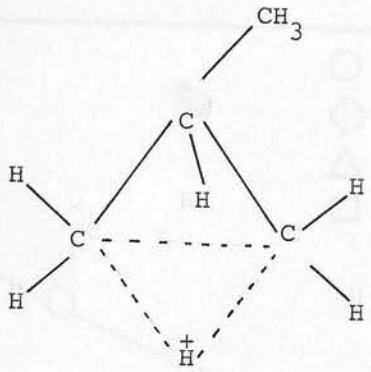


does not exist or plays a negligible part in the reaction, substantial amounts of isobutene would otherwise be observed.

A possible energy profile for the isomerisation of MCP to n-butenes over zeolite Ω is illustrated in Fig. 7.23. The transition state through which the MCP passes must be much higher than those involved in n-butene interconversion because of the thermodynamic instability of MCP relative to the butenes.

b) 1,1 Dimethylcyclopropane Isomerisation

The isomerisation of 1,1 DMCP was investigated over samples of zeolite Ω which had been outgassed at 823 K for 40 hours. The reaction occurred much more rapidly than that of butene or MCP, and was studied in the temperature range 213-277.5 K using appropriate slush baths. A typical reaction profile is illustrated in Fig. 7.24. Good first order kinetics for disappearance of reactant were observed (Fig. 7.24(b)) although there appeared to be an initial acceleratory period after which first order kinetics were maintained. The first order rate constants and Arrhenius parameters are tabulated in Table 7.14.

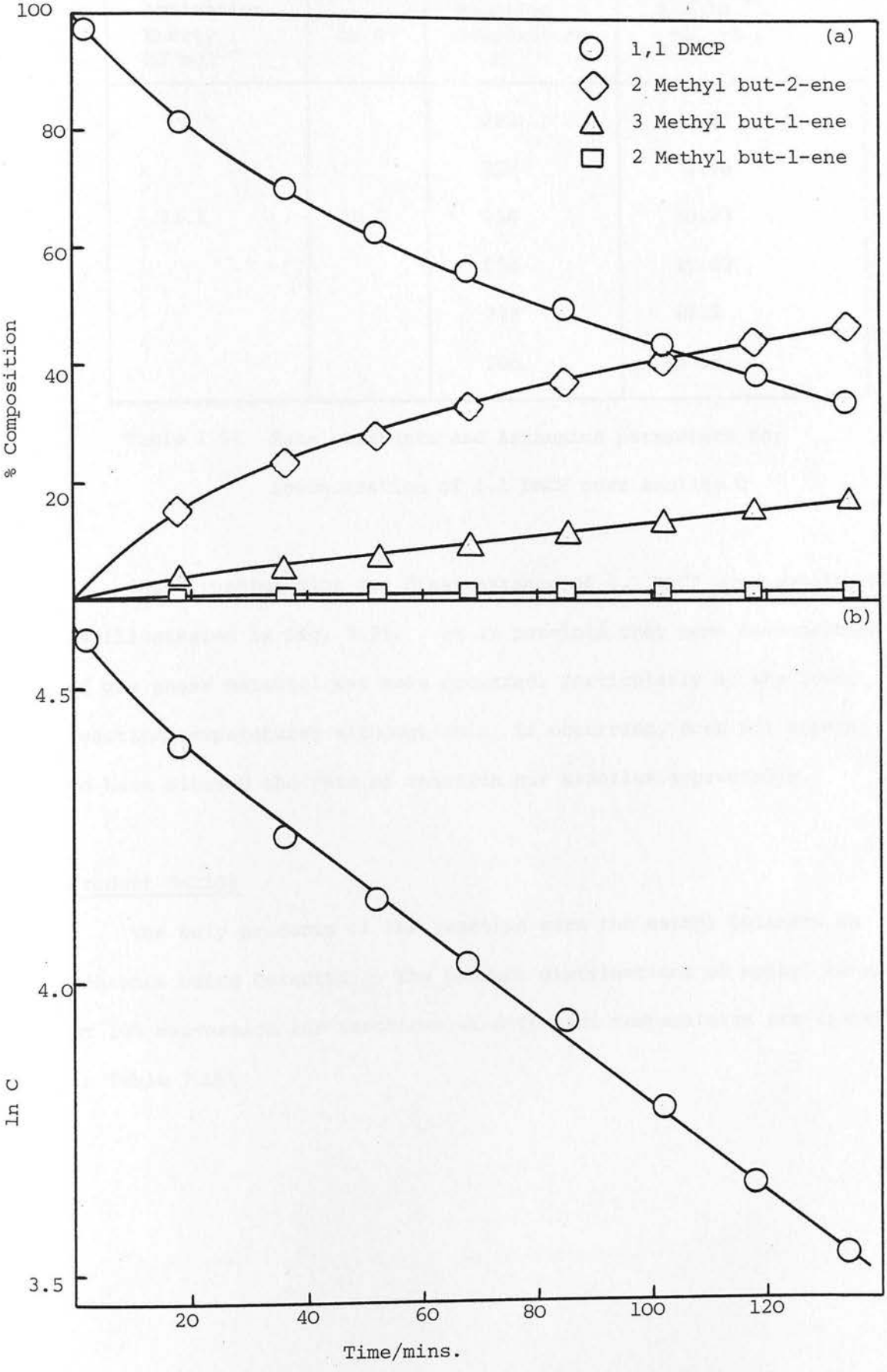


Fig. 7.24 (a) Reaction Profile of Isomerisation of 11 DMCP over Zeolite Ω at 238 K

(b) Derived First Order Plot.

| Activation Energy $kJ\ mol^{-1}$ | ln A | Reaction Temperature K | $k \times 10^{-4}$ $s^{-1}\ g^{-1}$ |
|---|---|---|---|
| 35.1 | 10.7 | 213 | 1.07 |
| | | 228 | 3.76 |
| | | 238 | 10.23 |
| | | 250 | 19.03 |
| | | 273 | 85.2 |
| | | 280 | 107.3 |

Table 7.14 Rate constants and Arrhenius parameters for isomerisation of 1,1 DMCP over zeolite Ω

The Arrhenius plot for disappearance of 1,1 DMCP over zeolite Ω is illustrated in Fig. 7.25. It is possible that some condensation of gas phase material may have occurred, particularly at the lower reaction temperatures although this, if occurring, does not appear to have altered the rate of reaction nor kinetics appreciably.

Product Ratios

The only products of the reaction were the methyl butenes, no pentenes being detected. The product distributions of methyl butenes at 10% conversion for reactions at different temperatures are listed in Table 7.15.

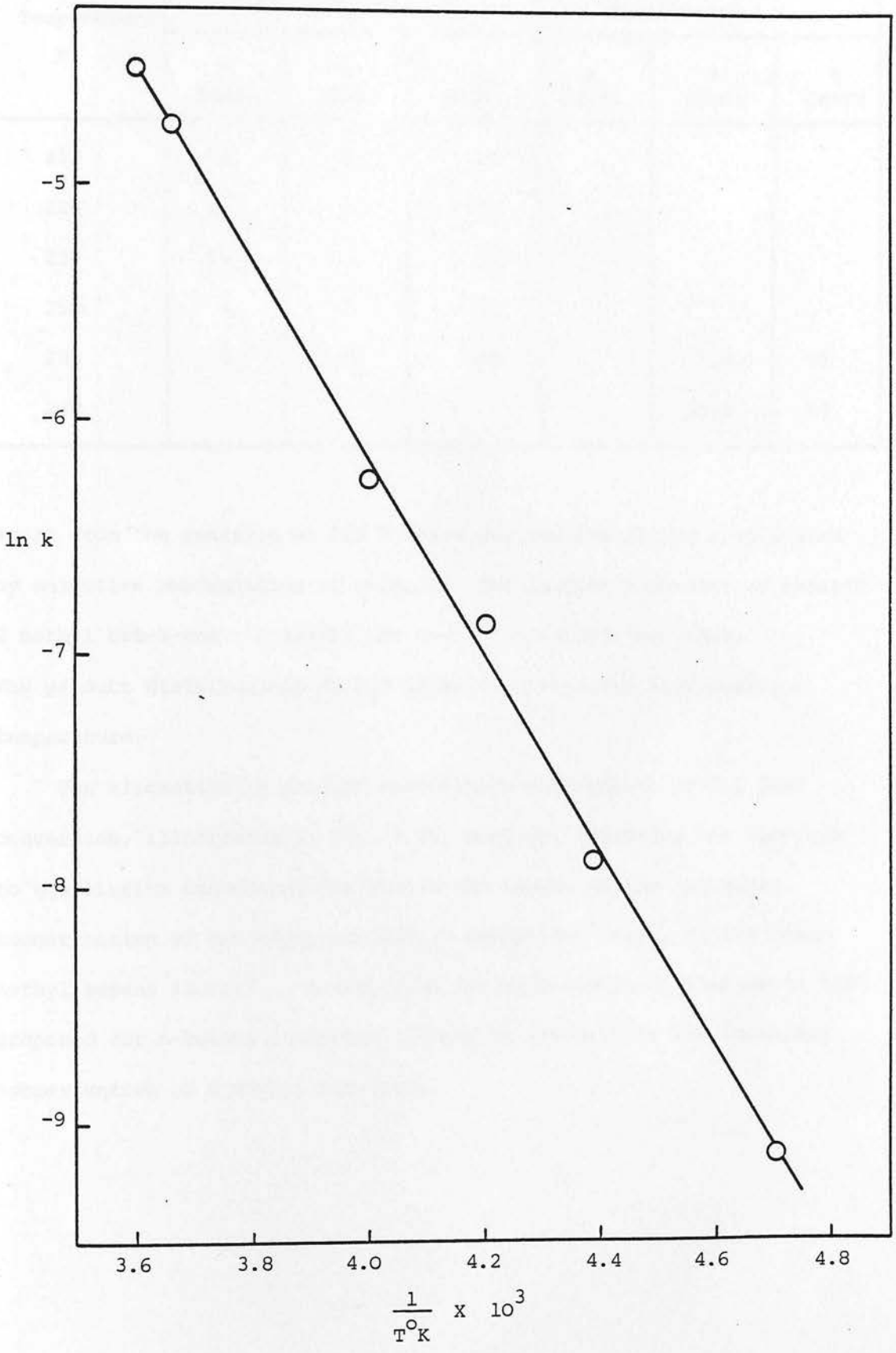


Fig. 7.25. Arrhenius Plot for Isomerisation of 1,1 DMCP over Zeolite Ω

Table 7.15. Product Composition from 1,1 DMCP Isomerisation over Zeolite Ω

| Reaction Temperature K | Product Composition at 10% Conversion | | | Product Composition at Equilibrium | | |
|---|---|---|---|---|---|---|
| | % 3MeBl | % 2MeBl | % 2MeB2 | % 3MeBl | % 2MeBl | % 2MeB2 |
| 213 | 54 | 0 | 46 | | | |
| 228 | 11 | 0 | 88 | | | |
| 238 | 16 | 1 | 82 | | | |
| 250 | 6 | 0 | 94 | | | |
| 280 | 8 | 4 | 88 | .5 | 7.0 | 92 |
| 298 | | | | .2 | 10.8 | 89 |

Apart from the reaction at 213 K where the results may be complicated by selective condensation of products, the product compositions exhibit 2 methyl but-2-ene > 3 methyl but-1-ene > 2 methyl but-1-ene. The product distributions do not alter significantly with reaction temperature.

The alteration in product composition with extent of 1,1 DMCP conversion, illustrated in Fig. 7.26, does not represent the approach to equilibrium concentrations but is the result of the secondary isomerisation of the major product, 2 methyl but-2-ene, to the other methyl butene isomers. A carbonium ion type mechanism similar to that proposed for n-butene isomerisation may be invoked for the secondary isomerisation of 2 methyl but-2-ene.

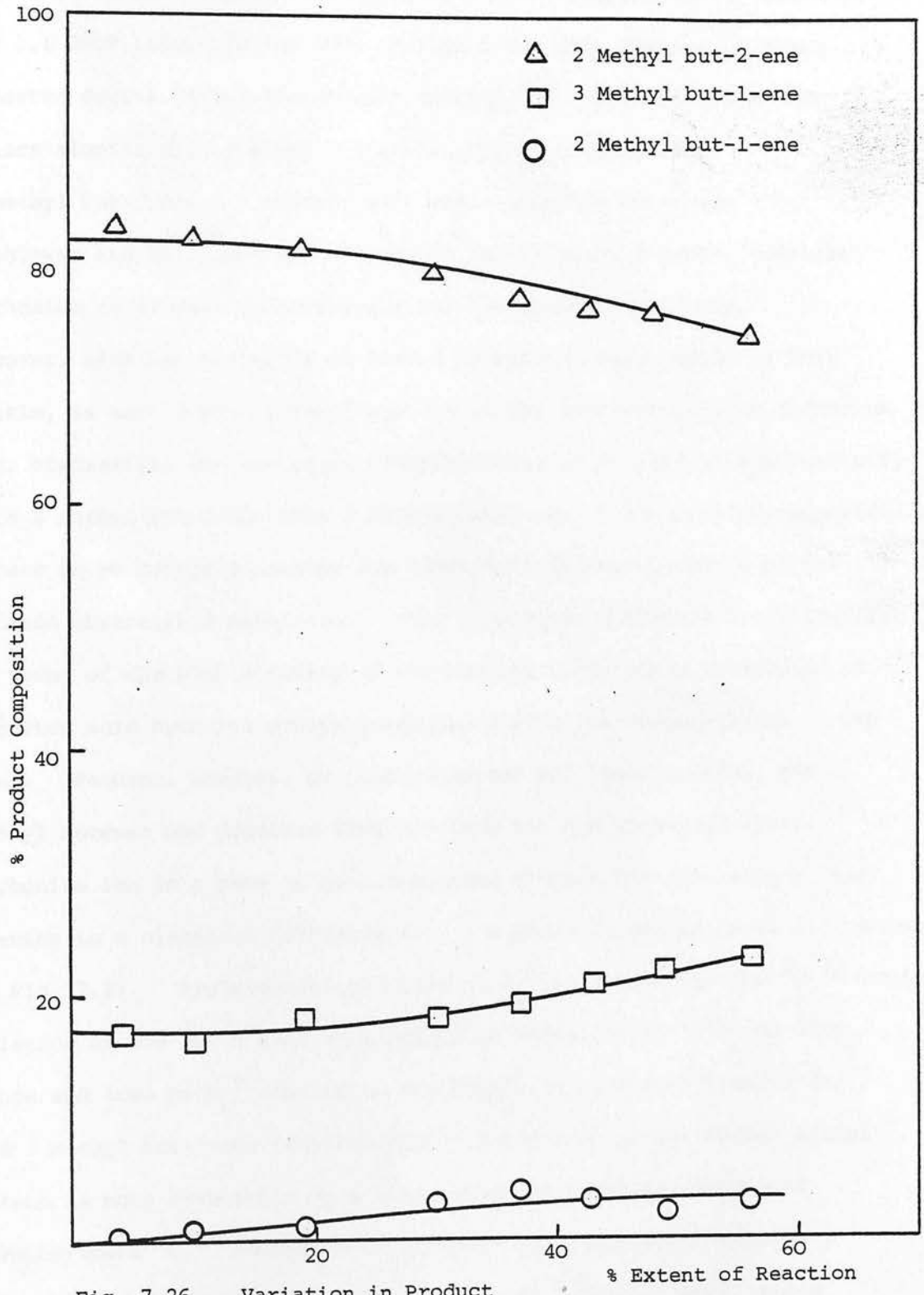


Fig. 7.26. Variation in Product Composition with Extent of Reaction of 1,1 DMCP over Zeolite Ω at 238 K

Discussion

Product distribution, activity and the activation energy observed for 1,1 DMCP isomerisation over zeolite Ω are very similar to those reported over a cerium exchanged X zeolite.[218] Isomerisation over silica alumina[211] also yielded a similar product composition;

2 methyl but-2-ene > 2 methyl but-1-ene > 3 methyl but-1-ene ≃ 0.

Hightower and Hall[211] have postulated the operation of a proton addition mechanism to account qualitatively for the observed products. However, although operation of such a mechanism would result in very little, if any, 3 methyl but-1-ene due to the involvement of a carbonium ion, statistical and energetic considerations would predict substantially more 2 methyl but-1-ene than 2 methyl but-2-ene. The product compositions appear to be better accounted for quantitatively by operation of the hydride abstraction mechanism. This is however difficult to rationalise in terms of the high activity of the zeolite, previously attributed to Brönsted acid hydroxyl groups generated during the decomposition of TMA ions. Perhaps, however, as postulated for MCP isomerisation, the methyl butenes are produced directly from the non-classical cyclic carbonium ion in a more or less concerted process not involving a ring opening to a classical carbonium ion. A possible mechanism is illustrated in Fig. 7.27. Preferential addition of $H_e^+$ occurs across the $^1C$-$^2C$ bond, scission of the $^1C$-$^2C$ bond accompanied by formation of $^2C$-$H_c$ or $^1C$-$H_c$ bonds and loss of $H_b^+$ results in the formation of 2 methyl but-2-ene and 3 methyl but-1-ene respectively. Production of the former methyl butene is more favourable as a consequence of the lower degree of crowding round $^2C$. Formation of 2 methyl but-1-ene would require formation of $^2C$-$H_c$ bond and loss of a proton from the methyl group on $^1C$. Product selectivity results suggest that if this type of

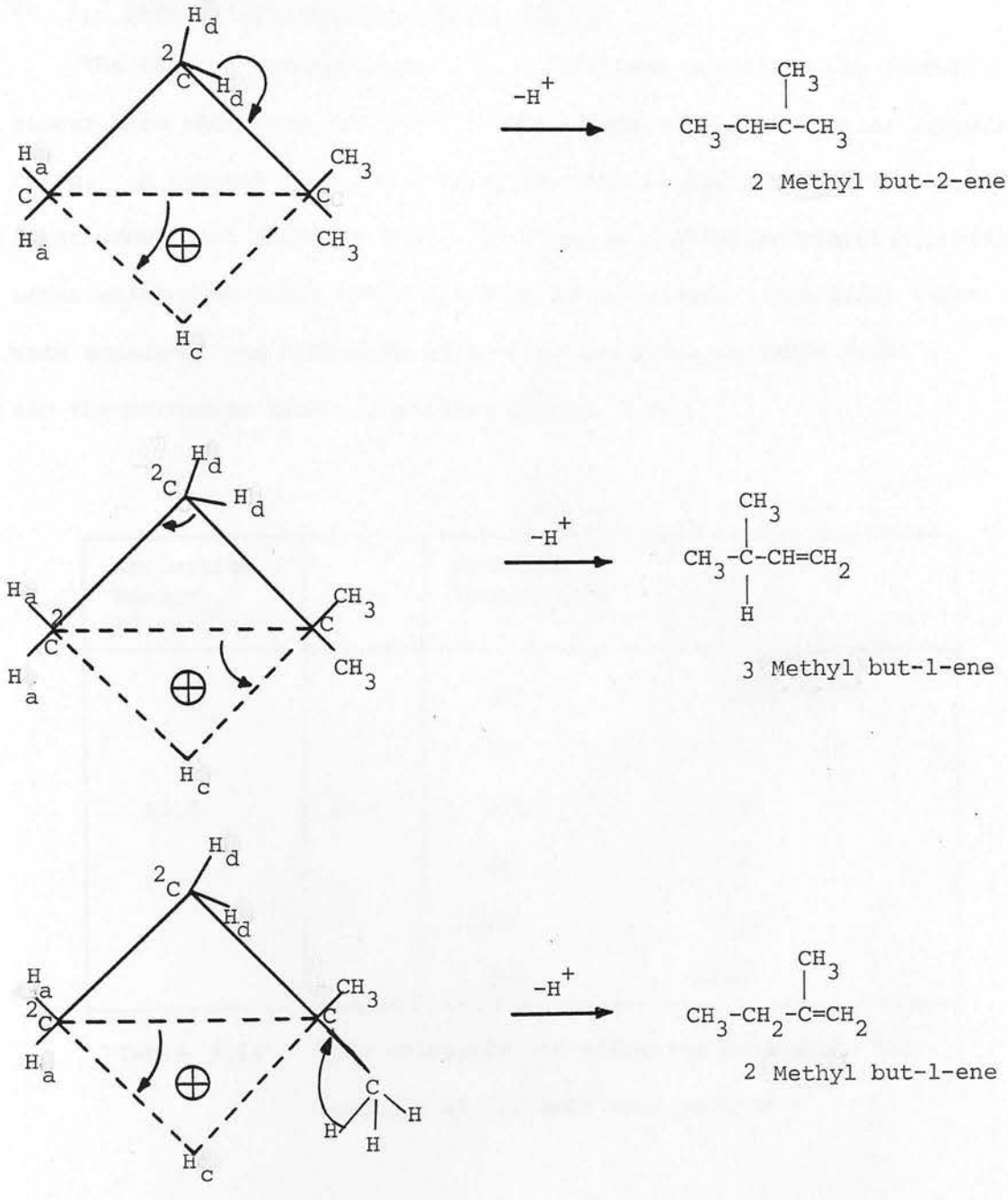


Fig. 7.27. Proposed Mechanism for Isomerisation of 1,1 DMCP

mechanism is operative for 1,1 DMCP isomerisation loss of methyl hydrogens is much less favoured than loss of $H_b$.

c) 1,2 Dimethylcyclopropane Isomerisation

The rate of isomerisation of 1,2 DMCP over zeolite Ω was somewhat slower than that observed for 1,1 DMCP isomerisation at similar temperatures. A typical reaction profile is given in Fig. 7.28. The typical first order plot shown in Fig. 7.29 shows an initial accelerating period after which good first order kinetics are observed. The first order rate constants and Arrhenius parameters are given in Table 7.16 and the Arrhenius plot illustrated in Fig. 7.30.

| Activation Energy $kJ\ mol^{-1}$ | ln A | Reaction Temperature K | $k \times 10^{-4}$ $s^{-1}g^{-1}$ |
|---|---|---|---|
| | | 229 | .05 |
| | | 242 | .25 |
| 60.5 | 19.4 | 247 | .40 |
| | | 261 | 2.3 |
| | | 280 | 9.61 |
| | | 293 | 63.8 |

Table 7.16 Rate constants and Arrhenius parameters for Reaction of 1,2 DMCP over zeolite Ω

Product Ratios

The major products of the reaction are 3 methyl but-1-ene and 2 methyl but-2-ene with small amounts of 2 methyl but-1-ene, pent-1-ene and cis and trans pent-2-enes being observed. The product distributions of methyl butenes at 10% conversion are given in Table 7.17.

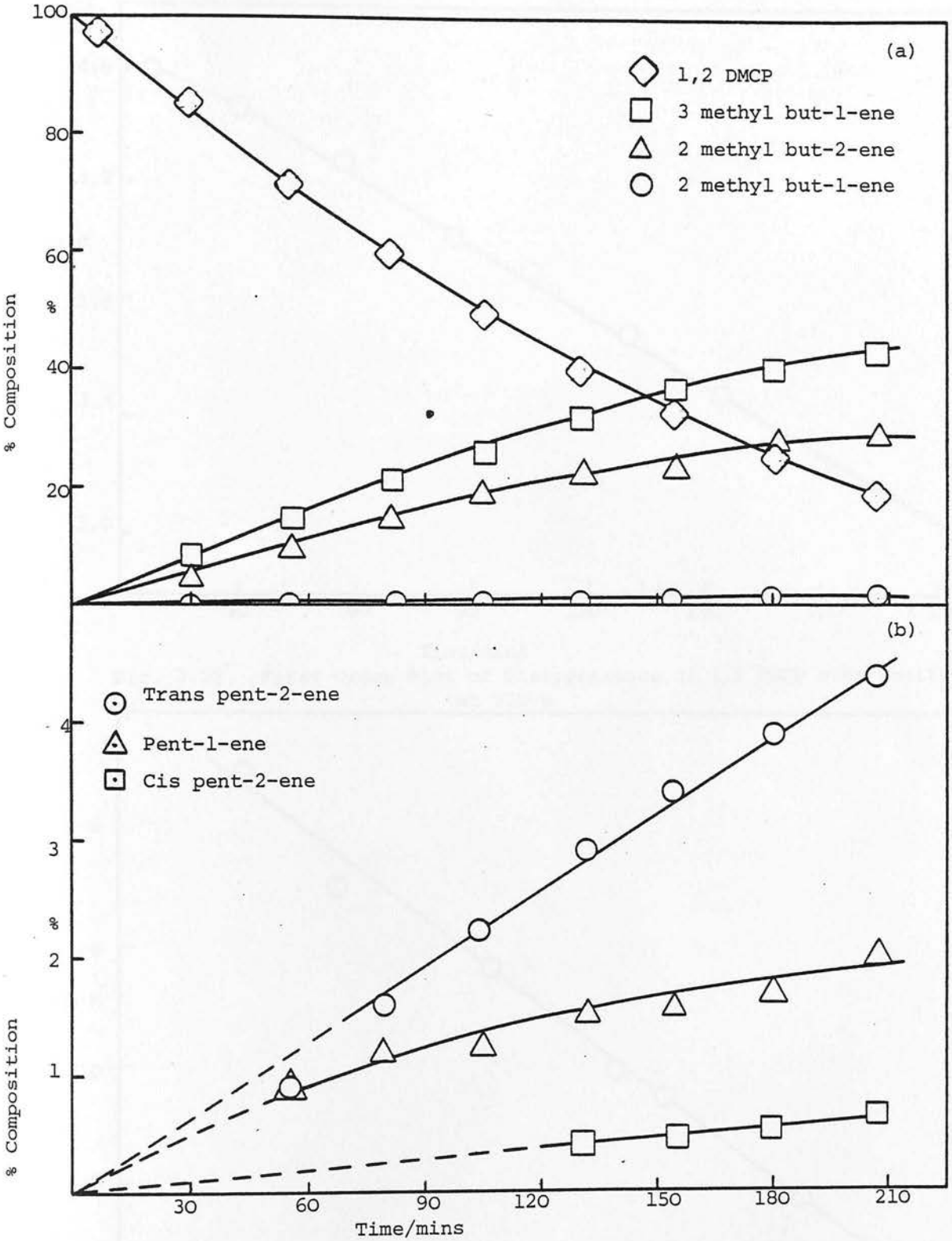


Fig. 7.28. Reaction of 1,2 DMCP on Zeolite Ω at 280 K

(a) Methyl butene products

(b) Pentene products

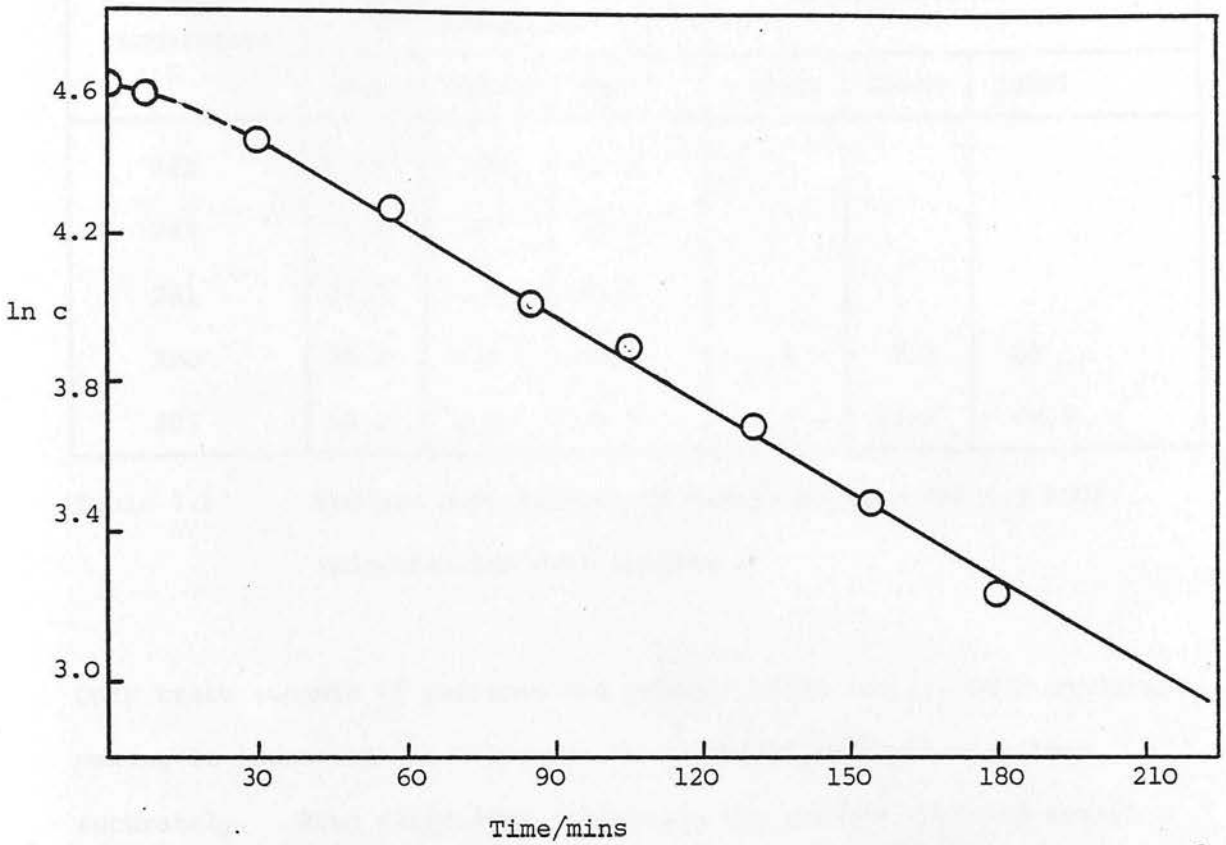


Fig. 7.29. First Order Plot of Disappearance of 1,2 DMCP over zeolite Ω at 280 K

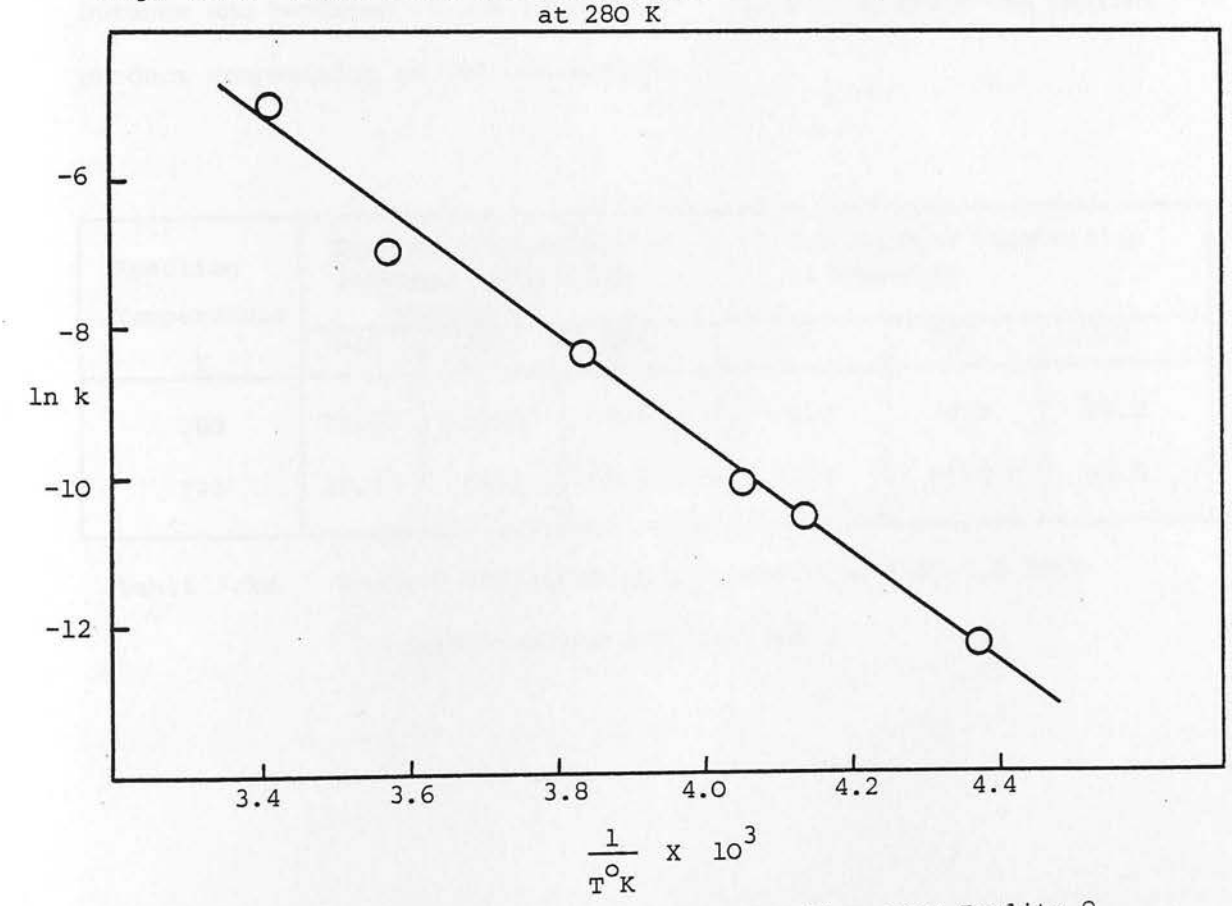


Fig. 7.30. Arrhenius Plot for 1,2 DMCP Reaction over Zeolite Ω

| Reaction Temperature K | Product Composition of Methyl butenes after 10% Conversion | | | Equilibrium Composition of Methyl butenes | | |
|---|---|---|---|---|---|---|
| | 3MeBl | 2MeBl | 2MeB2 | 3MeBl | 2MeBl | 2MeB2 |
| 242 | 83.6 | .06 | 16.3 | | | |
| 247 | 71.1 | 0 | 28.9 | | | |
| 261 | 63.7 | .6 | 35.7 | | | |
| 280 | 56.3 | 4.6 | 39.1 | .5 | 7.0 | 92 |
| 293 | 59.6 | 1.9 | 38.5 | .2 | 10.9 | 88.9 |

Table 7.17 Product Distribution of Methyl butenes for 1,2 DMCP Isomerisation over zeolite Ω

Only trace amounts of pentenes are present after 10% 1,2 DMCP conversion making it impossible to determine the pentene product composition accurately. Even after 100% conversion the product contains methyl butenes and pentenes in the ratio 9:1. Table 7.18 lists the pentene product composition at 50% conversion.

| Reaction Temperature K | Product Composition of Pentenes, after 50% Conversion | | | Equilibrium Composition of Pentenes | | |
|---|---|---|---|---|---|---|
| | P1 | TP2 | CP2 | P1 | TP2 | CP2 |
| 280 | 33.3 | 58.6 | 8.1 | 1.0 | 74.0 | 25.0 |
| 293 | 32.3 | 59.3 | 8.4 | 1.5 | 69.0 | 29.5 |

Table 7.18. Product Distribution of n-Pentenes from 1,2 DMCP Isomerisation over Zeolite Ω

Assuming negligible interconversion of the pentenes has occurred n-pentenes are produced from 1,2 DMCP isomerisation in the order trans > pent-1-ene > cis. This is the same order as observed for the formation of the n-butenes from MCP isomerisation.

As observed for 1,1 DMCP isomerisation, secondary reactions occur, 2 methyl but-2-ene isomerising to 3 methyl but-1-ene and 2 methyl but-1-ene.

Discussion

The product composition from 1,2 DMCP isomerisation over zeolite Ω correlates well with the operation of a classical proton addition mechanism, the relative amounts of the methyl butenes and pentenes being rationalised in terms of steric and energetic considerations. Hence the trace amount of 2 methyl but-1-ene observed may be attributed to the involvement of a primary carbonium ion in its formation whereas the other products are formed via secondary carbonium ions. In contrast to 1,1 DMCP isomerisation over zeolite Ω, the product composition from 1,2 DMCP is far removed from that predicted for a hydride abstraction mechanism.

It seems improbable that the isomerisation of various methyl-substituted cyclopropanes should occur by different types of mechanisms. Hence in view of the previous results for butenes and MCP it seems likely that a proton addition mechanism is operative for all these isomerisations. Moreover, mechanisms involving a non-classical carbonium ion have been postulated for the isomerisations of MCP and 1,1 DMCP. A similar mechanism may therefore be operating for 1,2 DMCP even though the observed results are in very good agreement with, those predicted from a classical proton addition ring-opening reaction.

## 7.2.2. Reactions over Erionite

a) Methylcyclopropane

Erionite (T) was a more active catalyst for the isomerisation of MCP than erionite (N). Typical reaction profiles for MCP isomerisation over erionite (N) and erionite (T) are shown in Figs. 7.31. and 7.32. respectively. Reactions over erionite (T) were followed in the temperature range 273-317 K, throughout which zero order kinetics for disappearance of MCP were observed. Over erionite (N) however although zero order kinetics were observed for reaction temperatures below 325 K, the results of a reaction carried out at 346 K appeared to fit either zero or first order kinetics (Fig. 7.33.). It was not possible to establish the kinetics of MCP isomerisation at higher temperatures, using the same quantities of catalyst and reactant, due to analytical restrictions.

The Arrhenius parameters and zero order rate constants are given in Tables 7.19. and 7.20.

| Activation Energy kJ $mol^{-1}$ | ln A | Reaction Temperature K | k x $10^{-3}$ % $s^{-1}$ $g^{-1}$ |
|---|---|---|---|
| 72.1 | 24.15 | 292 | 3.8 |
| | | 297 | 6.4 |
| | | 307 | 15 |
| | | 315 | 39 |
| | | 320 | 49 |
| | | 325 | 78 |

Table 7.19. Rate constants and Arrhenius parameters for MCP Isomerisation over Erionite (N)

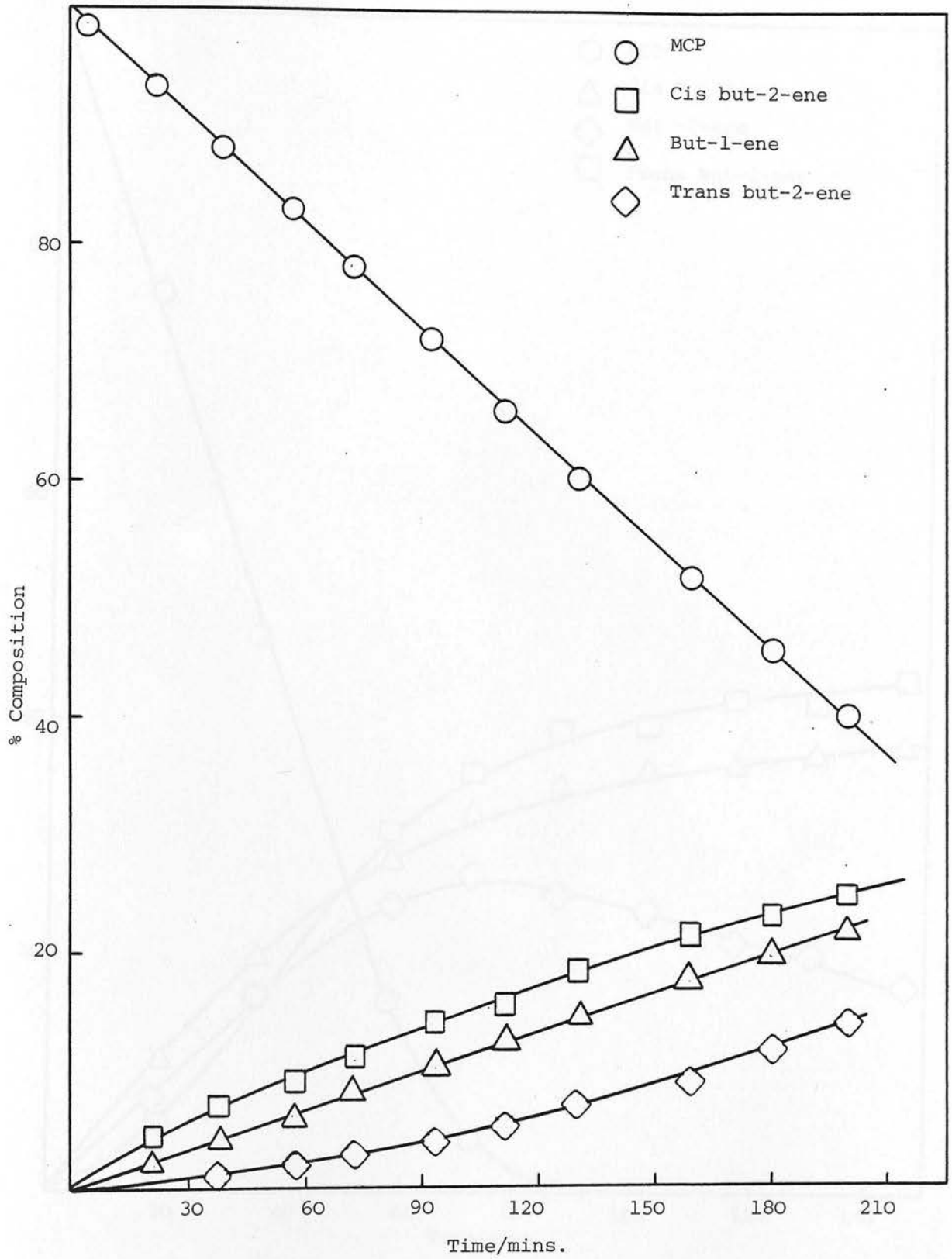


Fig. 7.31. Reaction Profile for Isomerisation of MCP over Erionite (N) at 315 K

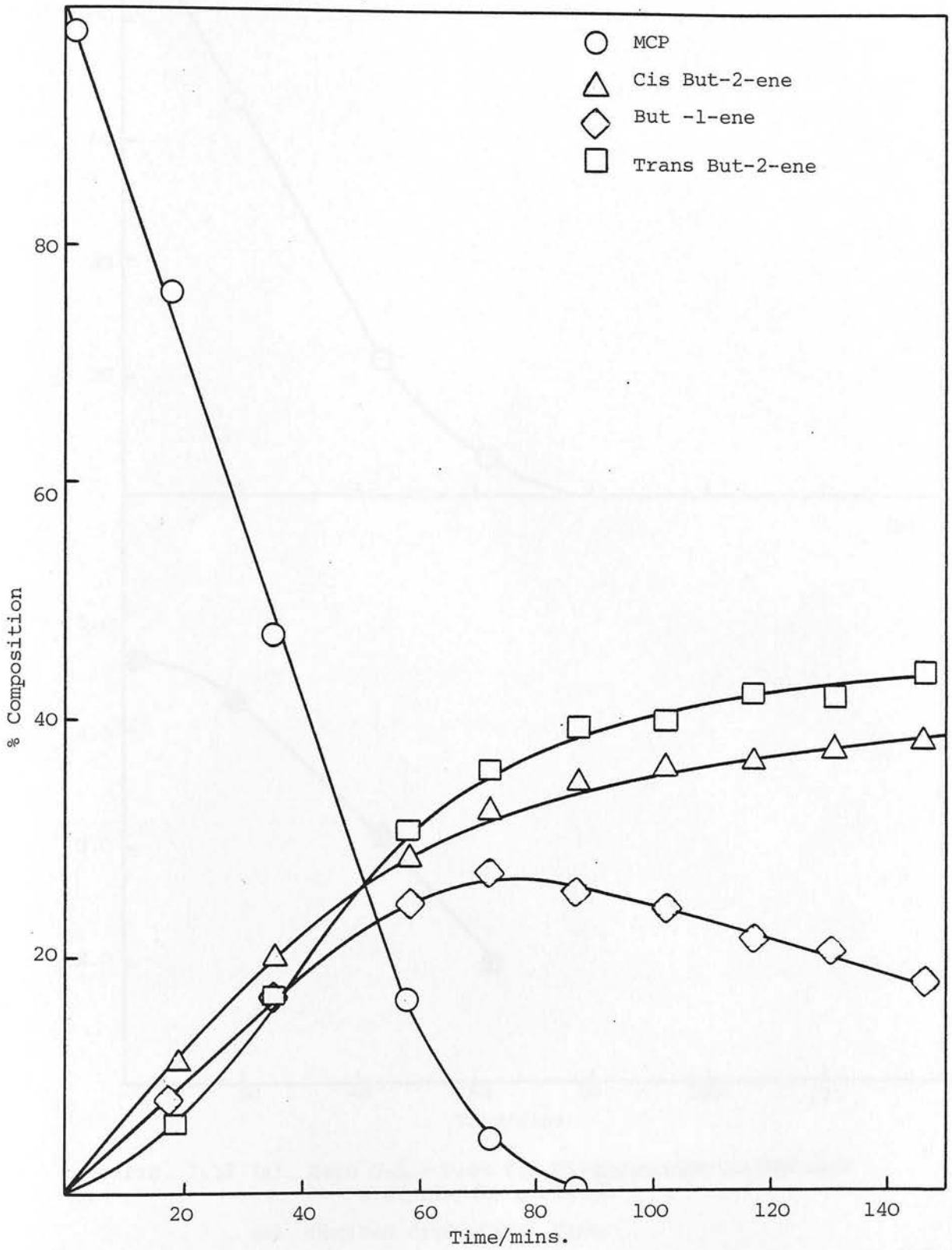


Fig. 7.32. Reaction Profile for Isomerisation of MCP over Erionite (T) at 317 K

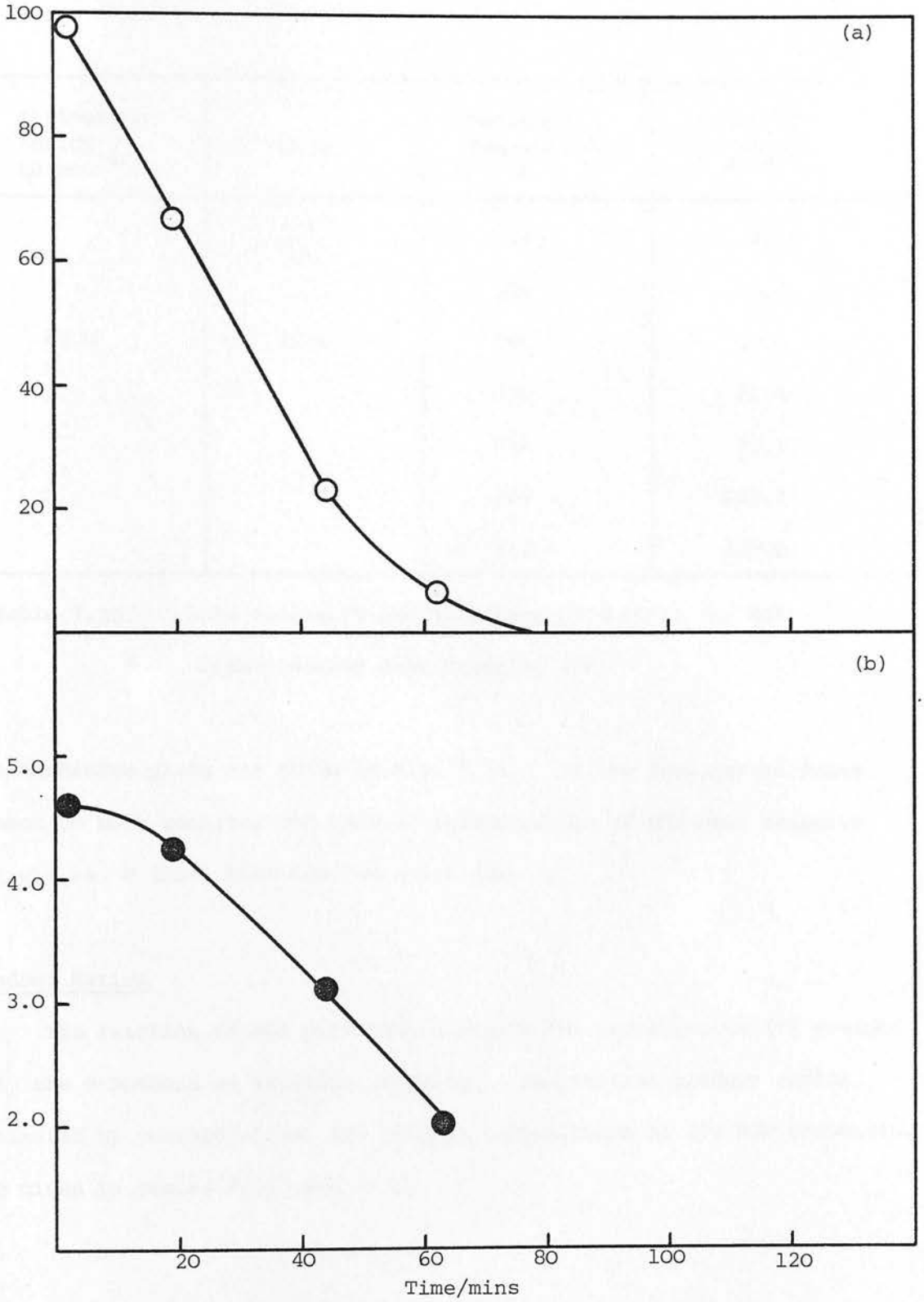


Fig. 7.33 (a) Zero Order Plot for Disappearance of MCP over Erionite (N) at 346 K

(b) Derived First Order Plot.

| Activation Energy $_{-1}$ kJ mol | ln A | Reaction Temperature K | k x $10^{-3}$ % $s^{-1}$ $g^{-1}$ |
|---|---|---|---|
| 63.0 | 22.4 | 273 | 4.33 |
| | | 286 | 18.4 |
| | | 289 | 20.5 |
| | | 290 | 22.4 |
| | | 296 | 39.1 |
| | | 309 | 133.4 |
| | | 317 | 192.0 |

Table 7.20. Rate constants and Arrhenius parameters for MCP isomerisation over Erionite (T)

The Arrhenius plots are shown in Fig. 7.34. In the temperature range common to both zeolites the rate of isomerisation of MCP over erionite (T) was ca. 8 times that over erionite (N).

Product Ratios

The reaction of MCP over both erionite (N) and erionite (T) yielded only the n-butenes as reaction products. The initial product ratios, estimated by extrapolation, and product compositions at 10% MCP conversion are given in Tables 7.21 and 7.22.

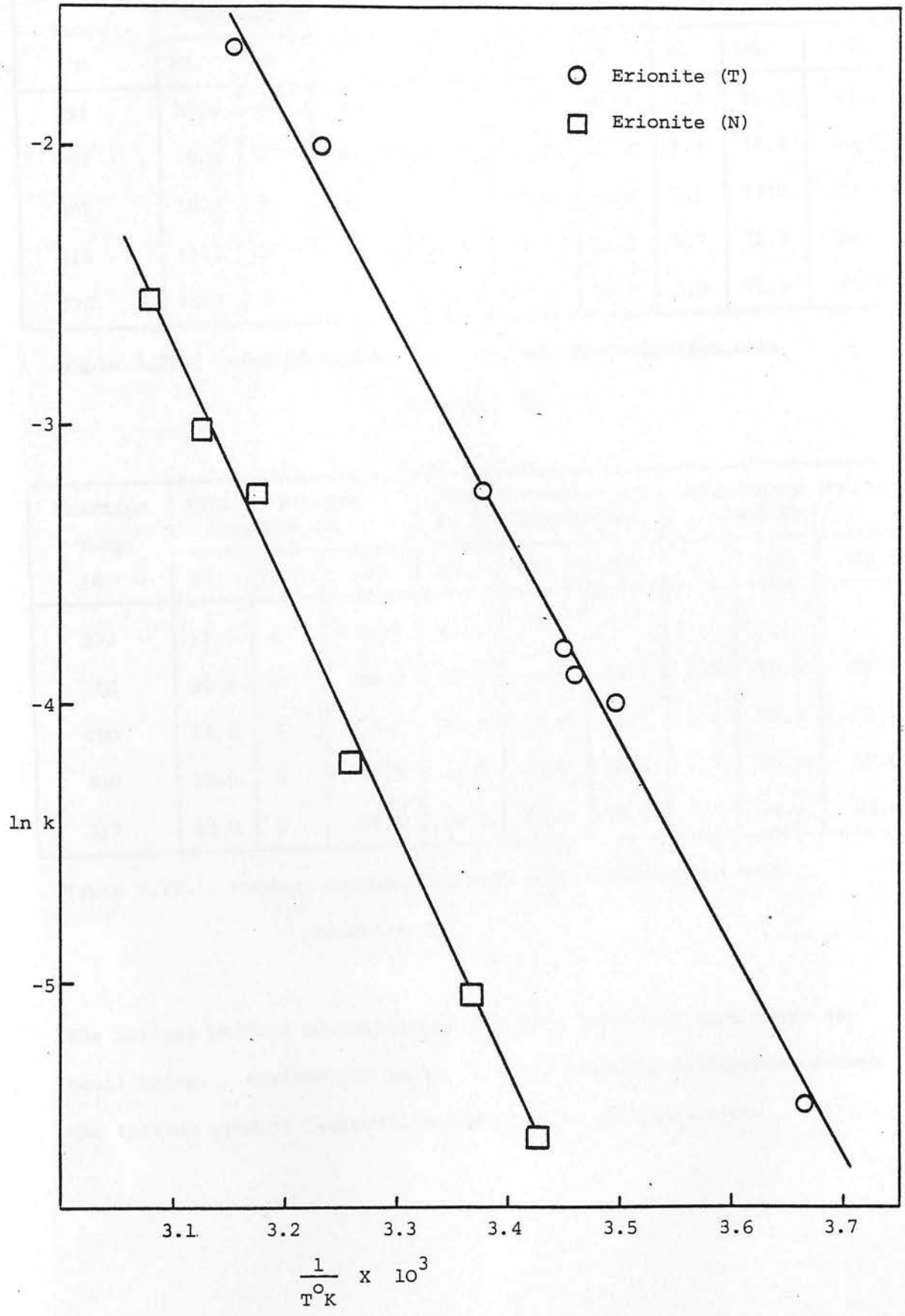


Fig. 7.34. Arrhenius Plots for Isomerisation of MCP over Erionite

| Reaction Temp. | Initial Product Composition | | | Product Composition at 10% Conversion | | | Equilibrium Product Composition | | |
|---|---|---|---|---|---|---|---|---|---|
| K | B1 | TB2 | CB2 | B1 | TB2 | CB2 | B1 | TB2 | CB2 |
| 292 | 20.9 | 0 | 79.1 | 32.9 | 6.9 | 60.2 | 2.2 | 75.3 | 22.5 |
| 297 | 19.0 | 0 | 81.0 | 32.4 | 6.8 | 60.8 | 2.4 | 74.3 | 23.3 |
| 307 | 18.1 | 0 | 81.9 | 35.0 | 8.0 | 57.0 | 2.5 | 74.0 | 23.5 |
| 315 | 11.3 | 0 | 88.7 | 35.6 | 8.2 | 56.3 | 2.7 | 72.5 | 24.8 |
| 325 | 15.8 | 0 | 84.2 | 37.3 | 10.1 | 52.6 | 3.0 | 71.5 | 25.5 |

Table 7.21. Product Composition form MCP Isomerisation over Erionite (N)

| Reaction Temp. | Initial Product Composition | | | Product Composition at 10% Conversion | | | Equilibrium Product Composition | | |
|---|---|---|---|---|---|---|---|---|---|
| K | B1 | TB2 | CB2 | B1 | TB2 | CB2 | B1 | TB2 | CB2 |
| 273 | 11.5 | 0 | 88.5 | 21.3 | 7.8 | 70.9 | | | |
| 286 | 20.0 | 0 | 80.0 | 28.0 | 14.9 | 57.1 | 2.1 | 75.6 | 22.3 |
| 290 | 24.8 | 0 | 75.2 | 25.8 | 7.9 | 66.2 | 2.2 | 75.3 | 22.5 |
| 309 | 35.5 | 0 | 46.7 | 33.7 | 16.8 | 49.5 | 2.5 | 73.9 | 23.6 |
| 317 | 32.0 | 0 | 68.0 | 32.0 | 12.0 | 56.0 | 2.7 | 72.4 | 24.9 |

Table 7.22. Product Composition from MCP Isomerisation over Erionite (T)

The initial product distributions are very different from those at equilibrium. Furthermore there is a considerable difference between the initial product composition and that at 10% conversion.

Fig. 7.35 illustrates the substantial variation in product composition with conversion of MCP. Secondary isomerisation of products (Fig. 7.32) does not seem to be responsible for such a change.

The estimated initial product ratios are similar to those observed in n-butene conversion; cis but-2-ene > but-1-ene > trans but-2-ene, although as discussed previously these may be apparent, the intrinsic ratios probably being distorted by the selective adsorption characteristics of the zeolite.

Reaction of But-1-ene after MCP Isomerisation

The profile of an extended reaction (Fig. 7.32) shows that isomerisation of product but-1-ene to but-2-ene occurs after all the MCP has been converted. This reaction will occur in parallel with MCP isomerisation to a small extent illustrated by the small alteration in the % composition of but-1-ene in the product with extent of MCP conversion (Fig. 7.35). The disappearance of but-1-ene, after 100% MCP conversion, follows first order kinetics yielding rate constants identical to those observed when but-1-ene was the initial reactant. Reactions were also carried out in which, after complete MCP conversion, the gas phase was evacuated and a dose of $10^{20}$ molecules admitted to the used catalyst. Rate constants similar to those already reported were observed, although an initial accelerating period of ca. 20 minutes was required before a steady first order rate was maintained. In contrast isomerisation of but-1-ene admitted to erionite (T) immediately after pretreatment exhibited an initial decelerating period before achieving a steady first order rate. The MCP reaction therefore does not appear to poison the sites necessary for n-butene conversion. Although MCP

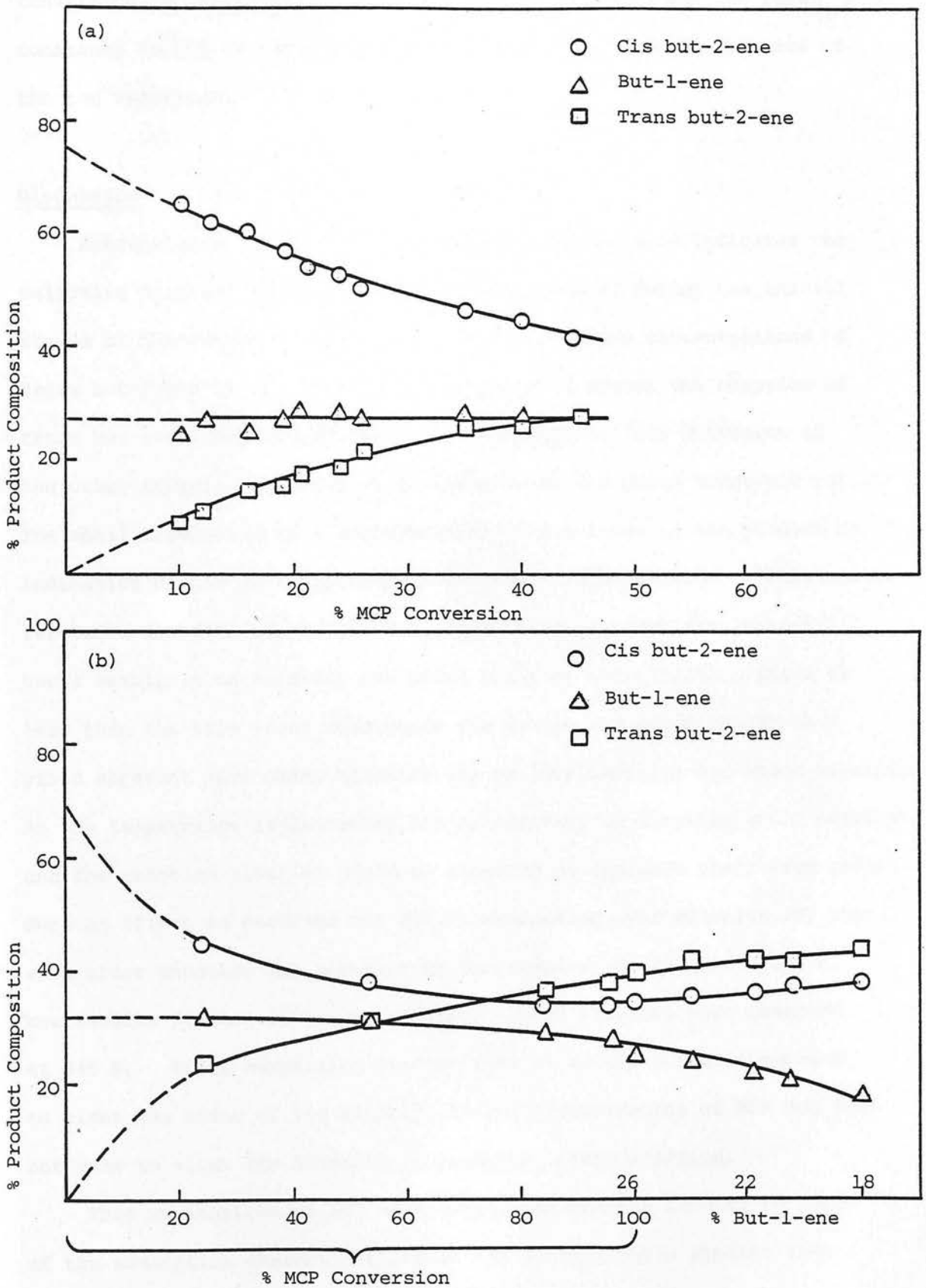


Fig. 7.35. Variation in Product Composition with Extent of MCP Conversion

(a) Reaction over erionite (T) at 286 K

(b) Reaction over erionite (T) at 317 K

conversion is substantially faster than that of but-1-ene the rate constants cannot be compared in view of the difference in kinetics of the two reactions.

Discussion

Extrapolation of product ratios to zero conversion indicates the selective sorption of any trans but-2-ene produced during the initial stages of the reaction leading to initial gas phase concentrations of trans but-2-ene of ca. 0%. As the reaction proceeds the sorption of trans but-2-ene may be limited by the intracrystalline diffusion of the other isomers resulting in an increase in gas phase trans/cis ratio. The small alteration in % concentration of but-1-ene in the product is indicative of its participation in secondary isomerisation. Furthermore selective sorption of one or more of the products over the reactant would result in an apparent gas phase reactant concentration which is less than the true value throughout the system and could conceivably yield apparent zero order kinetics for an intrinsically 1st order reaction. As the temperature is increased the selectivity of sorption would decrease and the reaction kinetics would be expected to approach their true order. Such an effect is observed for MCP isomerisation over erionite (N) where zero order kinetics are apparent in the temperature range 292-325 K, but results fitting both zero and first order kinetics were observed at 346 K. It is surprising however that selective sorption appears to alter the order of the kinetics in the isomerisation of MCP but does not seem to alter the kinetics of n-butene interconversion.

This explanation of MCP selectivity and kinetic results in terms of the adsorption characteristics of the zeolite again implies that the majority of the reaction occurs on the external surface.

Moreover, because of the apparent nature of the results it is not possible to postulate whether the isomerisation of MCP involves the same intermediate as n-butene interconversion or a different one as postulated for reaction over zeolite Ω. The absence of isobutene and cyclobutane from the observed products is however suggestive of a proton addition mechanism.

b) 1,1 Dimethylcyclopropane

A typical reaction plot for the isomerisation of 1,1 DMCP over erionite (N) is shown in Fig. 7.36. The derived first order plot shows that although an initial decelerating period occurs the reaction eventually follows first order kinetics. Similar reaction profiles and kinetics are observed for erionite (T). The eventual steady first order rates, attained after ca. 20% conversion over erionite (T) and after ca. 50% conversion over erionite (N), and derived Arrhenius parameters are listed in Tables 7.23 and 7.24. The initial first order rate constants are approximately three times greater than the steady values and result in a similar value of activation energy (35.8 kJ $mol^{-1}$ for erionite (N)).

| Activation Energy $\pm_1$ kJ $mol^{-1}$ | ln A | Reaction Temperature K | k x $10^{-4}$ $s^{-1}$ $g^{-1}$ |
|---|---|---|---|
| 34.3 | 6.8 | 278 | 3.11 |
| | | 290 | 5.08 |
| | | 294 | 5.67 |
| | | 303 | 8.55 |
| | | 314 | 15.74 |
| | | 320 | 19.4 |

Table 7.23. Rate constants and Arrhenius parameters for 1,1 DMCP Isomerisation over Erionite (N)

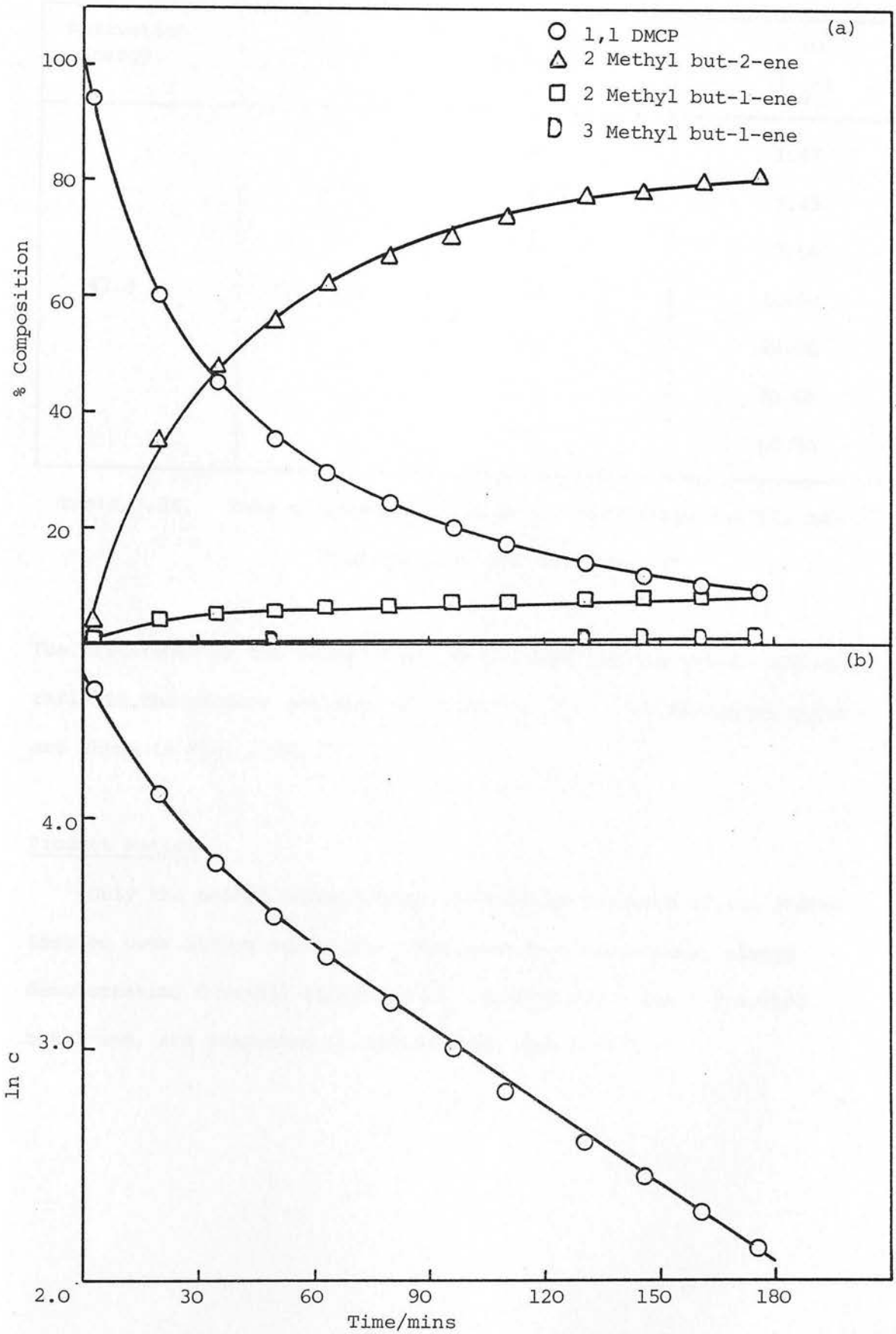


Fig. 7.36. (a) Reaction Profile for 1,1 DMCP Isomerisation over Erionite (N) at 314 K

(b) Derived First Order Plot.

| Activation Energy | ln A | Reaction Temperature K | k x $10^{-4}$ $s^{-1}$ $g^{-1}$ |
|---|---|---|---|
| 43.3 | 14.0 | 229 | 1.47 |
| | | 242 | 5.45 |
| | | 246 | 7.66 |
| | | 257 | 18.28 |
| | | 260 | 22.56 |
| | | 264 | 31.06 |
| | | 273 | 60.70 |

Table 7.24. Rate constants and Arrhenius parameters for 1,1 DMCP Isomerisation over Erionite (T)

The difference in the temperature ranges used for the two erionites reflects the greater activity of erionite (T). The Arrhenius plots are shown in Fig. 7.37.

Product Ratios

Only the methyl butenes were observed as products of the isomerisation over either erionite. The product compositions, always demonstrating 2 methyl but-2-ene >> 2 methyl but-1-ene > 3 methyl but-1-ene, are presented in Tables 7.25, and 7.26.

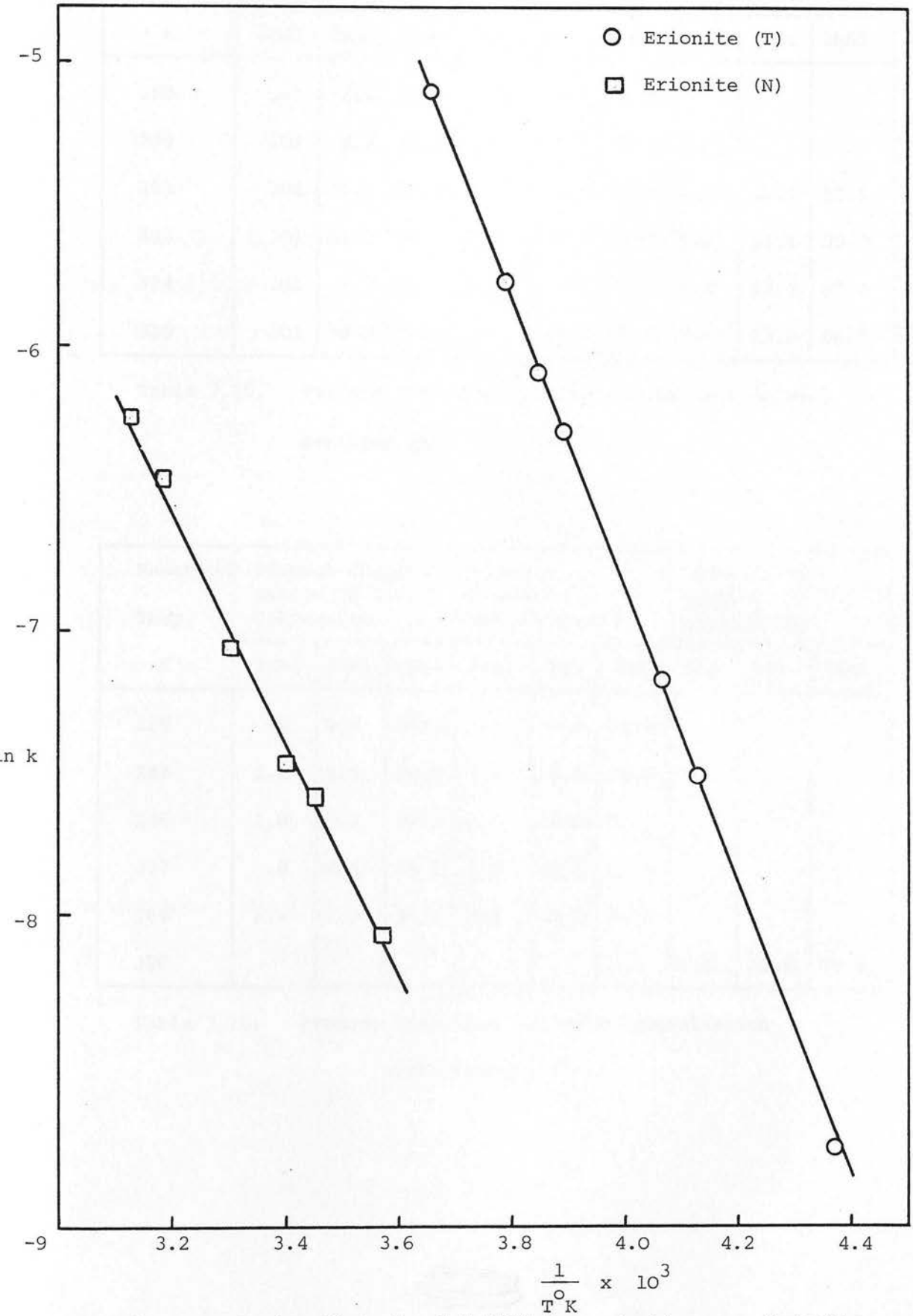


Fig. 7.37. Arrhenius Plots for 1,1 DMCP Isomerisation over Erionite.

| Reaction Temp. | Product Composition at 10% Conversion | | | Product Composition at 50% Conversion | | | Equilibrium Product Composition | | |
|---|---|---|---|---|---|---|---|---|---|
| K | 3MB1 | 2MB1 | 2MB2 | 3MB1 | 2MB1 | 2MB2 | 3MB1 | 2MB1 | 2MB2 |
| 280 | .01 | 7.6 | 92.4 | 2.1 | 6.8 | 91.1 | | | |
| 290 | .01 | 9.2 | 90.8 | 1.7 | 7.6 | 90.6 | | | |
| 294 | .01 | 9.2 | 90.8 | 1.7 | 7.9 | 90.4 | 0.2 | 10.7 | 89.1 |
| 303 | .01 | 11.1 | 88.9 | 1.6 | 9.9 | 88.4 | 0.2 | 11.1 | 88.7 |
| 314 | .01 | 7.3 | 91.7 | 1.6 | 9.5 | 88.9 | 0.4 | 12.2 | 87.4 |
| 320 | .01 | 10.0 | 90.0 | 2.1 | 10.1 | 87.8 | 0.5 | 13.0 | 86.5 |

Table 7.25. Product Data from 1,1 DMCP Isomerisation over Erionite (N)

| Reaction Temp. | Product Composition at 10% Conversion | | | Product Composition at 50% Conversion | | | Equilibrium Product Composition | | |
|---|---|---|---|---|---|---|---|---|---|
| K | 3MB1 | 2MB1 | 2MB2 | 3MB1 | 2MB1 | 2MB2 | 3MB1 | 2MB1 | 2MB2 |
| 229 | .9 | 4.3 | 94.8 | 1.2 | 4.5 | 89.8 | | | |
| 242 | 1.1 | 4.4 | 94.5 | 1.4 | 5.5 | 93.0 | | | |
| 246 | 1.8 | 6.3 | 92.9 | 1.3 | 5.5 | 93.1 | | | |
| 257 | .8 | 4.1 | 95.1 | 2.6 | 4.7 | 92.6 | | | |
| 264 | 2.6 | 3.0 | 94.4 | 9.4 | 2.8 | 87.8 | | | |
| 298 | | | | | | | 0.2 | 10.8 | 89.0 |

Table 7.26. Product Data from 1,1 DMCP Isomerisation over Erionite (T)

The occurrence of secondary reactions of the products is evident in an extended reaction profile illustrated in Fig. 7.38 where 2 methyl but-2-ene appears to isomerise to 3 methyl but-1-ene. However this is slow in comparison to the rate of isomerisation of 1,1 DMCP and thus won't alter product compositions appreciably. It is however possible that the small amount of 3 methyl but-1-ene observed during isomerisation of 1,1 DMCP may be a product of the secondary reaction. The shape of the curve for appearance of 3 methyl but-1-ene with time (Fig. 7.38) lends support to this suggestion.

Although the pressure of gas admitted to the catalyst was less than the saturated vapour pressure, loss of material from the gas phase was indicated from summation of the chromatographic peak areas. After 9 samples were removed from the reaction vessel at 242 K the total peak area was ca. 24% of the initial value. In contrast removal of 9 samples from the reaction vessel at 294 K yielded a total peak area of ca. 84% of the original. This phenomenon has already been discussed in Chapter 6 and appears to be due to condensation rather than to a slow selective sorption.

## Discussion

The product composition observed from 1,1 DMCP isomerisation over both samples of erionite is very similar to that observed over zeolite Ω and, according to previous reports, to that over CeX[218] and silica-alumina.[211] As discussed previously such a distribution is neither wholly compatible with either a hydride abstraction nor a proton addition mechanism, the presence of 2 methyl but-2-ene as the major product favouring the former and the presence of small amounts of 3 methyl but-1-ene agreeing with the latter. It is therefore possible

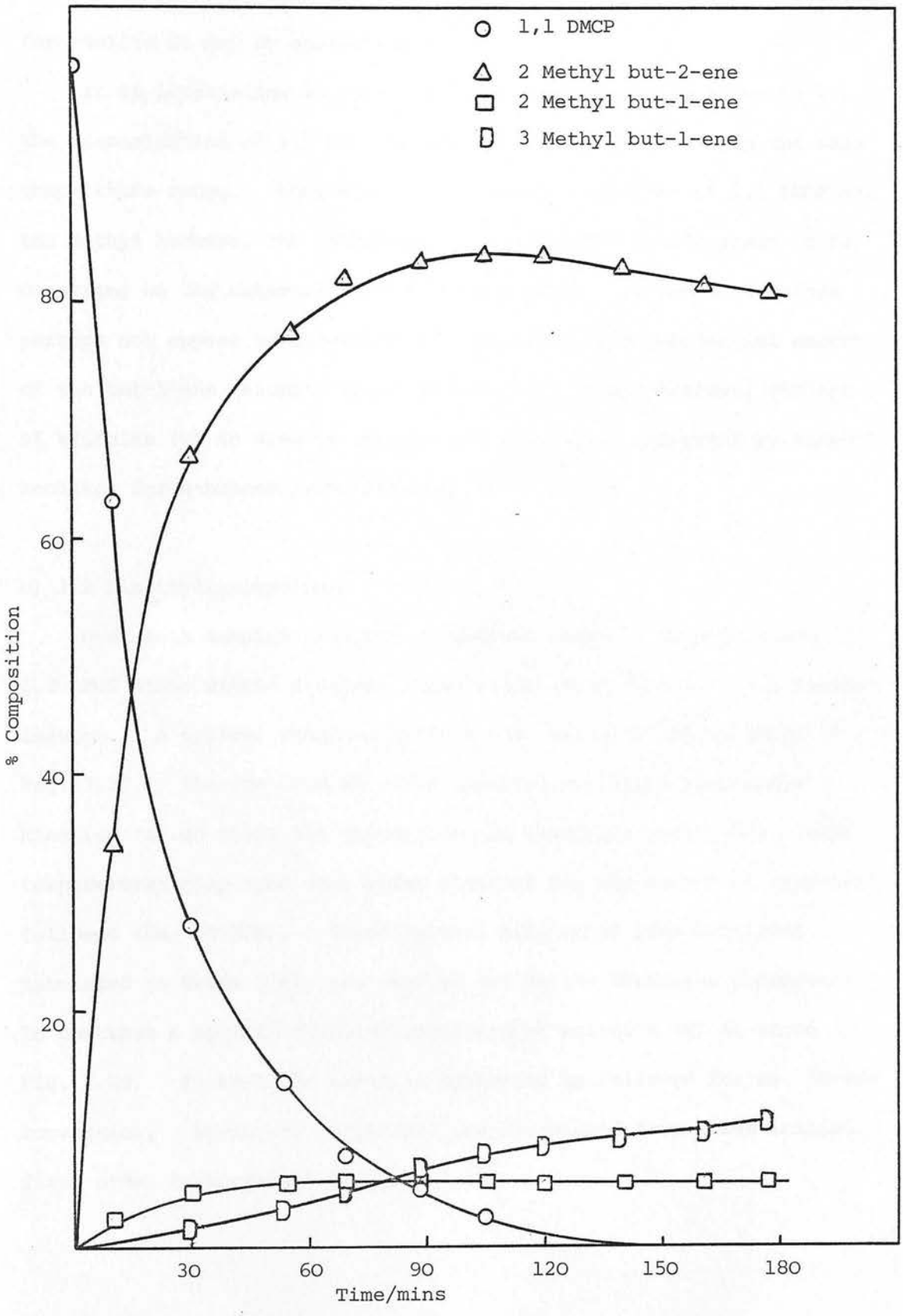


Fig. 7.38. Reaction Profile of 1,1 DMCP Isomerisation over Erionite (T) at 273 K.

that a mechanism involving a non-classical carbonium ion, as suggested for zeolite Ω, may be operative.

It is interesting to note that over zeolites Ω and erionite (T) the isomerisation of 1,1 DMCP occurs at similar rates within the same temperature range. However, in view of the bulkiness of 1,1 DMCP and the methyl butenes, the isomerisation of 1,1 DMCP would appear to be occurring on the external surface of erionite. It would therefore perhaps not appear unreasonable to conclude that a substantial amount of the but-1-ene reaction was also occurring on the external surface of erionite (T) in view of the similar activities exhibited by these zeolites for n-butene isomerisation.

c) 1,2 Dimethylcyclopropane

Over both samples of erionite similar rates of isomerisation of 1,2 DMCP occur within a higher temperature range than 1,1 DMCP isomerisation. A typical reaction profile over erionite (N) is shown in Fig. 7.39. The reaction at 348 K appeared to follow zero order kinetics for at least 50% conversion and reactions observed at lower temperatures displayed zero order kinetics for the extent of reaction followed (ca. 20-30%). These initial zero order rate constants, tabulated in Table 7.27, are used to derive the Arrhenius parameters. In contrast a typical reaction profile over erionite (T) is shown in Fig. 7.40. First order kinetics appear to be followed for ca. 50-60% conversion. Arrhenius parameters are calculated from these initial first order rates listed in Table 7.28.

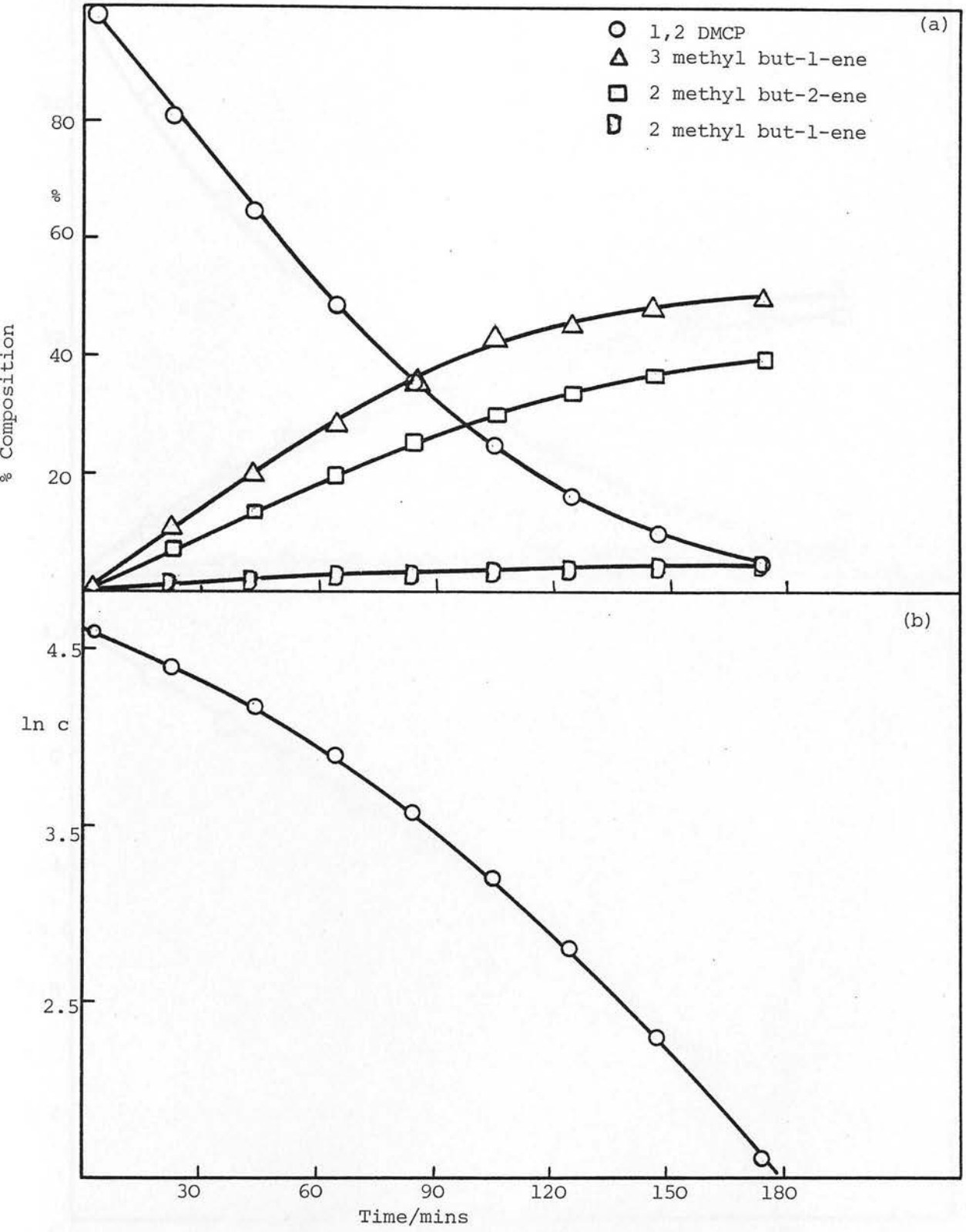


Fig. 7.39 (a) Reaction Profile of 1,2 DMCP Isomerisation over Erionite (N) at 348 K

(b) Derived First Order Plot.

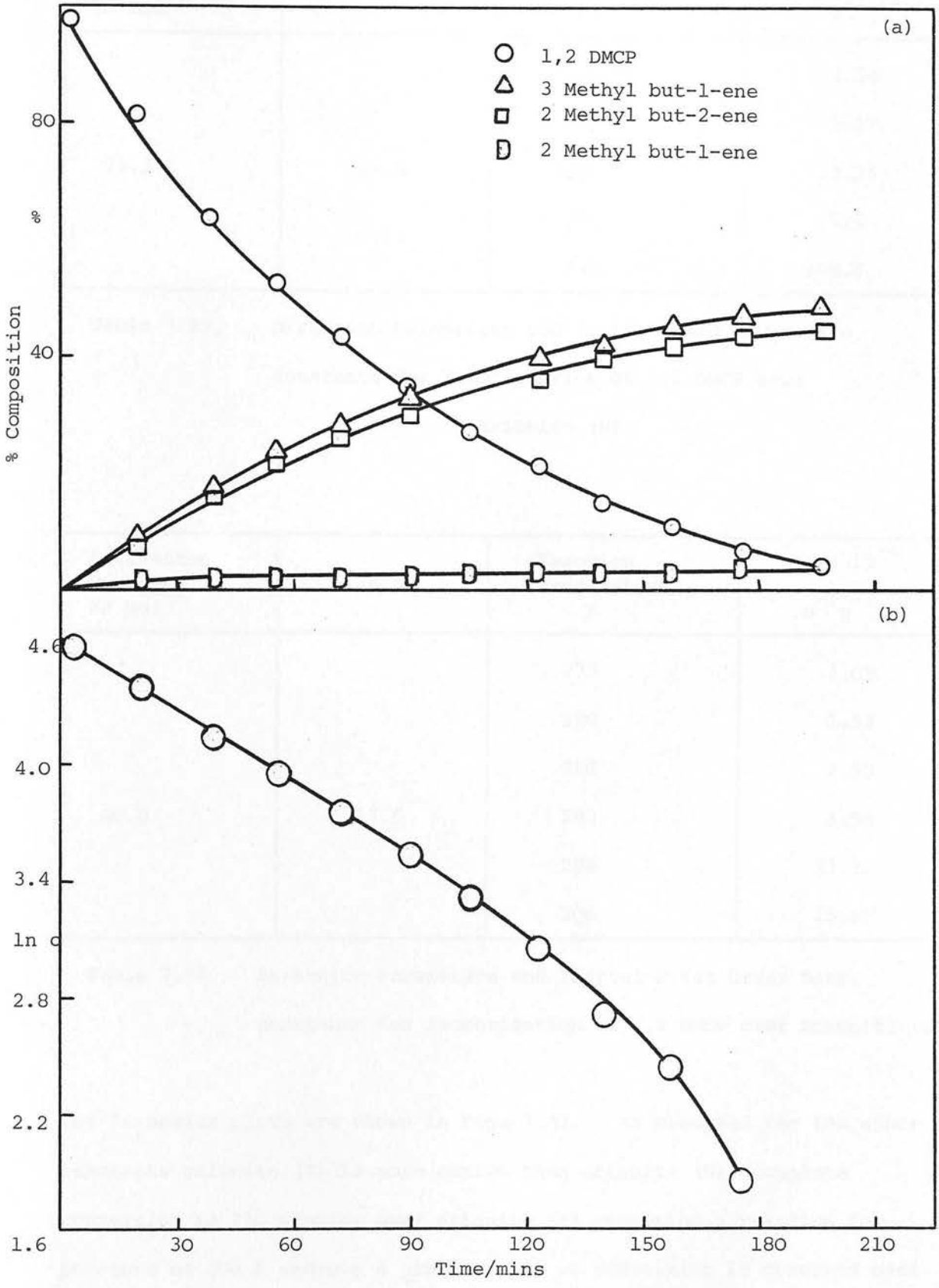


Fig. 7.40. (a) Reaction Profile of 1,2 DMCP Isomerisation over Erionite (T) at 306 K

(b) Derived First Order Plot.

| Activation Energy $kJ\ mol^{-1}$ | ln A | Reaction Temperature K | $k \times 10^{-3}$ % $s^{-1}g^{-1}$ |
|---|---|---|---|
| 73.3 | 22.9 | 311 | 4.54 |
| | | 317 | 7.27 |
| | | 326 | 13.24 |
| | | 344 | 55.9 |
| | | 348 | 101.8 |

Table 7.27. Arrhenius Parameters and Initial Zero Order Rate constants for Isomerisation of 1,2 DMCP over Erionite (N)

| Activation Energy $kJ\ mol^{-1}$ | ln A | Reaction Temperature K | $k \times 10^{-4}$ $s^{-1}g^{-1}$ |
|---|---|---|---|
| 60.8 | 17.5 | 273 | 1.05 |
| | | 280 | 1.53 |
| | | 286 | 2.90 |
| | | 293 | 5.56 |
| | | 299 | 11.15 |
| | | 306 | 15.58 |

Table 7.28. Arrhenius Parameters and Initial First Order Rate constants for Isomerisation of 1,2 DMCP over Erionite (T)

The Arrhenius plots are shown in Fig. 7.41. As observed for the other reactants erionite (T) is more active than erionite (N), complete conversion in 210 minutes over erionite (T) requiring a reaction temperature of 308 K whereas a similar rate of conversion is observed over

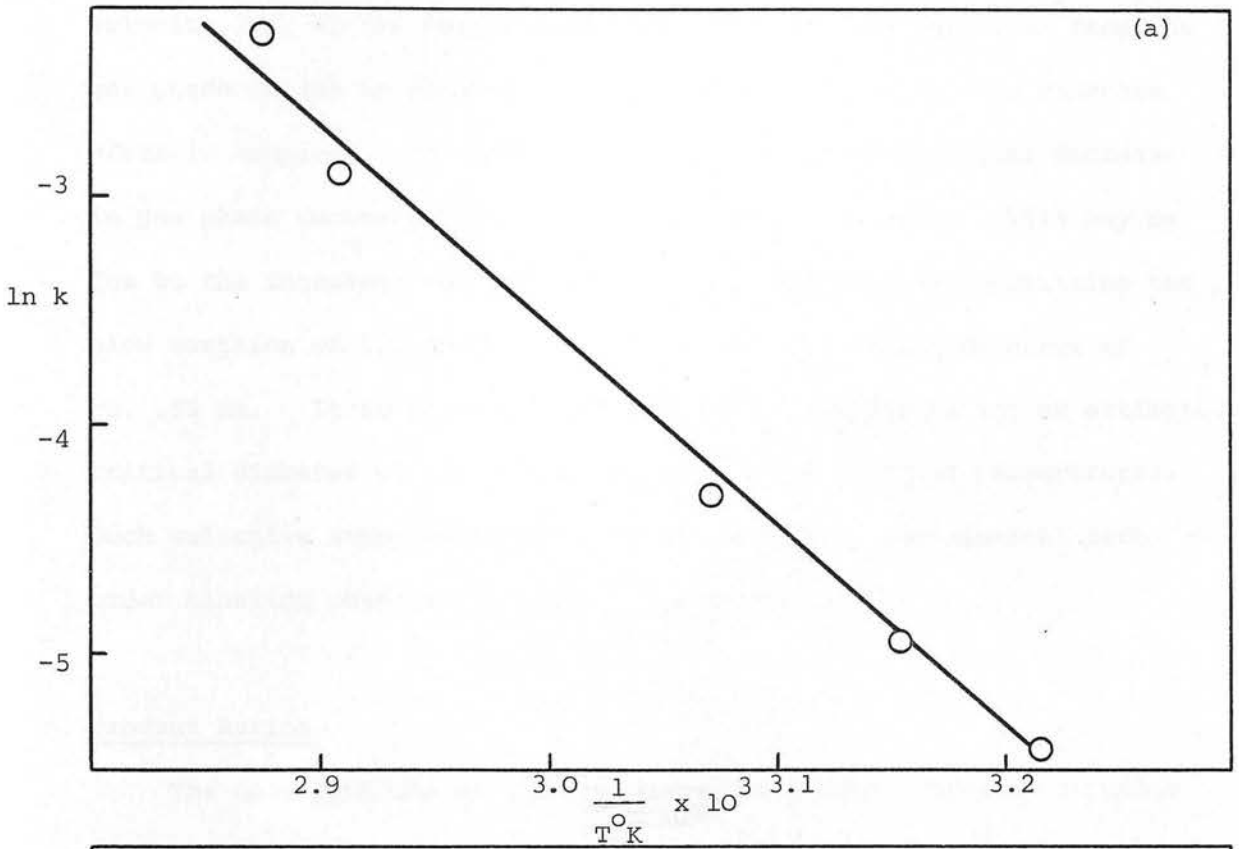


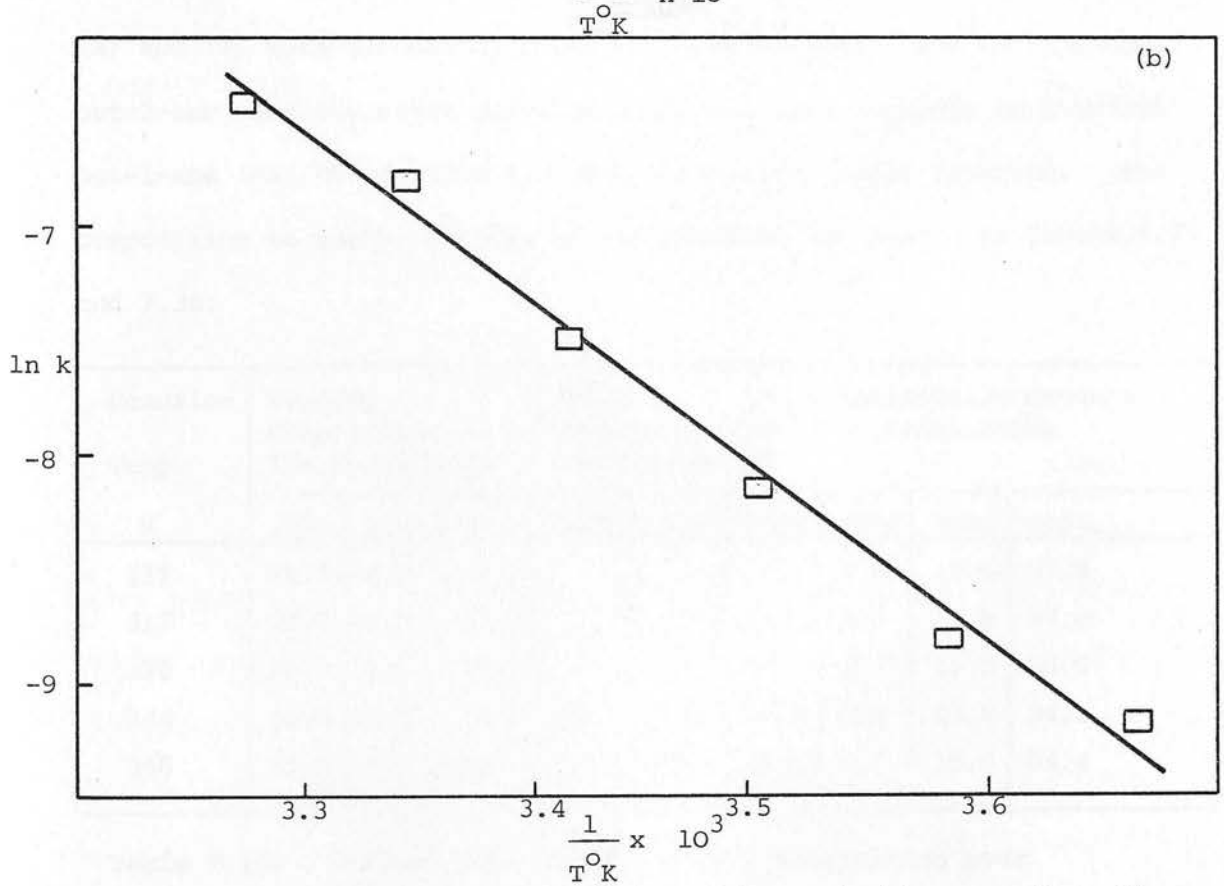


Fig. 7.41. Arrhenius Plots for 1,2 DMCP Isomerisation over Erionite

(a) Erionite (N)

(b) Erionite (T)

erionite (N) at 348 K. Gas phase analysis indicates that over erionite (T), in the temperature range studied, the only loss from the gas phase is due to removal of samples resulting in ca. 25% decrease after 10 samples. In contrast, with erionite (N) a similar decrease in gas phase concentration is observed after 3 samples. This may be due to the increased temperatures used for erionite (N) permitting the slow sorption of 1,2 DMCP estimated to have a critical diameter of ca. .56 nm. It is unlikely that the methyl butenes having an estimated critical diameter of ca. .58 nm will be sorbed at these temperatures. Such selective sorption of reactant may result in the apparent zero order kinetics observed initially over erionite (N).

Product Ratios

The only products of the reaction of 1,2 DMCP over both erionite (N) and (T) were the methyl butenes; 3 methyl but-1-ene and 2 methyl but-2-ene were the major products with only small amounts of 2 methyl but-1-ene (ca. 5% at 100% 1,2 DMCP conversion) being detected. The composition of methyl butenes in the products are listed in Tables 7.29 and 7.30.

| Reaction Temp. | Product Composition at 10% Conversion | | | Product Composition at 50% Conversion | | | Equilibrium Product Composition | | |
|---|---|---|---|---|---|---|---|---|---|
| K | 3MB1 | 2MB1 | 2MB2 | 3MB1 | 2MB1 | 2MB2 | 3MB1 | 2MB1 | 2MB2 |
| 311 | 56.9 | 2.8 | 40.3 | | | | 0.5 | 12.0 | 87.5 |
| 317 | 52.3 | 4.0 | 43.7 | | | | 0.5 | 12.5 | 87.0 |
| 326 | 53.9 | 3.1 | 43.0 | | | | 0.5 | 13.0 | 86.5 |
| 344 | 52.5 | 6.6 | 40.9 | 51.5 | 5.6 | 42.9 | 0.6 | 14.6 | 84.8 |
| 348 | 52.8 | 6.6 | 40.6 | 48.7 | 5.5 | 45.7 | 0.6 | 15.0 | 84.4 |

Table 7.29. Product Data for 1,2 DMCP Isomerisation over Erionite (N)

| Reaction Temp. | Product Composition at 10% Conversion | | | Product Composition at 50% Conversion | | | Equilibrium Product Composition | | |
|---|---|---|---|---|---|---|---|---|---|
| K | 3MB1 | 2MB1 | 2MB2 | 3MB1 | 2MB1 | 2MB2 | 3MB1 | 2MB1 | 2MB2 |
| 273 | 61.8 | 1.1 | 37.1 | 59.5 | 1.6 | 38.9 | | | |
| 280 | 54.6 | 1.1 | 44.3 | 51.8 | 1.7 | 46.5 | | | |
| 286 | 53.0 | 3.1 | 43.9 | 52.4 | 2.2 | 45.4 | | | |
| 293 | 58.8 | 2.2 | 39.0 | 54.2 | 2.4 | 43.4 | 0.4 | 10.9 | 88.7 |
| 299 | 52.5 | 3.5 | 44.0 | 50.8 | 5.0 | 44.2 | 0.4 | 11.1 | 88.5 |
| 306 | 52.6 | 4.0 | 43.4 | 49.7 | 5.8 | 44.5 | 0.5 | 11.5 | 88.0 |
| 322 | 53.0 | 3.9 | 43.1 | 52.1 | 4.0 | 43.9 | 0.5 | 13.0 | 86.5 |

Table 7.30. Product Data for 1,2 DMCP Isomerisation over Erionite (T)

No pentenes were observed at any stage of the reaction nor at any reaction temperature.

Discussion

The relative amounts of the methyl butenes produced from the isomerisation of 1,2 DMCP over both samples of erionite are similar to those observed for zeolite Ω; 3 methyl but-1-ene > 2 methyl but-2-ene >> 2 methyl but-1-ene. However, in contrast with zeolite Ω and results reported previously over other acidic catalysts,[211,218] no pentenes were observed. Control analysis of the 1,2 DMCP before use demonstrated the presence of a small amount of pent-1-ene impurity which was not detected in the sample after passage over either erionite. This suggests the selective sorption of pent-1-ene by this zeolite. Therefore the absence of pentenes in the gas phase products of 1,2 DMCP isomerisation

does not necessarily imply that these species are not products of the reaction, only that they are not the major products.

Criteria outlined in Appendix 1 demonstrate that the relative amounts of the methyl butenes produced from 1,2 DMCP isomerisation over both types of erionite are strongly indicative of a classical proton addition type mechanism. Operation of this mechanism would also produce small amounts of pentenes, which may be being selectively sorbed into the erionite cavities. Both the bulkiness of the 1,2 DMCP and methyl butenes and the indication of selective sorption of pentenes from the gas phase throughout the reaction are suggestive of the occurrence of 1,2 DMCP isomerisation mainly on the external surface of erionite.

## 7.3 Double bond Shift of 1,1 [$^2H_2$] Propene

### 7.3.1 Reactions over Zeolite Ω

Plots of the disappearance of [$^2H_2$] propene according to first order kinetics yield straight lines from which the first order rate constants and Arrhenius parameters listed in Table 7.31 are evaluated.

| Activation Energy $kJ\ mol^{-1}$ | ln A | Reaction Temperature K | k x $10^{-4}$ $s^{-1}\ g^{-1}$ |
|---|---|---|---|
| 35.0 | 3.99 | 340 | 2.28 |
| | | 353 | 3.44 |
| | | 357 | 4.12 |
| | | 371 | 6.43 |

Table 7.31. First order rate constants and Arrhenius Parameters for Disappearance of [$^2H_2$] propene over zeolite Ω.

The Arrhenius plot is shown in Fig. 7.42.

| Normalised Deuterium Distribution/% | | | Total |
|---|---|---|---|
| $CD_2$=CH-$CH_3$ | $CH_2$=CH-$CHD_2$ | CHD=CH-$CH_2D$ | [$^2H_2$]propene/% |
| 82 | 18 | 0 | 88 |
| 65 | 34 | 1 | 78 |
| 55 | 45 | 0 | 65 |
| 10 | 30 | 60 | 35[c] |

Table 7.32. Composition of [$^2H_2$] Propenes as a Function of Extent of Reaction.

| Normalised Deuterium Distribution/% | | Total |
|---|---|---|
| CDH=CH-$CH_3$ | $CH_2$=CH-$CH_2D$ | [$^2H_2$]propene/% |
| 87 | 13 | 88 |
| 89 | 11 | 78 |
| 75 | 25 | 65 |
| 100 | 0 | 100[a] |
| 50 | 50 | 100[b] |
| 40 | 60 | 35[c] |

Table 7.33. Composition of [$^2H_1$] Propenes as a Function of Extent of Reaction

[a] Product distribution by operation of the associative or concerted mechanism.

[b] Product distribution by operation of the dissociative mechanism.

[c] Equilibrium distribution with 5 exchangeable hydrogen atoms.

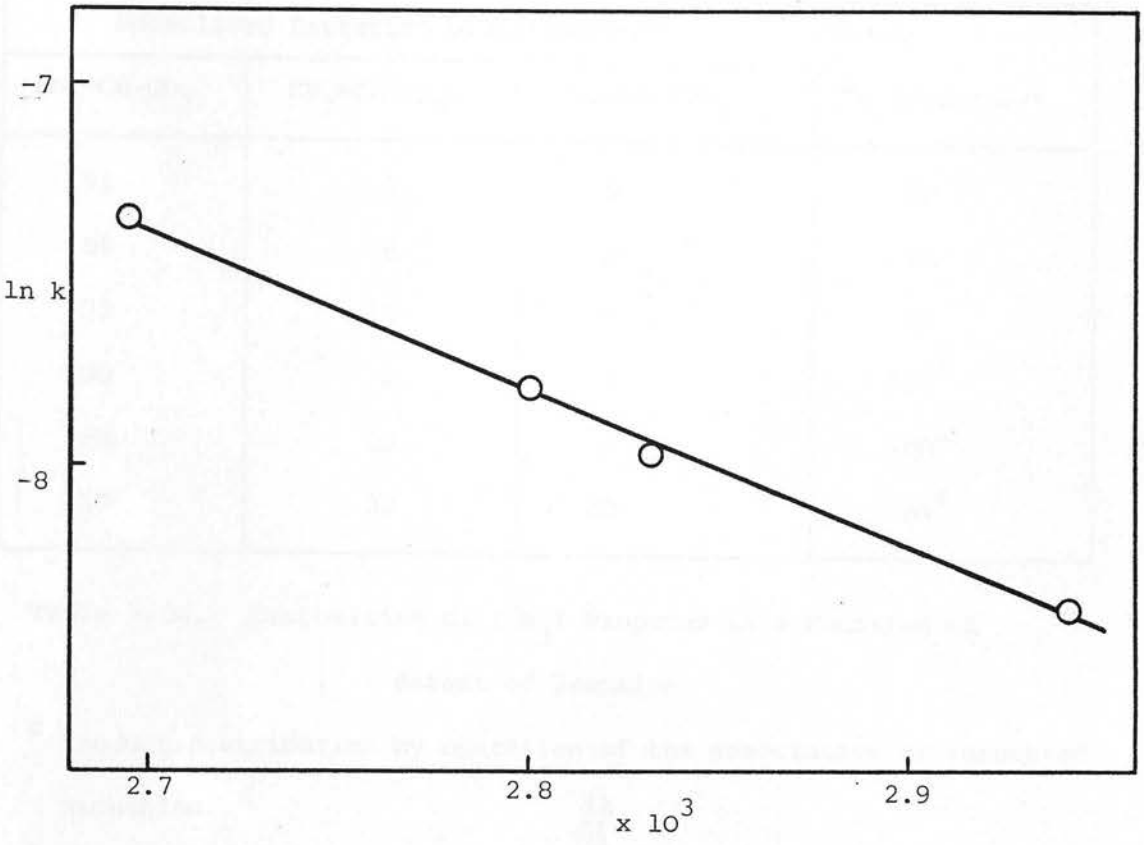


Fig. 7.42. Arrhenius Plot for Isomerisation of $CD_2=CH-CH_3$

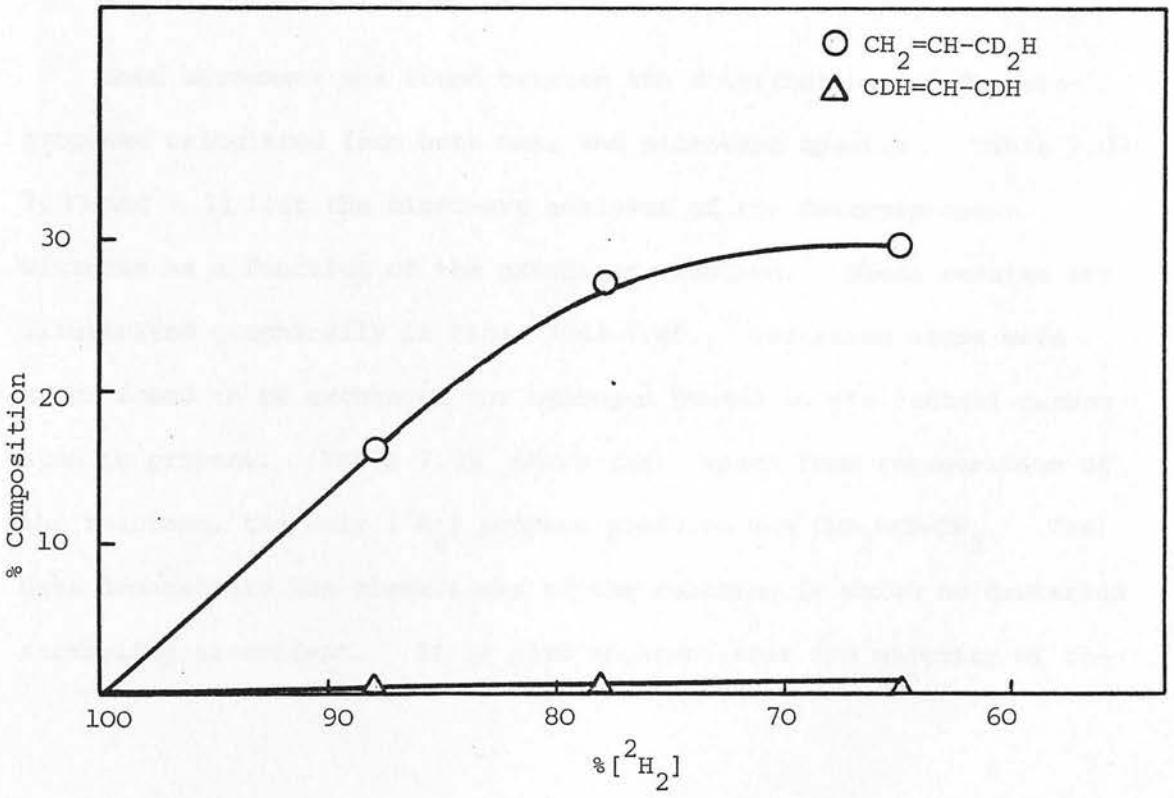


Fig. 7.43. Composition of $[^2H_2]$ Propenes as a Function of Extent of Reaction

| Normalised Deuterium Distribution/% | | | Total |
|---|---|---|---|
| $CH_2$=CH-$CD_3$ | $CD_2$=CH-$CH_2D$ | CHD=CH-$CHD_2$ | [$^2H_2$]propene/% |
| 91 | 9 | 0 | 88 |
| 87 | 6 | 8 | 78 |
| 73 | 18 | 9 | 65 |
| 100 | 0 | 0 | 100[a] |
| 50 | 50 | 0 | 100[b] |
| 10 | 30 | 60 | 35[c] |

Table 7.34. Composition of [$^2H_3$] Propenes as a Function of Extent of Reaction

[a] Product distribution by operation of the associative or concerted mechanism.

[b] Product distribution by operation of the dissociative mechanism.

[c] Equilibrium distribution with 5 exchangeable hydrogen atoms.

Good agreement was found between the distributions of deuteropropenes calculated from both mass and microwave spectra. Table 7.32 7.33 and 7.34 list the microwave analyses of the deuteropropene mixtures as a function of the extent of reaction. These results are illustrated graphically in Figs. 7.43-7.45. Deuterium atoms were never found to be exchanged for hydrogen bonded to the central carbon atom in propene. Table 7.32 shows that, apart from regeneration of the reactant, the only [$^2H_2$] propene produced was $CHD_2$-CH=$CH_2$. The data demonstrate the cleanliness of the reaction in which no deuterium scrambling is evident. It is also apparent that the majority of the

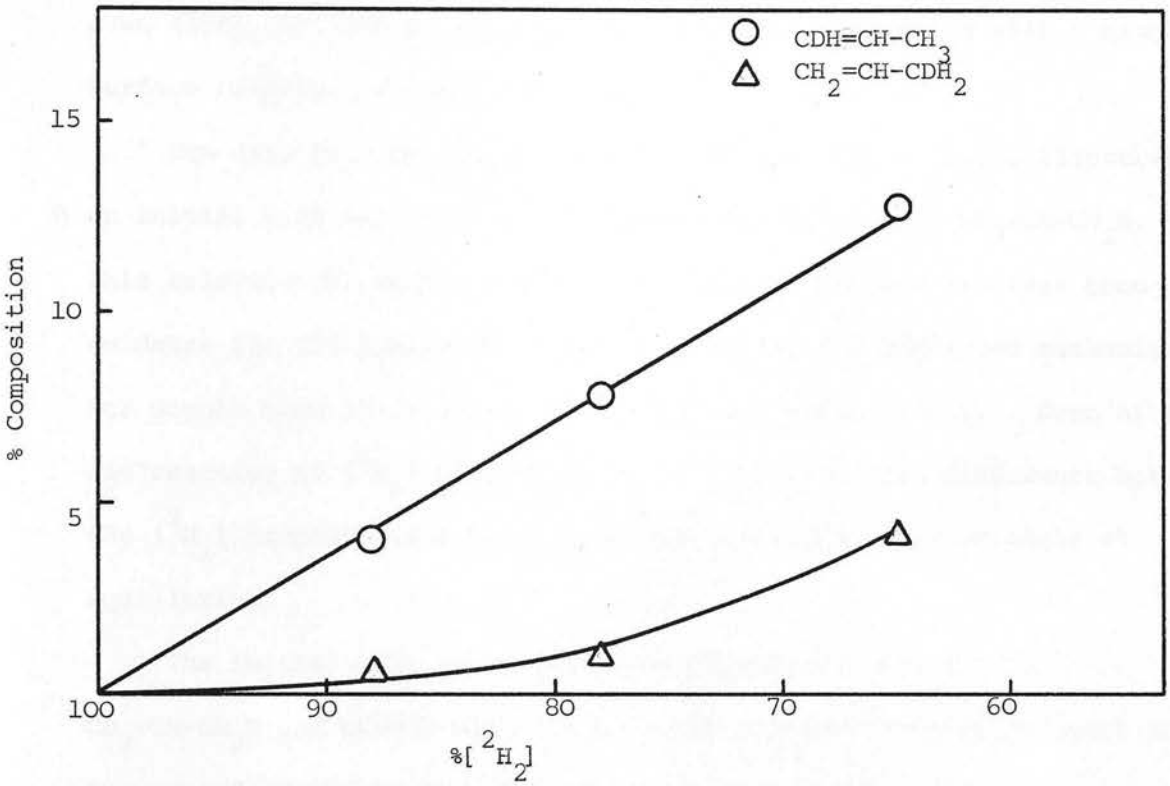


Fig. 4.44. Composition of [ $^{2}H_{1}$ ] Propenes as a Function of Extent of Reaction

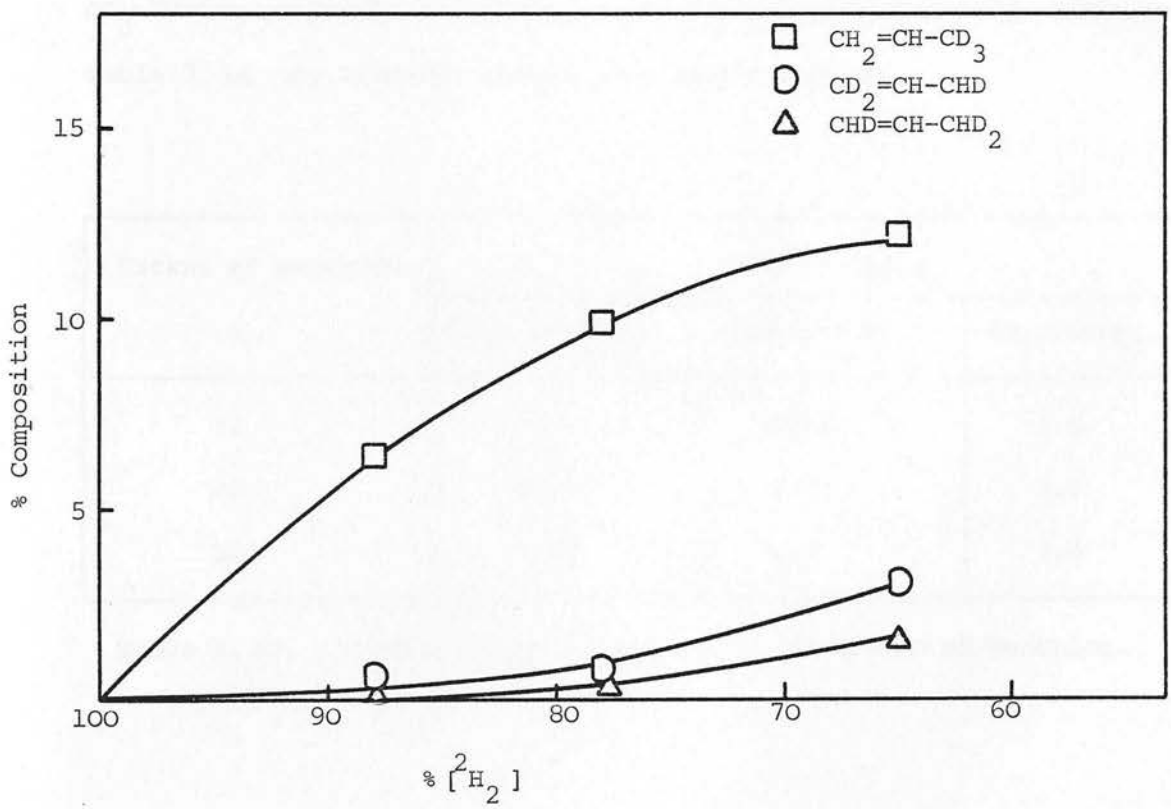


Fig. 7.45. Composition of [ $^{2}H_{3}$ ] Propenes as a Function of Extent of Reaction

molecules have undergone only a single surface reaction. The data for the [$^2H_1$] and [$^2H_3$] propenes and the absence of [$^2H_o$] propene, even after 35% loss of [$^2H_2$] propene are also consistent with a single surface reaction for most molecules.

The data for the [$^2H_1$] propenes, shown in Table 7.33 , illustrates an initial high selectivity for $CDH=CH-CH_3$ relative to $CH_2=CH-CH_2D$. This selectivity, maintained as the reaction proceeds provides good evidence for the operation of an associative or a concerted mechanism for double bond shift (Figs. 4.31, 4.33 and Table 7.33 ). Even after 35% reaction of [$^2H_2$] propene there is a considerable difference between the [$^2H_1$] propene distribution and that predicted statistically at equilibrium.

The initial high selectivity for $CH_2=CH-CH_3$ relative to $CD_2=CH-CH_2D$ and $CHD=CH-CHD_2$ (Table 7.34) provides further evidence for the operation of the associative or concerted mechanism.

The ratios of the amounts of $CD_2H-CH=CH_2$, $CHD=CH-CH_3$ and $CD_3-CH=CH_2$ produced as a function of the extent of reaction, given in Table 7.35, are constant within experimental error.

| Extent of Reaction | Product Ratio | | |
|---|---|---|---|
| % | $CD_2H-CH=CH_2$ | $CHD=CH-CH_3$ | $CD_3-CH=CH_2$ |
| 12 | 2.5 | 0.64 | 1.0 |
| 22 | 2.7 | 0.80 | 1.0 |
| 35 | 2.4 | 1.0 | 1.0 |

Table 7.35. Product Ratio as a Function of Extent of Reaction.

This observation is consistent with the operation of an associative mechanism for double bond shift. This type of mechanism would result in the production of these three deuteropropenes as primary products and as such their ratios would not be expected to alter with extent of reaction during the initial course of the reaction. In contrast, the concerted mechanism would produce $CHD=CH-CH_3$ and $CD_3-CH=CH_2$ as secondary products from the subsequent reaction of $CD_2H-CH=CH_2$. The difference in the average ratio of $CD_2H-CH=CH_2$ to $CDH=CH-CH_3$ (ca. 3:1) from the predicted ratio (1.5:1) may be due to the operation of a kinetic isotope effect in the rate determining step which is therefore associated with rupture of a C-H or C-D bond in the carbonium ion. The ease of breaking a C-H bond compared to a C-D bond is therefore deduced to be ca. 2, a value which is reasonable both with regard to predicted values from difference in zero point energies of the bonds and to previous values deduced for reaction over MgO and $TiO_2$.[224]

It is therefore possible to conclude that double bond shift of 1,1 [$^2H_2$] propene proceeds via an associative mechanism, the active sites for the reaction being of the Brönsted acid type. These sites must be relatively few in number as no experimentally detectable decrease in deuterium content of the hydrocarbon is apparent.

It seems reasonable that the mechanistic conclusion reached for [$^2H_2$] propene isomerisation is a general one and may at least be applied to the n-butenes. At 370 K it was found that the reversible first order rate constants for but-1-ene isomerisation ($k_b$) and [$^2H_2$] propene loss ($k_p$) were related as $k_b \simeq 8\ k_p$. It is shown on purely statistical grounds in Fig. 4.31 that if 10 molecules of $CD_2=CH-CH_3$ react, 6 will remain as [$^2H_2$] propenes whereas 4 will be transferred into [$^2H_1$] and [$^2H_3$] propenes. The statistical probability of loss

of $[^2H_2]$ propene in a single surface reaction is $^2/_5$. Similarly Fig. 7.46 shows that the statistical probability of but-1-ene loss in a single surface reaction is also $^2/_5$.

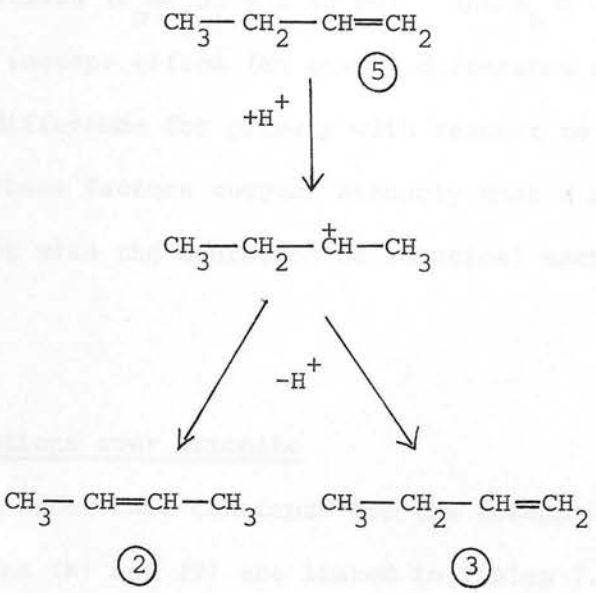


Fig. 7.46. Associative mechanism for double bond shift of but-1-ene. The circled numbers show the statistically predicted concentration of products from reaction of 5 molecules of but-1-ene.

Therefore, if it can be assumed that both processes proceed through identical rate determining steps and their heats of adsorption are similar, $k_b$ should equal $k_p$. However the ratio of products observed from propene suggests the operation of a kinetic isotope effect of ca. 2 and hence the involvement of C-H bond rupture in the rate determining step. As loss of $[^2H_2]$ propene is limited by the rate of breaking a C-D bond whereas butene isomerisation involves breaking a C-H bond, $K_b \simeq 2k_p$ may be predicted. Furthermore loss of $H^+$ from the sec-butyl carbonium ion by secondary C-H bond rupture to produce

the but-2-enes would proceed more readily than regeneration of but-1-ene through primary C-H bond rupture. A factor of 4 in rates would correlate with an activation energy difference for the breaking of these bonds of ca. 4.3 kJ $mol^{-1}$. Interestingly the derived activation energies for the two reactions ($E_p \simeq 35 \pm 2$ kJ $mol^{-1}$ and $E_b \simeq 29 \pm 2$ kJ $mol^{-1}$) reflect the kinetic isotope effect (an energy difference of ca. 2.1 kJ $mol^{-1}$) and the energy difference for primary with respect to secondary C-H bond rupture. These factors suggest strongly that a ratio of $k_b/k_p \simeq 8$ is consistent with the operation of identical mechanisms for the two reactions.

7.3.2 Reactions over Erionite

The first order rate constants for the disappearance of [$^2H_2$]propene over erionites (N) and (T) are listed in Tables 7.36 and 7.37 respectively. The Arrhenius plots are shown in Fig. 7.47

| Activation Energy kJ $mol^{-1}$ | ln A | Reaction Temperature K | k x $10^{-4}$ $s^{-1}g^{-1}$ |
|---|---|---|---|
| 64.5 | 11.0 | 383 | .96 |
| | | 396 | 1.87 |
| | | 409 | 3.48 |
| | | 419 | 5.45 |

Table 7.36. First order rate constants and Arrhenius parameters for disappearance of [$^2H_2$] propene over erionite (N)

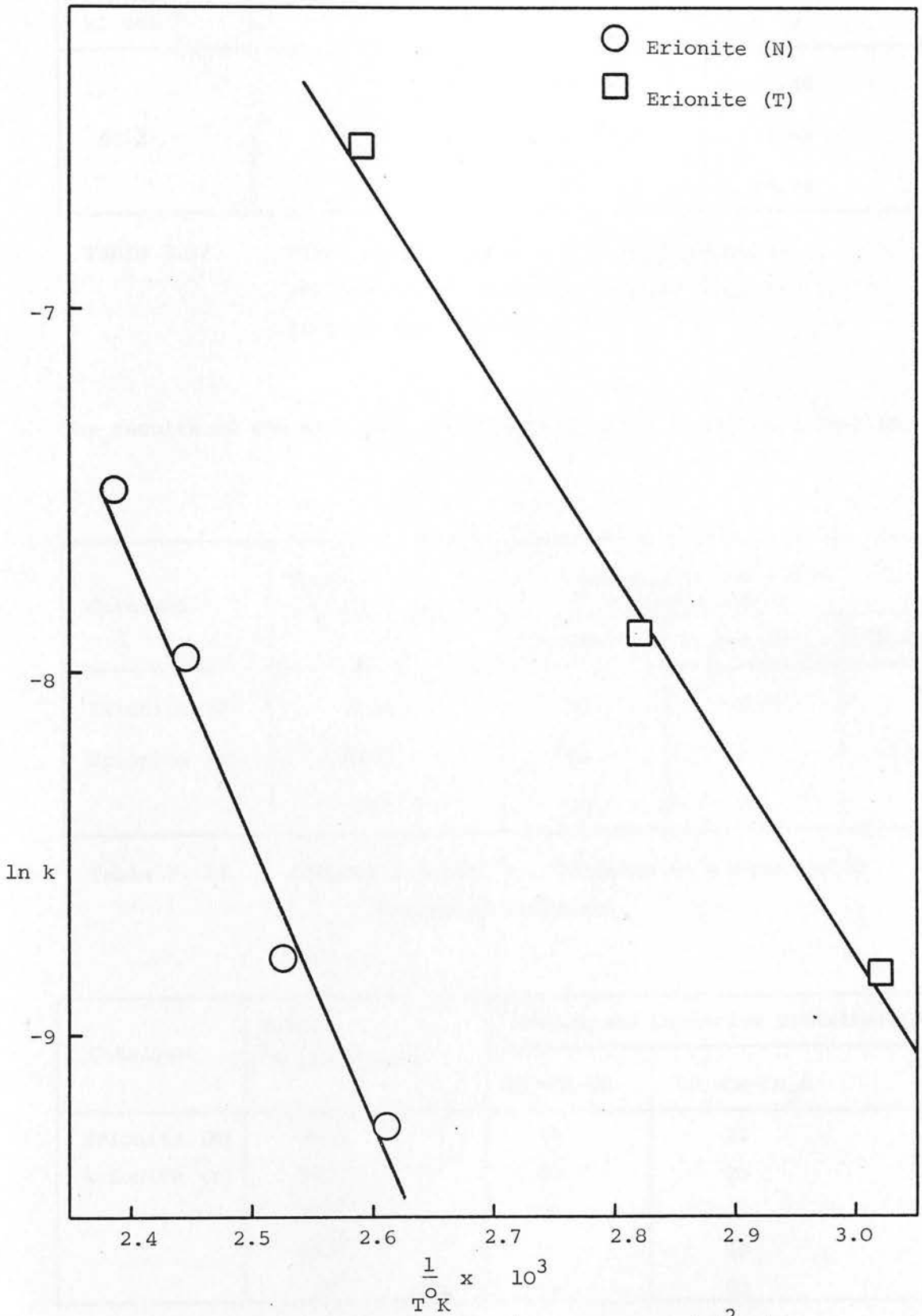


Fig. 7.47. Arrhenius Plots for Disappearance of [$^2H_2$] Propene on Erionite

| Activation Energy $_{-1}$ kJ mol | ln A | Reaction Temperature K | k x $10^{-4}$ $s^{-1}g^{-1}$ |
|---|---|---|---|
| 44.2 | 6.8 | 331 | 1.46 |
| | | 361 | 3.69 |
| | | 383 | 14.24 |

Table 7.37. First order rate constants and Arrhenius parameters for disappearance of [$^2H_2$] propene over erionite (T)

The results of the microwave analyses are given in Tables 7.38-7.40.

| Catalyst | Total [$^2H_2$]Propene/% | Normalised Deuterium Distribution/% | | |
|---|---|---|---|---|
| | | $CD_2$=CH-$CH_3$ | $CH_2$=CH-$CHD_2$ | CHD=CH-$CH_2D$ |
| Erionite (N) | 70.0 | 55 | 42.3 | 2.7 |
| Erionite (T) | 74.3 | 61 | 38 | 1 |
| | 35[c] | 10 | 30 | 60 |

Table 7. 38. Composition of [$^2H_2$] Propenes as a Function of Extent of Reaction

| Catalyst | Total [$^2H_2$]Propene/% | Normalised Deuterium Distribution/% | |
|---|---|---|---|
| | | CDH=CH-$CH_3$ | $CH_2$=CH-$CH_2D$ |
| Erionite (N) | 70.0 | 78 | 22 |
| Erionite (T) | 74.3 | 80 | 20 |
| | 100[a] | 100 | o |
| | 100[b] | 50 | 50 |
| | 35[c] | 40 | 60 |

Table 7. 39 Composition of [$^2H_1$] Propenes as a Function of Extent of Reaction

| Catalyst | Total [$^2H_2$]propene/% | Normalised Deuterium Distribution/% | | |
|---|---|---|---|---|
| | | $CH_2$=CH-$CD_3$ | $CD_2$=CH-$CH_2D$ | CHD=CH-$CHD_2$ |
| Erionite (N) | 70.0 | 77 | 12 | 11 |
| Erionite (T) | 74.3 | 80 | 13 | 7 |
| | 100[a] | 100 | 0 | 0 |
| | 100[b] | 50 | 50 | 0 |
| | 35[c] | 10 | 30 | 60 |

Table 7.40. Composition [$^2H_3$] Propenes as a Function of Extent of Reaction

In Tables 7.38-7.40.

[a]Product distribution by operation of the associative or concerted mechanism

[b]Product distribution by operation of the dissociative mechanism

[c]Equilibrium distribution with 5 exchangeable hydrogen atoms

The product selectivities demonstrated by both types of erionite are very similar to those observed over Ω zeolite. No deuterium bound to the central carbon atom in propene was detected. Apart from regeneration of the reactant ($CD_2$=CH-$CH_3$), $CH_2$=CH-$CHD_2$ is the only [$^2H_2$] propene formed initially. Tables 7.39 and 7.40 show the preferential formation of CDH=CH-$CH_3$ and $CH_2$=CH-$CD_3$. Comparison of experimental results with those predicted from operation of the 3 possible mechanisms indicate that the observed selectivity is indicative of the operation of an associative or concerted mechanism. The ratios of the amounts of $CD_2H$-CH=$CH_2$, CHD=CH-$CH_3$ and $CD_3$-CH=$CH_2$ at ca. 30% reaction were 3.2 : 1.0 : 1.0 and 2.6 : 1.0 : 1.0 erionite (N) and (T) respectively. These are similar to ratios observed over Ω at varying

extents of reaction hence it would seem reasonable to conclude that an associative mechanism was also operative for double bond shift reaction of 1,1[$^2H_2$]propene over both samples of erionite.

Similar mechanistic conclusions may also be attained for but-1-ene isomerisation. Both types of erionite exhibit greater activity for but-1-ene isomerisation than [$^2H_2$] propene loss. The first order rate constants are related as $k_b \simeq 8.7\ k_p$ for erionite (N) at 381 K and $k_b \simeq 7.6\ k_p$ for erionite (T) at 334 K. Such a ratio can be rationalised in terms of energetic considerations as discussed for zeolite Ω. For erionite (N) $E_b \simeq 56 \pm 2$ kJ mol$^{-1}$ and $E_p \simeq 64.5 \pm 2$ kJ mol$^{-1}$ while for erionite (T) $E_b \simeq 40 \pm 2$ kJ mol$^{-1}$ and $E_b \simeq 44 \pm 2$ kJ mol$^{-1}$. The differences in activation energy for but-1-ene isomerisation and [$^2H_2$] propene loss for both erionites reflect the contributions from operation of a kinetic isotope effect (ca. 2.1 kJ mol$^{-1}$) and an energy difference for primary with respect to secondary C-H bond rupture, a difference of 4.3 kJ mol$^{-1}$ leading to a factor of 4 in the rates.

It is therefore apparent that, similar to zeolite Ω, but-1-ene isomerisation and double bond shift of 1,1[$^2H_2$] propene over erionite proceed via associative mechanisms involving C-H bond rupture in the rate determining step. Such a mechanism proceeds on Brönsted acid sites, the number of which must be relatively small as no significant dilution of hydrocarbon deuterium content was observed.

## 7.4. Conclusion

### a) Zeolite Ω

The catalytic activity of zeolite Ω was markedly dependent on pretreatment conditions; the decomposition and subsequent removal of the tetramethylammonium cations resulting in the formation of protonic acid sites. Variations in the catalytic activity towards molecules too large to enter the gmelinite cages led to the postulate that these active sites are generated in the main channels of the zeolite.

Complete removal of the organic cations yielded a zeolite, H-Ω, which displayed catalytic activity similar to that previously reported for HX and CeX zeolites and much greater than that of copper and nickel exchanged zeolites. Moreover the cis/trans product ratio from but-1-ene isomerisation resembled the literature values for HX and CeX zeolites.[238]

Initial product ratios observed for n-butene interconversion suggested the operation of carbonium ion type mechanism. In common with studies over silica-alumina and other zeolites the sec butyl carbonium ion has been postulated as an intermediate. Although products resulting from methylcyclopropane isomerisation were also indicative of a carbonium ion type mechanism an alternative intermediate to the sec butyl carbonium ion must be invoked since initial product distributions are different from those predicted from the interconversion of the n-butenes. A non-classical cyclopropylium ion has been postulated.

Product compositions from 1,1- and 1,2 dimethylcyclopropane isomerisation also implied a carbonium ion type mechanism, that of 1,1 DMCP fits a non classical mechanism while that of 1,2 DMCP agrees with the product distribution predicted from the classical mechanism.

It is unlikely that these three methyl-substituted cyclopropanes react by completely different intermediates and is therefore probable that all three isomerise via a non classical carbonium ion formed in an associative manner.

Studies of the reaction of a specifically labelled deuteropropene, $CD_2=CH-CH_3$, showed conclusively that double bond shift of propene occurred by an associative carbonium ion type mechanism over zeolite H-Ω. Furthermore, arguments in terms of reaction rates and activation energies have been presented to show that this mechanism also fits the results for the isomerisation of but-1-ene on this catalyst.

b) Erionite

Very different sorptive and catalytic activities were exhibited by the two types of erionite studied. The faster rates of sorption observed for erionite (T) were attributed to the exchange of the majority of the sodium ions by iron (III) ions resulting in less hindered entry to and diffusion along the erionite channels. Unlike the wide-pore zeolite Ω both types of erionite displayed different rates of sorption for the three n-butenes dependent on their critical molecular diameters.

The alteration of the intrinsic product distributions from n-butene and methylcyclopropane isomerisation by selective sorption of the products made it impossible to postulate mechanisms for these reactions on the basis of initial product ratios. The isomerisation of 1,1 dimethylcyclopropane has however been postulated to proceed via a non classical carbonium ion as proposed for zeolite Ω. The distribution of methyl butenes from isomerisation of 1,2 dimethylcyclopropane was similar to that over zeolite Ω, however no pentenes were observed. This is

probably in consequence of their selective sorption. Hence, as for zeolite Ω, product composition resulting from 1,2 dimethylcyclopropane isomerisation was indicative of a classical carbonium ion type mechanism involving proton addition to the reactant.

The products observed from the reaction of specifically labelled deuteropropene, $CD_2=CH-CH_3$, over both erionites indicated that double bond shift occurred via a carbonium ion intermediate formed in an associative manner. Comparison of reaction rates and activation energies showed that this mechanism was also applicable to the isomerisation of but-1-ene over these catalysts.

The results presented in this thesis suggest that all reactions studied over zeolites Ω and erionite occur via a classical or non classical carbonium ion formed by proton addition and hence involving Brönsted acid sites. In zeolite Ω it has been proposed that the active sites formed during the decomposition and removal of TMA ions are located in the wide channels. The position of the active Brönsted acid sites in erionite has not been established. Further investigations, involving poisoning experiments similar to those of Detreköy *et al*[91], may establish whether these sites are located on the external surface or within the erionite cavities.

## Appendix 1

## Mechanistic Schemes for Alkylcyclopropane Isomerisation

(A) $H^-$ Loss

(1) MCP

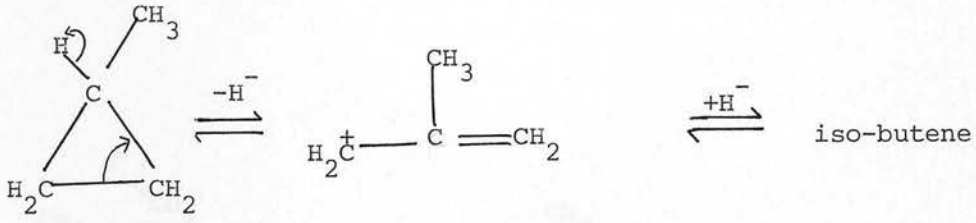


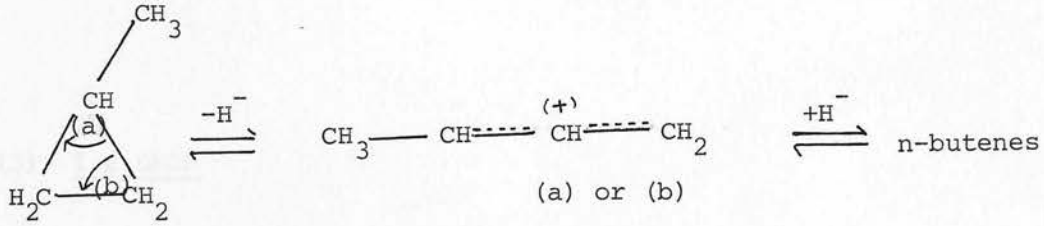


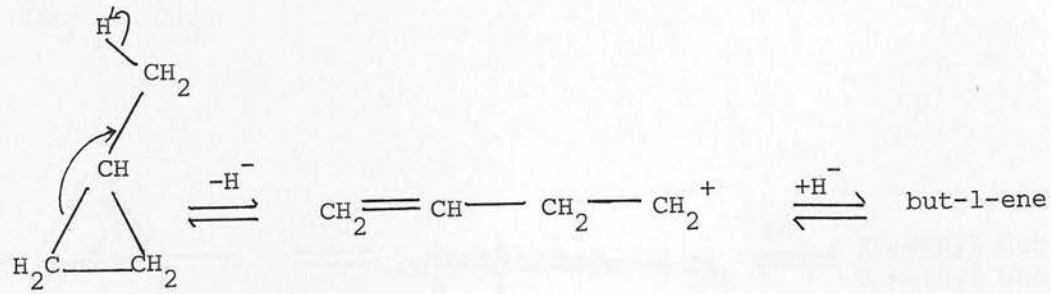

(A) $H^-$ Loss (contd.)

(2) 1,1 DMCP

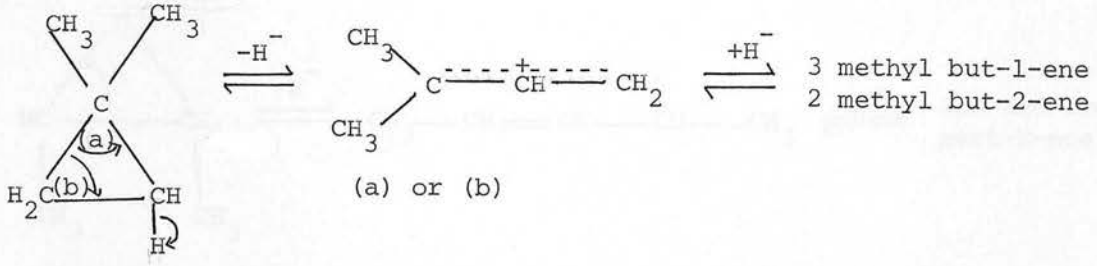


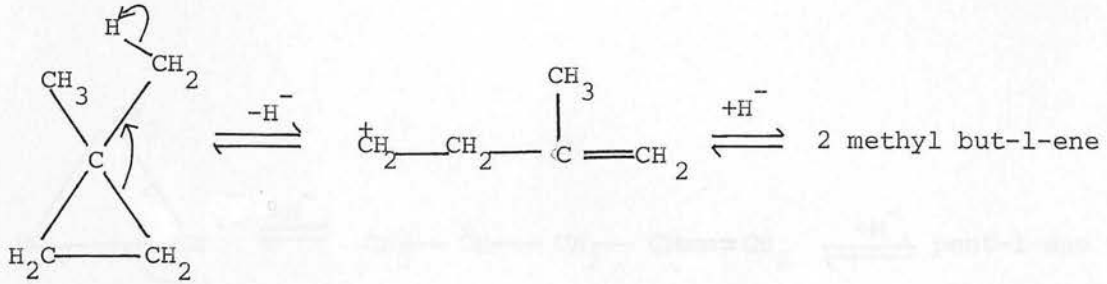


(3) 1,2 DMCP

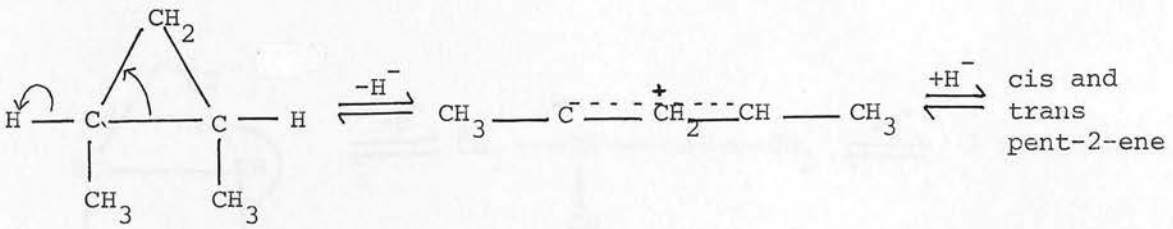


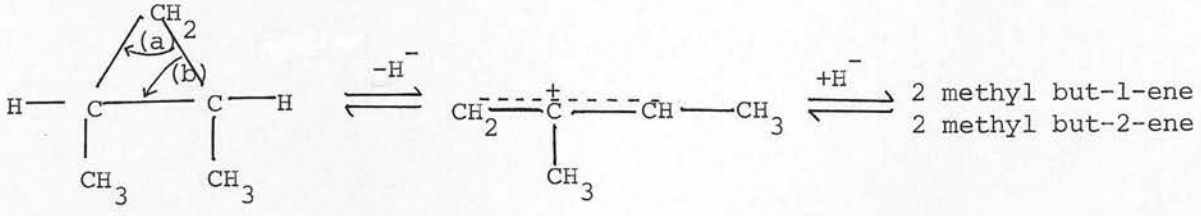


(a) or (b)

(A) $\underline{H^-}$ Loss (contd.)

(3) 1,2 DMCP (contd.)

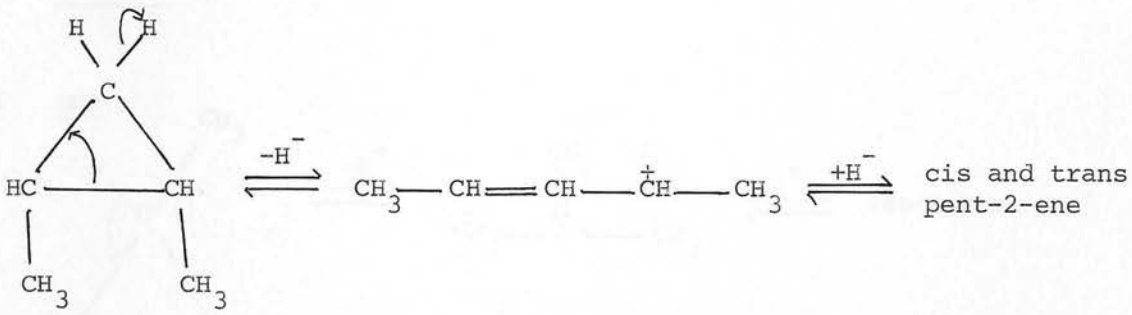


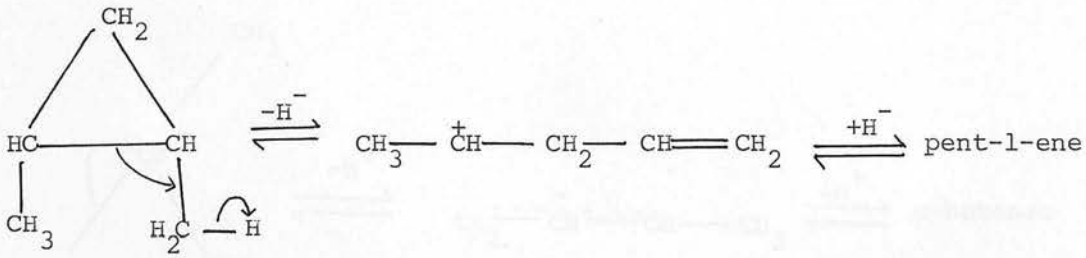


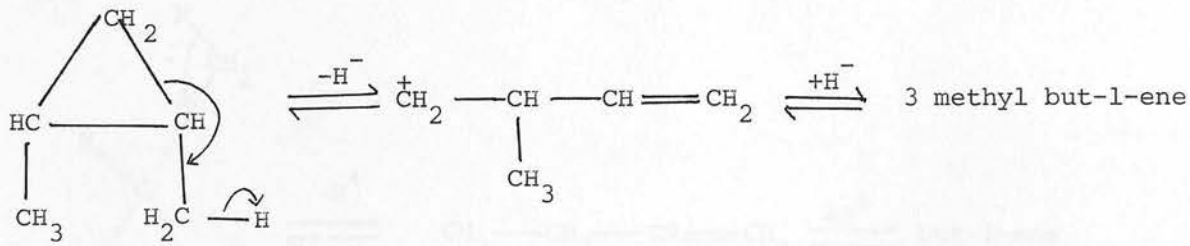

(B) $H^+$ Loss

(1) MCP

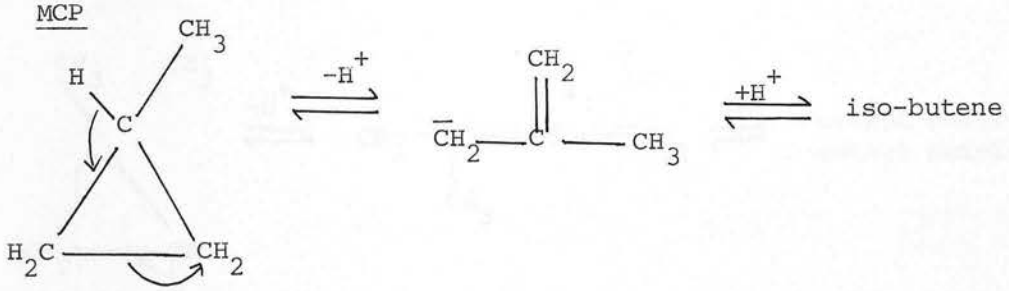
CH3
H
C
H2C
CH2
-H+
CH2
CH2
C
CH3
+H+
iso-butene

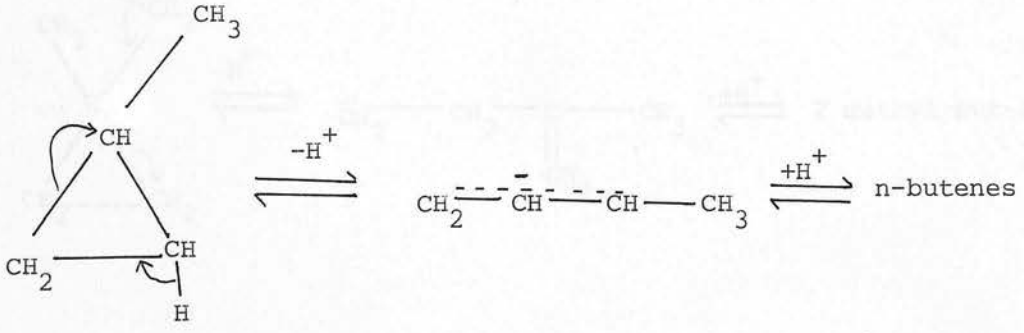
CH3
CH
CH2
CH
H
-H+
CH2
CH
CH
CH3
+H+
n-butenes

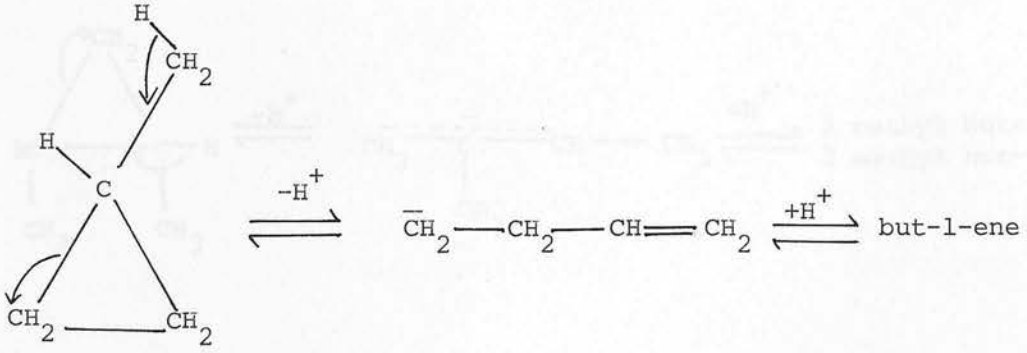
H
CH2
H
C
CH2
CH2
-H+
CH2
CH2
CH
CH2
+H+
but-1-ene

(B) $H^+$ Loss (continued)

(2) 1,1 DMCP

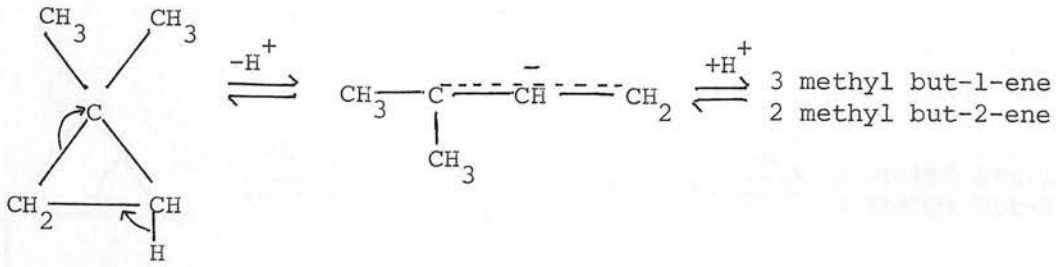


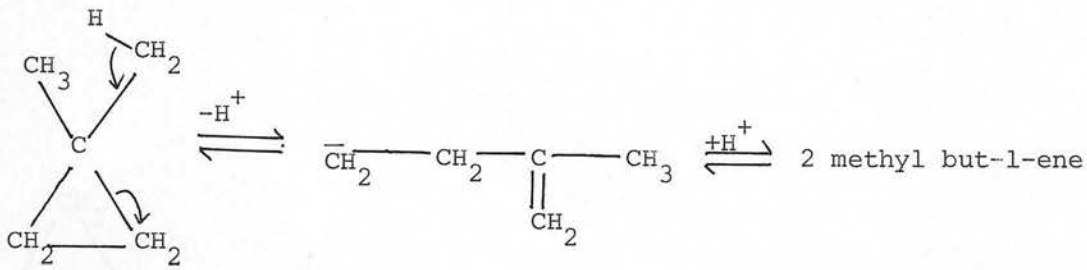


(3) 1,2 DMCP

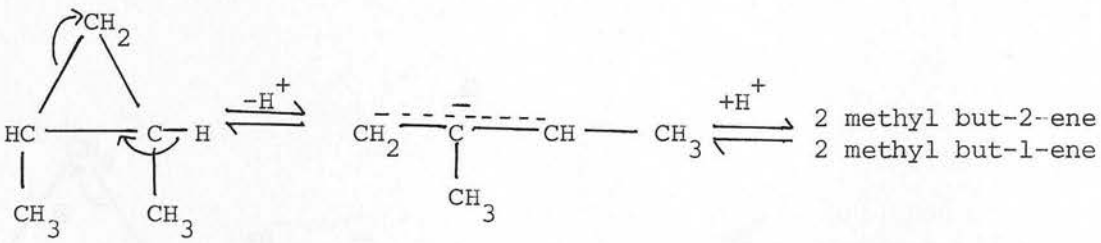


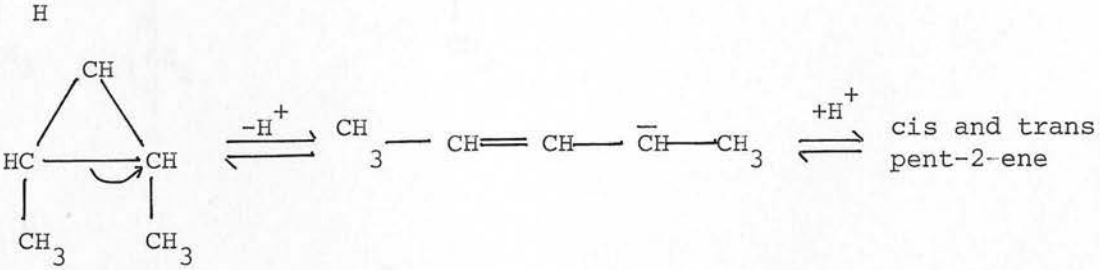

(B) $H^+$ Loss (contd.)

(3) 1,2 DMCP (contd.)

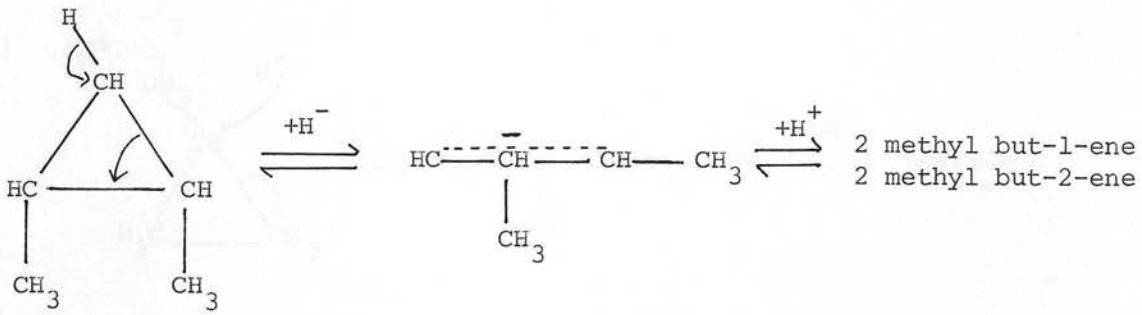


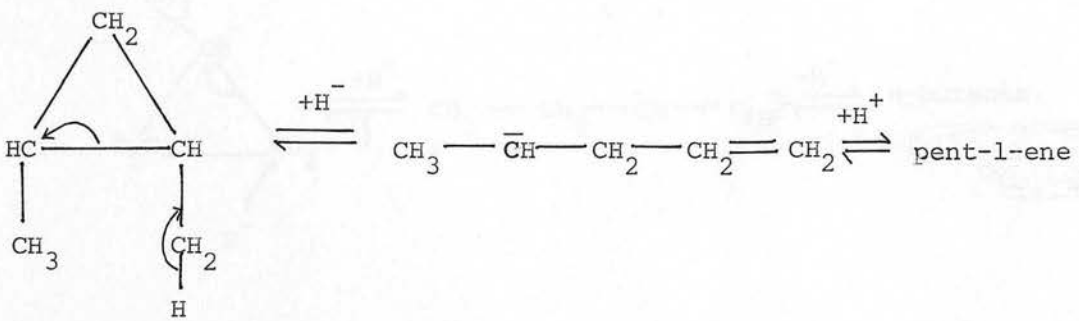


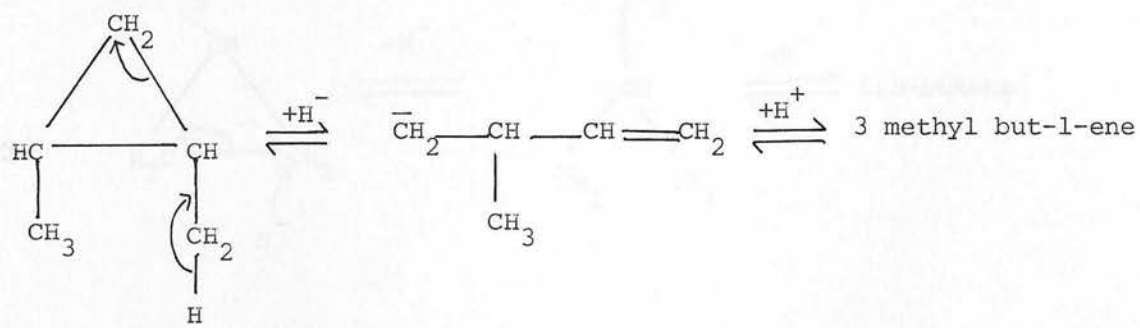

(C) $H^-$ Gain

(1) MCP

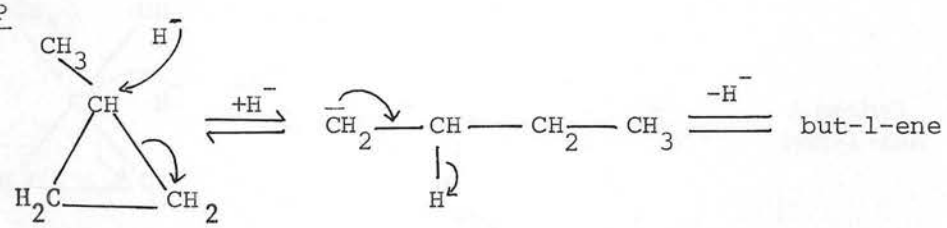
CH3
H⁻
CH
H2C
CH2
+H⁻
CH2
CH
CH2
CH3
H
-H⁻
but-1-ene

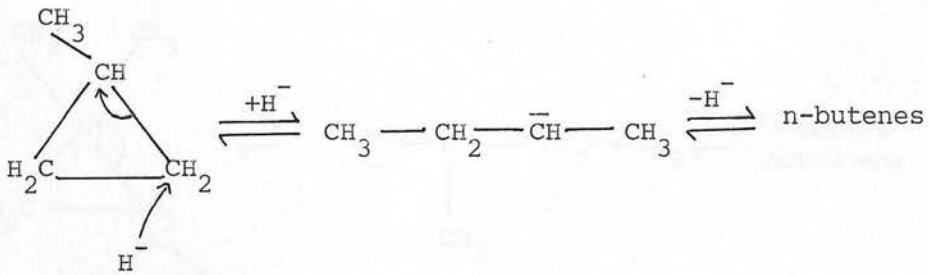
CH3
CH
H2C
CH2
H⁻
+H⁻
CH3
CH2
CH
CH3
-H⁻
n-butenes

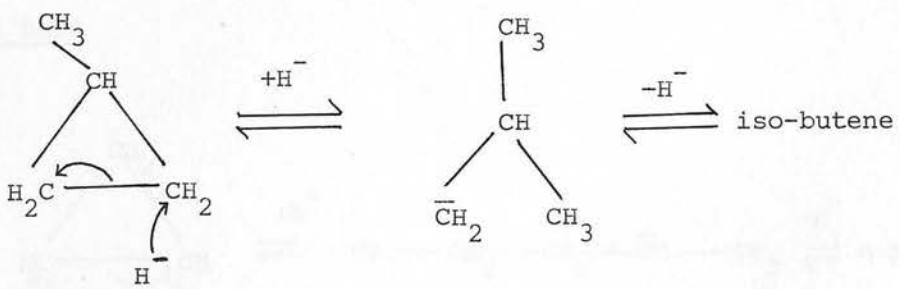
CH3
CH
H2C
CH2
H⁻
+H⁻
CH3
CH
CH2
CH3
-H⁻
iso-butene

(C) $H^-$ Gain (contd.)

(2) 1,1 DMCP

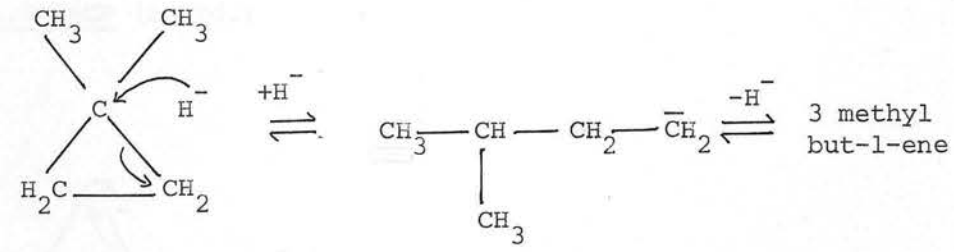


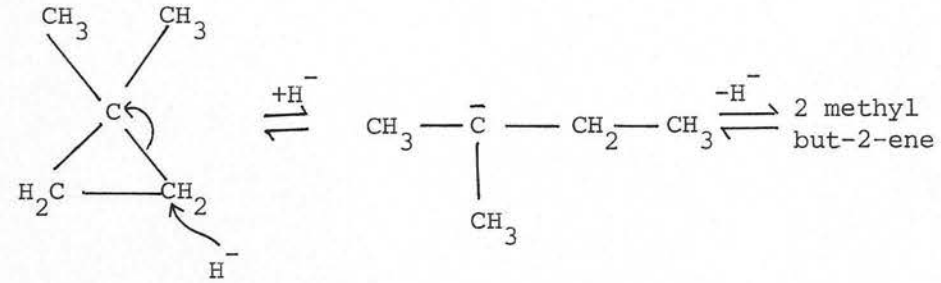


(3) 1,2 DMCP

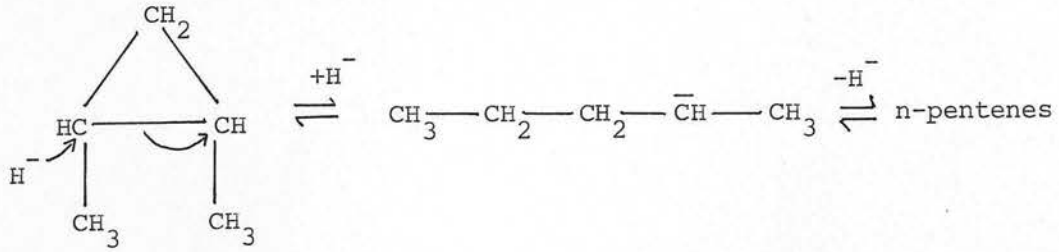

(C) $H^-$ Gain (contd.)

1,2 DMCP (contd.)

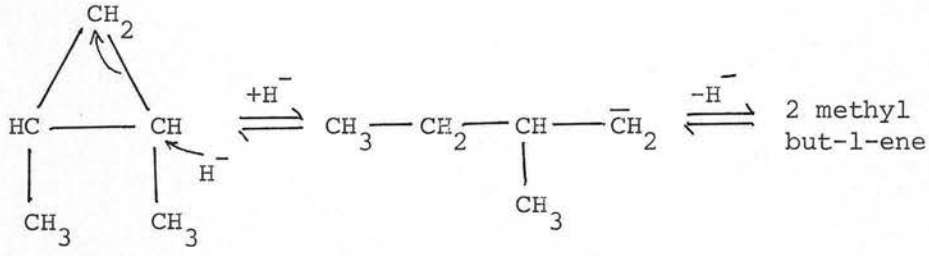


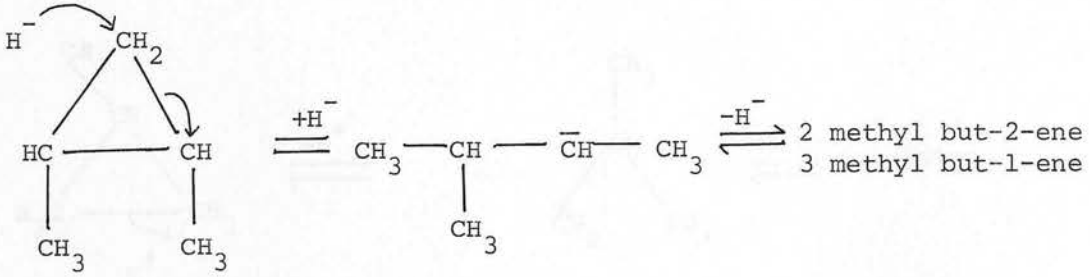

(D) $H^+$ Gain

(1) MCP

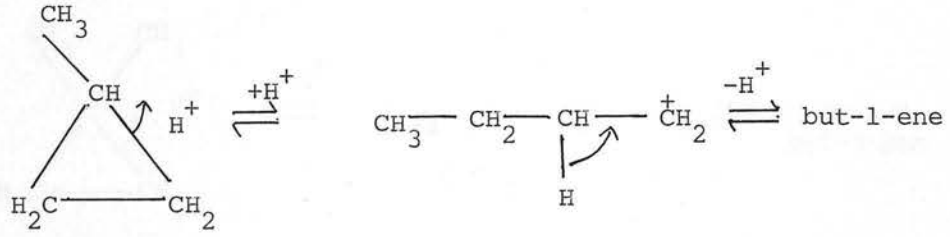
CH3
CH
H+
+H+
H2C
CH2
CH3 CH2 CH CH2
H
-H+
but-1-ene

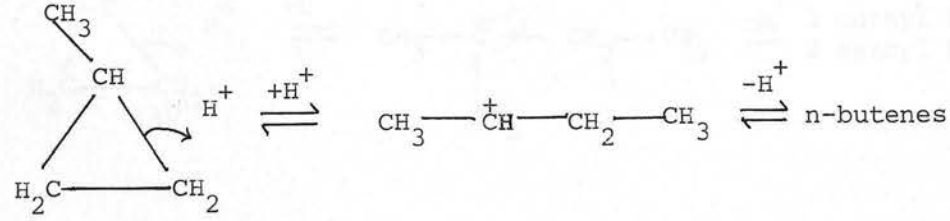
CH3
CH
H+
+H+
H2C
CH2
CH3 CH CH2 CH3
-H+
n-butenes

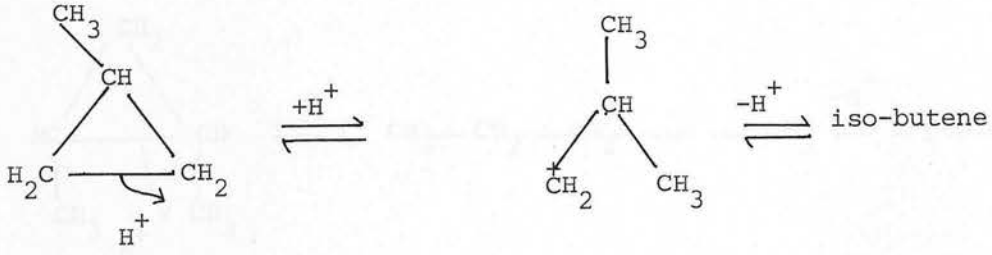
CH3
CH
+H+
H2C
CH2
H+
CH3
CH
CH2
CH3
-H+
iso-butene

(D) $H^+$ Gain (contd.)

(2) 1,1 DMCP

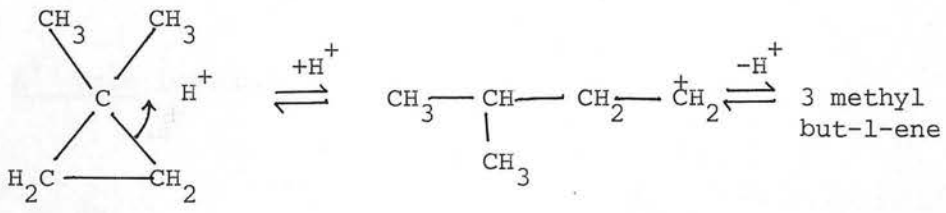


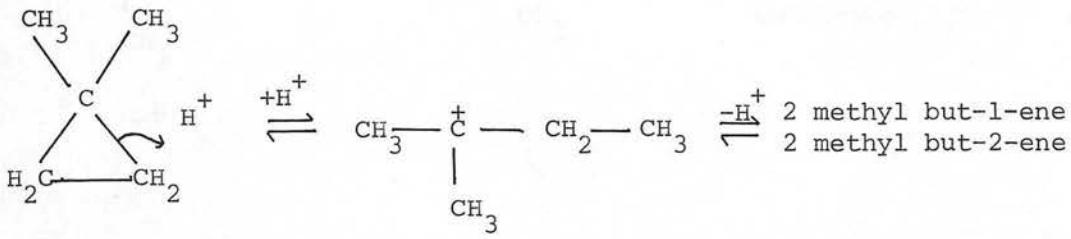


(3) 1,2 DMCP

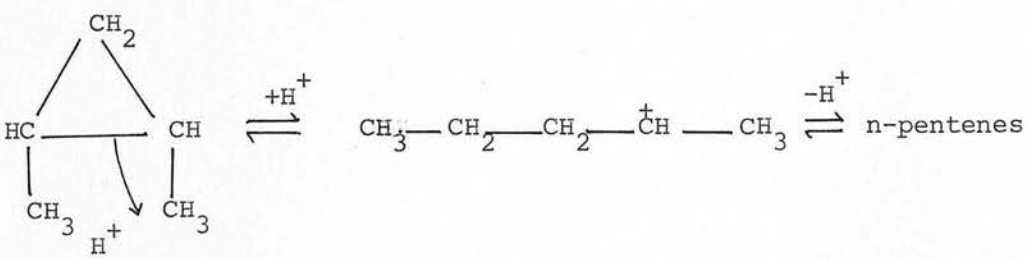


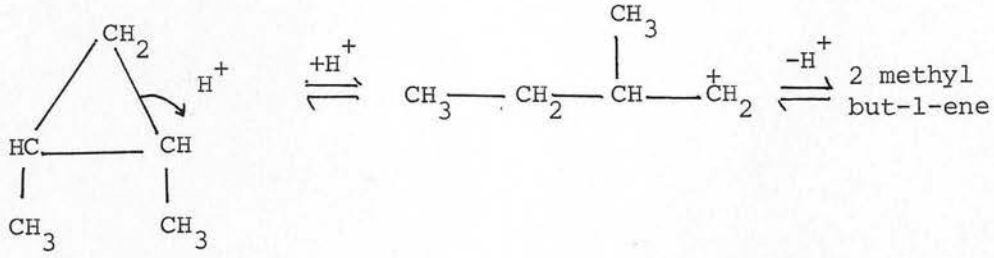

(D) $H^+$ Gain (contd.)

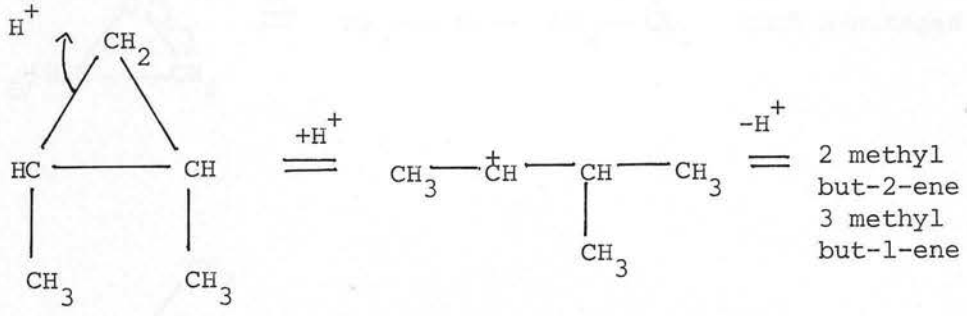

(E) $H^{\bullet}$ Loss

(1) MCP

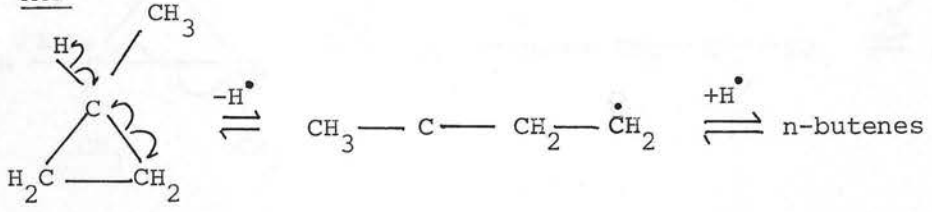


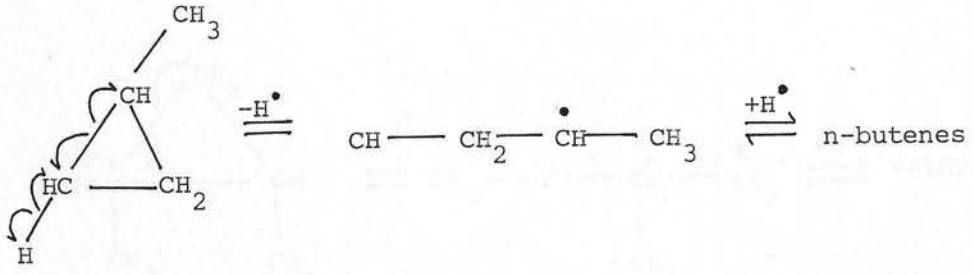


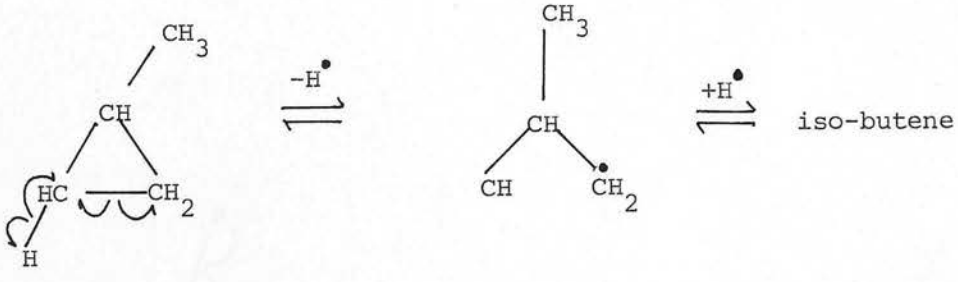


(2) 1,1 DMCP

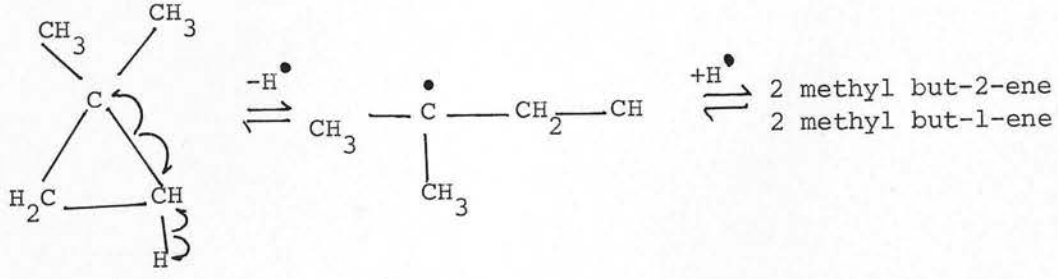

(E) $H^{\bullet}$ Loss (continued)

(3) 1,2 DMCP

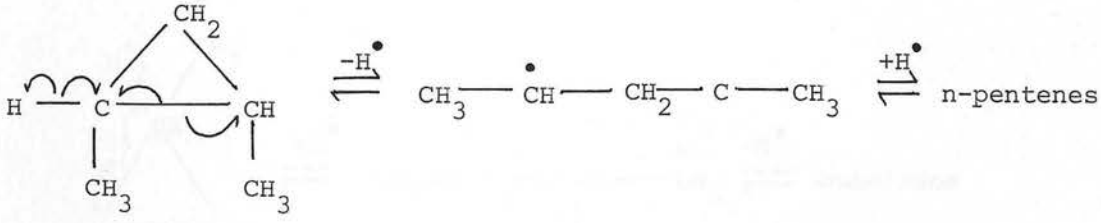


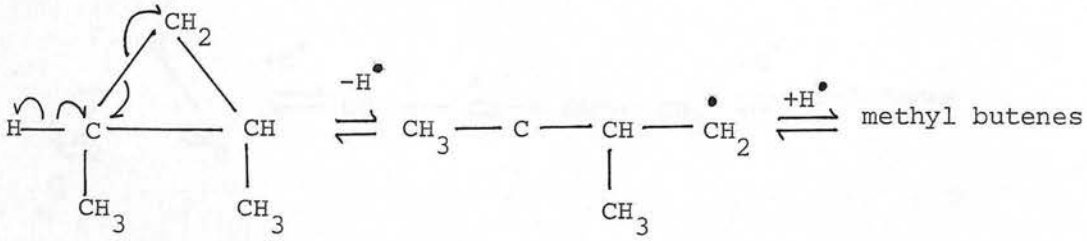


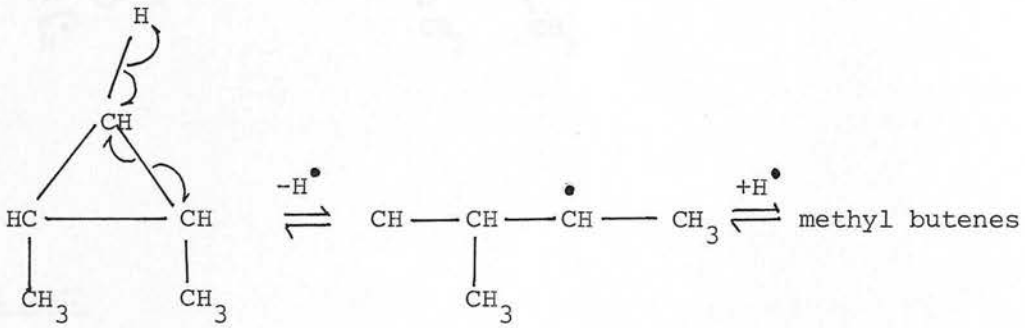

(F) $H^{\bullet}$ Gain

(1) MCP

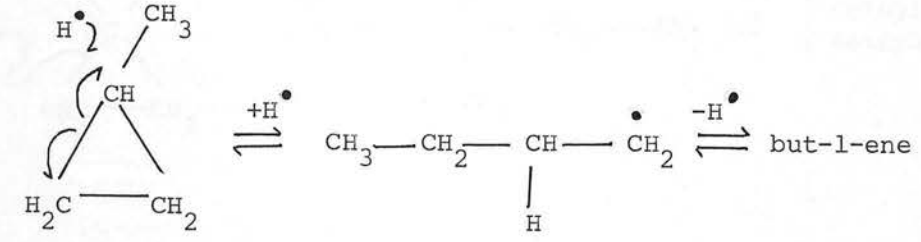


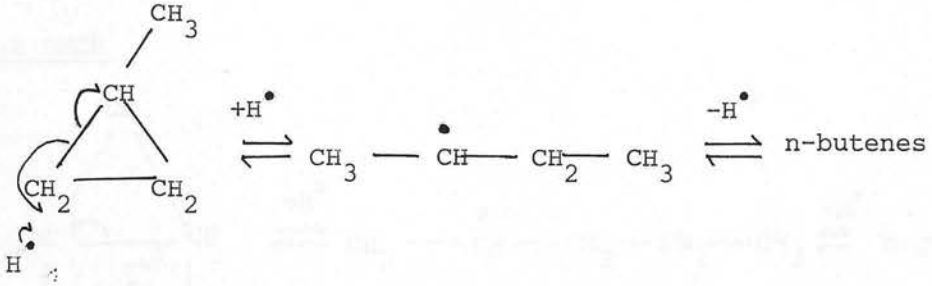


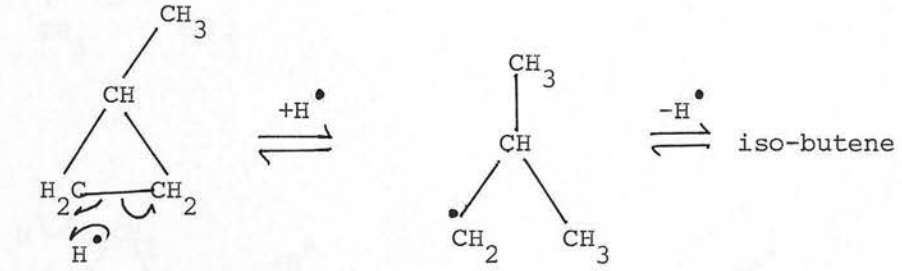


(2) 1,1 DMCP

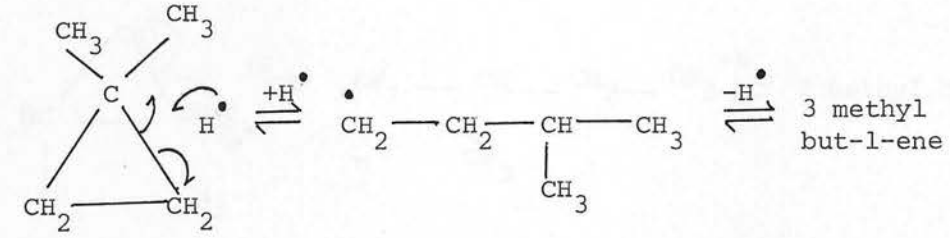

(F) $H^{\bullet}$ Gain (contd.)

(2) 1,1 DMCP (contd.)

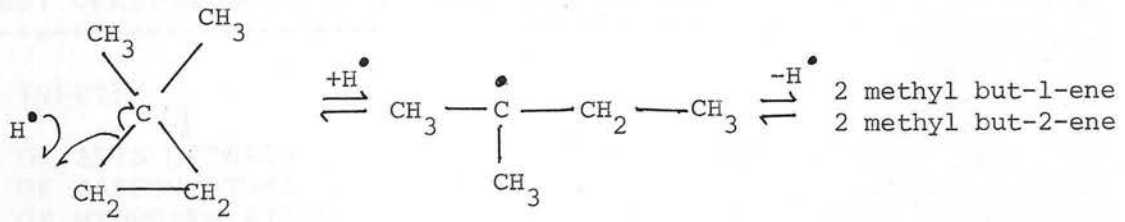


(3) 1,2 DMCP

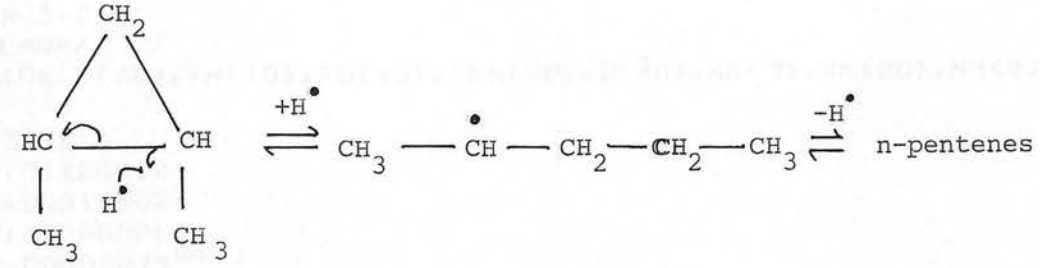


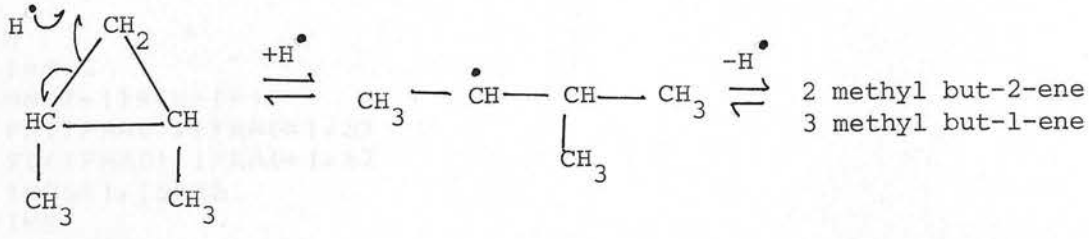


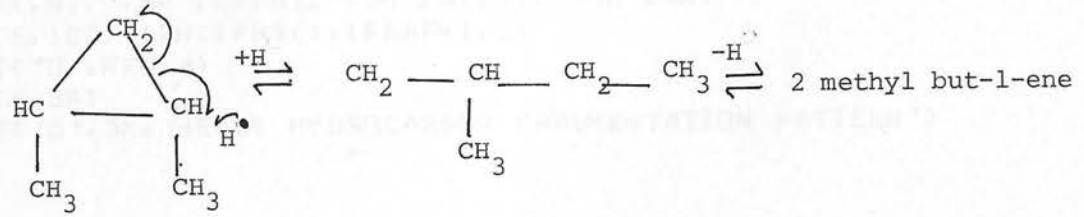

Appendix 2

```
C       LATEST VERSION OF MS10 CORRECTION PROGRAM
C       -----------------------------------------
C
C
C       DATA INPUT:
C
C       1 NO OF SETS OF DATA
C       2 NO OF CARBON ATOMS
C         NO OF HYDROGEN ATOMS
C         NO OF OXYGEN ATOMS
C         NO OF FRAGMENTS
C       3 LIGHT FRAGMENTATION PATTERN
C       4 HEAVY FRAGMENTATION PATTERN
C       5 TIME OF SAMPLE
C       6 EXPERIMENTAL PEAK HEIGHTS
C               (N=NO OF CARBON+NO OF HYDROGEN+1)
C
C
C
      INTEGER S,C,O
      DATA BLANK/' '/
      DIMENSION P(40),FH(10),FD(10),PEK(20),D(20),KK(7),NN(20),NH(8),
     WND(8)
      READ,ISETS
      ONEC=0.01120414
      ONED=0.00015602
      TWOD=0.00000001
      TWOC=0.00006277
      CANDD=0.00000175
      READ,C,N,O,M
      K=N+M+1
      IPEAK=N+M+2
      S=M+1
      NN(1)=N
      DO 47 I=2,N
   47 NN(I)=NN(I-1)*(N-I+1)
      READ,(FH(IFRAG),IFRAG=1,S)
      READ,(FD(IFRAG),IFRAG=1,S)
      DO 56 INOS=1,ISETS
      READ,TIME
      READ,(P(J),J=1,K)
      WRITE(6,37)
   37 FORMAT('0',///3X,'LIGHT HYDROCARBON FRAGMENTATION PATTERN')
      WRITE(6,1003) (BLANK,LULU=1,M)
 1003 FORMAT('0',2X,6HPARENT,2X,A1,'-1H',4X,A1,'-2H',4X,A1,'-3H',4X,A1,'
     W-4H',4X,A1,'-5H',4X,A1,'-6H',4X,A1,'-7H',4X)
      WRITE(6,102) (FH(IFRAG),IFRAG=1,S)
  102 FORMAT('0',8F8.4)
      WRITE(6,38)
   38 FORMAT('0',3X,'HEAVY HYDROCARBON FRAGMENTATION PATTERN')
```

```
      J=IPEAK-I
      IF(J.EQ.M) GO TO 45
      L=J-S
      IF (P(J).LT.0.0) GO TO 4
      NH(1)=1
      ND(1)=1
      NH(2)=N-L
      ND(2)=L
      IF(S.LT.3) GO TO 901
      DO 46 IVY=3,S
      NH(IVY)=NH(IVY-1)*(NH(2)-IVY+2)
   46 ND(IVY)=ND(IVY-1)*(L-IVY+2)
  901 CONTINUE
      ZH=GAMMA**L
      ZD=PI**(N-L)
      DO 4 NPL=1,M
      NB=NPL+1
      DO 4 NA=1,NB
      NHL=NA-1
      NDL=NPL-NHL
      NWAYS=NPL
      IF(NHL.EQ.0) NWAYS=1
      IF(NHL.LT.2) GO TO 902
      DO 48 IRIS=2,NHL
   48 NWAYS=NWAYS*(NPL-IRIS+1)/IRIS
  902 CONTINUE
      CORR=NWAYS*(NHL*FH(NPL)+NDL*FD(NPL))*ND(NDL+1)*NH(NHL+1)/
     W(NN(NPL)*NPL)*ZD**NDL*ZH**NHL
              KEY=J-NHL-2*NDL
              IF(KEY.LE.0) GO TO 4
  207   P(KEY)=P(KEY)-CORR*P(J)
    4 CONTINUE
   45 WRITE (6,300)
  300 FORMAT ('0',10X,22HCORRECTED PEAK HEIGHTS)
      DO 125 KZ=1,7
  125 KK(KZ)=8-KZ
      NHIGH=8-M
      WRITE(6,1002) (BLANK,KK(KZ),KZ=NHIGH,7)
      WRITE(6,25) (P(J),J=1,M)
      WRITE(6,1001) (BLANK,LULU=1,N)
      WRITE (6,25) (P(J),J=S,K)
      DO 82 NHIGH=1,M
      IFRAG=S-NHIGH
      FD(IFRAG+1)=FD(IFRAG)
   82 FH(IFRAG+1)=FH(IFRAG)
      FD(1)=1.0000
      FH(1)=1.0000
      TOTAL=0.0
      DO 60 J=S,K
      IF (P(J).LT.0.0) GO TO 60
```

```
      TOTAL=TOTAL+P(J)
   60 CONTINUE
      WRITE (6,400)
  400 FORMAT ('0',10X, 30HPERCENTAGE OF ISOTOPIC SPECIES)
      WRITE(6,1001) (BLANK,LULU=1,N)
      DO 810 J=S,K
  810 PER(J)=P(J)*100/TOTAL
      WRITE(6,25) (PER(J),J=S,K)
      PHI=0.0
      DO 80 J=S,K
      L=J-S
      IF(PER(J).LT.0.0) GO TO 80
      PHI=PHI+L*PER(J)
   80 CONTINUE
      WRITE(6,410) TIME,TOTAL,PHI
  410 FORMAT('0',9X,4HTIME,9X,5HTOTAL,9X,3HPHI/F14.1,F15.2,F13.2)
      WRITE(6,34) PHI
   34 FORMAT('0',10X,31HBINOMIAL DISTRIBUTION WITH PHI=,F9.2,2X)
      YY=PHI/(100*N)
      XX=1.0000-YY
      D(1)=100*XX**N
      JEAN=N+1
      DO 59 JIM=2,JEAN
   59 D(JIM)=D(JIM-1)*(JEAN-JIM+1)*YY/(XX*(JIM-1))
      WRITE(6,1001) (BLANK,LULU=1,N)
      WRITE(6,25) (D(JIM),JIM=1,JEAN)
   56 CONTINUE
 3000   STOP
      END
```

REFERENCES


1. Schwab, G.M., Catalysis, 1, 3, (Macmillan, London, 1937)
2. Van Marum, D. J.der Phys., 3, 369 (1796)
3. Kirchhoff, G.R., Schweigger's Journal, 4, 108 (1812)
4. Davy, H., Phil. Trans., 107, 45,(1817)
5. Döbereiner, J.W., Annls.Chim.Phys., 24, 91, (1823)
6. Dulong, P.L. and Thenard, L.G., Annls.Chim.Phys., 23, 440, (1823)
7. Phillips, P. English Patent 6069,(1831)
8. Berzelius, J.J., Annls.Chim.Phys., 61, 146, (1836)
9. Ostwald, W., Physik Z., 3, 313, (1902)
10. Faraday, M., Phil.Trans., 124, 55, (1834)
11. Sabatier, P., La Catalyse en Chemie Organique, (Paris and Liege, 1913)
12. Langmuir, I., Phys.Rev., 6, 79, (1915)
13. Brunauer, S., Emmett, P.H. and Teller, E., J.Amer.Chem.Soc., 60, 309, (1938)
14. Eischens, R.P. and Pliskin, W.A., Adv. Catalysis, 10, 1, (1958)
15. Cornaz, P.F., van Hooff, J.H.C., Pluijm, F.J., and Schuit, G.C.A., Disc.Farad.Soc., 41, 290, (1966)
16. Langmuir, I., Trans.Farad.Soc., 17, 607, 621, (1922)
17. Hinshelwood, C.N., The Kinetics of Chemical Change,(Clarendon Press, Oxford, 1940)
18. Rideal, E.K., J.Soc.Chem.Ind., 62, 335, (1943)
19. Eley, D.D., Quart Rev., 3, 209,(1949)
20. Bond, G.C., Catalysis by Metals,(Academic Press, London, 1962)
21. Sosman, R.B., The Phases of Silica, (Rutger's University Press, New Brunswick, N.J., 1965)
22. Hey, M.H., Trans. Brit.Ceram. Soc., 36, 84, (1937)

23. Rinaldi, R. and Smith, J.V., Int. Mineral Soc. Mtg., (Berlin, 1974)

24. Morey, G.W. and Ingerson, E., Econ.Geol., 38, 607, (1937)

25. Barrer, R.M., J.Chem.Soc., 2158, (1948)

26. Barrer, R.M. and Ibbitson, D.A., Trans.Farad.Soc., 40, 195,(1944)

27. Breck, D.W., Eversole, W.G. and Milton, R.M., J.Amer.Chem.Soc., 78, 2338,(1956).

28. Milton, R.M., U.S. Patent, 2,882,243,(1959)

29. Milton, R.M., U.S. Patent, 2,882,244,(1959)

30. Breck, D.W. and Flanigen, E.M., S.C.I. Conf. on Mol. Sieves, (London, 1967)

31. Barrer, R.M., Baynham, J.W., Bultitude, F.W. and Meier, W.M., J.Chem.Soc., 195,(1959)

32. Flanigen, E.M. and Grose, R.W., Adv.Chem.Series, 101, 76,(1971)

33. McNicol, B.D., Pott, G.T. and Loos, K.R., J.Phys.Chem., 76, 3388, (1972)

34. Barrer, R.M. and Denny, P.J., J.Chem.Soc., 971, (1961)

35. Aiello, R. and Barrer, R.M., J.Chem.Soc.(A),1470, (1970)

36. Taylor, W.H., Z. Krist., 74, 1, (1930)

37. Dent, L.S. and Smith, J.V., Nature, 181, 1794,(1958)

38. Meier, T.B. and Breck, D.W., J.Amer.Chem.Soc., 78, 5972, (1956)

39. Meier, W.M., Z. Krist., 115, 439,(1961)

40. Kerr, G.T., J.Phys.Chem., 70, 1047,(1966)

41. Loewenstein, W., Amer.Miner., 39, 92,(1954)

42. Breck, D.W., Adv.Chem.Series, 101, 1, (1971)

43. Meier, W.M., S.C.I. Conf. on Mol. Sieves, (London, 1967)

44. Barrer, R.M., J.Chem.Soc., 2342, (1950)

45. Keough, A.H. and Sand, L.B., J.Amer.Chem.Soc., 83, 3536, (1961)

46. Barrer, R.M. and Makki, M.B., Can.J.Chem., 42, 1481, (1964)

47. Breck, D.W., Zeolite Molecular Sieves, 570, (1973)

48. Uytterhoeven, J.B., Christner, L.G. and Hall, W.K., J.Phys.Chem., 69, 2117, (1965)

49. Ward, J.W., J.Catalysis, 9, 225, (1967)

50. Kazanskii, V.B., Kinet.Catal., 11, 378, (1970)

51. Rabo, J.A., Angell, C.L., and Schoemaker, V., Preprint 54, 4th Internat.Congr.Catalysis, (Moscow, 1968)

52. Mikheikin, I.D., Shvets, V.A. and Kazanskii, V.B., Kinet.Catal. 11, 609, (1970)

53. Mikheikin, I.D., Brotikovskii, O.I. and Kazanskii, V.B., Kinet. Catal., 13, 481, (1972)

54. Barrer, R.M. and Bratt, G.C., J.Phys.Chem.Solids, 12, 130, (1960)

55. McDaniel, C.V. and Maher, P.K., S.C.I. Conf. on Mol.Sieves, (London, 1967)

56. Kerr, G.T., J.Phys.Chem., 71, 4155, (1967)

57. Kerr, G.T., J.Phys.Chem., 72, 2594, (1968)

58. Kerr, G.T. and Shipman, G.F., J.Phys.Chem., 72, 3071, (1968)

59. Kerr, G.T., J.Phys.Chem., 73, 2780, (1969)

60. Kerr, G.T., J.Catalysis, 15, 200, (1969)

61. Weigel, O. and Steinhoff, E., Z. Krist., 61, 125, (1925)

62. McBain, J.W., The Sorption of Gases and Vapours by Solids, Chapter 5, (Rutledge and Sons, London, 1932)

63. Kington, G.L. and McLeod, A.C., Trans.Farad.Soc., 55, 1799, (1959)

64. Ruthven, D.M., Derrah, R.I. and Loughlin, K.F., Can.J.Chem., 51, 3514, (1973)

65. Barrer, R.M. and Kerr, I.S., Trans.Farad.Soc., 55, 1915, (1959)

66. Breck, D.W., Eversole, W.G., Milton, R.M., Reed, T.B. and Thomas, T.L., J.Amer.Chem.Soc., 78, 5963, (1956)

67. Venuto, P.B. and Landis, P.S., Adv.Catalysis, 18, 259, (1968)

68. Kondis, E.F. and Dranoff, J.S., Adv.Chem.Series, 102, 171, (1971)

69. Antonson, C.R. and Dranoff, J.S., Chem.Eng.Progr.Symp.Series, 65, 27, (1969)

70. Barrer, R.M., Adv.Chem.Series, 102, 42, (1971)

71. Eagan, J.D., Kindl, B. and Anderson, R.B., Adv.Chem.Series, 102, 164, (1971)

72. Satterfield, C.N. and Cheng, C.S., A.I.Ch.E. Symp. Series, No 117, 67, 43, (1971)

73. Barrer, R.M. and Brook, D.W., Trans.Farad.Soc., 49, 1049, (1953)

74. Ruthven, D.M. and Derrah, R.I., J.Colloid Interface Sci., 52, 397, (1975)

75. Doetsch, I.H., Ruthven, D.M. and Loughlin, K.F., Can.J.Chem., 52, 2717, (1974)

76. Gorring, R.L., J.Catalysis, 31, 13, (1973)

77. Eberly, P.E. Jr., Adv.Chem.Series, 171, 414, (1976)

78. Yates, D.J.C., Catalysis Rev., 2, 113, (1969)

79. Ward, J.W., Adv. Chem.Series, 101, 380, (1971)

80. Angell, C.L. and Schaeffer, D.C., J.Phys.Chem., 69, 3463, (1965)

81. Ward, J.W., J.Catalysis, 9, 396, (1967)

82. Best, D.F., Larson, R.W. and Angell, C.L., J.Phys.Chem., 77, 2183, (1973)

83. Eberly, P.E. Jr., Kimberlin, C.N. Jr., and Voorhies, A. Jr., J. Catalysis, 22, 419, (1971)

84. Lefrancois, M. and Malbois, G., J.Catalysis, 20, 350, (1971)

85. Hattori, H. and Shiba, T., J.Catalysis, 12, 111, (1968)

86. Ward, J.W., J.Catalysis, 17, 355, (1971)

87. Kiselev, A.V., Kitiashvili, D.G. and Lygin, V.I., Kinet.Catal., 12, 959, (1971)

88. Kiselev, A.V., Kitiashvili, D.G. and Lygin, V.I., Kinet.Catal., 14, 222, (1973)

89. Zhdanov, S.P. and Kotov, E.I., Adv.Chem.Series, 121, 240, (1973)

90. Wu, E.L., Whyte, T.E. Jr. and Venuto, P.B., J.Catalysis, 21, 384, (1971)

91. Detrekö̈y, E.J., Jacobs, P.A., Kallo̅, D. and Uytterhoeven, J.B., J.Catalysis, 32, 442, (1974)

92. Yashima, T. and Hara, N., J.Catalysis, 27, 329, (1973)

93. Mestdagh, M.M., Stone, W.E.E. and Fripiat, J.J., Trans.Farad.Soc.1., 154, (1976)

94. Mestdagh, M.M., Stone, W.E.E. and Fripiat, J.J., J.Phys.Chem., 76, 1220, (1973)

95. Angell, C.L. and Howell, M.V., J.Colloid Interface Sci., 28, 279, (1968)

96. Eberly, P.E. Jr., J.Phys.Chem., 71, 1717, (1967)

97. Bielanski, A., Datka, T., Drelinkiewicz, A. and Malecka, A., Bull.Acad.Pol.Sci.Ser.Sci.Chem., 24, 137, (1976)

98. Hennig, H.J. and Wechert, H., Proc. 3rd.Internat.Conf.Mol.Sieves, 319, (1973)

99. Hirschler, A.E., Neikam, W.C., Barmby, D.S., and James, R.L., J.Catalysis, 4, 628, (1965)

100. Corio, P.L. and Shih, S., J.Catalysis, 18, 126, (1970)

101. Corio, P.L. and Shih, S., J.Phys.Chem., 75, 3475, (1971)

102. Minachev, Kh.M., Kinet.Catal., 11, 342, (1970)

103. Miale, J.N., Chen, N.Y. and Weisz, P.B., J.Catalysis, 6, 278, (1966)

104. Hansford, R.C. and Ward, J.W., J.Catalysis, 13, 316, (1969)

105. Otouma, H., Arai, Y. and Ukihashi, H., Bull.Chem.Soc.Japan, 42, 2449, (1969)

106. Ikemoto, M., Tsutsumi, K. and Takahashi, H., Bull.Chem.Soc.Japan, 45, 1330, (1972)

107. Turkevich, J., Catalysis Rev., 1, 1, (1968)

108. Venuto, P.B., Adv.Chem.Series, 102, 260, (1971)

109. Leach, H.F., Ann.Reports (A), 195,(1971)

110. Minachev, Kh.M. and Isakov, Y.I., Adv.Chem.Series, 121, 451, (1973)

111. Venuto, P.B., Chem.Tech., 18, 215, (1971)

112. Rabo, J.A. and Poutsma, M.L., Adv.Chem.Series, 102, 284, (1971)

113. Weisz, P.B. and Miale, J.N., J.Catalysis, 4, 527, (1965)

114. Weisz, P.B. and Frillete, V.J., J.Phys.Chem., 64, 382, (1960)

115. Benesi, H.A., J.Catalysis, 8, 368, (1967)

116. Frillete, V.J., Weisz, P.B. and Golden, R.L., J.Catalysis, 1, 301, (1962)

117. Aldridge, L.P., McLaughlin, J.R. and Pope, C.G., J.Catalysis, 30, 409, (1973)

118. Bryant, D.E. and Kranich, W.L., J.Catalysis, 8, 8, (1967)

119. Gourisetti, B., Cosyns, I. and Leprince, P., Bull.Soc.Chim.France, 3, 1085, (1966)

120. Kladnig, W. and Noller, H., J.Catalysis, 29, 385, (1973)

121. Nishizawa, T., Hattori, H., Uematsu, T. and Shiba, T., Preprint 55, 4th Internat.Congr.Catalysis, (Moscow,1968)

122. Cross, N.E., Kemball, C. and Leach, H.F., Adv.Chem.Series, 102, 389, (1971)

123. Dimitrov, Chr. and Leach, H.F., J.Catalysis, 14, 336, (1969)

124. Cross, N.E., Kemball, C. and Leach, H.F., J.Chem.Soc.(A), 3315, (1971)

125. Ward, J.W., J.Catalysis, 13, 321, (1969)

126. George, Z.M. and Habgood, H.W., J.Phys.Chem., 74, 1502, (1970)

127. Hall, W.K., Lombardo, E.A. and Sill, G.A., J.Catalysis, 22, 54, (1971)

128. Norton, C.J., Ind.Eng.Chem.Process Design Dev., 3, 230, (1964)

129. Venuto, P.B., Hamilton, L.A. and Landis, P.S., J.Catalysis, 5, 484, (1966)

130. Liengme, B.V. and Hall, W.K., Trans.Farad.Soc., 62, 3229, (1966)

131. Weisz, P.F., Frillette, V.J., Maatman, R.W. and Mower, R.F., J. Catalysis, 1, 307, (1962)

132. Voorhies, A. and Hopper, J.R., Adv.Chem.Series, 102, 410, (1971)

133. Robson, H.E., Hamner, G.P. and Arey, W.F. Jr., Adv.Chem.Series, 102, 417, (1971)

134. Chen, N.Y. and Garwood, W.E., Adv.Chem.Series, 121, 575, (1973)

135. Penchev, V., Davidova, N., Kanazirev, V., Minchev, H. and Neinska, Y., Adv.Chem.Series, 121, 461, (1973)

136. Galich, P.N., Golubchenka, I.T., Gutyrya, V.S., Il'in, V.G. and Neimark, I.E., Ukr.Khim.Zh., 31, 1117, (1965)

137. Chen, N.Y. and Weisz, P.B., Chem.Eng.Progr.Symp.Series, 63, 86, (1967)

138. Yashima, T. and Hara, N., J.Catalysis, 27, 329, (1972)

139. Turkevich, J., Nozaki, F. and Stamires, D., Proc.3rd Internat. Congr.Catalysis, 1, 586, (Amsterdam, 1965)

140. Pickert, P.E., Rabo, J.A., Dempsey, E. and Schoemaker, V., Proc. 3rd Internat.Congr.Catalysis, 1, 714, (1965)

141. Jacobs, P.A., Leeman, H.E. and Uytterhoeven, J.B., J.Catalysis, 33, 17, (1974)

142. Jacobs, P.A., Leeman, H.E. and Uytterhoeven, J.B., J.Catalysis, 33, 31, (1974)

143. Ward, J.W., J.Catalysis, 26, 470, (1972)

144. Hatada, K., Ono, Y. and Keii, T., Adv.Chem.Series, 121, 501, (1973)

145. Yashima, T., Sato, K., Hayasaka, T. and Hara, N., J.Catalysis, 26, 303, (1972)

146. Yashima, T., Suzuki, H. and Hara, N., J.Catalysis, 33, 486, (1974)

147. Smith, J.V., Adv.Chem.Series, 171, 1, (1976)

148. Eakle, A.S., Amer.J.Sci., 6, 66, (1898)

149. Deffeyes, K.S., Amer.Mineral., 44, 501, (1959)

150. Hey, M.H., Mineral Mag., 32, 343, (1959)

151. Staples, L.W. and Gard, J.A., Mineral Mag., 32, 261, (1959)

152. Barrer, R.M. and Kerr, I.S., Trans.Farad.Soc., 55, 1915, (1959)

153. Hey, M.H. and Fejer, E.E., Mineral Mag., 33, 66, (1962)

154. Bennett, J.M. and Gard, J.A., Nature, 214, 1005, (1967)

155. Zhdanov, S.P., Izv.Akad. Nauk.SSSR.Ser.Khim.Nauk., 2, 950, (1965)

156. Breck, D.W. and Acara, N.A., U.S. Patent, 2,950,952, (1960)

157. Sheppard, R.A. and Gude, J.A., Amer.Mineral., 54, 875, (1969)

158. Eberly, P.E. Jr., Amer.Mineral., 49, 30, (1964)

159. Peterson, D.L., Helferlich, F. and Blytas, G.C., J.Phys.Chem.Solids, 26, 385, (1965)

160. Kawahara, A. and Curien, H., Bull. Soc.Franc.Mineral Crist., 92, 250, (1969)

161. Gard, J.A. and Tait, J.M., Proc. 3rd Internat. Conf. Mol. Sieves, 94, (1973)

162. Aiello, R., Barrer, R.M., Davies, J.A. and Kerr, I.S., Trans. Farad.Soc., 66, 1610, (1970)

163. Eberly, P.E. Jr., Ind.Eng.Chem.Prod.Res.Dev., 8, 140, (1969)

164. Barrer, R.M. and Peterson, D.L., J.Phys.Chem., 68, 3427, (1964)

165. Tsitsishvili, G.V., Andronikashvili, T.G., Sabelashvili, Sh.D. and Osipova, N.A., J.Chromat., 130, 13, (1977)

166. Chen, N.Y., Lucki, S.J. and Mower, E.B., J.Catalysis, 13, 328, (1968)

167. Chen, N.Y., Proc. 5th Internat.Congr.Catalysis, 1343,(Florida,1972)

168. Rollman, L.D., J.Catalysis, 47, 113, (1977)

169. Chen, N.Y., Hill, C. and Rosinski, E.J., U.S. Patent, 3,630,966, (1971)

170. Kokotailo, G.T. and Lawton, S.L., U.S. Patent, 3,640,680, (1972)

171. Burgess, W.P., U.S. Patent, 3,925,191, (1975)

172. Scherzer, J. and Albers, E.W., Can.Patent, 998381, (1976)

173. Barrer, R.M. and Villiger, H., Chem.Comm., 12, 659, (1969)

174. Cole, J.F. and Kouwenhoven, H.W., Adv.Chem.Series, 121, 583, (1973)

175. Flanigen, E.M. and Kellberg, E.R., Netherlands Patent, 6,710,729, (1967)

176. Weeks, T.J.Jr., Kimak, D.G., Bujalski, R.L. and Bolton, A.P., Trans.Farad.Soc.1, 72, 575, (1976)

177. Breck, D.W., Zeolite Molecular Sieves, 620, (1973)

178. Bond, G.C. and Wells, P.B., Adv. Catalysis, 15, 91, (1964)

179. Cvetanović, R.J. and Foster, N.F., J.Amer.Chem.Soc., 82, 4274, (1960)

180. Turkevich, J. and Smith, R.K., J.Phys.Chem., 16, 466, (1948)

181. Haag, W.O. and Pines, H., J.Amer.Chem.Soc., 82, 2488, (1960)

182. Lucchesi, P.J., Baeder, D.L. and Longwell, J.P., J.Amer.Chem.Soc., 81, 3235, (1959)

183. Leftin, H.P. and Hermana, E., Proc.3rd Internat.Congr. Catalysis, 2, 1065, (1965)

184. Gerberich, H.R., Larson, J.G. and Hall, W.K., J.Catalysis, 4, 523, (1965)

185. Gerberich, H.R. and Hall, W.K., J.Catalysis, 5, 99, (1966)

186. Hightower, J.W., Gerberich, H.R. and Hall, W.K., J.Catalysis, 7, 57, (1967)

187. Hightower, J.W. and Hall, W.K., J.Phys.Chem., 71, 1014, (1967)

188. Hightower, J.W. and Hall, W.K., J.Amer.Chem.Soc., 89, 778, (1967)

189. Ballivet, D., Barthomeuf, D. and Trambouze, Y., J.Catalysis, 34, 423, (1974)

190. Misono, M., Sarto, Y. and Yoneda, Y., J.Catalysis, 9, 135, (1967)

191. Misono, M. and Yoneda, Y., J.Phys.Chem., 76, 44, (1972)

192. Hoser, H. and Krzyanowski, S., J.Catalysis, 38, 366, (1975)

193. Lombardo, E.A. and Velez. J., Adv.Chem.Series, 121, 553, (1973)

194. Lombardo, E.A., Sill, G.A. and Hall, W.K., J.Catalysis, 22, 54, (1971)

195. Jacobs, P.A., Declerck, L.J., Vandamme, L.J. and Uytterhoeven, J.B., Trans.Farad.Soc. 1, 71, 1545, (1975)

196. Declerck, L.J., Vandamme, L.J. and Jacobs, P.A., Paper 164, Proc. 3rd Internat. Congr.Mol.Sieves, (1973)

197. Haag, W.O. and Pines, H., J.Amer.Chem.Soc., 82, 387, (1960)

198. Pines, H., Vesely, J.A. and Ipatieff, V.N., J.Amer.Chem.Soc., 77, 347, (1955)

199. Wells, P.B. and Wilson, G.R., J.Catalysis, 9, 70 (1967)

200. Raphael, R.A., The Chemistry of the Carbon Compounds, II, 26, (Elsevier Publishing Co., Amsterdam and N.Y., 1953)

201. Noller, C.R., Chemistry of Organic Compounds, 922, (1965)

202. Lawrence, C.D. and Tipper, C.F.H., J.Chem.Soc., 713, (1955)

203. Tipper, C.F.H. and Walker, D.A., Chem. and Ind., 730, (1957)

204. Newham, J., Chem.Rev., 63, 123, (1963)

205. Anderson, J.R. and Avery, N.R., J.Catalysis, 8, 48, (1967)

206. Roth, J., J.Amer.Chem.Soc., 92, 6658, (1970)

207. Roginski, S.Z. and Rathmann, F.H., J.Amer.Chem.Soc., 55, 2800, (1933)

208. Roberts, R.M., J.Phys.Chem., 63, 1400, (1959)

209. Larson, J.G., Gerberich, H.R. and Hall, W.K., J.Amer.Chem.Soc., 87, 1880, (1965)

210. Hall, W.K., Lutinski, F.E. and Gerberich, H.R., J.Catalysis, 8, 391, (1967)

211. Hightower, J.W. and Hall, W.K., J.Amer.Chem.Soc., 90, 851, (1968)

212. Baird, R.L. and Aboderin, A.A., J.Amer.Chem.Soc., 86, 252, (1964)

213. Bullivant, J., Shapiro, J.S. and Swinbourne, E.S., J.Amer.Chem.Soc. 91, 7703, (1969)

214. Bassett, D.W. and Habgood, H.W., J.Phys.Chem., 64, 769, (1960)

215. Habgood, H.W. and George, Z.M., S.C.I. Conf. on Mol.Sieves, 130, (London, 1967)

216. Bartley, B.H., Habgood, H.W. and George, Z.M., J.Phys.Chem., 72, 1689, (1968)

217. Nguyen, T.T., Cooney, R.P. and Curthoys, G., J.Catalysis, 44, 81, (1976)

218. Coutts, N.M. Ph.D. Thesis, University of Edinburgh, (1973)

219. Flockhart, B.D., McLoughlin, L. and Pink, R.C., Chem.Comm., 818, (1970)

220. Lide, D.R. Jr. and Christiansen, D., J.Chem.Phys., 35, 1374, (1961)

221. Hirota, E. and Morina, Y., J.Chem.Phys., 45, 2326, (1966)

222. Naito, S., Kondo, T., Ichikawa, M. and Tamaru, K., J.Phys.Chem., 76, 2184, (1972)

223. Hughes, B.T., Kemball, C. and Tyler, J.K., Trans.Farad.Soc.1, 71, 1285, (1975)

224. John, C.S., Kemball, C., Dickinson, R. and Tyler, J.K., Trans. Farad.Soc.1, 72, 1782, (1976)

225. Naito, S., Sakurai, Y., Shimizu, H., Onishi, T. and Tamaru, K., Trans.Farad.Soc., 67, 1529, (1971)

226. Stark, J.G. and Wallace, H.G., Chemistry Data Book

227. Haag, W.O. and Pines, H., J.Amer.Chem.Soc., 82, 387, (1960)

228. Selected Values of Physical and Thermodynamic Properties of Hydrocarbons and Related Compounds, (Carnegie Press, 1953)

229. McNaught, W.G.M., Ph.D. Thesis, University of Edinburgh, (1970)

230. Gruber, H.L. and Shipley, C.S., Vac.Microbalance Tech., 3, 131, (1963)

231. Cahn, L. and Schultz, H.R., Vac.Microbalance Tech., 3, 29, (1963)

232. Day, R.E., Parfitt, G.D. and Peacock, J., Progr.Vac.Microbalance. Tech., 2, 61, (1973)

233. Adler, I. and Rose, H.J. Jr., Trace Analysis - Physical Methods, (Ed. Morrison, G.H., 1965)

234. Weeks, T.J. Jr., Angell, C.L. and Bolton, A.P., J. Catalysis, 38, 461, (1975)

235. McClellan, A.L. and Harnsberger, H.F., J.Colloid Interface Sci., 23, 577, (1967)

236. Hammond, G.S., J.Amer.Chem.Soc. 77, 334, (1955)

237. Nishizawa, T., Hattori, H., Uematsu, T. and Shiba, T., Preprint 55, 4th Internat.Congr. Catalysis (1968)

238. Riekert, L., A.I.Ch.E.J. 17, 446, (1971)

239. Tempere, J.F. and Imelik, B., Bull.Soc.Chim.France, 12, 4228, (1970)